Development of Monoclonal Antibodies Targeting T Cell Co-Inhibitory Proteins TIM-3 and TIM-4

February 2024

Mariana Grima

A thesis presented to the Faculty of Health Sciences of the University of Malta in partial fulfilment of the requirements for the degree of Master of Science in Applied Biomedical Science

Supervisor: Prof. David Saliba B.Sc. (Hons) Ph.D. (Edin.)

L-Università ta' Malta

FACULTY/INSTITUTE/CENTRE/SCHOOL Faculty of Health Sciences

DECLARATIONS BY POSTGRADUATE STUDENTS

(a) Authenticity of Dissertation

I hereby declare that I am the legitimate author of this Dissertation and that it is my original work.

No portion of this work has been submitted in support of an application for another degree or qualification of this or any other university or institution of higher education.

I hold the University of Malta harmless against any third party claims with regard to copyright violation, breach of confidentiality, defamation and any other third party right infringement.

(b) Research Code of Practice and Ethics Review Procedures

I declare that I have abided by the University's Research Ethics Review Procedures. Research Ethics & Data Protection form code FHS-2022-00429.

As a Master's student, as per Regulation 77 of the General Regulations for University Postgraduate Awards 2021, I accept that should my dissertation be awarded a Grade A, it will be made publicly available on the University of Malta Institutional Repository.

Dedications

I dedicate this thesis to my loving family, thoughtful partner and cherished friends, whose unwavering support and encouragement have been the cornerstone of my academic journey.

Acknowledgements

I would like to extend my heartfelt gratitude to my supervisor, Prof. David Saliba, for his expertise throughout the research process, valuable guidance and continuous support.

I am grateful to Prof. Jean Paul Ebejer for his invaluable guidance and expertise in the field of bioinformatics, which helped enrich the scientific depth of this research.

I wholeheartedly thank all the staff at the University of Malta and especially at the Centre of Molecular Medicine and Biobanking for their constant assistance.

I also express deep gratitude to Prof. Ted Hupp from the University of Edinburgh for his crucial collaboration and contributions.

My profound gratitude also goes out to the Tertiary Education Scholarship Scheme, without whom my research would not have been possible.

Abstract

Immune checkpoint inhibition (ICI) therapy uses antibodies to block checkpoint proteins from binding with their partner proteins to help overcome dysfunctional T cells and promote the recognition and elimination of tumour cells. The exploration of novel immune checkpoint targets, like T cell immunoglobulin mucin 3 and 4 (TIM-3 and TIM-4), stems from trying to improve the efficacy of ICI therapies (e.g. against cytotoxic T-lymphocyte antigen 4 (CTLA-4) and/or programmed cell death protein 1 (PD-1)) which are currently being used to treat certain cancers like breast, colon and lung cancer either as sole agents or in combination with other immune checkpoint inhibitors or alternative treatments. Targeting TIM-3 and TIM-4 may reverse immune tolerance and suppress tumour cell growth and migration but no effective TIM-4 inhibitors have been developed yet. In this study, monoclonal single chain variable fragment (scFv) antibodies against TIM-3-Fc and TIM-4 were identified using phage display biopanning which isolated antibodies from large immunoglobulin gene repertoires displayed on the surface of bacteriophages. Thirty monoclones from each of the polyclonal pools of anti-TIM-3-Fc and anti-TIM-4 scFv antibodies displayed on phages were picked for validation. Enzyme-linked immunosorbent assay was used to determine the specificity of the phage clones to the target proteins TIM-3-Fc and TIM-4 respectively versus non-target proteins severe acute respiratory syndrome coronavirus 2 (SARS-CoV-2) spike S1 and SARS-CoV-2 receptor-binding domain proteins respectively. This revealed 21 anti-TIM-3-Fc scFv antibody phage monoclones with affinity and specificity to TIM-3-Fc and 8 anti-TIM-4 scFv antibody phage monoclones binding with affinity and specificity to TIM-4. Finally, sanger sequencing was used to determine the DNA sequence of the anti-TIM-3-Fc and anti-TIM-4 scFv antibodies and to compare the resulting amino acid sequences to confirm that different scFv antibodies were identified for TIM-3-Fc versus TIM-4.

Table of Contents

Dedications ii

Acknowledgements iv

Abstract v

List of Figures viii

List of Tables x

List of Abbreviations xi

Chapter 1: Introduction 1

1.1 Tumour Microenvironment 1

1.2 T Cell Activation and Deactivation 4

1.3 Immune Checkpoint Inhibition 8

1.4 TIM-3 and its Ligands 10

1.5 TIM-4 and its Ligands 17

1.6 Combination Therapy 22

1.7 Phage Display Biopanning for the Development of Monoclonal Antibodies 25

Principal Aim and Objectives 33

Chapter 2: Methodology 34

2.1 Maintenance of Escherichia coli ER2738 34

2.1.1 Media Preparation 34

2.1.2 Glycerol Stock Culture 35

2.1.3 Primary Streak Plate 36

2.1.4 Mid-log phase Liquid Culture 36

2.2 Applications of the phage library 37

2.2.1 Phage Display Biopanning 37

2.2.2 Phage Library Titration 41

2.2.3 ELISA Screening of the Enriched Phage Library from Biopanning 43
2.2.4 Preparation of Candidate Phage Clones 46
2.2.5 Monoclonal ELISA 48
2.3 Plasmid extraction from phage precipitate from PEG-precipitated individual clones 51
2.4 Data Analysis 52
2.4.1 GraphPad Prism analysis for monoclones 52
2.4.2 BLAST search 54
Chapter 3: Results 56
3.1 Homology analysis between TIM-3 and TIM-4 56
3.2 Biopanning 59
3.2.1 TIM-4 failed biopanning rounds 59
3.2.2 TIM-4 successful biopanning rounds 63
3.3 Analysis of Monoclones 67
3.3.1 Anti-TIM-3-Fc and anti-IgG-Fc phage clones 67
3.3.2 TIM-3-Fc versus SARS-CoV-2 Spike S1 bait ELISA 71
3.3.3 TIM-4 versus SARS-CoV-2 RBD bait ELISA 75
3.4 Sanger sequencing 78
3.4.1 TIM-3 78
3.4.2 IgG 80
3.4.3 TIM-4 82
3.4.4 No protein control 84
3.4.5 Comparison of all Fully Sequenced Monoclones 85
Chapter 4: Discussion 93
References 108
Appendix 153

List of Figures

Figure 1.1: Immune cells in the TME. 2

Figure 1.2: T cell activation. 5

Figure 1.3: Co-stimulation and co-inhibition of T cells. 6

Figure 1.4: Anti-PD-1 antibodies permit activation of T cells. 9

Figure 1.5: TIM-3 and its ligands. 11

Figure 1.6: Structure of TIM-4. 18

Figure 1.7: Infection of E. coli by M13 phages. 27

Figure 1.8: Structure of scFv. 28

Figure 1.9: Phage Display Biopanning Technique. 29

Figure 2.1: Inoculating LB agar plates. 36

Figure 2.2: Schematic diagram showing binding of fluorescently labelled anti-M13 antibody, M13 phages and target protein. 44

Figure 2.3: ELISA plate layout for testing of phage polyclonal pools. 45

Figure 2.4: ELISA plate layout for testing of phage monoclones. 49

Figure 3.1: Structures of TIM-3 and TIM-4. 57

Figure 3.2: Alignment from the homology analysis of extracellular domains of TIM-3 and TIM-4... 58

Figure 3.3: Graphs of failed TIM-4 biopanning and no protein control 61

Figure 3.4: Graphs of phage dilutions for rounds 2-4 of biopanning of TIM-4, TIM-3, trimer and no protein control phages against anti-M13-PE antibody (a.u.). 64

Figure 3.5: Estimation plot for comparison of round 4 of TIM-4 and round 4 of NPC. 66

Figure 3.7: Graph of anti-TIM-3-Fc scFv antibody-displaying monoclones bound to TIM-3-Fc and SARS-CoV-2 Spike S1 baits respectively vs anti-M13-PE antibody (a.u.). 73

Figure 3.8: Graph of anti-TIM-4 scFv antibody-displaying monoclones vs anti-M13-PE antibody. .. 77

Figure 3.9: Alignments of anti-TIM-3-Fc scFv antibody-displaying monoclones grouped by sequence similarity..... 79

Figure 3.10: Structure of scFv displayed by anti-TIM-3-Fc scFv antibody-displaying phage clone 11. 80

Figure 3.11: Alignments of anti-IgG-Fc scFv antibody-displaying monoclones grouped by sequence similarity..... 81

Figure 3.12: Structure of scFv displayed by anti-IgG-Fc scFv antibody-displaying phage clone 6. ... 82

Figure 3.13: Alignments of TIM-4 monoclones grouped by sequence similarity..... 83

Figure 3.14: Structure of scFv displayed by anti-TIM-4 scFv antibody-displaying phage clone 9. 84

Figure 3.15: Alignments of NPC monoclones. 85

Figure 3.16: Structure of scFv displayed by NPC phage clone 5. 85

Figure 3.17: Alignments of fully sequenced monoclones grouped by sequence similarity. 87

Figure 3.18: Heatmaps of CDR region comparisons between clones binding to different targets..... 91

Figure 3.19: Heatmaps of CDR regions of clones binding to the same targets. 92

Figure 4.1: Binding specificity of scFv antibodies identified. 94

Figure 4.2: Structure of proline. 101

List of Tables

Table 2.1: Dilutions used for phage titering. 42

Table 2.2: Legend of symbols for statistical significance and their meaning. 54

List of Abbreviations

ADAM - A disintegrin and metalloprotease

ADCC - antibody dependent-cellular cytotoxicity

AlphaLISA - amplified luminescent proximity homogenous

AMPKα1 - adenosine monophosphate activating kinase-α1

APC - antigen presenting cell

ATP - adenosine triphosphate

AU - arbitrary unit

AUC - area under the curve

BAT3 - HLA-B associated transcript 3

Bcl-2 - B-Cell Leukemia/Lymphoma 2

Bcl-xL - B-cell lymphoma-extra large

BiTEs - bispecific T-cell engager antibodies

BSA - bovine serum albumin

CAR - chimeric antigen receptor

CC' - coiled-coil

CCL - chemokine ligand

CD - cluster of differentiation

CDR – complementarity-determining region

CEACAM1 - carcinoembryonic antigen-related cell adhesion molecule 1

CFU – colony forming unit

CHO - Chinese hamster ovary

CI – confidence interval

CMMB – Centre for molecular medicine and biobanking

CTLA-4 - cytotoxic T-lymphocyte-associated protein 4

DAMP - damage-associated molecular pattern

DNA - deoxyribonucleic acid

ECD – extracellular domain

EGFP - enhanced green fluorescent protein

ELISA - enzyme-linked immunosorbent assay

ERK - extracellular-signal-regulated kinase inhibitor

E-value – expect value

F - fertility

Fc - crystallizable fragment

FDA - food and drug administration

FG - phenylalanine glycine

FOXP3 - fork head box $P3^{+}$

FR - framework

GHBP - growth hormone binding protein

HAMA - human anti-mouse antibodies

HAVCR1 - hepatitis A virus cellular receptor 1

HAVCR2 – hepatitis A virus cellular receptor 2

HLA - human leukocyte antigen

HMGB-1 - high mobility group box protein 1

HSP90 - heat shock protein 90

ICCVS – international centre for cancer vaccine science

ICI - immune checkpoint inhibition

ICOS - inducible T cell co-stimulator

IFN - interferon

Ig - immunoglobulin

IgV - immunoglobulin variable

IL - Interleukin

ITIM - immunoreceptor tyrosine based inhibitory motif

ITK - inducible T-cell kinase

KIM-1 - Kidney injury molecule-1

LB - lysogeny broth

LAG-3 - lymphocyte activation gene-3

LcK - lymphocyte-specific protein tyrosine kinase

LMIR5 - leukocyte mono-Ig–like receptor 5

mAb - monoclonal antibody

MAPK - mitogen-activated protein kinase

MHC - major histocompatibility complex

MILIBS - metal-ion-dependent ligand binding site

NK - natural killer

NKG2D - natural killer group 2-member D

NPC – no protein control

NO - nitric oxide

Ns – not significant

NSCLC - non-small cell lung carcinoma

PC – phage culture

PD-1 - programmed cell death 1

PD-L1 - programmed death ligand 1

RBD – receptor binding domain

RGD - arginine-glycine-aspartic acid

Rpm – revolutions per minute

ROS - reactive oxygen species

SARS-CoV-2 - severe acute respiratory syndrome coronavirus 2

scFv - single chain variable fragment

SEM - standard error of the mean

STAT6 - signal transducer and activator of transcription 6

TCF-1 - T cell factor-1

TCR - T cell receptor

TEA - triethylamine

TGF - transforming growth factor

TIGIT - T cell immunoreceptor with Ig and ITIM domains

TIL - tumor infiltrating lymphocyte

Th-1 - T helper 1

TLR - toll-like receptors

TIM-1 - T cell immunoglobulin mucin-1

TIM-3 - T cell immunoglobulin mucin-3

TIM-4 - T cell immunoglobulin mucin-4

TIMD4 - T cell immunoglobulin and mucin domain containing 4

TME - tumor microenvironment

TNF - tumor necrosis factor

TRAIL - TNF-related apoptosis-inducing ligand

Tregs - regulatory T cells

VH - variable heavy

VL – variable light

Vs – versus

Chapter 1: Introduction

1.1 Tumour Microenvironment

The environment surrounding a tumour is known as the tumour microenvironment (TME) and is composed of a diverse matrix of various cell types and molecules (Labani-Motlagh, Ashja-Mahdavi et al. 2020). It is generated and dominated by tumour-induced intercellular interactions (Whiteside, T. L. 2008) involving complex and dynamic systems of cytokines, chemokines, growth factors, inflammatory and matrix remodelling enzymes with disruptions to the physical and chemical properties of the tissue (Grivennikov, Greten et al. 2010, Hanahan, Weinberg 2011, Martinez, Sica et al. 2008). The cell and tissue types which can be found in TME include: proliferating tumour cells and stroma, blood vessels, lymphatics, fibroblasts and pericytes (Joyce, Pollard 2009).

One of the functions of TME is immune surveillance which utilises both innate and adaptive immunity (Swann, Smyth 2007) and explains the recruitment of immune cells to the TME as in **Figure 1.1**. Immune infiltrated tumours show an active immune response as immune cells are homogenously distributed throughout the tumour. Contrarily, in immune excluded tumours, immune cells are found around the periphery of the tumour and not infiltrated into the TME. Yet other tumours are known as immune silent tumours and completely lack immune cell infiltration (Anderson, Simon 2020).

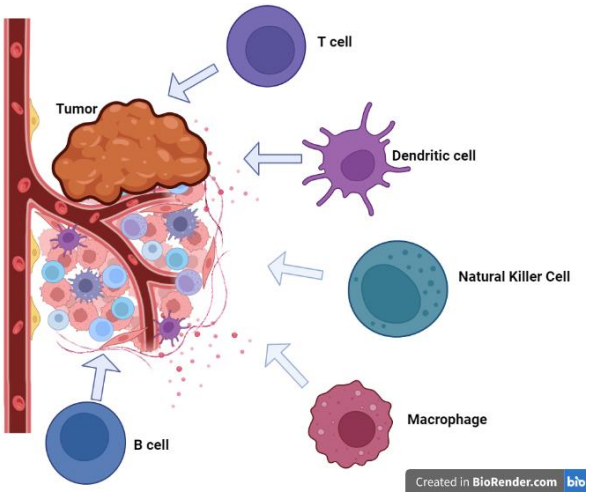

Figure 1.1: Immune cells in the TME. *A multitude of immune cells are recruited to the TME; namely T cells, dendritic cells, B cells and to a lesser extent also macrophages, natural killer cells and neutrophils.*

During the elimination phase of cancer immunoediting, each immune cell performs an important function. For example, dendritic cells coordinate the immune reactions and macrophages eliminate tumour cells by releasing lytic enzymes, tumour necrosis factor-alpha (TNF-α), oxygen and nitrogen intermediates and by promoting antibody-dependent cell-mediated cytotoxicity (ADCC) (Gul, Babes et al. 2014, Martin, Edwards 1993, Urban, Shepard et al. 1986). Furthermore, infiltration of TME with cytotoxic T cells is regulated by basophils through release of chemokine ligand 3 (CCL3) and CCL4 among others (Sektioglu, Carretero et al. 2017) and T cell activation is mediated by eosinophils which are recruited to the TME by molecules released by the tumour. The anti-tumour response provided by eosinophils also includes degranulation and secretion of granzyme A and TNF-α through binding of natural killer group 2-member D (NKG2D) to NKG2D ligands on tumour cells (Kataoka, Konishi et al. 2004, Legrand, Driss et al. 2010). Additionally, neutrophils can activate anti-tumour T cell immunity and tumour death by TNF-related apoptosis-inducing ligand (TRAIL) as well as through release of reactive oxygen species (ROS) and ADCC. T helper 1 (Th1) cells are pro-inflammatory and assist cytotoxic T cells by secreting IL-2 and interferon (IFN)-γ (Anderson, Simon 2020).

In healthy individuals, cluster of differentiation (CD)8^+ cytotoxic T cells recognise abnormal proteins synthesised by pathological cells and provide anti-tumour immunity (Dhatchinamoorthy, Colbert et al. 2021) whereas in cancer progression there is evasion of recognition and elimination of tumour cells by

$CD8^+$ T cells. Avoidance of the elimination phase results in tumour formation and as the tumour and its environment advance during the equilibrium phase, suppression of anti-tumour immunity is achieved. This is known as the escape phase and is brought about by multiple mechanisms including the release of immunosuppressive extravascular vesicles and molecules such as IL-10. Additionally, tumour cells achieve immune evasion by down-regulating major histocompatibility class I (MHC I) which results in less immune control over the cancer and prevents immunotherapies from functioning properly (Dhatchinamoorthy, Colbert et al. 2021). Furthermore, tumours successfully evade cytotoxic T cells by undergoing variations which decrease antigen processing capabilities and upregulating anti-apoptotic molecules or dysregulating death receptor expression. In addition, T cells self-regulate by expressing increased numbers of checkpoint inhibitors such as cytotoxic T lymphocyte-associated antigen-4 (CTLA-4) and T cell immunoglobulin (Ig) and mucin domain-containing protein 3 (TIM-3) which induces T cell exhaustion and anergy (De Sousa Linhares, Leitner et al. 2018).

Regulatory T cells (Tregs) control autoimmunity by suppressing inflammatory responses and producing an immunosuppressive environment. In tumours this results in elimination of anti-tumour immunity which then favours tumorigenesis (Takeuchi, Nishikawa 2016, Shimizu, Yamazaki et al. 1999, Shitara, Nishikawa 2018). The secretion of growth factors by Tregs and interaction with stromal cells results in enhanced Treg generation (Lindau, Gielen et al. 2013). Furthermore, endothelial cells enhance Treg migration and induce Treg generation under inflammatory conditions (Brinkman, Iwami et al. 2016, Fu, Kishore et al. 2014, Taflin, Favier et al. 2011).

Forkhead box P3 (FoxP3) plays an important role in management of regulatory T cell differentiation and development and is a lineage specification factor of Treg cells (Fontenot, Rasmussen et al. 2005, Hori, Nomura et al. 2003, Khattri, Cox et al. 2003, Takeuchi, Nishikawa 2016). The main role of $FoxP3^+$ Treg cells is immunologic self-tolerance through suppression of excessive immune responses toward self-antigens and pathogens (Sakaguchi, Yamaguchi et al. 2008, Josefowicz, Lu et al. 2012). There is apoptosis and inhibition of activation and proliferation of effector T cells, natural killer cells, monocytes, macrophages and antigen presenting cells (APC) using a multitude of mechanisms (Saleh, Elkord 2019). Additionally, there is increased utilisation of interleukin (IL)-2 (Thornton, Lu et al. 2019,

Chinen, Kannan et al. 2016), increased release of IL-10, IL-35, transforming growth factor-beta (TGF-β) (Collison, Workman et al. 2007, Taylor, Verhagen et al. 2006), granzyme B and perforin (Cao, Cai 2007) and upregulated levels of inhibitory immune checkpoints such as CTLA-4, Programmed cell death-1 (PD-1), lymphocyte activation gene-3 (LAG-3), T-cell immunoreceptor with Ig and immunoreceptor tyrosine based inhibitory motif (ITIM) domains (TIGIT) and TIM-3 (Sasidharan Nair, Elkord 2018).

The levels of tumour-infiltrating lymphocytes (TILs) are one of the most important prognostic factors for patients with solid tumours as it reveals the strength of the anti-tumour immune response and therefore predicts the clinical response to therapy (Galon, Cotes et al. 2006, Leffers, Gooden et al. 2009, Sato, Olson 2005). In cancer patients the levels of circulating regulatory $CD4^+$ helper T cells are significantly elevated in comparison to healthy individuals (Sakaguchi, Miyara 2010, Takeuchi, Nishikawa 2016). Elevated levels of Th1 cells in TME is associated with positive prognosis (Anderson, Simon 2020). Additionally, higher levels of $CD8^+$ T cells surrounding tumour is associated with better clinical outcomes following therapy (Chiba, Ohtani et al. 2004, Kawai, Ishii et al. 2008) whereas elevated ratios of $FoxP3^+$ Tregs:$CD8^+$ T cells in TME is a major contributor to tumour progression and immunosuppression (DeLeeuw, Kost et al. 2012, Peng, Zhuang et al. 2012, Yoon, Orrock et al. 2012). Studies show that high levels of Treg cells are associated with poor prognosis and low survival rate in patients with lung, ovarian, gastric, pancreatic cancers, head and neck squamous cell carcinoma and melanoma (Chaudhary, Elkord 2016, Sasidharan Nair, Elkord 2018, Shang, Liu et al. 2015). $FoxP3^+$ Tregs also help develop tumour resistance to immunotherapies (Facciabene, Motz et al. 2012, Maj, Wang et al. 2017, Petersen, Campa et al. 2006, Saleh, Elkord 2019, Simpson, Li et al. 2013, Yu, Lee 2005) meaning that immunotherapies such as immune checkpoint inhibition (ICI) therapy should be given in combination with targeting of Tregs.

1.2 T Cell Activation and Deactivation

Immature dendritic cells in TME engulf and process tumour antigens and transport this antigenic information to the cell surface where it is displayed to be recognised by immune cells

(Dhatchinamoorthy, Colbert et al. 2021). Dendritic cell maturation and activation is evoked by damage-associated molecular patterns (DAMPs) and results in decreased antigen capture and processing and increased antigen presentation to lymphocytes. Mature dendritic cells then migrate to lymph nodes where there is activation of cytotoxic and helper T cells through antigen presentation on MHC class I and II respectively (Mueller, Jenkins et al. 1989).

With only the first signal, T cells can become anergic to successive stimulation by the same antigen or there can be T cell apoptosis (Mueller, Jenkins et al. 1989). Therefore, apart from the signal between the MHC on the cell surface of APCs and the T cell receptor (TCR), the second signal needed is through antigen-independent co-stimulatory molecules such as CD28 with CD80/86 (Sharpe 2009) as in **Figure 1.2**. There is elevated costimulatory ligand expression including from the B7 and TNF families and increased cytokine release (Curtsinger, Schmidt et al. 1999, Hernandez, Aung et al. 2002, Schmidt, Mescher 1999, Schmidt, Mescher 2002). For example, dendritic cells release the cytokine IL-12 which is essential for strong proliferation, development of cytolytic function and establishment of long-lived memory cells (Schmidt, Mescher 1999, Schmidt, Mescher 2002).

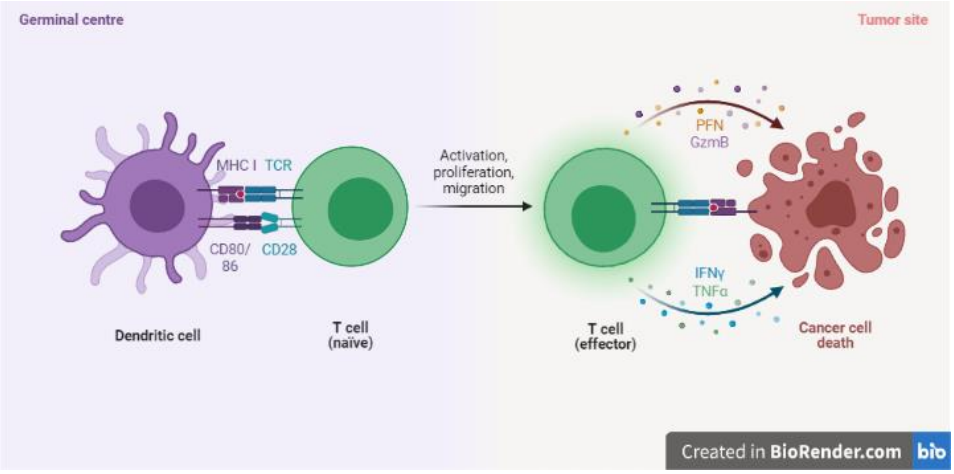

Figure 1.2: T cell activation. *T cells are fully activated if both the MHC/TCR interaction and the co-stimulatory receptor are present. Tumour cells are then apoptosed by perforins and granzymes released by the effector T cells.*

A study by Curtsinger et al. (2003) reveals that with high antigen levels and co-stimulation of naïve T cells there is strong *in vitro* proliferation and clonal expansion *in vivo*, however, without IL-12 as a third signal, the T cells do not perform their effector functions. Apart from this, T cells that expand

without the presence of a third signal become tolerant and fail to perform their effector functions even upon re-stimulation that is usually sufficient for full activation of naïve T cells.

T cells infiltrate the TME to perform their functions via signalling molecules such as chemokines and their receptors (Schmidt, Mescher 1999, Schmidt, Mescher 2002). Apoptosis of cancer cells is mediated by death receptor ligation, Fas ligand, TRAIL, perforin and granzyme B secretions (refer to **Figure 1.2**) (Dhatchinamoorthy, Colbert et al. 2021). Cytotoxic T cells also secrete IFN-γ which suppresses angiogenesis (Anderson, Simon 2020).

The cross-presentation of antigens by dendritic cells to T cells can result in full T cell activation and effector functions as above or it can result in tolerance depending on the co-signalling molecules being expressed as per **Figure 1.3** (Heath, Carbone 2001a, Heath, Carbone 2001b). Co-signalling molecules are transmembrane proteins known as immune checkpoints which cause an intracellular signalling cascade through their cytoplasmic tail, modifying the T-cell-receptor-mediated signal (Mueller, Jenkins et al. 1989).

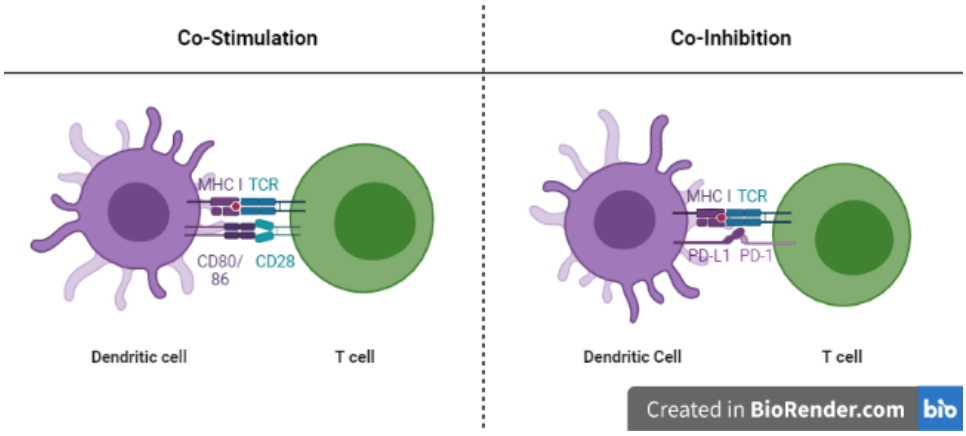

Figure 1.3: Co-stimulation and co-inhibition of T cells. *Co-regulatory molecules determine the fate of the T cell and it either becomes activated or anergic.*

These can be co-stimulatory resulting in full T cell activation or co-inhibitory immune checkpoints which prevent autoimmunity by suppressing potentially autoreactive naïve T cells in lymph nodes, or in peripheral tissue when T cells are further along in development (Franzin, Netti et al. 2020).

CD28 is a co-stimulatory molecule found on all helper T cells and most cytotoxic T cells. Its known ligands are B7-1 and B7-2 which can be expressed on activated T cells (Taylor, Lees et al. 2004) and

on subpopulations of APCs (Hathcock, Laszlo et al. 1994). B7-1 and B7-2 are rapidly upregulated upon activation of APCs. If there is chronic stimulation, this leads to downregulation of CD28 expression which shows a negative feedback mechanism to prevent devastating immune responses (Posnett, Edinger et al. 1999).

CD28 is the most significant pathway of co-stimulation for initial naïve T cell activation. There is ligation of CD3 and CD28 which stimulates production of IL-4 and IL-5 and seems to be unique in its ability to induce high levels of IL-2 production. This increases proliferation in an autocrine manner, provides resistance to apoptosis and results in long-term expansion of T cells (Harding, McArthur et al. 1992, Jenkins, Taylor et al. 1991, Rulifson, Sperling et al. 1997).

Apart from co-stimulatory molecules, co-inhibitory molecules such as CTLA-4 can be expressed on the same cells either simultaneously or consecutively making this intrinsic process more complex (Beier, Hutloff et al. 2000).

CTLA-4 is transported from inside the cell to be expressed on the surface of T cells after activation to inhibit further T cell activation (Brunet, Denizot et al. 1987, Walunas, Lenschow et al. 1994). CTLA-4 also binds to B7-1 and B7-2 but with a higher affinity than CD28 since it produces a lattice structure upon binding with these ligands. This prevents CD28 from binding and results in T-cell deactivation. Furthermore, CTLA-4 restricts autocrine production of IL-2 and inhibits progression of the cell cycle (Schwartz, Zhang et al. 2002).

PD-1 is another co-inhibitory molecule but is not limited to expression on T cells as it is also found on B cells and myeloid cells after activation. PD-1 binds to PD-L1 (Dong, Zhu et al. 1999) and PD-L2 (Freeman, Latchman et al. 2001, Tseng, Otsuji et al. 2001) which have different functions at differing parts of immune responses. PD-L1 is known to be expressed on T cells, B cells, macrophages and dendritic cells in thymus and nonlymphoid tissues including the heart, kidney and liver. PD-L2 is expressed solely on activated macrophages and dendritic cells (Yamazaki, Akiba et al. 2002). PD-1 binding to its ligands results in downregulation of T cell response and arrests the cell cycle (Agata, Kawasaki 1996) as in **Figure 1.3**. However, co-stimulation by CD28 or exogenous IL-2 can overcome

the inhibition of proliferation and cytokine production caused by PD-1. Therefore, PD-1 suppression is important in cases where there is limited IL-2 production such as when there is inducible T cell co-stimulator (ICOS) co-stimulation (Bennett, Luxenberg et al. 2003).

Co-signalling molecules have significant potential as targets for therapeutic treatments since they are vital for regulating T cells especially in T-cell-regulated or T-cell-mediated immune disorders (Beier, Hutloff et al. 2000).

1.3 Immune Checkpoint Inhibition

The complexity of anti-tumour immunity provides a significant challenge for production of effective therapies for cancer patients. Oncogenesis is strongly attributed to dysfunction of the immune system and evasion of anti-tumour immunity which hampers the traditional treatment strategy of many cancers (Vinay, Ryan et al. 2015). One of the main difficulties is exhaustion of T cells. In this cellular state there is compromised proinflammatory cytokine production and development of cytotoxicity due to continuous antigen exposure (Hashimoto, Kamphorst et al. 2018). Traditionally, chemotherapy and radiotherapy target the tumour directly whereas novel immunotherapies target the TME as well as effector immune cells, killing tumour cells indirectly (Labani-Motlagh, Ashja-Mahdavi et al. 2020).

ICI immunotherapy is an antibody-based therapy that relies on stimulation of immune cells to promote their function by increasing recognition and elimination of tumour cells (Yang 2015). The antibodies block inhibitory molecules and allow immune cells to function properly as in **Figure 1.4**. In recent years immunotherapy has been used to treat a multitude of cancers which includes renal cell carcinoma, bladder carcinoma, melanoma, non-small cell lung cancer (NSCLC), Hodgkin lymphoma (Das, Johnson 2019), rectal cancer (Karagkounis 2022), head and neck cancer, gastric cancers, triple-negative breast cancer among others (Witkowska, Smolewski 2018).

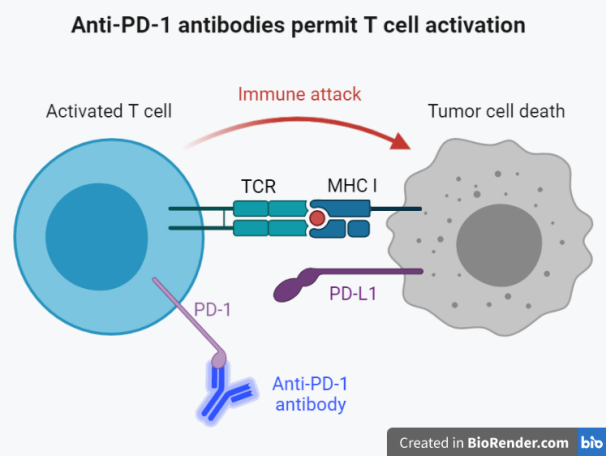

Figure 1.4: Anti-PD-1 antibodies permit activation of T cells. *The binding of antibodies to co-inhibitory molecules prevents ligands from binding and results in T cell activation leading to tumour cell death.*

Ipilimumab which is an anti-CTLA-4 antibody is the first immune checkpoint inhibitor approved for therapy and shows significant responses when used to treat metastatic melanoma (Spagnuolo, Gridelli 2018). Nivolumab or anti-PD-1 is approved for treatment of classic Hodgkin lymphoma since 2016 for patients who relapse after autologous hematopoietic stem cell transplant (Vaddepally, Kharel et al. 2020). Pembrolizumab which is another anti-PD-1 antibody treatment approved since 2017, is used to treat relapsed or refractory classic Hodgkin lymphoma after multiple lines of therapy and since 2020 it is approved to treat patients even after one line of therapy (Vaddepally, Kharel et al. 2020).

A study by Ansell et al. enrols 23 patients with heavily pre-treated relapsed or refractory classic Hodgkin lymphoma. These patients are treated with nivolumab and show an 87% overall response rate which includes a 17% complete response and 70% partial response. Their rate of progression-free survival at 24 weeks is 86% (Ansell, Lesokhin et al. 2015).

For many cancer patients, ICI therapy has greatly improved their prognosis, however, it has also been associated with ill-defined adverse events due to the resulting uncontrolled activation of immune cells. This is because the physiological breaks provided by the immune checkpoints are inhibited. Such an adverse event is known as an immune-related adverse event and clinically resembles auto-immune disorders (Benfaremo, Manfredi et al. 2018, Jenkins, Barbie et al. 2018). Immune checkpoint inhibitors are also associated with kidney toxicity (Perazella, Shirali 2020) and this issue is further complicated

because renal toxicities caused by anticancer agents are frequently reported as an increase in creatine levels without further understanding of the pathogenic effects on the patient (Franzin, Netti et al. 2020).

Furthermore, several patients fail to respond to therapy. Primary and acquired resistance commonly occur and this emphasises the importance of identifying new biomarkers to determine patients who would reap the most benefit from particular checkpoint inhibitors (Darvin, Toor et al. 2018, Havel, Chowell et al. 2019, Sharma, Hu-Lieskovan et al. 2017) and to identify and develop various antibodies against different targets (Pineda, Castaneda Hernandez et al. 2016, Carter, Lazar 2018). Research is also important to develop new therapeutic strategies and to better understand tumorigenesis, especially how TME contributes to tumour growth.

Notwithstanding, ICI therapy is a more well-tolerated therapy for patients especially when used as monotherapy in comparison to other immunotherapies such as chimeric antigen receptor (CAR)T-cell therapy and bispecific T-cell engager antibodies (BiTEs) (Hatic, Sampat et al. 2021). In CAR T-cell therapy, the patient's T cells are used to attack tumour cells using a CAR molecule. This therapy is approved for use in diffuse large B-cell lymphoma and mantle cell lymphoma which allows for ICI to potentially be used in patients with CAR-T progression since their immune system will be modified to favour ICI therapy use (Hatic, Sampat et al. 2021). BiTEs target an antigen on lymphoma cells and another antigen on T cells forming a bridge and resulting in cell-mediated cytotoxicity. Combination therapy with ICI can be performed with chemotherapy or CAR-T cell therapy to mediate antigen presentation by APCs (Zitvogel, Galluzzi et al. 2013). Otherwise, two immune checkpoint inhibitors can be used to potentially overcome defective antigen presentation by enhanced T-cell activation depending on the response of individual patients (Hatic, Sampat et al. 2021).

1.4 TIM-3 and its Ligands

TIM-3 is an immunoregulatory protein and has an amino-terminal immunoglobulin variable (IgV) domain with five noncanonical cysteines, a mucin stalk, a transmembrane domain and a cytoplasmic tail as in **Figure 1.5** but lacks any known inhibitory signalling motifs (McIntire 2001, Meyers, Sabatos et al. 2005). It is part of the TIM family which are encoded by HAVCR1, HAVCR2 and T cell

immunoglobulin and mucin domain containing 4 (TIMD4) genes in humans found on chromosome bands 5q33.2 and 11B1.1. This region in the genome is towards the end of IL4, IL5 and IL13 gene loci associated with allergy and asthma (McIntire 2001, Meyers, Sabatos et al. 2005).

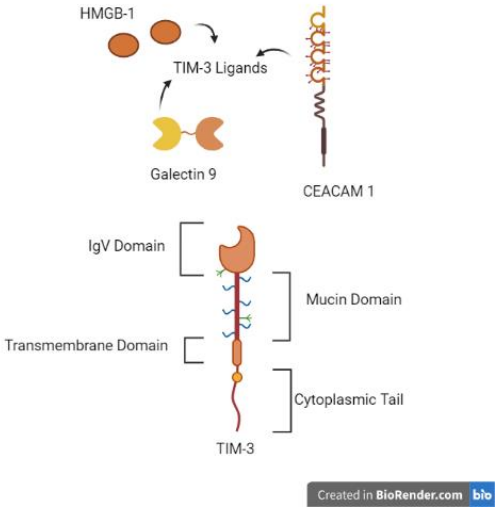

Figure 1.5: TIM-3 and its ligands. *The structure of TIM-3 consists of an IgV domain, mucin stalk, transmembrane domain and cytoplasmic tail. Its known ligands include carcinoembryonic antigen-related cell adhesion molecule 1 (CEACAM1), galectin 9 and high mobility group box 1 (HMGB-1).*

TIM-3 is linked with regulation of the immune response in autoimmunity and cancer. It is expressed by IFN-γ-producing $CD4^+$ helper and $CD8^+$ cytotoxic T cells (Kuchroo, Monney et al. 2002), regulatory T cells (Gao, Zhu et al. 2012), myeloid cells (Anderson, Anderson et al. 2007), natural killer cells (Ndhlovu, Lopez-Verges et al. 2012) and mast cells (Phong, Avery 2015).

Upon T cell activation, TIM-3 is recruited to the immunological synapse where human leukocyte antigen (HLA)-B associated transcript 3 (BAT3) binds to its cytoplasmic tail and there is recruitment of the active and catalytic form of lymphocyte-specific protein tyrosine kinase (LCK) (Clayton, Haaland et al. 2014). In this state TIM-3 can activate the T cell. However, upon binding of TIM-3 to its ligands such as soluble lectin galectin 9 and adhesion molecule carcinoembryonic antigen-related cell adhesion molecule 1 (CEACAM1), there is phosphorylation of Try256 and Try263 by IL-2 inducible T-cell kinase (ITK) (Van De Weyer, Muehlfeit et al. 2006, Huang, Zhu et al. 2015). BAT3 is then released and TIM-3 exerts its inhibitory functions (Rangachari, Zhu et al. 2012).

Tyrosine-protein kinase Fyn (FYN) may also result in TIM-3 mediated inhibitory signalling since it can bind to the same region as BAT3 resulting in competition for binding. FYN induces T cell anergy through activation of phosphoprotein associated with glycosphingolipid-enriched microdomains 1 (PAG). There is recruitment of c-terminal Src tyrosine kinase which phosphorylates LCK on an inhibitory residue and therefore suppresses TCR signalling (Davidson, Schraven et al. 2007). Additionally, TIM-3 binding to CD45 and CD148 disrupts the immunological synapse which also results in T cell inhibition (Clayton, Haaland et al. 2014).

Galectin 9 is one of the known ligands of TIM-3 and is a C-type lectin broadly expressed and secreted by multiple haematopoietic cells. It has two carbohydrate recognition domains and can form a molecular bridge between TIM-3 complexed with other ligands and phosphatases CD45 and CD148 at the immunological synapse (Clayton, Haaland et al. 2014). It binds to the carbohydrate motifs on the IgV domain of TIM-3 and can generate intracellular calcium influx and cell death (Kuchroo, Zhu, 2005). Upon binding there is oligomerization of TIM-3 on the cell surface which induces the release of BAT3 from the intracellular tail of TIM-3. Consequently, there is T cell inhibition and eventually cell death (Rangachari, Zhu et al. 2012).

It is hypothesised that galectin 9 binding may promote binding of TIM-3 to other ligands by inducing an allosteric change to make the cleft framed by phenylalanine glycine (FG) and coiled-coil (CC') loops, making it more accessible to other ligands (Wolf, Anderson et al. 2019).

By secreting TIM-3 and galectin 9, cancer cells can evade immune surveillance (Goncalves, Yasinska et al. 2017). Expression of galectin 9 may be caused by TIM-3 as an inhibitory feedback mechanism. For example, in acute myeloid leukemia patients, an autocrine TIM-3-galectin-9 loop results in self-renewal of acute myeloid leukemia stem cells through activation of nuclear factor-κB and β-catenin pathways (Kikushige, Miyamoto et al. 2015).

Galectin 9 can also work independently of TIM-3 through O-linked glycosylation of an unknown glycoprotein and IL-2 (Oomizu, Arikawa et al. 2012). *In vitro* experiments show that galectin 9 can enhance production of cytokines by Th1 and Th2 cells (Su, Bi et al. 2011) and supress Th17 cell

differentiation. Galectin 9 can also bind to cell-surface glycoprotein CD44 in Tregs via binding of N-linked sugars of defined configuration and this regulates their function (Wu, Thalhamer et al. 2014).

Phosphatidylserine is another ligand which binds to TIM-3 and other members of the TIM family (Kobayashi, Karisola et al. 2007, DeKruyff, Bu et al. 2010). It is a phospholipid which acts as a surface marker for apoptotic cells (Freeman, Casasnovas et al. 2010). It binds to the FG and CC' loop pocket in the TIM-3 IgV domain (DeKruyff, Bu et al. 2010) with coordinated calcium binding (Cao, Cai 2007) involving amino acids Asn119 and Asp120 (Gandhi, Kim et al. 2018). This binding site is on the opposite side of the IgV domain to the site predicted to bind with galectin 9 (Freeman, Casasnovas et al. 2010). In comparison to other TIM family members, TIM-3 binds with much lower affinity to phosphatidylserine and does not lead to engulfment and phagocytosis of apoptotic material by T cells. However, it is presumed to be important for antigen cross-presentation by TIM-3^{+} dendritic cells (Nakayama, Akiba 2009).

High mobility group box 1 (HMGB1) is another known ligand of TIM-3 found specifically on dendritic cells and thought to bind through the CC' and FG loops of TIM-3 (Chiba, Baghdadi et al. 2012, Nakayama, Akiba et al. 2009, Sabatos-Peyton, Nevin et al. 2018, Tang, Lotze 2012). HMGB1 can also be secreted by tumour cells (Curtin, Liu et al. 2009). It binds to deoxyribonucleic acid (DNA) released by dying cells and aids nucleic acid sensing by toll-like receptors (TLRs). It is possible that TIM-3^{+} myeloid cells act as a molecular sink for HMGB1, interfering with its function in innate immune activation. Furthermore, it is suggested that TIM-3 interaction with HMGB1 is independent of other TIM-3 ligands (Sabatos-Peyton, Nevin et al. 2018, Tesniere, Schlemmer et al. 2010). Testing whether TIM-3 blockade increases the efficacy of other chemotherapeutic drugs that result in HMGB1 release would be interesting (Wolf, Anderson et al. 2019).

CEACAM1 also binds to TIM-3 and is known to aid in regulation of antiviral responses (Khairnar, Duhan et al. 2018). *In vitro* studies with CEACAM1 showed that it is co-expressed with TIM-3 on ovalbumin peptide-stimulated and *Staphylococcus aureus* endotoxin B-stimulated T cells after repeated

exposure to these antigens. Therefore, it likely contributes to establishing T cell tolerance (Huang, Zhu et al. 2015).

CEACAM1 is thought to bind to the CC' and FG loops of TIM-3 (Huang, Zhu et al. 2015) and has been found to bind intracellularly which appears important for TIM-3 maturation (Huang, Zhu et al. 2015). The binding of CEACAM1 can release BAT3 from TIM-3, mediating TIM-3 inhibition of TCR signalling (Huang, Zhu et al. 2015). Additionally, CEACAM1 is also expressed on dendritic cells (Kammerer, Stober et al. 2001), monocytes (Horst, Bickert et al. 2009) and macrophages (Coutelier, Godfraind et al. 1994). This suggests that TIM-3-CEACAM1 binding can inhibit immune responses in *cis* or in trans in T cells and myeloid cells. Interaction through *cis* improves the stability of mature TIM-3 on the cell surface while both *cis* and trans interactions mediate the inhibitory function of TIM-3 (Wolf, Anderson et al. 2019). Contrarily, while Linhares et al. (2020) confirm CEACAM1-mediated-inhibition, they argue that TIM-3 and CEACAM1 do not functionally interact in *cis* and in *trans*. The results of this study suggest that TIM-3 functions independently of CEACAM1. TIM-3 interaction with CEACAM1 in TME is highly complex and needs to be further molecularly dissected to determine regulatory mechanisms.

Nevertheless, TIM-3-CEACAM1 binding is potentially a very important target for immunotherapy. All antibodies directed against mouse TIM-3 have shown functional efficacy *in vivo* in mouse cancer models and these interfere with phosphatidylserine and CEACAM1 binding (Sabatos-Peyton, Nevin et al. 2018). CEACAM1 is also highly expressed by tumour cells such as melanoma cells where it is thought to dampen T cell responses (Weiner, Kohalmi et al. 2007). However, CEACAM1 may have tumour-suppressor functions under certain circumstances as mice lacking CEACAM1 developed higher tumour burden in a chemically induced model of colorectal cancer (Leung, Turbide et al. 2006).

It is important to note that polymorphisms in coding and non-coding regions of HAVCR2 have been linked to autoimmune conditions and allergies (Lee, Phong et al. 2011). The main polymorphisms are -1516G/T (rs10053538) and -574G/T (rs10515746) in the promotor region and +4259T/G (rs1036199) in the coding region. Some conditions associated with these polymorphisms are rhinitis (Chae, Park et

al. 2004), gastrointestinal tract cancer (Gao, Yang et al. 2016), NSCLC (Bai, Li et al. 2013), pancreatic cancer (Tong, Zhou et al. 2012) and renal cell carcinoma (Cai, Wang et al. 2012).

Glycosylation is vital for proper folding of protein (Shentel-Bechor, Levy 2008) and stability (Sola, Griebenow 2009). The afore mentioned variations occur close to the predicted glycosylation sites of TIM-3 and therefore likely result in TIM-3 misfolding. Tyr82Cys and Thr101Ile presumably hinder glycosylation of the N-linked or O-linked glycosylation sites and are in a pocket suspected to bind to galectin 9. Therefore, this possibly results in interference with galectin 9 binding and prevention of cell-surface expression. These variations may also impact TIM-3 interaction with CEACAM-1 which aids TIM-3 glycosylation, maturation and transport to the cell surface (Huang, Zhu et al. 2015). Future research using animal models with these point mutations and modelling of the crystal structure of the misfolded protein will give a better understanding of how these variations result in different TIM-3 biology (Wolf, Anderson et al. 2019).

The link between germline HAVCR2 mutations and human disease solidifies the role of TIM-3 as co-inhibitory (Dixon, Das et al. 2018, Gayden, Sepulveda et al. 2018, Polprasert, Takeuchi et al. 2019). Variation c.245A>G (Tyr82Cys) in the IgV domain of TIM-3 results in misfolding of TIM-3 and loss of expression on the cell surface of T cells and myeloid cells. This results in TIM-3 aggregation intracellularly and patients have severe autoinflammatory and autoimmune phenotype with excessive production of proinflammatory molecules such as soluble CD25 and IL-18. There is hyperactivation of macrophages which results in excessive IL-1 and TNF levels in serum. Furthermore, in patients with HAVCR2 variations there is earlier onset of subcutaneous panniculitis-like T cell lymphoma and the disease is more severe when compared to patients without such variations (Wolf, Anderson et al. 2019).

Data by Sabatos-Peyton, Nevin et al. 2018 suggests that antibodies targeting TIM-3 can interfere with phosphatidylserine and CEACAM1 binding but not with galectin 9 binding which brings into question the role of galectin 9 in TIM-3 signalling in tumours. It is not known what the affinity of TIM-3 to its ligands is but there is speculation that the concentration of each ligand in certain tissues may be different and determines the signalling through TIM-3. For example, gastrointestinal tract tissue is known to

express high levels of CEACAM1 whilst liver is known to highly express galectin 9 (Golden-Mason, Rosen 2017, Yan, Zhang et al. 2013).

It is worth noting that since TIM-3 expression is restricted to intratumoral regulatory T cells, blockade of TIM-3 may prevent some of the toxic effects caused by blockade of for example CTLA-4 which is expressed by all regulatory T cells. TIM-3 expression is also limited to terminally differentiated IFNγ-producing T cells whereas CTLA-4 is expressed on all T cells upon activation (Wolf, Anderson et al. 2019).

TIM-3 can also be found in soluble form without the mucin and transmembrane domains because of metalloproteinase-dependent cleavage which facilitates its shedding from the cell surface (Moller-Hackbarth, Dewitz et al. 2013). In the plasma of patients with graft-versus-host disease (Hansen, Hanash et al. 2013) and osteosarcoma patients (Ge, Li et al. 2017), there are elevated plasma levels of TIM-3 (Xu, Yuan et al. 2015). Therefore, TIM-3 can be used as a biomarker for these diseases. The function of soluble TIM-3 is not yet known but it is hypothesised that it may act as a 'molecular sink' for ligands of TIM-3 and this interferes with its inhibitory functions. Contrary to this, *in vitro* experiments suggest that soluble TIM-3 can reduce IL-2 production by T cells (Goncalves, Yasinska et al. 2017).

Tcf7 encodes for T cell factor-1 (TCF1) which is a transcription factor that maintains stemness and restrains effector differentiation. It has been shown that TIM-3 expression is a marker for T cells which have lost the expression of TCF1 (Im, Hashimoto et al. 2016). This negative correlation between TIM-3 and TCF1 expression can be used to mark terminally differentiated effector cells which are exhausted and cannot be reinvigorated by checkpoint blockade and stem-like cells respectively (Brummelman, Mazza et al. 2018, Im, Hashimoto et al. 2016, Kurtulus, Madi et al. 2019, Miller, Sen et al. 2019, Siddiqui, Schaeuble et al. 2019, Wu, Ji et al. 2016). Expression of TCF1 in $PD1^-$ or $PD1^+$ T cells determines response to checkpoint blockade (Kurtulus, Madi et al. 2019, Siddiqui, Schaeuble et al. 2019). It is unknown whether a regulatory mechanism between TIM-3 and TCF1 exists and whether this exists transcriptionally or post-transcriptionally (Wolf, Anderson et al. 2019).

Additionally, TIM-3 can be used as a prognostic marker for solid tumours such as colon, gastric, NSCLC, clear cell renal carcinoma and cervical cancer. Higher levels of TIM-3 expression are correlated to lower survival rates and low TIM-3 expression is correlated to higher survival rates (Zhang, Cai et al. 2017). The same is observed for elevated TIM-3 levels in patients with HBV-associated hepatocellular carcinoma where TIM-3^+ T cells are correlated with lower chances of survival (Li, Wu et al. 2012). Interestingly, in patients with HBV-negative hepatocellular carcinoma, TIM-3 expression on helper and cytotoxic T cells is low (Li, Wu et al. 2012).

TIM-3^+ Tregs have improved suppressor function when compared to TIM-3^- Tregs, therefore, blocking the TIM-3-galectin 9 pathway reduces their suppressive capacity (Ju, Shang et al. 2014). Furthermore, malignant haematopoietic cells show TIM-3 expression, especially in acute myeloid leukemia (Kikushige, Miyamoto 2013). In these tumours, TIM-3 expression is high in leukemic stem cells but not in normal haematopoietic stem cells (Kikushige, Miyamoto et al. 2015, Jan, Chao et al. 2011, Haubner, Perna et al. 2019). The role of TIM-3 on these cells is not known but in a xenograft model of acute myeloid leukemia, blockade of TIM-3 resulted in improved prognosis. Therefore, TIM-3 can be used as biomarker as well as a clinical target (Kikushige, Shima et al. 2010).

1.5 TIM-4 and its Ligands

The SMUCKLER gene encodes for type I transmembrane protein TIM-4 (Liu, Xu et al. 2020). TIM-4 consists of an extracellular IgV domain, mucin-like domain, transmembrane domain and an intracellular cytoplasmic tail as can be seen in **Figure 1.6**. Unlike TIM-3 it has a conserved arginine-glycine-aspartic acid (RGD) motif in the IgV domain that binds integrin proteins (Zhang, Wang et al. 2015). TIM-4 has the longest mucin-like domain of the TIM family and it is rich in threonine, serine and proline residues. The intracellular region of TIM-4 is the most highly conserved region of mouse and human homologs and contains 42-77 amino acids (Liu, Xu et al. 2020).

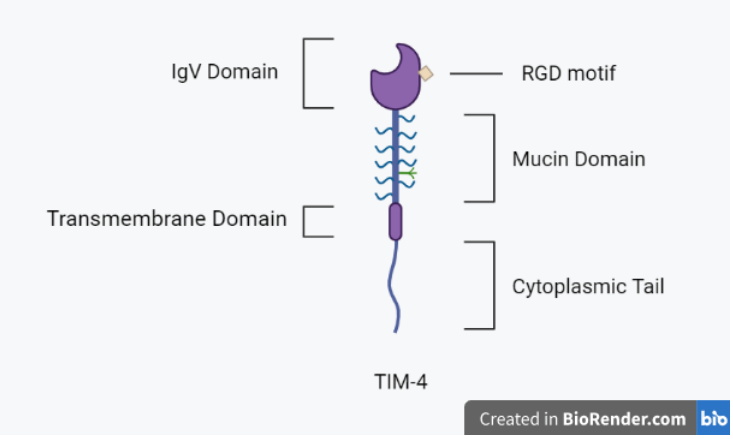

Figure 1.6: Structure of TIM-4. *The structure of TIM-4 includes an IgV domain with an RGD motif, mucin-like domain, transmembrane domain and an intracellular cytoplasmic tail.*

TIM-4 has roles in allergy, asthma, pathogen infection, chronic metabolic disease and tumours (Liu, Xu et al. 2020) and research has confirmed the selective presence of TIM-4 on macrophages, mature dendritic cells, peritoneal B1 cells and invariant natural killer T cells (Cao, Ryan et al. 2011, Wang, Chen et al. 2023, Wong, Valdez et al. 2010, Zhang, Gu et al. 2016). However, it is mainly expressed on antigen-presenting cells instead of T cells unlike other TIM molecules which tend to be mainly expressed on T cells (Kuchroo, Meyers et al. 2005). TIM-4 is also a key marker of resident macrophages in different tissues, whereas, recruited macrophages don't express TIM-4 (Liu, Xu et al. 2020).

Peripheral lymphoid tissues such as thymus, spleen, lymph nodes, tonsils and Peyer's nodule are noted to have high expression of TIM-4. Contrarily, it is expressed at low levels in lung, liver and kidney tissues (Kobayashi, Karisola et al. 2007, Kuchroo, Meyers et al. 2005, Wong, Valdez et al. 2010). TIM-4 has also been found expressed ectopically on tumour cells. Namely in lung cancer (Zhang, Wang et al. 2015), colorectal cancer (Tan, Zhang et al. 2018) and parapharyngeal liposarcoma (Dorfman, Hornick et al. 2010).

The expression of TIM-4 is regulated by different stimulators such as lipopolysaccharide, cholera toxins, cytokines, DAMPs among others (Baghdadi, Yoneda et al. 2013, Feng, Chen et al. 2008, Kim, Kim et al. 2010, Xu, Qi et al. 2010, Xu, Qi et al. 2015). Its expression is greatly increased in the presence

of IL-6 or TGF-β in the TME (Fisher, Appenheimer et al. 2014, Seoane, Gomis 2017, Zhang, Wang et al. 2015).

Interestingly, probiotics are reported to decrease TIM-4 expression on dendritic cells through inhibition of its transcription factor signal transducer and activator of transcription 6 (STAT6) (Yang, Luo et al. 2018). Additionally, vitamin D may repress TIM-4 gene transcription and expression through vitamin D receptor (Liu, Li et al. 2017). Conversely, exposure to cigarette smoke extract results in upregulation of TIM-4 expression in immature dendritic cells from murine bone marrow. This upregulation is inhibited by extracellular-signal-regulated kinase inhibitor (ERK) but not by p38 or c-Jun N-terminal kinase inhibitor (Jiang, Jiang et al. 2019). The mechanisms surrounding TIM-4 expression are still mostly unknown and studies need to be carried out to determine the drivers of transcriptional and translational regulation of TIM-4.

It is speculated that TIM-4 may have an inhibitory role in activation of macrophages (Liu, Xu et al. 2020). TIM-4 is known to inhibit CD80, CD86 and MHC-II expression in macrophages and production of TNF-α in lipopolysaccharide-treated macrophages (Xu, Qi et al. 2010). It also suppresses nitric oxide (NO) production in lipopolysaccharide or IFN-γ-activated macrophages (Liu, Xu et al. 2020).

Kobayashi, Karisola et al. (2007) and Uchiyama, Koike et al. (2007) recognise TIM-4 as a receptor for engulfment of apoptotic cells. Phagocytosis of apoptotic thymocytes is lower upon pre-treatment with TIM-4 blocking antibody. A study by Santiago et al. found that TIM-4 has a metal-ion-dependent ligand binding site (MILIBS) for binding of phosphatidylserine and any amino acid deficiency or variation in this region results in impaired phagocytosis (Santiago, Ballesteros et al. 2007).

A different study revealed that glioma-derived macrophages expressing high levels of TIM-4 contribute to tolerance of tumours by phagocytosis of T cells after exposure to phosphatidylserine (Xu, Xiao et al. 2011). Furthermore, overexpression of TIM-4 on APC's in transgenic mice results in decreased secondary T cell responses and antigen-specific T cell numbers (Albacker, Karisola et al. 2010), therefore, TIM-4 plays a negative role in anti-tumour immunity through induction of tumour immune

tolerance. Consequently, there is potential for blockade of TIM-4 to enhance anti-tumour immunity and improve cancer chemotherapy.

Baghdadi et al. reports high expression of TIM-4 on tumour related macrophages and dendritic cells stimulated by DAMPs such as HMGB1, heat shock protein 90 (HSP90), monosodium urate crystals, S100A8 and adenosine triphosphate (ATP) secreted from dying or stressed tumour cells induced by chemotherapy. After ingesting apoptotic B16-F10 tumour cells, there is activation of autophagy in macrophages through TIM-4-adenosine monophosphate activating kinase-α1 (AMPKα1) interaction. This results in degradation of ingested tumour cells, decreased antigen presentation and impaired cytotoxic T cell responses. Therefore, blocking the TIM-4-AMPKα1-autophagy pathway causes increased tumour-specific cytotoxic T cell responses and thus increases the anti-tumour effect of chemotherapeutics. Targeting this pathway may be a useful strategy for increasing anti-tumour immunity and improving cancer chemotherapy (Baghdadi, Yoneda et al. 2013).

Research performed by Rodriguez-Manzanet et al. (2008) finds that proliferation of T cells incubated with TIM-4^+ Chinese hamster ovary (CHO) cells is significantly higher than that of control cells. Using anti-TIM-4 results in partial inhibition of T cell proliferation induced by TIM-4^+ CHO cells which suggests that TIM-4 is involved in promoting T cell activation. CHO cells also express endogenous co-stimulatory molecules which together with TIM-4 potentially have a synergistic role in activation of T cells (Rodriguez-Manzanet, Meyers et al. 2008). When a higher dose of anti-TIM-4 antibody is used there is more T cell proliferation and amplification *in vitro* and *in vivo* and when lower concentrations are used there is inhibition of T cell proliferation via anti-CD3 and anti-CD28 antibodies (Kuchroo, Meyers et al. 2005). This suggests that TIM-4 can have different functions depending on the activation status of T cells.

A study reveals that TIM-4-Ig binds with CHO cells transfected with TIM-1 and not with those transfected with TIM-3 or TIM-4. This suggests that TIM-4 and TIM-1 interact (Kuchroo, Meyers et al. 2005). Upon addition of anti-TIM-1 antibodies, this binding is blocked confirming that TIM-4 is a natural ligand of TIM-1 (Kuchroo, Meyers et al. 2005). Both proteins bind to phosphatidylserine on the

surface of apoptotic cells or exosomes which means that TIM-1 interaction with TIM-4 occurs indirectly through a phosphatidylserine bridge (Uchiyama, Koike et al. 2007).

TIM-4 has been reported to bind to naïve $CD4^{+}TIM\text{-}1^{-}$ T cells resulting in inhibition of proliferation of naïve $CD4^{+}TIM\text{-}1^{-}$ T cells but not of pre-activated T cells (Mizui, Shikina et al. 2008). Contrastingly, in a study by Cao et al., TIM-4 Fc is found to inhibit both naïve and pre-activated T cell activation, proliferation and cytokine production through a TIM-1 independent pathway (Cao, Ryan et al. 2011). This could be due to differing experiment conditions.

T cell proliferation and differentiation requires the mitogen-activated protein kinase (MAPK) pathway (Nakahara, Moroi et al. 2006, Dong, Davis et al. 2002, Yamashita, Shinnakasu et al. 2005). Anti-TIM-4 antibody could result in Akt phosphorylation and an increase in B-Cell Leukemia/Lymphoma 2 (Bcl-2) expression which protects T cells from apoptosis but does not increase B-cell lymphoma-extra large (Bcl-xL) protein expression (Rodriguez-Manzanet, Meyers et al. 2008). This suggests that TIM-4 may promote proliferation of T cells by inducing anti-apoptotic signals and cell division. Nevertheless, TIM-4 Fc inhibits ERK phosphorylation of T cells stimulated with coated anti-CD3 and anti-CD28 (Mizui, Shikina et al. 2008). This indicates that TIM-4 Fc could inhibit the MAPK pathway even in pre-activated $TIM\text{-}1^{+}$ T cells.

Cao et al. (2011) confirm that TIM-4 Fc could inhibit the MAPK pathway in T cells, prevent differentiation of Th17 cells and block IL-17 production in Th17-polarized cultures. Also, IgV and mucin domains are necessary for TIM-4 mediated inhibition of T cell activation and Th17 differentiation through the MAPK pathway (Cao, Ryan et al. 2011).

Ge, Zeng et al. (2016) suggest that TIM-4 could bind to TIM-3 on the surface of polarized Th1 cells increasing phosphorylation and levels of Fas ligand in these cells and resulting in apoptosis. The conclusion from this research is that TIM-4 can regulate T cell activation via cross-linkage of different receptors. TIM-4 is also suggested as a ligand for leukocyte mono-Ig–like receptor 5 (LMIR5) which does not bind to phosphatidylserine and has no effect on TIM-4 mediated phagocytosis of apoptotic cells (Yamanishi, Kitaura et al. 2010).

Additionally, TIM-4 can be sheared into soluble TIM-4 by A disintegrin and metalloprotease (ADAM) 10 and ADAM 17 without impacting phosphatidylserine binding (Schweigert, Dewitz et al. 2014). It is speculated that soluble TIM-4 acts as an antagonist of membrane surface TIM-4 but this role is not confirmed *in vivo* (Liu, Xu et al. 2020). Soluble TIM-4 can be detected in serum or bodily fluids and changes in its levels can indicate pathological conditions. For example, in ankylosing spondylitis patients, the soluble TIM-4 levels in serum are significantly elevated which is positively correlated to TNF-α levels and Bath ankylosing spondylitis disease activity index (Chen, He et al. 2015).

A study by Caronni et al. (2021) found that TIM-4 may be used as a biomarker for stratification of human lung tumours. Levels of TIM-4 expression are found to be significantly higher in non-small-cell lung cancer tissues and have adverse prognosis. TIM-4 is identified as a lung type 1 conventional dendritic cell phagocytic receptor implicated in immune surveillance of early murine tumours that is targeted at a later stage of tumour progression and impairs antitumor responses. In a study by Zhang, Wang et al. (2015), TIM-4 expression in NSCLC tissues is negatively correlated with the prognosis of lung cancer patients. The expression of TIM-4 promoted the growth, proliferation and cell cycle progression of lung cancer cells via RGD motif.

TIM-4 expression is also found to be significantly elevated in glioma tissues and here it promotes growth, suppresses apoptosis and enhances clonogenicity (Li, Li et al. 2016). In colorectal cancer, higher expression of TIM-4 results in activation of angiogenesis and recruitment of tumour-associated macrophages through certain signalling pathways (Tan, Zhang et al. 2018). Therefore, targeting TIM-4 may reverse immune tolerance and suppress tumour cell growth and migration which provides a promising tool for tumour therapy. To date, no effective TIM-4 inhibitors have been developed and more research must be performed to determine the anti-tumorigenic actions (DuPage, Cheung et al. 2011, DuPage, Mazumdar et al. 2012, Liu, Xu et al. 2020).

1.6 Combination Therapy

Studies find that most cytotoxic T cells co-express TIM-3 and PD-1 in many solid tumours and TIM-3 marks the most dysfunctional subset of tumour-infiltrating $CD8^{+}PD1^{+}$ T cells by account of there being

less expression of effector cytokines compared to TIM-3$^-$ cells (Jin, Anderson et al. 2010, Fourcade, Zhaojun et al. 2014, Sakuishi, Apetoh et al. 2010). Additionally, the upregulation of TIM-3 and co-expression of PD-1 on melanoma specimens shows unfavourable immune responses (Fourcade, Sun et al. 2010). Combination blockade is suggested since both co-inhibitors are markers of T cell exhaustion and blocking both may result in restoration of T cell proliferation and cytokine production which generates an immune response (Friedlander, Addeo et al. 2019). There is also research being performed on the use of a bispecific antibody targeted at TIM-3 and PD-1 (Klein, Schaefer et al. 2019).

In a study using mouse models genetically engineered with adenocarcinoma of the lung, treatment with anti-PD-1 antibody exhibits progression of tumour and upregulation of other immune checkpoints. This is noted mostly with upregulation of TIM-3 especially on T cells bound to therapeutic antibody. Therefore, TIM-3 overexpression can be used as a marker of resistance to treatment. Treatment of these mice with TIM-3 blockade determines whether it is still efficacious at the point of resistance and in fact, a clinical benefit is observed. To check this applicability in patients treated with PD-1 blockade, specimens from two patients who show an initial response to the PD-1 blockade and eventually develop progressive disease are analysed. Both cases show upregulation of TIM-3 on therapeutic antibody-bound TILs. Therefore, targeting other immune checkpoints which are upregulated when using blockade therapy can expand the clinical benefit in responsive tumours (Koyama, Akbay et al. 2016).

Moreover, treatment of CT26 tumour-bearing mice with only anti-PD-L1 tends to delay tumour growth but shows a lot of variation between experiments and does not give a statistical significance. Meanwhile, using anti-TIM-3 antibodies independently results in little to no difference in tumour burden and treatment. However, when these antibodies are used in combination, there is a substantial decrease in tumour growth and half the mice show complete tumour regression (Sakuishi, Apetoh et al. 2010).

Consequently, most clinical trials using anti-TIM-3 antibodies also make use of anti-PD-1 treatment, provided that dose escalation and safety criteria are met for single agent treatment using anti-TIM-3 antibodies. For example, Tesaro developed a humanized anti-TIM-3 IgG4 antibody (TSR-022) and the

first trial data reported shows that administration of TSR-022 results in stable disease in 31 patients and a partial response in a patient with leiomyosarcoma with no dose-limiting toxicity (Murtaza, Laken et al. 2016). Therefore, combination treatment is trialled with TSR-042 which is an anti-PD-1 antibody. The dose of TSR-022 is increased whilst that of TSR-042 is maintained. This therapy is used in 202 patients with anti-PD1 or anti-PDL-1-antibody-refractory NSCLC and is well-tolerated with no dose-limiting toxicity observed (Chen, Song et al. 2019).

Sabatomimab and spartalizumab are humanized monoclonal antibodies which block the binding of TIM-3 to phosphatidylserine and PD-1 to PD-L1/2 respectively (Tian, Li 2021). The safety and efficacy of sabatomimab with or without spartalizumab in patients with advanced solid tumours is studied in a phase I/II study (Curigliano, Gelderblom et al. 2021). Around half the patients are treated with sabatolimab and the rest with both sabatomimab and spartalizumab. When sabatolimab is used there is no response. However, when combination treatment is used, 6% of patients have partial responses in colorectal cancer, NSCLC, malignant perianal melanoma and small cell lung cancer lasting 12 to 27 months. Some of these patients have elevated expression of immune markers in baseline biopsies and some have positive TIM-3 staining including an NSCLC patient with preceding PD-1 therapy (Curigliano, Gelderblom et al. 2021).

Another phase Ia/b study determines the safety, tolerability, dose, immunogenicity, pharmacodynamics and efficacy of a novel TIM-3 monoclonal antibody LY3321367 when used by itself and when used in combination with anti-PD-L1 antibody LY300054 (Harding, Moreno et al. 2021). The dose escalation study shows no dose limiting toxicity by itself or when used in combination therapy. For NSCLC patients, prior exposure to blockade of PD-1 impacts the clinical outcomes. Patients who are resistant to anti-PD-1/L1 have an objective response rate of 0% and a disease control rate of 35% with a median progression-free survival of 1.9 months. For anti-PD-1/L1 responders, the objective response rate is 7% and the disease control rate is 50% with a median progression-free survival of 7.3 months. When combination therapy is used, objective response rate is 4% and disease control rate is 42% (Harding, Moreno et al. 2021).

LY3415244 which is a bispecific antibody that targets TIM-3 and PD-L1 is studied for its safety and efficacy in advanced solid tumours during a phase I trial (Hellmann, Bivi et al. 2021). Of 12 patients, 2 develop clinically significant anaphylactic infusion related reactions and all patients develop anti-drug antibodies. High levels of the anti-drug antibodies have a negative impact on soluble TIM-3 target engagement. Notably, the anti-drug antibodies have epitope specificity for both the TIM-3 and PD-1 arms (Hellmann, Bivi et al. 2021). This study shows the importance of proper analysis for potentially pre-existing anti-drug antibodies which should be part of immunogenicity risk assessment of novel antibodies (Tian, Li 2021).

Combination therapy can also be used with anti-TIM-3 and anti-TIM-4 antibodies. Models of tumour prove that combined treatment with anti-TIM-3 and anti-TIM-4 antibodies increases the efficacy of cancer vaccines (Cheng, Ruan 2015) compared to TIM-3 and TIM-4 blockade individually. For example, when combinatorial blockade of TIM-3 and TIM-4 is used to treat B16 melanoma, there is a significant increase in vaccine-induced anti-tumour responses by increasing the numbers and effector functions of natural killer cells and cytotoxic T cells (Baghdadi, Nagao et al. 2013).

1.7 Phage Display Biopanning for the Development of Monoclonal Antibodies

Over 100 monoclonal antibodies have been approved for use clinically and a large number are in pre-clinical and clinical development (Manis 2023). In the past century, 4 Nobel prizes have been awarded for technologies related to antibody development. Most recently in 2018, George P. Smith and Sir Gregory P. Winter were awarded the Nobel prize in chemistry for the development of the phage display technique for peptides and antibodies (McCafferty, Griffiths et al. 1990, Smith 1985, Winter, Milstein 1991). Also, in 2018, James P. Allison and Tasuku Honjo were awarded the Nobel Prize in Physiology and Medicine for discovering cancer immunotherapy using antibody blockade of T-cell inhibitory receptors to improve anti-tumour immune responses (Leach, Krummel et al. 1996, Ledford, Else et al. 2018).

Hybridoma technology was the first technique used to generate monoclonal antibodies in mice and when it was first developed, it was ground-breaking. It is still being used today, however, murine-

derived monoclonal antibodies have limited therapeutic efficacy as many patients develop human anti-mouse antibodies (HAMA). In these patients there is quicker clearance of the monoclonal antibody and there can also be an undesirable allergic reaction upon repeated administration (Legouffe, Liautard et al. 1994, Berger, Shankar et al. 2002).

This HAMA response is combatted by engineering chimeric or humanized antibodies with murine variable regions or complementarity-determining regions (CDR) but with human constant regions to maintain specificity whilst reducing the HAMA response (Jones, Dear et al. 1986, Morrison, Oi 1989, Studnicka, Soares et al. 1994). Nowadays, fully human antibodies are generated using hybridoma technology in transgenic mice models such as HuMabMouse and XenoMouse where the mouse immunoglobulin gene loci are replaced with human loci in the transgenic mouse genome (Lonberg 2005, Lonberg, Taylor et al. 1994, Mendez, Green et al. 1997). However, not all antigens are suitable for development using hybridoma. These include conserved, toxic and unstable antigens or proteins with allosteric conformational changes as well as transmembrane proteins (Frenzel, Schirrmann et al. 2016).

Monoclonal antibodies can also be developed through phage display biopanning which involves isolation of fully human-derived monoclonal antibodies from large immunoglobulin gene repertoires displayed on the surface of bacteriophages (Winter, Milstein 1991). The bacteriophage usually used is the filamentous phage M13 which has restricted infection range and does not display temperate or lytic behaviour found in other phages. M13 phages cause a chronic infection in the host by triggering continuous synthesis and release of new particles without compromising the integrity of its host. This is essential for performing multiple biopanning rounds. M13 phage contains a circular single-stranded DNA genome with nine genes that encode for assembly and replication proteins as well as coat proteins pIII, pVIII, pVI, pVII and pIX (Specthrie, Bullitt et al. 1992, van Wezenbeek, Hulsebos et al. 1980). M13 phages infect only *Escherichia coli* with F pilus expression which has a tubular structure and plays a key role in bacteria conjugation (Huang, Bishop-Hurley et al. 2012, Sokullu, Soleymani Abyaneh et al. 2019) through interaction with filamentous bacteriophage coat protein pIII (O'Callaghan, Bradley et al. 1973) as in **Figure 1.7**. Additionally, pIII protein has structural flexibility and can display large

proteins without loss of function (Kehoe, Kay 2005, Rakonjac, Bennett et al. 2011, Sheehan, Marasco 2015, Sidhu, Weiss et al. 2000). In a mature M13 phage virion, protein pIII is found as 5 copies grouped at one end of the virion (Rodi Makowski 1999, Russel Linderoth et al. 1997).

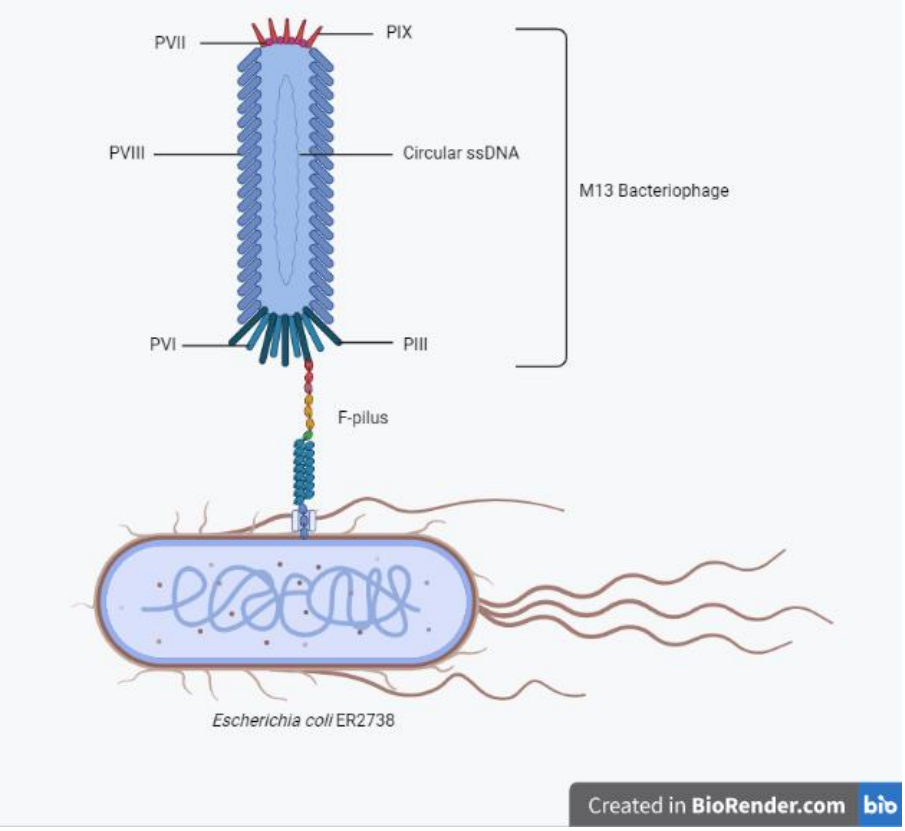

Figure 1.7: Infection of E. coli by M13 phages. *E. coli are infected through interaction of the pIII protein of the M13 bacteriophage with the F pilus of mid-log phase ER2738.*

The success of biopanning depends greatly on the quality and diversity of the antibody repertoire which in turn is dependent on the quality and source of antibody information. Generally, RNA is isolated from B cells or peripheral blood mononuclear cells and is transcribed into cDNA to serve as a template for amplification using a defined set of primers targeting the entire diversity of the host. The library can be constructed to include different antibody isotypes and formats. Single-chain variable fragment (scFv) is the most popular format for phage display as it contains heavy and light chains of the variable region joined by a flexible linker (Alfaleh, Alsaab et al. 2020, Funfrock 2020) as can be seen in **Figure 1.8**.

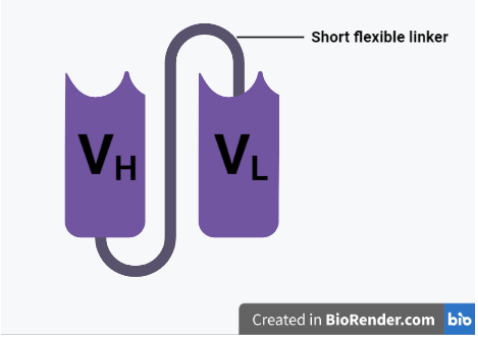

Figure 1.8: Structure of scFv. *VH and VL domains connected by a short flexible linker.*

The advancement of antibody phage display technology is partly due to the discovery of smaller recombinant antibody formats such as variable domain, single-chain variable domain, fragment antigen binding, diabodies, heavy-domain camelid and shark antibody fragments (Barbas, Kang et al. 1991, Bates, Power et al. 2019, Breitling, Dubel et al. 1991, Clackson, Hoogenboom et al. 1991, Kwon, Kim et al. 2019, Vincke, Muyldermans 2012). These smaller fragments can be expressed more easily on bacteria than full antibodies which require assembly of four polypeptide chains and extensive disulphide bond formation (Alfaleh, Alsaab et al. 2020).

The creation of combinatorial scFv library on M13 phage surfaces is achieved using a mix of variable heavy (VH) and variable light (VL)-domains joined by a flexible, protease resistance glycine-serine linker into a single DNA sequence (McCafferty, Griffiths et al. 1990). These sequences are then inserted and cloned as a gene fusion with the bacteriophage pIII gene which is reliant on a weak promoter in a phagemid vector - a plasmid carrying an antibiotic resistance gene as well as bacterial and phage origins of replication (Lowman, Bass et al. 1991, Bass, Greene et al. 1990, Sidhu 2001, Smith, Petrenko 1997).

Purified antigens can be presented to a phage antibody library by immobilisation on solid surfaces which can be nitrocellulose membranes, polystyrene tubes or plates, magnetic beads (as in **Figure 1.9**) or column matrices (Kang, Barbas et al. 1991, Marks, Hoogenboom et al. 1991, Schirrman, Meyer at al. 2011). Any sites which remain unbound to antigen are blocked using a blocking agent such as bovine serum albumin (BSA) to avoid non-specific binding (Menendez, Scott 2005, Shen, Li et al. 2012). After binding of phages to their target, any unbound phages are washed away as these are non-specific binders. The washing step can be regulated depending on what the outcome needed is. With every round

of biopanning, the washing steps are increased gradually so that the higher affinity phage clones are isolated (Smith, Petrenko 1997, Smith, Scott 1993). These high affinity phages are then eluted using different conditions such as change in pH, proteolytic cleavage or competition with free antigens (Haque, Tonks 2012, Kang, Barbas et al. 1991, Marks, Hoogenboom et al. 1991). To prevent degradation of phages and maintain their infectivity, it is essential to neutralise the pH of eluted phage antibodies to be around 8 (Kristensen, Winter 1998, Ward, Clark et al. 1996).

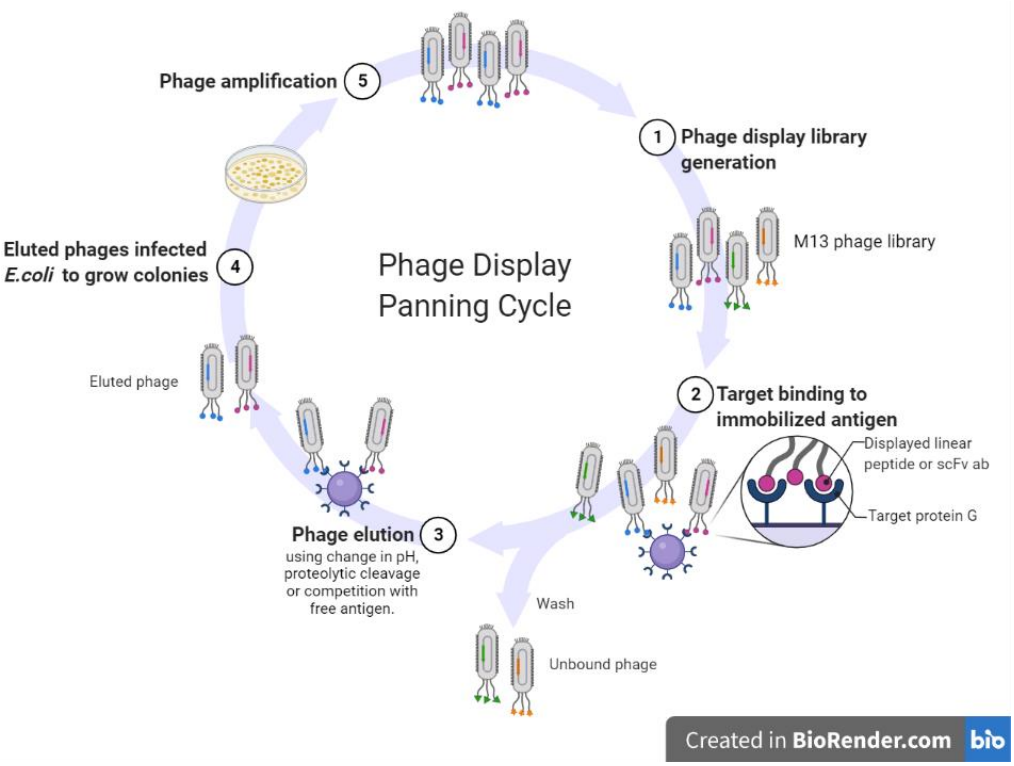

Figure 1.9: Phage Display Biopanning Technique. *This technique involves incubating a library of phage displayed antibodies on beads coated with target, washing away unbound phage, eluting and amplifying the bound phage.*

After multiple biopanning rounds, the phage pool from each round is tested, generally by enzyme-linked immunosorbent assay (ELISA) to determine whether there is enrichment of phage binders to the target in the polyclonal pool. The ELISA involves immobilisation of antigen to microtiter plates and addition of multiple phage pool dilutions from each round followed by a detection antibody against M13 phage. Individual clones from the final biopanning round showing the highest level of enrichment are then screened by ELISA to determine the individual phage clones isolated with highest specificity to the antigen of interest. Positive clones are analysed by restriction fragment length polymorphism to

determine the number of unique clones or by sequencing to determine the CDRs for heavy and light chains (Pande, Szewczyk et al. 2010).

The most important advantage of phage display when compared to *in vivo* methods of antibody generation is the possibility of using toxic and/or non-immunogenic antigens to develop antibodies. Furthermore, phage display is revolutionary in antibody discovery because of the simplicity of phage structure and the fast replication and turnover of bacterial systems. The technology allows for rapid screening of substantial repertoires from naïve or immune hosts obtained through amplification of antibody genes expressed by peripheral blood cells (Funfrock 2020).

Additionally, phage display can be used for known or unknown antigens and for antigens that are unavailable in their pure form (Dantas, Narbosa, de Macedo Brigido et al. 2012, Krag, Shukla et al. 2006, Rader, Barbas 1997, Siva, Kirkland et al. 2008). It can also be used to obtain binders to a unique conformational state of cell surface receptor (Eisenhardt, Schwarz et al. 2007a, Eisenhardt, Schwarz et al. 2007b, Paduch, Koide et al. 2013, Shwarz, Maede et al. 2006, Schwarz, Rottgen et al. 2004) and to identify new biomarkers expressed exclusively on rare cells in heterogenous solution (Kristensen, Sorensen 2011, Sorensen, Agerholm et al. 2010).

This versatile *in vitro* selection technology is successful if the therapeutic antibodies obtained are highly specific and have a high affinity to target. The solubility, viscosity, expression yield and thermal and long-term stability which are dependent on the amino acid sequence of the antibody are essential for success in clinical trials (Chennamsetty, Voynov et al. 2010, Jain, Sun et al. 2017, Lecerf, Kanyavuz et al. 2019). Additionally, low solubility that affects the biomanufacturing of antibodies (Bye, Platts et al. 2014, Garidel, Kuhn et al. 2017, Trevino, Scholtz et al. 2008) will impact the potency, bioavailability and immunogenicity of that antibody (Gibson, McCarty et al. 2011, Sormanni, Amery et al. 2017). Inadequate developability of antibodies can be due to high immunogenicity, physicochemical instability, self-association, high viscosity, poly-specificity, short half-life and poor expression (Lavoisier, Schaaeppi 2015, Dobson, Devine et al. 2016).

Important challenges in *in vitro* antibody display include the lack of natural affinity maturation and loss of natural pairing information. In naïve antibody repertoires there can be weaker affinity to specific antigens in comparison to hybridoma-derived antibodies. And in naïve and immune libraries, heavy and light chains are randomly paired which can result in less stability when compared to hybridoma-derived antibodies. One way of tackling these issues is by improving library quality through significant increase in diversity and improving library construction methods such as *in silico* evaluation of potential binders (Funfrock 2020).

Other limitations of biopanning can include poor availability of purified protein and potentially altered conformation when attached to solid surfaces. Methods which have been used to resolve this include in-solution biopanning followed by affinity capture of antigens tagged with biotin (Fellouse, Esaki et al. 2007) or calmodulin binding peptide (Mukherjee, Ure et al. 2015). Another limitation is that some membrane proteins (Santos, Ursu et al. 2016) are poorly soluble in aqueous media and because of this they don't form well during recombinant expression (Sarkar, Dodevski et al. 2008). For example, they can form aggregates and lose their tertiary structures when they are coated on immunotubes (Butler, Navarro et al. 1997, Butler, Ni et al. 1992, White, Wimley 1999) which results in antibody binders to epitopes that are not naturally exposed (Lipes, Chen et al. 2008, Nagy, Friedlander et al. 2005). This is combatted using cell-based biopanning which maintains the membrane proteins' native conformation (Alfaleh, Arora et al. 2019, Alfaleh, Jones et al. 2017, Jones, Alfaleh et al. 2016, McGuire, Li et al. 2009).

There are 14 FDA approved phage-display derived antibodies and antibody fragments with many others in clinical trials (Alfaleh, Alsaab et al. 2020). Research institutes, start-ups and industrial laboratories are continually developing methods for design, construction and screening of developable antibody-phage libraries to make the process more time-efficient and less expensive (Funfrock 2020). For example, beads have been found to be more effective and efficient for immobilisation of the target protein than plates (Grima 2022, Spiteri 2022). Apart from this, the high-throughput screening of antibody discovery has been greatly improved by the more recent advancements in next-generation sequencing technologies, bioinformatics and nanotechnology (Yoo, Lee et al. 2020, DeKosky, Ippolito

et al. 2013, Sormanni, Aprile et al. 2018, Noh, Kim et al. 2019). All this significantly reduces the time and amount of labour needed to discover antibodies and will make development of therapeutic monoclonal antibodies much quicker (Kelley 2020).

Principal Aim and Objectives

The main aim of this project was to identify scFv antibodies against TIM-3 and TIM-4. This was achieved by using:

- Phage display biopanning to isolate highest affinity scFv antibodies against TIM-3 and TIM-4 proteins,
- ELISA to determine the specificity of the phage pools and phage clones to the target protein,
- Sanger sequencing to determine the DNA sequence of the anti-TIM-3 and anti-TIM-4 scFv antibodies identified,
- Amino acid sequence alignment to determine how similar the complementarity-determining regions of the scFvs identified were.

Chapter 2: Methodology

2.1 Maintenance of Escherichia coli ER2738

The *Escherichia coli* ER2738 strain were provided by the International Centre for Cancer Vaccine Science (ICCVS). This strain was used because it was notably suited for propagation of M13 phages (Ph.D. phage display peptide library instruction manual, New England BioLabs). M13 phages are male-specific coliphages which infect through the fertility (F) pili of Enterobacteriaceae (Bari, Yeasmin 2014) as in **Figure 1.7**. ER2738 F-factor has a mini-transposon which gives them tetracycline resistance (Ph.D. phage display peptide library instruction manual, New England BioLabs). Therefore, tetracycline containing media was used as selective media. All cultures for M13 propagation were inoculated from bacterial colonies grown on tetracycline containing media, rather than from a glycerol culture (Ph.D. phage display peptide library instruction manual, New England BioLabs).

2.1.1 Media Preparation

Media was prepared in class 2 laminar flow cabinets [Faster S.R.L., Ferrara, Italy] in the Centre for Molecular Medicine and Biobanking (CMMB). These class 2 laminar flow cabinets were also used for the inoculation of *E. coli* onto Luria-Bertani (LB) agar [HiMedia Laboratories GmbH, Einhausen, Germany] and into LB broth [HiMedia Laboratories GmbH, Einhausen, Germany]. LB broth cultures were incubated in an Eppendorf New Brunswick™ Innova 42 Incubator Shaker [Massachusetts, United States] and LB agar cultures were incubated in a Binder BD53 Natural Convection incubator [Apeldoorn, The Netherlands].

A tetracycline stock was prepared by making a 70% ethanol solution in a conical tube using 100% ethanol and deionised water. A concentration of 10 mg/ml of tetracycline hydrochloride [Gibco, New York, United States, Catalogue# A39246, Lot# Q26H011A] was then added to this ethanol solution. An ampicillin stock was prepared by dissolving 100 mg/ml of ampicillin sodium salt [Gibco, New York, United States, Catalogue# 11593027, Lot# A0330966] in deionised water and a kanamycin stock was prepared by dissolving 50 mg/ml of kanamycin sulphate [Gibco, New York, United States, Catalogue#

11593-027, Lot# 2240842] in deionised water. The antibiotics were filter sterilised and aliquoted under a class 2 laminar flow cabinet into labelled and autoclaved microcentrifuge tubes for storage in a -20°C freezer. When needed, only one of the tubes was thawed, preventing multiple unnecessary freeze thaw cycles to avoid disrupting the structure of the antibiotic.

LB agar was prepared using a concentration of 35 g/L LB agar powder in deionised water. Half the deionised water was added to the powder until it dissolved. Then the remaining volume of deionised water was added. The LB agar was autoclaved at 121°C for 15 minutes and allowed to cool to about 55°C. Once cool, 10 μg/ml of tetracycline stock were added. Plates were prepared by pouring 25 ml of tetracycline LB agar into petri dishes. These were left to solidify. The lids were left ajar to allow ventilation and prevent condensation during the cooling process. They were then stored in a fridge at 4°C and used for primary streak plates. Similarly, ampicillin plates were made by adding 100 μg/ml of ampicillin to the agar instead of tetracycline. These plates were used for determination of phage titre.

LB broth was made to a concentration of 25 g/L LB broth powder in deionised water. It was autoclaved at 121°C for 15 minutes and allowed to cool completely. When it was needed for overnight cultures, mid-log phase bacteria and phage titering, 10 μg/ml of tetracycline or 100 μg/ml of ampicillin and/or 50 μg/ml of kanamycin was added depending on the procedure being carried out.

2.1.2 Glycerol Stock Culture

A class 2 laminar flow cabinet was used to prepare the glycerol stock culture. Tetracycline LB broth was inoculated with *E. coli* in a conical flask and incubated at 37 °C and 250 revolutions per minute (rpm) in an Eppendorf New Brunswick™ Innova 42 Incubator Shaker overnight. The mouth of the conical flask was covered with aluminium foil to prevent leaks and avoid contamination. A 50% glycerol solution was prepared in a sterile conical tube using deionised water and glycerol. The tube was placed on a rotator for a few minutes to allow the glycerol and water to homogenise. The 50% glycerol solution was filter sterilised and syringed into another sterile conical tube. A volume of 500 μl 50% glycerol solution were aliquoted into several labelled screw top tubes together with 500 μl overnight culture and gently mixed to ensure a uniform solution without layers. These glycerol stock

cultures were stored in a -80°C freezer until needed. To recover frozen cells, a small portion of the frozen glycerol stock was streaked onto LB agar using a 1 µl loop without allowing the stock to thaw and the inoculated plate was incubated at 37°C overnight in a Binder BD53 Natural Convection incubator.

2.1.3 Primary Streak Plate

To prepare primary streak plates, tetracycline LB agar plates were streaked using frozen glycerol stock of *E. coli* ER2738 strain. In a class 2 laminar flow cabinet, 10 µl frozen glycerol stock was pipetted onto one side of the plate. A 1 µl loop was used to make the pool. This loop was turned over to streak that side of the plate with the unused loop surface. A new loop was used to inoculate the rest of the plate as per **Figure 2.1**. One tetracycline LB agar plate was left uninoculated to act as a sterility check. The inoculated and sterility plates were incubated at 37 °C overnight in a Binder BD53 Natural Convection incubator. The next day, they were removed from the incubator, sealed with parafilm tape and stored in a fridge at 4°C. Unless contamination was visible, a new working stock plate needed only be prepared from the glycerol stock or from another primary streak plate every 2 weeks.

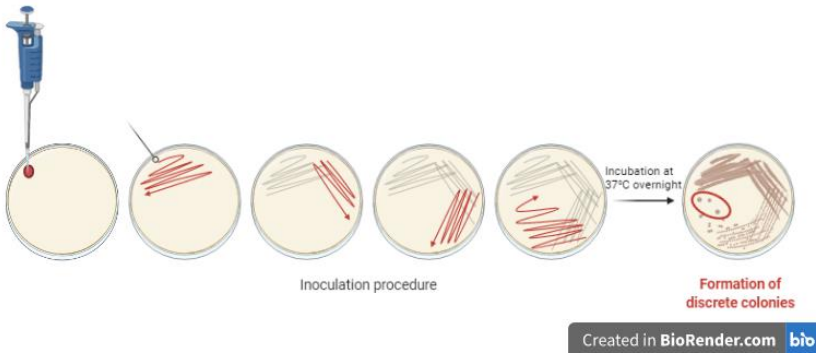

Figure 2.1: Inoculating LB agar plates. *A pool was made by pipetting 10 µl of ER2738 glycerol stock onto a plate and a 1µl loop was used to spread out the pool. The loop was turned over to make streaks towards the side of the plate and a new loop was used for the following streaks, repeating the same technique.*

2.1.4 Mid-log phase Liquid Culture

Grima's (2022) optimization of the mid-log phase of bacterial growth identified the specific timing when *E. coli* exhibited the F pilus. The expression of this F pilus played a crucial role in infecting ER2738, as the infection process relied on its interaction with the pIII protein of the M13 bacteriophage

(Huang, Bishop-Hurley et al. 2012, O'Callaghan, Bradley et al. 1973, Sokullu, Soleymani Abyaneh et al. 2019). It was concluded that mid-log phase was reached after 1.5 hours. The F pilus was required for infection by M13 phages in phage titering as in **Sections 2.2.1, 2.2.2 and 2.3**. The F factor of ER2738 provides resistance to tetracycline (Ph.D. phage display peptide library instruction manual, New England BioLabs) which makes tetracycline LB broth specific to F factor-containing ER2738 and prevents contamination by other bacteria.

To obtain mid-log phase bacteria, 10 μg/ml tetracycline stock were pipetted into LB broth in a sterile falcon tube in a laminar flow cabinet and the tube was inverted to obtain a homogenous solution. A single colony was picked from a primary streak plate with a pipette tip and the tip was dropped into the broth to inoculate it. The falcon tube was incubated at 37°C and 220 rpm for 16 hours in an Eppendorf New Brunswick™ Innova 42 incubator shaker. After the overnight incubation, the broth was moved from the incubator to the fridge and kept at 4°C until needed.

To make the mid-log phase ER2738, a concentration of 10 μg/ml tetracycline was added to a falcon tube containing fresh LB broth and mixed gently by inversion. A volume of 250 μl of the overnight growth was inoculated in the LB/tetracycline broth and incubated at 37°C and 250 rpm. The Eppendorf BioPhotometer spectrophotometer [Eppendorf Corporate, Hamburg, Germany] was blanked using 100 μl fresh LB/tetracycline broth in a cuvette and measurements of the ER2738 were then taken after 1.5 hours of incubation by transferring 100 μl from the corresponding tube into cuvettes and measuring their spectrophotometric readings. This was performed until the OD600 reached 0.4-0.6.

2.2 Applications of the phage library

2.2.1 Phage Display Biopanning

Phage display allowed expression of exogenous scFv antibodies on the surface of bacteriophages in fusion with phage coat protein, linking the phage phenotype with its encapsulated genotype (Rodi, Makowski 1999, Saw, Song 2019, Smith 1985, Ss 2000).

In this project a naïve canine scFv phage library was used. The phage library was provided through collaboration with Prof. Ted Hupp (University of Edinburgh) and Dr Lisowska (ICCVS, University of Gdansk). The scFv antibodies were composed of VH and VL domains connected by a short flexible linker as in **Figure 1.8** and were displayed as N-terminal fusions to minor coat proteins pIII of phages. Each phage displayed a single antibody species (Winter Griffiths et al. 1994, Ahmad Yeap et al. 2012).

In vitro biopanning was used also in Grima (2022) to obtain the highest affinity phages towards target protein TIM-3 using affinity selection. The phage library was incubated with beads and plates which acted as a support by immobilizing the bait protein. As concluded by Grima (2022), beads were more efficient for immobilisation of the target molecule. His-tag beads were used instead of magnetic protein G beads since clumping was observed in Grima (2022) when using magnetic protein G beads. The use of cobalt beads that bind to histidine-tagged target proteins (Dynabeads™ His-Tag Isolation & Pulldown package insert), effectively circumvented the problem.

In this experiment the target proteins used were: SARS-CoV-2 Spike S1+S2 (D614G) trimer Protein (ECD, His tag) [Sino Biological Inc., Beijing, China, Catalogue# 40589-V08H8, Lot# LC15DE0803] as a positive control (since antibodies were successfully isolated before in our lab using the same procedure but by a different scientist) and human TIM4/TIMD4 Protein (His Tag) [Sino Biological Inc., Beijing, China, Catalogue# 12161-H08H, Lot# LC12DE1307].

The selection process of phage display biopanning was initiated with a large phage library of approximately $1x10^{13}$ phage particles expressing a wide diversity of antibodies. This library was used to select subpopulations of specific phage that bind the desired target. The phages which remained unbound and other non-specific phages were removed through repetitive washing steps. The target-bound phages were eluted by incubating in a high pH buffer (a low pH buffer could also be used) to disrupt the interaction between phage-displayed proteins and their targets and to disturb protein folding. The eluted phages were amplified by infecting them into bacteria. Then the amplified elute was collected through a series of centrifugation steps. Further binding and amplification cycles were performed to refine the pool to obtain the phages with the highest affinity for the target (refer to **Figure**

1.9). ELISA and DNA sequencing were then performed to determine the increasing titre of phage with affinity towards the target protein throughout the rounds and to determine the sequence of the antibodies identified respectively (Saw, Song 2019).

For this experiment, the following preparations were made. The preparation of 100mM Triethylamine (TEA) was made by adding 700 µl of TEA into 50ml of deionised water. The pH of the solution was checked using a well-calibrated pH meter and was found to be 11.5. TEA was then stored at 8°C. To prepare sterile 20%PEG 8000/2.5M NaCl, 50g of PEG 8000 were added to 36.5g of NaCl in distilled water up to a final volume of 250ml. This was heated up to 50°C to dissolve while stirring and then autoclaved. To prevent phase separation the magnetic stirrer was left inside the bottle. The solution was stirred while allowed to cool after autoclaving. This solution was also used in **Section 2.2.4**.

In all procedures, every step involving phages was performed using filter tips to prevent contamination of the pipettes.

SARS-CoV-2 Spike S1+S2 trimer protein and human TIM4/TIMD4 Protein were reconstituted in sterile PBS to a concentration of 100 µg/ml. Three labelled low retention 1.5 ml tubes were prepared:

1. Tube 1 labelled as R1 NPC (no protein control)
2. Tube 2 labelled as R1 TIM-4
3. Tube 3 labelled as R1 Trimer

In each tube except the control, 10µl of reconstituted protein in 90µl of binding buffer (PBS + 0.01% Tween-20) were diluted accordingly to have a final volume of 100 µl. For the control, 100 µl of binding buffer were used.

Dynabeads™ His-Tag Isolation & Pulldown contained 40 mg beads/ml in 20% ethanol and had a capacity of isolating 40 µg of a 28 kDa histidine tagged protein/mg (25 µl) beads (Dynabeads™ His-Tag Isolation & Pulldown package insert, 2023). The following calculation was used to determine the volume of beads required per tube for 2.5ug of protein (optimisation experiments were carried out to determine the optimal concentration of protein for correct saturation of His-tag beads).

Dynabeads concentration= 40mg/ml

Binding capacity= 40µg of protein/25µl of beads

Therefore, 2.5 µg of protein requires 1.5625 µl of beads

Prepared as follows: 2µl of beads/tube to counteract the loss of beads during washing steps.

Using a Dynamag™-2 magnet [Invitrogen, Massachusetts, United States, Catalogue# 12321D, Lot# 0714], 6 µl of Dynabeads™ His-Tag Isolation and Pulldown [Invitrogen, Massachusetts, United States, Catalogue# 10103D, Lot# 1162748] were washed once with 500 µl of binding buffer and reconstituted in 70 µl of binding buffer. In each tube, 20µl of beads (120 µl final volume) were pipetted and incubated at room temperature for 30 minutes on a rotator. The beads were washed twice with 500 µl of wash buffer (PBS + 0.05% Tween-20) and blocked with 150 µl of blocking buffer (3% BSA in PBS+0.1% Tween-20) for 1 hour on a rotator. The blocking buffer was then removed.

The original scFv dog library (titre $5x10^{12}$PFU/ml) was diluted in blocking Buffer (final volume was 150 µl/tube). For the first panning round, 2 µl of the original library was used for each tube. For subsequent rounds, 5 µl of enriched library from the previous panning round was used for each tube. If the previous round was stored in glycerol, 10 ul was used. To each tube, 150 µl of diluted library was added and incubated for 1 hour at room temperature on a rotator. A volume of 500 µl of wash buffer was used to wash the beads with phages 10 times. The microcentrifuge tubes were then spun down before using the magnet to remove the final wash to ensure maximum elution in the following step. The phages were then eluted with 150 µl of 100 mM TEA solution (pH=11.3) for 10 minutes on rotator. The eluate was transferred to fresh labelled low retention tube containing 35 µl of 1M TRIS (pH 6.8) and stored at 4°C.

The method in **Section 2.1.4** was carried out to obtain mid-log phase ER2738. To 1 ml ER2738 culture in 5 ml tubes for aeriation, 90 µl of neutralized phage eluate was transferred and incubated for 15 minutes at 37°C on a thermoblock. The culture with phage was diluted in 20ml of LB broth with 20µl ampicillin (working concentration of ampicillin was 100 µg/ml and stock concentration was 100 mg/ml) and incubated at 37°C for 1.5 hours while shaking at 250 rpm. This allowed phage to infect bacteria

and created ampicillin resistance. A volume of 20 µl of helper phage M13KO7 (stock titre was $6.9x10^{11}$ PFU/ml) was added and incubated for 10 minutes static, then for 1.5 hours with shaking at 250 rpm at 37°C. The helper phage provided the bacteria with the Kanamycin resistance gene. A volume of 10µl of Kanamycin (kanamycin working concentration was 50 µg/ml and stock concentration was 50 mg/ml) was added and incubated overnight (16 hours) at 30°C with shaking at 250rpm.

The next day, the samples were centrifuged at 4000 rpm for 10 minutes and approximately 20 ml of the supernatant was transferred to a clean Falcon tube using a pipette gun without disturbing the pellet. A volume of 3.5 ml of PEG/NaCl was added to the supernatant to precipitate the phage and mixed by inversion several times followed by incubation on ice for 2 hours. The tubes were then centrifuged at 4000 rpm for 20 minutes at 4°C and the supernatant was discarded using a pipette gun. The centrifugation was repeated, and the supernatant was carefully removed with a pipette. The phage was resuspended in 200µl of sterile PBS, transferred to labelled microcentrifuge tubes and centrifuged at 10000 rpm at 4°C for 10 minutes. The supernatant was transferred to labelled low retention tubes and stored at 4°C. This was referred to as the enriched (purified) phage library. The enriched library could be stored at 4°C for about a month. For long-term storage, sterile glycerol was added to have 50% final glycerol concentration and it was stored at -20°C. The enriched library was taken through another 3 rounds to further enrich the pool in favour of binding phage. The enriched phage library after each round of biopanning was then titrated.

2.2.2 Phage Library Titration

Phage titering was performed to calculate colony forming units (CFU) and determine whether the phage titre remained constant after each biopanning round for each target protein and control. This would ensure that the amplification steps were successful. The ELISA would then ensure that the phage library grew more specific to the target protein throughout the rounds. The CFUs were calculated by infecting ER2738 with phages and counting the number of colonies which grew. For bacterial infection, the pIII proteins of phages bind to the F pilus of bacteria as in **Figure 1.7** (Ph.D. phage display peptide library instruction manual, New England BioLabs).

For phage titering to be carried out, the ER2738 needed to be in the mid-log phase so the procedure in **Section 2.1.4** was carried out first. Once the required OD reading was obtained, the bacteria were chilled immediately to prevent them from reaching the stationary phase at which point the F pilus tends to be lost (Sambrook 1989, Ready-To-Use Phage Display Library Manual Spring Bioscience). Different phage dilutions were used to infect *E. coli* and obtain a plate with 30-300 countable colonies from which the CFU was calculated. Ampicillin was used because after infection with phage, ER2738 obtained the phagemid vector conferring ampicillin resistance.

A volume of 198 µl LB broth was pipetted into one microcentrifuge tube and 180 µl LB broth were pipetted into another 8 microcentrifuge tubes. A volume of 2 µl phage library was pipetted into tube 2. A new pipette tip was used to homogenise the solution in tube 2 by pipetting up and down 10 times. A volume of 20 µl were pipetted from tube 2 to tube 3 and the pipette tip was discarded. The same was performed from tube 3 to tube 9 as per **Table 2.1**.

Table 2.1: Dilutions used for phage titering. *Dilutions 10^{-2}-10^{-10} were made using LB broth and phage library.*

Tube	Dilution	LB broth	Phage library
1	10^{-2}	198µl	2 µl from the stock
2	10^{-3}	180 µl	20µl from tube 1
3	10^{-4}	180 µl	20µl from tube 2
4	10^{-5}	180 µl	20µl from tube 3
5	10^{-6}	180 µl	20µl from tube 4
6	10^{-7}	180 µl	20µl from tube 5
7	10^{-8}	180 µl	20µl from tube 6
8	10^{-9}	180 µl	20µl from tube 7
9	10^{-10}	180 µl	20µl from tube 8

From previous experiments it was observed that 10^{-9} and 10^{-10} were the best dilutions to test for the canine scFv library so a volume of 100 µl of pre-chilled mid-log phase bacterial culture was transferred to fresh, prelabelled tubes and 100 µl of the 10^{-8}, 10^{-9} and 10^{-10} dilutions of the phage library were added respectively. The microcentrifuge tubes were gently mixed and incubated at room temperature for 5 minutes to allow infection.

The 200 µl of infected cells was dispensed onto LB/ampicillin plates (working concentration of ampicillin is 100 µg/ml) for inoculation. Using a sterile bent inoculating stick, these were spread evenly on the surface. Sterility plates were made before and after inoculating the 10^{-8}, 10^{-9} and 10^{-10} dilutions. The sterility plates were inoculated with un-infected mid-log phase ER2738 before and after the titration to ensure there was no contamination during the procedure. Any excess liquid on the inoculated plates was left to dry under a laminar flow cabinet. The ampicillin plates were incubated upside-down overnight (16 hours) at 37°C in a Binder BD53 Natural Convection incubator. The next day, the sterility plates were checked to ensure there was no growth and if so, the colonies were counted. The CFU was then calculated from the plate containing a colony count of between 30 and 300. Plating the infected cells on ampicillin-containing medium ensured that only cells harbouring the phagemid will grow and the low multiplicity of infection ensured that a host cell will be infected by only one phage. Thus, the titre (CFU/ml) of infected cells correlated to the titre (PFU/ml) of the library. The titre (CFU/ml) of the infected cells and hence of the phage was calculated as follows:

$$\text{CFU/ml=PFU/ml=} \frac{\text{Number of colonies on the plate x Total dilution factor}}{\text{Volume of culture plated in ml}}$$

2.2.3 ELISA Screening of the Enriched Phage Library from Biopanning

The enriched library was screened by ELISA using the same immobilized bait used for panning to confirm target binding. Additionally, the increasing specificity of the phages to the target protein after rounds 2, 3 and 4 of biopanning were compared. In this procedure a microtiter plate was coated with

the target protein and the enriched library from Rounds 2, 3 and 4 was applied to the plate at various dilutions. Bound phage was then detected with an anti-M13-PE antibody as in **Figure 2.2**. A no library control was used to determine background signal.

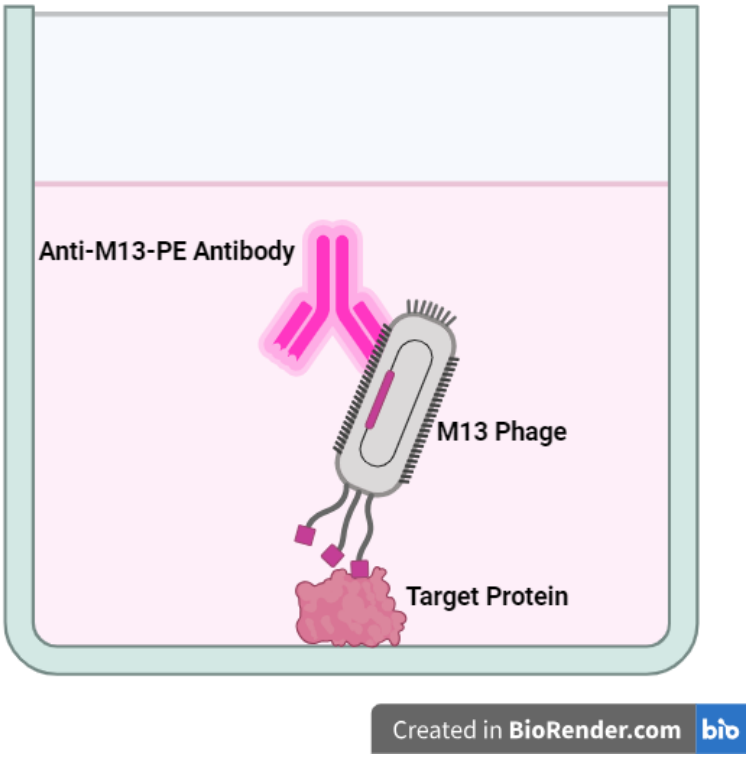

Figure 2.2: Schematic diagram showing binding of fluorescently labelled anti-M13 antibody, M13 phages and target protein. *The target protein was bound to the ELISA plate and M13 phages displaying scFv antibodies bound to the target protein. Anti-M13-PE labelled antibody then bound to the M13 phage.*

A 96-well, black (for fluorescence), flat bottom, non-treated, polystyrene COSTAR assay plate [Corning Inc., New York, United States, Catalogue# 3915, Lot# 36310018] was coated with 250ng of protein/well as per **Figure 2.3**. Proteins used here: human TIM4/TIMD4 Protein (His Tag), SARS-CoV-2 (2019-nCoV) Spike S1-His Recombinant Protein (HPLC-verified) [Sino Biological Inc., Beijing, China, Catalogue# 40591-V08H, Lot# LC1GMA2610], Recombinant Human IgG-Fc Protein, CF [R&D Systems, Minnesota, United States, Catalogue# 110-HG-100], Recombinant Human TIM-3 Fc Chimera Protein, CF [R&D Systems, Minnesota, United States, Catalogue# 2365-TM-050] and SARS-CoV-2 (2019-nCoV) Spike receptor binding domain (RBD) (L452R, T478K) Protein (His Tag) [Sino Biological Inc., Beijing, China, Catalogue# 40592-V08H90, Lot# LC16MA022] as was

necessary. The target protein and a no protein control were used for each enriched library tested. The experiment was conducted in duplicate, with a total of 24 technical replicates taken for the fluorescent measurements (12 replicates per duplicate).

Plate layout	1	2	3	4	5	6
A	R2 TIM-4 (1 in 10) on TIM-4	R2 TIM-4 (1 in 10) on TIM-4	R4 TIM-4 (1 in 10) on TIM-4	R4 TIM-4 (1 in 10) on TIM-4	R3 NPC (1 in 10) on TIM-4	R3 NPC (1 in 10) on TIM-4
B	R2 TIM-4 (1 in 100) on TIM-4	R2 TIM-4 (1 in 100) on TIM-4	R4 TIM-4 (1 in 100) on TIM-4	R4 TIM-4 (1 in 100) on TIM-4	R3 NPC (1 in 100) on TIM-4	R3 NPC (1 in 100) on TIM-4
C	R2 TIM-4 (1 in 1000) on TIM-4	R2 TIM-4 (1 in 1000) on TIM-4	R4 TIM-4 (1 in 1000) on TIM-4	R4 TIM-4 (1 in 1000) on TIM-4	R3 NPC (1 in 1000) on TIM-4	R3 NPC (1 in 1000) on TIM-4
D	R3 TIM-4 (1 in 10) on TIM-4	R3 TIM-4 (1 in 10) on TIM-4	R2 NPC (1 in 10) on TIM-4	R2 NPC (1 in 10) on TIM-4	R4 NPC (1 in 10) on TIM-4	R4 NPC (1 in 10) on TIM-4
E	R3 TIM-4 (1 in 100) on TIM-4	R3 TIM-4 (1 in 100) on TIM-4	R2 NPC (1 in 100) on TIM-4	R2 NPC (1 in 100) on TIM-4	R4 NPC (1 in 100) on TIM-4	R4 NPC (1 in 100) on TIM-4
F	R3 TIM-4 (1 in 1000) on TIM-4	R3 TIM-4 (1 in 1000) on TIM-4	R2 NPC (1 in 1000) on TIM-4	R2 NPC (1 in 1000) on TIM-4	R4 NPC (1 in 1000) on TIM-4	R4 NPC (1 in 1000) on TIM-4
G	No library control (PBS on TIM-4)	No library control (PBS on TIM-4)				

Figure 2.3: ELISA plate layout for testing of phage polyclonal pools. *The target protein (TIM-4 in this case) was bound to the ELISA plate and M13 phage pools displaying scFv antibodies against TIM-4 bound to the target protein. Anti-M13-PE labelled antibody then bound to the target-protein-specific M13 phages and fluorescent intensity was measured on a spectrophotometer.*

A volume of 50 µl of protein diluted in PBS per well was added and incubated for 2 hours at room temperature. The wells were washed 3 times with 100 µl of wash buffer (PBS+0.1% Tween-20)/well and incubated with 200 µl/well of blocking buffer (1%BSA in wash buffer) overnight at 4°C.

The next day, enriched library dilutions were prepared from round 2, 3 and 4 at 1/10, 1/100 and 1/1000 in PBS. A volume of 100 µl/well was added according to the plate layout after removing the blocking

buffer and incubated for 1 hour at room temperature. In 2 wells labelled ‘No library’, 100 µl/well of PBS with no phage library was added. The wells were then washed 5 times with 100µl of wash buffer/well and incubated with 70µl Anti-M13 Antibody (PE), Mouse Monoclonal [Sino Biological Inc., Beijing, China, Catalogue# 11973-MM05T-P, Lot# HR15SE2906] for 1 hour at room temperature in the dark. The antibody was used at 1µg/ml diluted in blocking Buffer. The wells were washed 5 times with 100 µl of wash buffer/well and once with 100 µl of PBS/well. A volume of 100 µl of PBS/well was added and the fluorescence was read on TECAN Spark using the following settings:

Mode: Fluorescence Top Reading
Excitation: Monochromator
Excitation wavelength: 561 nm
Excitation Bandwidth: 20 nm
Emission: Monochromator
Emission wavelength: 606 nm
Emission Bandwidth: 20 nm
Gain: Optimal
Mirror: AUTOMATIC
Number of flashes: 10
Integration Time: 40 µs
Lag time: 0 µs
Settle time: 0 ms
Z-Position: 20000 µm
Z-Position mode: Manual
Multiple Reads per Well (Circle (filled)): 4 x 4
Multiple Reads per Well (Border): 450 µm

2.2.4 Preparation of Candidate Phage Clones

To identify single positive clones from the enriched library, individual clones from round 4 enriched library were amplified, purified and then screened by ELISA.

Sterile 1.5ml tubes were prepared and labelled with round number, clone number and phage culture 1 (PC1). A volume of 400 µl of LB/ampicillin (working concentration of ampicillin was 100 µg/ml and stock concentration was 100 mg/ml) was added to all tubes. Using a sterile 10µl filter pipette tip, 30 well-isolated, single colonies from the LB/Ampicillin agar plate of the round 4 titration were picked and each was used to separately inoculate the medium in the microcentrifuge tubes. Each colony picked was labelled. The tubes were incubated at 37°C overnight (around 16 hours) with shaking at 250 rpm. These were the master stocks of individual phagemid clones in ER2738.

The following day, fresh 1.5 ml tubes were prepared and labelled with round and clone number and PC2. A volume of 400 µl of LB/ampicillin medium containing $5x10^8$ CFU of M13KO7 helper phage carrying the kanamycin resistance gene was added to each labelled PC2 tube. In this experiment the stock helper phage titre was $6.9x10^{11}$ PFU/ml. To calculate the volume of helper phage corresponding to $5x10^8$ CFU, the following formula was used:

$$6.9x10^{11} \text{ CFU: } 1ml = 5x10^8 \text{ CFU: X ml}$$

$$X = (5x10^8 \text{ CFU x 1 ml}) / 6.9x10^{11} \text{ CFU} = 0.72\mu l.$$

So, 0.72 µl of helper phage stock/tube which was rounded up to 1 µl/tube.

A volume of 50 µl of each overnight PC1 culture was transferred to the corresponding PC2 tube and incubated at 37°C for 2 hours with shaking at 250 rpm. To the remaining PC1 culture, sterile glycerol was added to prepare glycerol stocks with a final concentration of 15% and stored at -80°C. PC1 cultures could be stored in the fridge and glycerol stocks could be prepared within few days. The PC2 samples were centrifuged at 13300 rpm for 6 minutes at 25°C. The supernatant containing the phage was discarded and the cells pellet containing the permanent plasmid was resuspended in 500 µl of LB/amp/kan (ampicillin working concentration was 100 µg/ml and stock concentration was 100 mg/ml and kanamycin working concentration was 50 µg/ml and stock concentration was 50 mg/ml). The helper phage provided the bacteria with the Kanamycin resistance gene. The tubes were incubated at 37°C overnight (around 16 hours) with shaking at 250 rpm.

The following day, fresh low retention tubes were prepared and labelled with round number, clone number and PC3. The PC2 tubes were centrifuged at 13300 rpm for 6 minutes at 25°C. A volume of 400 µl of supernatant containing the phage was transferred to fresh PC3 tubes. When working with phage, aerosol resistant pipette tips with filters were used and one tube was opened at a time. A volume of 400 µl of blocking buffer (1% BSA in wash buffer) was added to help the PEG precipitate the phage. The tubes were incubated at 4°C on ice for 10 minutes. A volume of 160 µl of sterile 20% PEG/2.5M NaCl solution was added to each tube and incubated at 4°C on ice for 1 hour. The tubes were centrifuged at 10000 g for 20 minutes at 4°C. The supernatant was discarded, and the phage pellet was resuspended

in 100 µl of sterile PBS 1X. These were the individual purified phage clones. They could be stored in the fridge at 4°C for about a month.

2.2.5 Monoclonal ELISA

The monoclones were tested for target binding using ELISA. The target protein was bound to the ELISA wells and each individual monoclone was added to a separate well. Bound phage was then detected with an anti-M13-PE antibody. To eliminate clones that did not specifically interact with the target, each clone was tested against the target protein and a control protein with the same fusion-tag of the target (His-tag in this case). A positive control using target protein and the round 4 polyclonal pool was used to obtain high fluorescence and a no library control was used to determine background signal.

A 96-well flat bottom, non-treated, black polystyrene assay plate was coated with 50 ng of protein/well as per **Figure 2.4**. A volume of 50 µl of protein/well was added and incubated for 2 hours at room temperature. The proteins were diluted in PBS and the target protein and a control protein were used for each sample tested. Black plates were used for fluorescence-based assay and the fluorescent measurements were taken in 12 technical replicates.

Plate layout	1	2	3	4	5	6	7	8
A	Clone 1 on target protein	Clone 9 on target protein	Clone 17 on target protein	Clone 25 on target protein	Clone 1 on non target protein	Clone 9 on non target protein	Clone 17 on non target protein	Clone 25 on non target protein
B	Clone 2 on target protein	Clone 10 on target protein	Clone 18 on target protein	Clone 26 on target protein	Clone 2 on non target protein	Clone 10 on non target protein	Clone 18 on non target protein	Clone 26 on non target protein
C	Clone 3 on target protein	Clone 11 on target protein	Clone 19 on target protein	Clone 27 on target protein	Clone 3 on non target protein	Clone 11 on non target protein	Clone 19 on non target protein	Clone 27 on non target protein
D	Clone 4 on target protein	Clone 12 on target protein	Clone 20 on target protein	Clone 28 on target protein	Clone 4 on non target protein	Clone 12 on non target protein	Clone 20 on non target protein	Clone 28 on non target protein
E	Clone 5 on target protein	Clone 13 on target protein	Clone 21 on target protein	Clone 29 on target protein	Clone 5 on non target protein	Clone 13 on non target protein	Clone 21 on non target protein	Clone 29 on non target protein
F	Clone 6 on target protein	Clone 14 on target protein	Clone 22 on target protein	Clone 30 on target protein	Clone 6 on non target protein	Clone 14 on non target protein	Clone 22 on non target protein	Clone 30 on non target protein
G	Clone 7 on target protein	Clone 15 on target protein	Clone 23 on target protein	TIM-4 pool library on target protein	Clone 7 on non target protein	Clone 15 on non target protein	Clone 23 on non target protein	TIM-4 pool library on non target protein
H	Clone 8 on target protein	Clone 16 on target protein	Clone 24 on target protein	No library target on target protein	Clone 8 on non target protein	Clone 16 on non target protein	Clone 24 on non target protein	No library non target on non target protein

Figure 2.4: ELISA plate layout for testing of phage monoclones. *The target protein (was bound to the ELISA plate and M13 phage monoclones displaying scFv antibodies against target protein were added and allowed to bind. Anti-M13-PE labelled antibody then bound to the M13 phage clones binding to the target protein of interest and fluorescent intensity was measured on a spectrophotometer.*

The proteins used for this ELISA included; human TIM4/TIMD4 Protein (His Tag), SARS-CoV-2 (2019-nCoV) Spike S1-His Recombinant Protein (HPLC-verified), TIM-3 Protein, Human, Recombinant (ECD, hFc Tag) and SARS-CoV-2 (2019-nCoV) Spike RBD (V483I)-His Recombinant Protein as was required.

The wells were washed 3 times with 100 µl of wash buffer (PBS+0.1% Tween-20)/well and incubated with blocking buffer (200 µl/well) overnight at 4°C. A volume of 70µl of PBS was added to each PC3

preparation to have 170 µl of final volume. The enriched library from where the individual phage clones were purified was prepared at 1/100 dilution in PBS. A volume of 50 µl/well was applied according to plate layout and incubated for 2 hours at room temperature. In 2 wells labelled ‘No library’, 50 µl/well of PBS without phage library was added. The wells were washed 5 times with 100 µl of wash buffer/well and incubated with 70 µl/well anti-M13-PE monoclonal antibody diluted in blocking buffer to be used at 0.5 µg/ml for 1 hour at room temperature in the dark. The wells were washed 5 times with 100 µl of wash buffer/well and washed once with 100 µl of PBS/well. A volume of 100 µl of PBS/well was added and the fluorescence was read on TECAN Spark using the same settings as in **Section 2.2.3**.

2.3 Plasmid extraction from phage precipitate from PEG-precipitated individual clones

For rapid and reliable purification of high-quality plasmid DNA, the Monarch® Plasmid Miniprep Kit [New England BioLabs Inc., Massachusetts, United States, Catalogue# T1010L, Lot# 10132561] was used. This required the use of standard cell resuspension, alkaline lysis and neutralisation steps. The lysate was clarified by centrifugation and the DNA bound to the silica matrix under high salt conditions. The use of unique wash buffers ensured that salts, proteins, RNA and any other cellular component was removed to allow low-volume elution of concentrated and high-purity DNA which was used for DNA sequencing. This procedure was carried out for the monoclones of TIM-3, TIM-4, NPC, original phage library and IgG (Monarch® Plasmid Miniprep Kit Instruction Manual, 2021).

The procedure from **Section 2.1.4** was carried out. Once the required OD reading was obtained, 500 µl of mid-log phase ER2738 bacteria were infected with 1 µl of PEG-precipitated individual phage clones in 5 ml microcentrifuge tubes for aeration and incubated for 30 minutes at 37°C, at 220 rpm. A volume of 50 µl of the infected ER2738 bacteria were transferred into 3 ml of LB/Ampicillin (stock concentration of ampicillin was 100 mg/ml, working concentration 100 µg/ml) in culture tubes and incubated overnight (12-16 hours) at 37°C at 220rpm. For the control tubes, 3 ml of LB/ampicillin without bacteria and 3 ml of LB/ampicillin with uninfected bacteria were incubated.

The following day, the bacteria were transferred to microcentrifuge tubes (2 x 1.5 ml for each sample) and were centrifuged at 16000 g for 1 minute at room temperature. The Monarch® Plasmid DNA Miniprep Kit Protocol was used for the following steps. The supernatant was removed carefully using a pipette and the pellet was resuspended in 200 µl of pink resuspension buffer. The pellet was resuspended completely to achieve complete lysis of the bacteria in the next step. The tubes were vortexed for 10 seconds and were not incubated. A volume of 200 µl of blue Lysis Buffer was added immediately and mixed by inverting the tube gently 6 times, until the colour changed to dark pink. The tubes were incubated for no longer than 1 minute. A volume of 400 µl of yellow neutralization buffer stored at 4°C was added. The tubes were inverted until they were uniformly yellow, and a precipitate

formed. The tubes were incubated for 2 minutes. The samples were centrifuged for 5 minutes and New England Biolabs columns were prepared and labelled. To bind the DNA to column, the supernatant was carefully transferred to the columns and centrifuged for 1 minute. The flow through was discarded. The columns were reinserted to the collection tubes and 200 µl of Plasmid Wash buffer 1 was added. The tubes were centrifuged for 1 minute and the flow through was discarded again. A volume of 400 µl of Plasmid Wash Buffer 2 was added and the tubes were centrifuged for 1 minute. The flow through was discarded and another 400 µl of Plasmid Wash Buffer 2 were added. The tubes were centrifuged for 1 minute and the flow through was discarded. The columns were transferred to fresh tubes and a 1-minute dry spin was performed. The columns were transferred to a final labelled tube and 30 µl of Elution buffer were added in the centre of the matrix without puncturing it. The tubes were incubated for 1 full minute and spun for 1 minute. The flow through was collected and the eluate was stored at 4°C.

The NanoDrop™ 2000 Spectrophotometer [ThermoScientific, Massachusetts, United States, Catalogue# ND-2000] was used to quantify the DNA concentration of each monoclonal plasmid DNA extracted to ensure adequacy of the sample. The Nanodrop software was selected and the 'Nucleic Acid' application was chosen. The arm of the Nanodrop was lifted and after cleaning the pedestal, 2 µl of elution buffer was pipetted to act as a blank. The arm was closed, and the blank was measured. The procedure was repeated for plasmid DNA of each monoclone respectively.

Samples were then sent abroad to LGC Genomics in Berlin for sanger sequencing. The primer used for sequencing was M13-29R with a "CAGGAAACAGCTATGAC" sequence. Once the sequences were obtained, Snap Gene [GSL Biotech LLC, California, United States] was used to determine the protein sequences and compare clones together.

2.4 Data Analysis

2.4.1 GraphPad Prism analysis for monoclones

Fluorescence data obtained from ELISAs on the Tecan Spark® Multimode Microplate Reader was used to calculate the area under the curve for each biopanning round. A centralisation step of the data using

the trapezoidal rule was used to ensure that the data was normally distributed. The trapezoidal rule allowed for construction of a new data distribution based on normal distribution (Boonta, Boonthiem 2019). Welch's t-test was then used to compare the AUCs of the different rounds together. Estimation plots were used to compare certain AUCs together directly (Ho, Tumkaya, Aryal, Choi et al. 2019, Michel, Murphy, Motulsky 2020). These tests were performed using GraphPad Prism 10 software [GraphPad Software, San Diego, California, US] and the data was given as the mean ± the SEM. A p-value of less than 0.05 was considered statistically significant (Urban, Moosmeier et al. 2017). This was performed for all biopanning rounds and for the amplification of round 4 of TIM-3 as per Appendix Section B.

For the monoclonal ELISA data, the Shapiro-Wilk normality test was used since the sample size was smaller than 50 (Mishra, Pandey et al. 2019). The number of technical replicates used was 12. Data which was normally distributed was tested using the multiple unpaired t-test and data which was not normally distributed was tested using the Mann Whitney test. GraphPad Prism 10 was used for these tests and the data was given as the mean ± SEM. A p-value of less than 0.05 was considered statistically significant (Urban, Moosmeier et al. 2017). These tests were used to determine if there was a statistically significant difference between clones binding to target protein versus (vs) controls. Statistical analysis data was represented in the results section as per **Table 2.2**.

Table 2.2: Legend of symbols for statistical significance and their meaning. *Legend of symbols and the respective p-value meaning.*

Symbol	Meaning
****	$p \leq 0.0001$
***	$p \leq 0.001$
**	$p \leq 0.01$
*	$p \leq 0.05$
Not Significant (ns)	$p > 0.05$

2.4.2 BLAST search

Homology analysis was performed for proteins TIM-3 and TIM-4 to compare sequence similarity. High sequence similarity between TIM-3 and TIM-4 indicated that some clones could potentially bind to both proteins. This emphasised the importance of comparing the different clones obtained for TIM-3 with those obtained for TIM-4 (specifically the CDRs) using BLAST to check for the level of sequence similarity. BLAST analysis was also performed to compare TIM-3 monoclones with IgG monoclones and TIM-4 monoclones with NPC monoclones.

The National Library of Medicine [National Center for Biotechnology Information, Maryland, United States] was used to search for the gene that encoded for the target proteins. The FASTA amino acid sequences were obtained, downloaded and inserted into the BLAST (Basic Local Alignment Search) tool [National Center for Biotechnology Information, Maryland, United States]. In this case protein BLAST was used. For TIM-3, the HAVCR2 gene (HUMAN Homo sapiens Q8TDQ0) was used and for TIM-4, the TIMD4 gene (HUMAN Homo sapiens Q96H15) was used. For the monoclones, the amino acid sequence obtained from sanger sequencing was inserted into BLAST to compare them to each other.

The expect value (E-value) gave an indication of the statistical significance of a given pairwise alignment and reflected the size of the database and the scoring system used. The lower the E-value, the more significant the hit (The BLAST Sequence Analysis Tool, The NCBI Handbook). If $E > 10$,

the sequences under consideration were either unrelated or related by extremely distant relationships that fall below the limit of detection with the current method. Because the E-value was proportionally affected by the database size, an obvious problem was that as the database grew, the E-value for a given sequence match also increased (Alcock, Huynh et al. 2023).

The bit score gave an indication of the quality of the alignment. Bit scores were normalized based on the raw pairwise alignment score, which meant that the bit scores from different alignments could be compared, even if different scoring matrices were used. Sequence similarity was measured independent of query sequence length and database size (Alcock, Huynh et al. 2023, The BLAST Sequence Analysis Tool, The NCBI Handbook). Bit scores of more than 50 were considered significant. For a bit score of 40 or less, homology was only considered significant if an E-value of less than 0.001 was obtained for searches of protein databases with less than 7000 entries (Pearson 2013).

Chapter 3: Results

3.1 Homology analysis between TIM-3 and TIM-4

Computational homology analysis was used to determine the structural similarity of the extracellular domains (ECD) of proteins TIM-3 and TIM-4 by comparing protein to protein sequences using blastp - a reliable and widely used algorithm program. Only the ECDs of the proteins were compared as the target proteins used in biopanning consisted of only the ECDs. The TIM-3 ECD used was Fc tagged and the TIM-4 ECD used was His-tagged. Accurate statistical estimates were produced by the program to ensure that protein sequences which were highly similar were also structurally similar (Altschul, Madden et al. 1997, Pearson, 2013). The analysis aimed to determine whether anti-TIM-3-Fc ECD scFv antibodies could bind to TIM-4 ECD and *vice versa*, based on the similarity of the structures of TIM-3-Fc ECD and TIM-4 ECD. This is crucial for understanding the cross-reactivity potential of the antibodies, which could have implications for therapeutic and research purposes.

SWISS-MODEL [BIOZENTRUM, The Centre for Molecular Life Sciences, University of Basel, Basel, Switzerland] which is a structural bioinformatics web-server dedicated to homology modelling of 3D protein structures was used to produce 3D structures of TIM-3 and TIM-4 as in **Figure 3.1**. It was also used to produce the ECD structures of both proteins to visualise the differences in structure. Refer to Appendix Section D.2 for the Ramachandran plots of these structures, which were used to identify the permissible backbone conformations of the proteins and to assess the quality of the structures. These plots were essential for understanding the energetically favorable and unfavorable regions of protein folding, thus playing a fundamental role in the analysis of protein structure and function (Hollingsworth, Karplus 2010).

A) **TIM-3** **vs** **TIM-3 ECD**

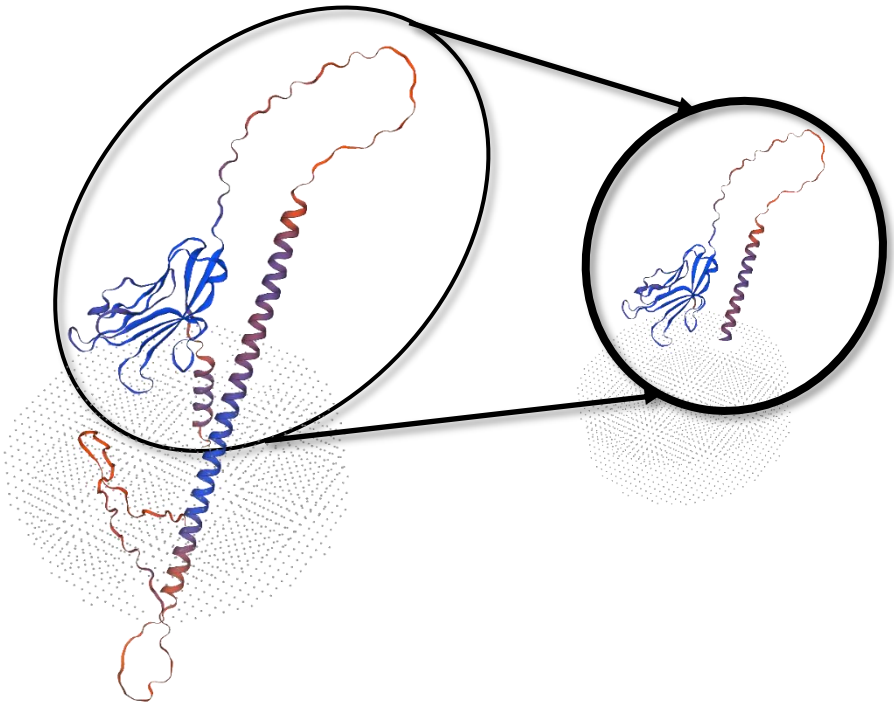

B) **TIM-4** **vs** **TIM-4 ECD**

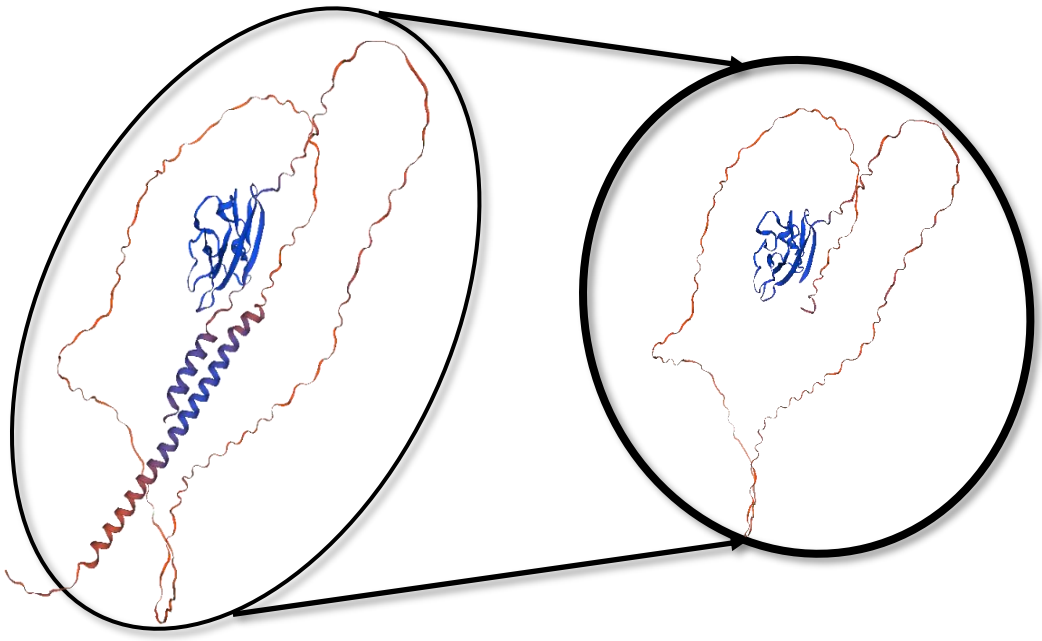

Figure 3.1: Structures of TIM-3 and TIM-4. *A) Structure of TIM-3 versus the ECD of TIM-3 and B) structure of TIM-4 versus the ECD of TIM-4.*

The blastp analysis was carried out using TIM-3 ECD as the subject sequence and TIM-4 ECD as the query sequence. The extracellular domain of TIM-4 consisted of 290 amino acids and that of TIM-3 consisted of 181 amino acids. A pairwise sequence alignment was performed. A higher bit score indicated better alignment and bit scores of more than 50 were considered significant (Pearson, 2013). The bit score obtained was of 93.6. Sequentially, a lower E-value implied more significant hits. E-values of less than 0.001 were considered significant. With an E-value of $4x10^{-28}$, the hits were statistically significant meaning that there was a very high chance that the result was due to a homologous relationship (Pearson, 2013). Analysis of the results as per **Figure 3.2** indicated that TIM-3 and TIM-4 proteins have highly similar ECD structures. Therefore, any antibodies produced through biopanning against TIM-3 could potentially bind to TIM-4 and *vice versa*.

TIM-3 ECD subject sequence vs TIM-4 ECD query sequence

Score	Expect	Method	Identities	Positives	Gaps
93.6 bits(231)	4e-28	Compositional matrix adjust.	59/159(37%)	83/159(52%)	9/159(5%)

```
Query  8    LGHRVTLPCLYSSWS-HNSNSMCWGKDQCPYSGCKEALIRTDGMRVTSRKSAKYRLQGTI  66
            +G    LPC Y+  +  N   +CWGK  CP   C   ++RTD  R  +  +++Y L G
Sbjct  9    VGQNAYLPCFYTPAAPGNLVPVCWGKGACPVFECGNVVLRTD-ERDVNYWTSRYWLNGDF  67

Query  67   PRGDVSLTILNPSESDSGVYCCRIEVPGWFNDVKINVRLNLQRASTTTHRTATTTTRRTT  126
             +GDVSLTI N + +DSG+YCCRI++PG  ND K N++L ++ A  T    A T  R  T
Sbjct  68   RKGDVSLTIENVTLADSGIYCCRIQIPGIMNDEKFNLKLVIKPAKVT---PAPTRQRDFT  124

Query  127  TTSPTTTRQMTTTPAALPTTVVTTPDLTTGTPLQMTTIA  165
              P    +M TT    P    T   L      Q++T+A
Sbjct  125  AAFP----RMLTTRGHGPAETQTLGSLPDINLTQISTLA  159
```

Figure 3.2: Alignment from the homology analysis of extracellular domains of TIM-3 and TIM-4. *Pairwise sequence alignment of the ECD of TIM-3 as the subject sequence and extracellular domain of TIM-4 as the query sequence. Analysis resulted in high bit score and low E-value indicating homology.*

3.2 Biopanning

3.2.1 TIM-4 failed biopanning rounds

Five rounds of biopanning were used to identify polyclonal populations of scFv anti-TIM-4 antibodies. ELISA was then used to ensure that the phage library grew more specific to the target protein throughout the rounds. The ELISA was constructed as follows:

- The enriched anti-TIM-4 scFv antibody displaying phage library from rounds 3-5 of biopanning was serially diluted and bound to the target protein in separate wells to compare the affinity of the phages towards the target TIM-4 throughout the panning rounds.
- The enriched no protein control (NPC) phage library from rounds 3-5 of biopanning which was biopanned against the His-tag beads in the absence of the target protein TIM-4 was also serially diluted and bound to the target protein in separate wells to compare the affinity of the phages towards the target TIM-4 throughout the panning rounds. This served as a negative control for biopanning as it was expected to have lower fluorescent values throughout the rounds when compared to the enriched anti-TIM-4 scFv antibody displaying phage library. Additionally, round 5 of NPC was expected to have the same or similar fluorescence to round 3 and round 4 of NPC since it was expected that there was no isolation of high affinity antibodies to TIM-4 throughout the rounds.
- A no library control which consisted of ELISA wells coated with target protein but no phage library which served as a blank for the ELISA.
- The enriched round 4 phages against TIM-3 protein from Grima (2022), which were successfully isolated through biopanning, against TIM-3 target on ELISA served as a positive control for the ELISA.

ELISA measured the fluorescence of anti-M13-PE detection antibody which bound to the phages in the ELISA wells and the measurements obtained were used to plot graphs of phage dilutions against anti-M13-PE antibody (arbitrary unit).

As can be observed from **Figure 3.3 A**, round 3 had the lowest values of fluorescence as expected. Very few phages in this round displayed antibodies specific to the target protein TIM-4. By round 4 and 5, the number of phages that were highly specific to TIM-4 remained low in comparison to the positive control. As anticipated, the no protein control (**Figure 3.3 B**) remained at low fluorescence throughout the rounds indicating that no scFv antibody-displaying phages were isolated. This outcome was expected since the beads were not coated with target protein for the NPC. Furthermore, the no library had the lowest fluorescence as was expected.

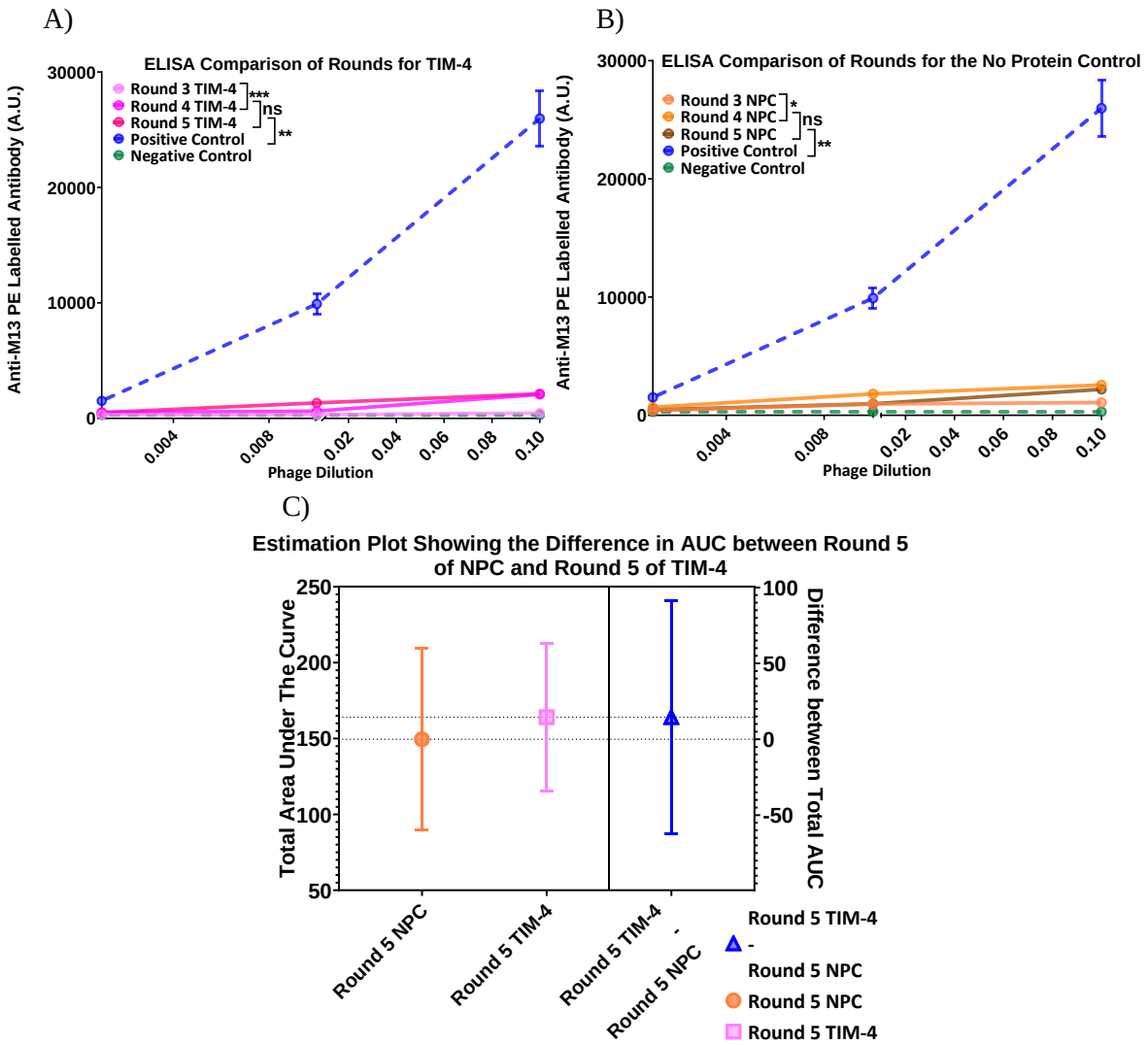

Figure 3.3: Graphs of failed TIM-4 biopanning and no protein control. *Graphs of phage dilutions for rounds 3-5 against anti-M13-PE antibody (a.u.) of A) TIM-4 and B) the no protein control. Each dilution was analyzed with 24 technical replicates and the error bars show the 95% confidence interval (CI). Round 5 of TIM-4 in comparison to the positive control shows a statistically significant difference confirming that biopanning was not successful and any binding was likely due to non-specific binding to the beads rather than to the target. This non-specific binding was confirmed by the NPC since the fluorescence of the detection antibody for rounds 3-5 were like those of TIM-4. C) The estimation plot compared the difference in the AUC of round 5 of the no protein control and round 5 of TIM-4 and confirmed further that biopanning was unsuccessful because there was no statistically significant difference between the AUCs of round 5 of the NPC versus round 5 of TIM-4.*

Statistical analysis was carried out to confirm these findings. The AUC was calculated for each round of TIM-4 and of the NPC to compare the rounds together. The difference between AUCs of round 3 and 4 for TIM-4 were statistically significant whereas the AUC of round 4 in comparison to that of round 5, was not statistically significant. Additionally, the AUC of round 5 of biopanning in comparison

to the positive control was statistically significant. This indicated that identification of monoclonal antibodies displayed on phages against TIM-4 was not successful by round 5 of biopanning.

Similarly, the difference between AUCs of round 3 and 4 of the NPC were statistically significant. However, when the AUC of round 4 was compared with that of round 5, there was not a significant difference. Furthermore, the AUC of round 5 in comparison to the positive control was also statistically significant.

This data indicated that there likely was non-specific binding during the biopanning rounds and no scFv antibodies highly specific to TIM-4 were identified.

Furthermore, statistical analysis was carried out to determine if there was a statistically significant difference between round 5 of TIM-4 and round 5 of the NPC. This was done because if a statistically significant difference was found, it would have indicated that biopanning may have been successful. The AUC values were used to make estimation plots to compare the two rounds as in **Figure 3.3 C**. There was no statistical significance between the AUCs of round 5 of TIM-4 and round 5 of the NPC confirming further that biopanning was unsuccessful.

It was concluded that the most probable reason for biopanning being unsuccessful was due to incorrect storage of the library at -20°C instead of -80°C. Furthermore, multiple freeze-thaw cycles over the course of a year may have led to proteolytic cleavage of scFvs from the surface of the phage particles (Andre, Moutinho et al. 2022, Baek, Suk 2002).

3.2.2 TIM-4 successful biopanning rounds

Following the outcome of the previous biopanning attempt, our collaborators at the University of Gdansk reconstituted the naïve canine scFv antibody phage library and sent us fresh aliquots. The aliquots were stored properly at -80°C. Biopanning was repeated to identify polyclonal populations of scFv anti-TIM-4 antibodies using this new original phage library and using SARS-CoV-2 trimer as a second positive control since it was previously successfully biopanned in our lab. Additionally, during the centrifugation steps a swingout bucket was used instead of a fixed bucket as it allowed for a more visible phage pellet to form which suggested better recovery of phage. If biopanning against trimer protein and other proteins failed, it would have indicated some other error in the procedure. If trimer biopanning had proved successful, while efforts against TIM-4 had remained unsuccessful, it would have indicated that phage display biopanning might not have been a viable method for identifying antibodies against TIM-4. The underlying reasons for this outcome would have required further investigation.

After 4 rounds of biopanning, ELISA was used to establish phage affinity throughout the rounds and was constructed as follows:

- Rounds 2, 3 and 4 of TIM-4
- Rounds 2, 3 and 4 of TIM-3 from Grima (2022) as positive control for ELISA
- Rounds 2, 3 and 4 of SARS-CoV-2 trimer as a positive control for biopanning
- Rounds 2, 3, and 4 of the NPC as a negative control for biopanning to facilitate the elimination of background fluorescence caused by non-specific binders
- No library control as a blank for the ELISA consisting of ELISA wells coated with target protein but no phage library.

The enriched libraries of each round were serially diluted and bound to the respective target protein and anti-M13-PE antibody was used as the detection antibody. The data obtained was used to plot graphs of phage dilutions against anti-M13-PE antibody (arbitrary unit) measured as fluorescence.

Figure 3.4 A shows the successful biopanning of TIM-4 protein. As expected, round 2 had the lowest values of fluorescence as few phages in this round displayed antibodies specific to the target protein TIM-4. By round 3, the number of phages specific to TIM-4 increased slightly and by round 4 there was a notable increase in fluorescence. This expected result was confirmed by the positive control as in **Figure 3.4 C** and the NPC as per **Figure 3.4 D**.

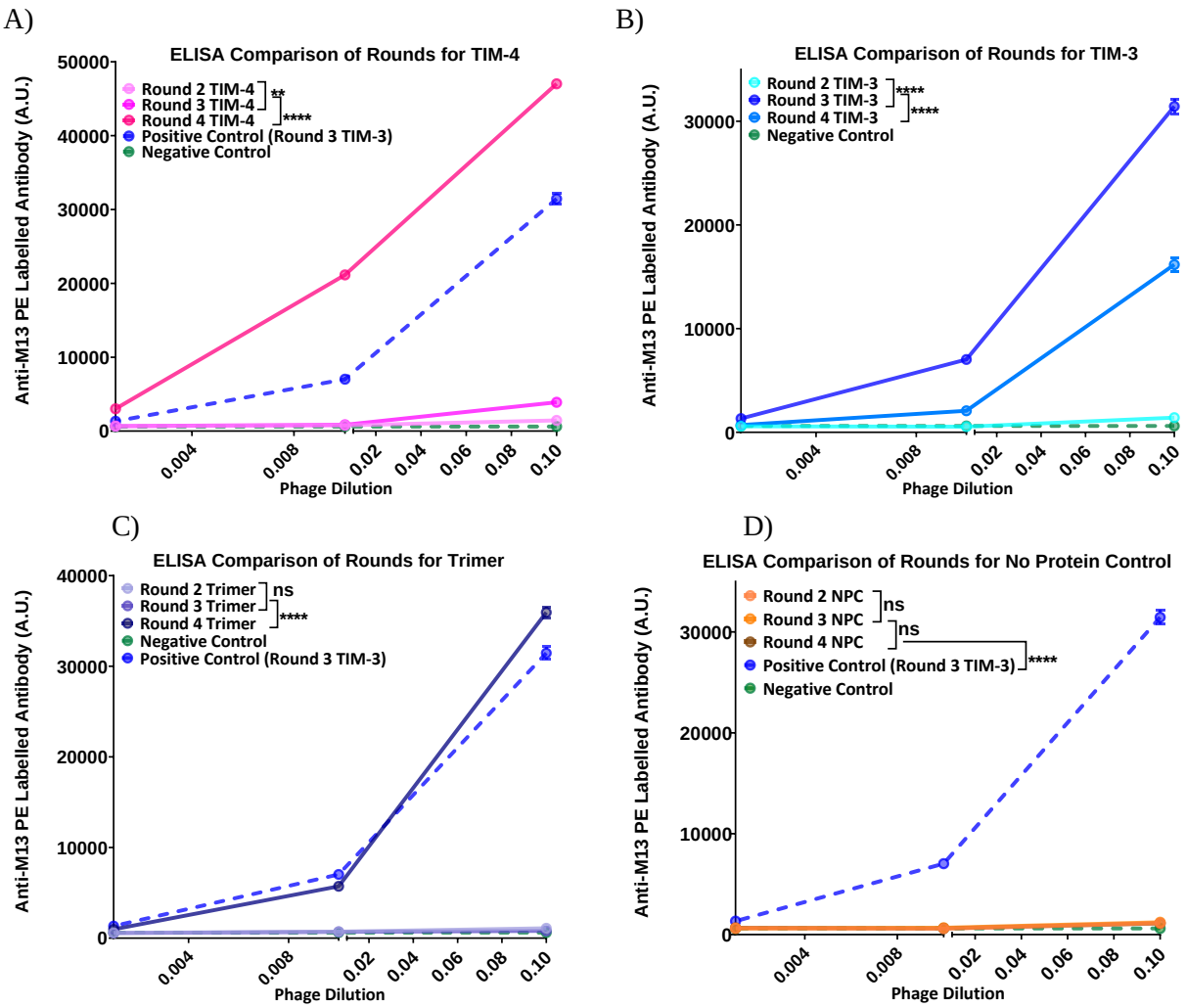

Figure 3.4: Graphs of phage dilutions for rounds 2-4 of biopanning of TIM-4, TIM-3, trimer and no protein control phages against anti-M13-PE antibody (a.u.). *Graphs of phage dilutions for rounds 2-4 against anti-M13-PE antibody (a.u.) of A) TIM-4, B) TIM-3, C) trimer and D) no protein control. Each dilution was analyzed with 24 technical replicates. The error bars show the 95% CI. Biopanning was successful for both TIM-4 and Trimer as round 2 gave the lowest fluorescence whilst round 4 gave the highest fluorescence. Despite round 4 of TIM-3 showing a lower fluorescence than round 3, the biopanning was successful in Grima (2022). The low fluorescence for round 2-4 of the NPC indicated non-specific binding to the His-tag beads, while the no library control showed the fluorescence measured in the absence of phages bound to the ELISA wells.*

When comparing the AUC of round 2 of TIM-4 with round 3 of TIM-4, a statistically significant difference in AUC was observed. Comparison of rounds 3 and 4 of TIM-4 also showed a statistically significant difference between AUCs. This statistical analysis confirmed that the biopanning was successful against the protein TIM-4 and a polyclonal pool of scFv antibodies with high affinity towards this protein was obtained.

TIM-3 biopanning was successful in Grima (2022) and was reanalysed in this study using ELISA. The statistical significance between round 2 and 3 remained as in the previous study. However, as per **Figure 3.4 B**, round 3 had a higher fluorescent value than round 4 of TIM-3 (refer to Appendix Section B for the amplification of round 4 of TIM-3 that was performed) and when comparing the AUC of round 3 to that of round 4, a statistical significance was obtained which was unlike the previous result in Grima (2022). Previously, round 4 of TIM-3 had a higher fluorescence than round 3 and there was no statistically significant difference between the AUCs. Since round 3 had the highest fluorescence, in **Figures 3.4 A, C and D**, round 3 of TIM-3 was used as the positive control. The enriched polyclonal pool of anti-TIM-3-Fc round 4 phages were used as a positive control for multiple experiments up to this point indicating that due to the multiple freeze-thaw cycles there may have been proteolytic cleavage of scFvs from the surface of the phages, hence the lower fluorescence compared to round 3 of TIM-3 (Andre, Moutinho et al. 2022, Baek, Suk 2002).

The biopanning rounds of SARS-CoV-2 trimer in **Figure 3.4 C** showed an increase in phages successfully binding to the target through the rounds as was expected. Rounds 2 and 3 had very low fluorescence whilst round 4 showed a remarkable increase in fluorescence. The difference between AUCs of round 2 and 3 for SARS-CoV-2 trimer were not statistically significant. However, when the AUC of round 3 was compared with that of round 4, there was a statistically significant difference. This indicated that development of scFv antibodies displayed on phages against trimer was successful and high affinity to the target protein was achieved by round 4 of biopanning.

The statistical analysis of the NPC strengthened the above results because between round 2 and 3 and between round 3 and 4 no statistically significant difference was obtained when comparing AUCs.

These results indicate that there was no significant difference in the binding of phages to the His-tag beads between the specified rounds and there was no isolation of scFv antibody-displaying phages against target protein TIM-4. Additionally, the no library control had the lowest fluorescence as per **Figure 3.4 A, B, C** and **D** as was expected.

Further statistical analysis was carried out to determine if there was a statistically significant difference between round 4 of TIM-4 and round 4 of the NPC to verify that biopanning was successful. This was confirmed using an estimation plot (refer to **Figure 3.5**).

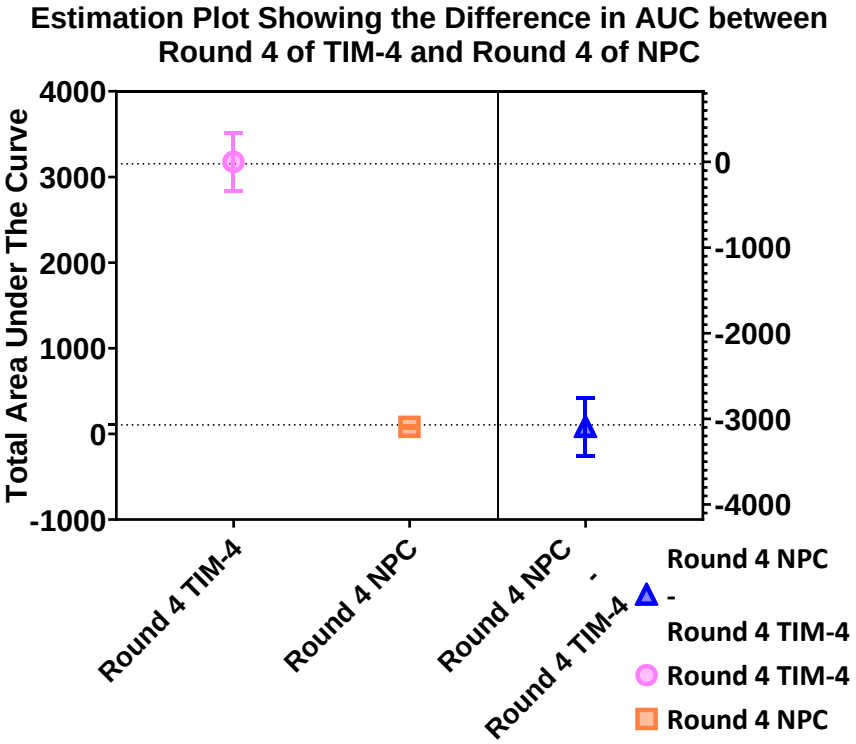

Figure 3.5: Estimation plot for comparison of round 4 of TIM-4 and round 4 of NPC. *The estimation plot compared the difference in the AUC of round 4 of TIM-4 with round 4 of the NPC. The error bars show the 95% CI. A statistical significance was observed between the AUCs of round 4 of TIM-4 and round 4 of NPC confirming that biopanning was successful.*

3.3 Analysis of Monoclones

3.3.1 Anti-TIM-3-Fc and anti-IgG-Fc phage clones

Phage titering was performed to determine whether the phage count was maintained after each round of biopanning for each target protein and control. This ensured that the amplification steps worked well. As per Appendix Section A, phage titre was maintained at around 10^{12} throughout.

To identify single positive clones from the enriched library after biopanning, 30 well-isolated, single colonies from the LB/Ampicillin agar plate of the round 4 titration were picked, labelled, amplified and purified.

ELISA was then performed as follows:

- Each individual monoclone was tested by coating separate ELISA wells with the target proteins TIM-3-Fc and IgG-Fc respectively and adding each monoclone to its own well.
- For the positive control, an ELISA well was coated with target protein and the enriched round 4 polyclonal pool was added.
- A no library negative control was used to determine background signal. This consisted of target coated ELISA wells without the addition of phages.

The fluorescence of anti-M13-PE antibody was measured for the 30 phages displaying anti-TIM-3-Fc and anti-IgG-Fc scFv antibody-displaying monoclones, the polyclonal anti-TIM-3-Fc and anti-IgG-Fc phage library pool and a negative control. Anti-TIM-3-Fc and anti-IgG-Fc scFv antibody-displaying monoclone phages after round 4 of biopanning were compared with the polyclonal pool and the no library negative control. The negative control with no phages was expected to give the lowest fluorescence and the polyclonal pool was expected to give the highest fluorescence. The variation in the measured fluorescence of anti-M13-PE detection antibody between monoclones was used to assess and compare binding affinity.

As can be seen from **Figure 3.6 A**, clones 8, 22 and 25 of TIM-3 had a lower fluorescence than the no library control. The polyclonal pool had the highest fluorescence and the clones with strongest binding

to target protein TIM-3 were clones 2, 11 and 23. **Figure 3.6 B** showed that all anti-IgG-Fc clones bound to the target protein IgG-Fc and the no library control had the lowest fluorescence. Unexpectedly, the polyclonal pool of anti-IgG-Fc scFv antibody-displaying phages did not have the highest fluorescence.

A)

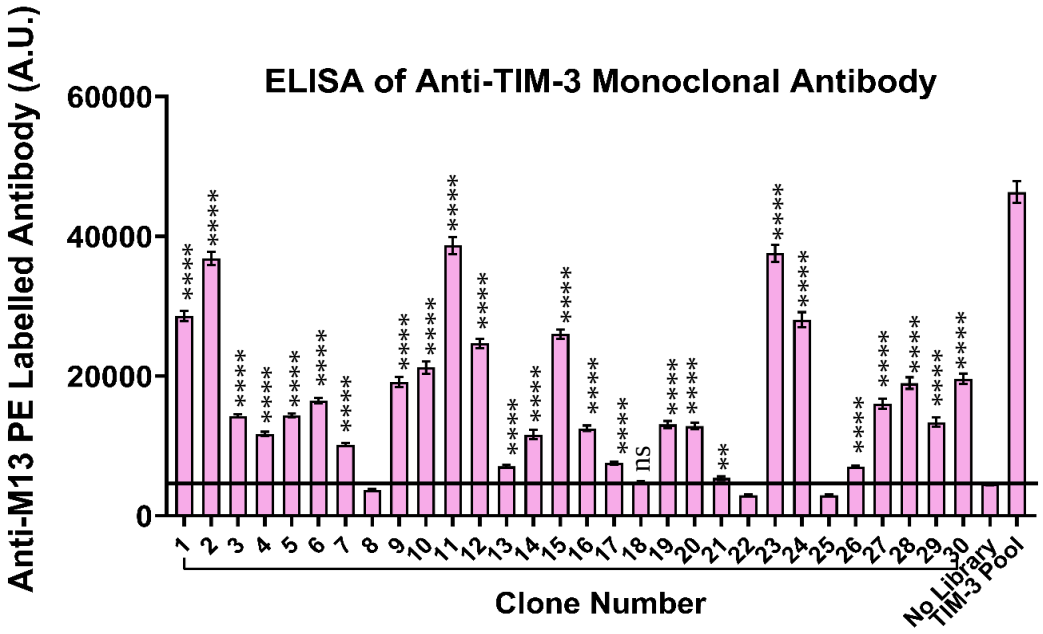

B)

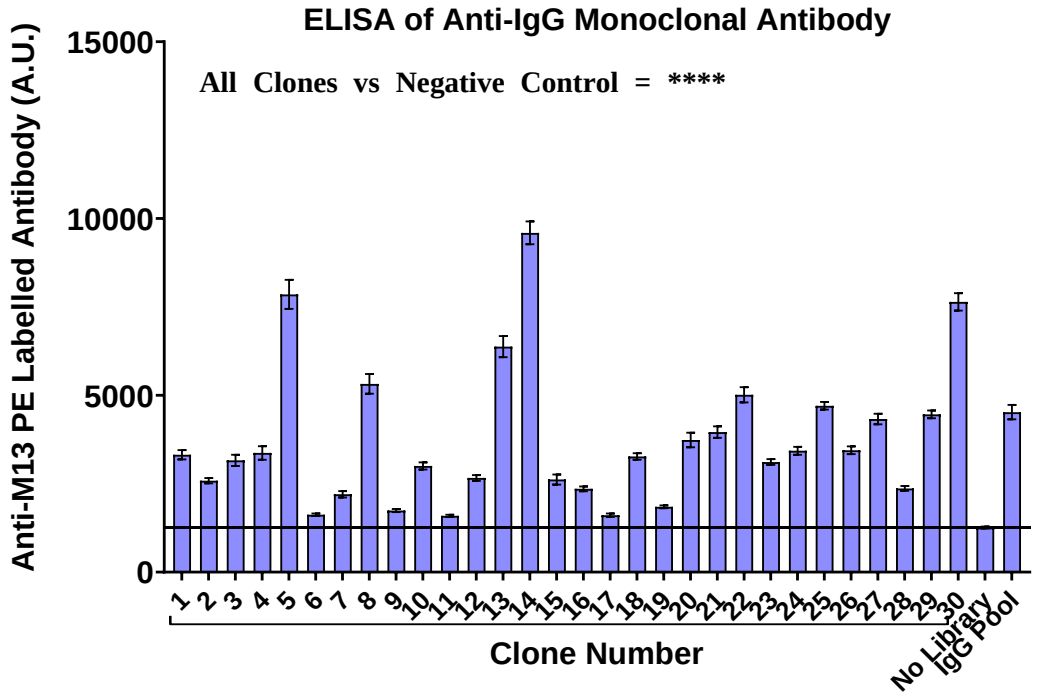

Figure 3.6: Graph of anti-TIM-3-Fc and anti-IgG-Fc scFv antibody-displaying monoclones vs anti-M13-PE antibody (a.u.). *Graphs of A) anti-TIM-3-Fc monoclones and B) anti-IgG-Fc monoclones vs anti-M13-PE antibody fluorescence. Each clone was analyzed with 12 technical replicates. The binding to target proteins TIM-3-Fc and IgG-Fc respectively was determined by comparing the fluorescence of the negative control as demonstrated by the black line with the fluorescence of the monoclones. For A) all clones except 8, 18, 22 and 25 showed significant binding to TIM-3. For B) all clones showed binding to the target protein IgG.*

Statistical analysis was carried out to compare each clone to the no library negative control to confirm positive binding to the respective target protein. All anti-TIM-3-Fc clones except clone 18 were found

to have a statistically significant difference in fluorescence when compared to the no library control. Since clones 8, 22 and 25 of TIM-3 had a lower fluorescence than the no library control, the statistically significant difference in fluorescence emphasised that there was no binding to the target protein for these clones. For the anti-IgG-Fc scFv antibody-displaying monoclones, all clones had a difference in fluorescence to the negative control which was statistically significant, indicating that all clones were binding to the target protein.

3.3.2 TIM-3-Fc versus SARS-CoV-2 Spike S1 bait ELISA

ELISA was performed again on the anti-TIM-3-Fc scFv antibody-displaying monoclones to compare the binding of the clones to the target protein TIM-3 versus non-target SARS-CoV-2 Spike S1 protein as a negative control. The control protein SARS-CoV-2 Spike S1 with the same fusion-tag of the target (His-tag in this case) was used to eliminate clones that did not specifically bind with the target protein TIM-3-Fc. Anti-TIM-3-Fc scFv antibody-displaying monoclones which showed equal binding to TIM-3-Fc and SARS-CoV-2 Spike S1 were not specific enough to the target protein and therefore would not be used in the future to develop anti-TIM-3-Fc monoclonal antibodies.

The ELISA wells were set up as follows:

- TIM-3-Fc target protein was added to separate wells and the 30 monoclones were added individually to each well.
- SARS-CoV-2 Spike S1 non-target protein was added to separate wells and the 30 monoclones were added individually to each well. This served as a negative control.
- A no library negative control consisted of TIM-3 bound to wells and no phage library as a blank.
- The polyclonal pool of anti-TIM-3-Fc scFv antibody displaying phages bound to TIM-3 as the positive control.

Yet another negative control using SARS-CoV-2 Spike S1 as bait protein for the polyclonal pool of anti-TIM-3-Fc should have been performed, however, this was determined whilst analysing the results. Therefore, this control was then included for **Section 3.3.3**.

Fluorescence of anti-M13-PE antibody was measured for each clone and control. The data obtained for the monoclones was compared with that obtained for the polyclonal pool of anti-TIM-3-Fc scFv antibodies and with the no library negative control. As expected, the no library negative control gave the lowest fluorescence and the polyclonal pool gave the highest fluorescence. **Figure 3.7** showed that

clones 4-7, 11-16, 20, 21, 23, 24 and 26-30 had the highest binding affinities. Clone 22 was also a binder but with less statistical significance. The strongest target binder was clone 23.

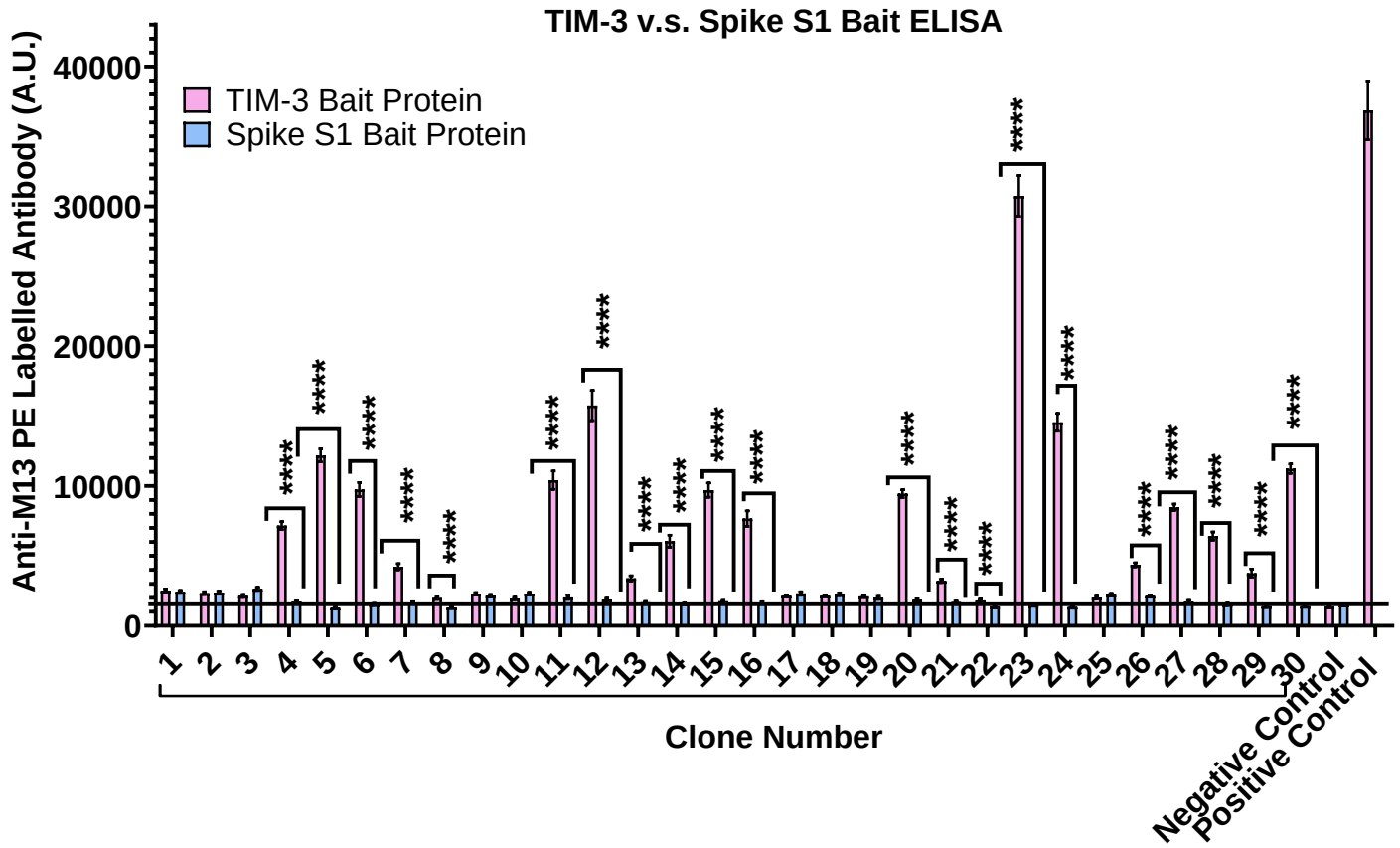

Figure 3.7: Graph of anti-TIM-3-Fc scFv antibody-displaying monoclones bound to TIM-3-Fc and SARS-CoV-2 Spike S1 baits respectively vs anti-M13-PE antibody (a.u.). *Graph of anti-TIM-3-Fc monoclones bound to TIM-3-Fc and SARS-CoV-2 Spike S1 bait proteins vs anti-M13-PE mAb used to determine the specificity of TIM-3 scFv antibodies to target protein TIM-3. Each clone was analyzed with 12 technical replicates. The binding of the clones towards target protein was confirmed by comparing the fluorescence of the negative control as demonstrated by the black line with the fluorescence of the clones. All anti-TIM-3-Fc scFv antibody displaying phage clones had significantly different fluorescence to the negative control suggesting that all clones bound to the target protein. Furthermore, the specificity of the monoclones was confirmed by comparing the fluorescence of the clones towards target protein TIM-3-Fc vs non-target protein SARS-CoV-2 Spike S1. It was concluded that the most specific binders were clones 4-8, 11-16, 20-24 and 26-30.*

Statistical tests were performed to compare fluorescence of anti-M13-PE antibody for anti-TIM-3-Fc scFv antibody-displaying clones with anti-SARS-CoV-2 Spike S1 scFv antibody-displaying clones and for anti-TIM-3-Fc scFv antibody-displaying monoclones versus the no library control. Comparison of anti-TIM-3-Fc clones versus anti-SARS-CoV-2 Spike S1 clones binding to TIM-3-Fc protein revealed that there was a statistically significant difference in fluorescence for clones 3-8, 11-16 and 20-30. Unexpectedly, clones 3, 10, 17, 18 and 25 were binding to target protein less than to non-target protein. Further comparison of anti-TIM-3-Fc clones to the negative no library control revealed that all clones had significantly different fluorescence to the negative control. This data was used to confirm which clones had binding affinities to the target protein without also binding to SARS-CoV-2 Spike S1 and it was concluded that the clones with binding affinity specific to TIM-3 were 4-8, 11-16, 20-24 and 26-30.

3.3.3 TIM-4 versus SARS-CoV-2 RBD bait ELISA

After successfully biopanning against TIM-4 protein, each individual anti-TIM-4 scFv antibody-displaying monoclone was tested for binding to its target (TIM-4) versus to a non-target protein (SARS-CoV-2 RBD) using ELISA. The ELISA was set up in the following way:

- The wells were coated with TIM-4 and each monoclone was added to a separate well to compare binding affinity between clones.
- Separate wells were coated with SARS-CoV-2 RBD and the individual anti-TIM-4 scFv antibody-displaying monoclones were added. This was performed to compare binding of monoclones to a non-target protein.
- One of the positive controls consisted of the polyclonal anti-TIM-4 scFv antibody-displaying phage pool binding to TIM-4 protein and another consisted of the polyclonal anti-TIM-3-Fc scFv antibody-displaying phage pool binding to TIM-3-Fc protein.
- A no library blank was used consisting of TIM-4 coated wells without addition of phages.
- A negative control was used which consisted of the anti-TIM-4 scFv antibody-displaying phage pool but SARS-CoV-2 RBD as bait protein. This negative control with SARS-CoV-2 RBD bait protein was used to confirm that the polyclonal pool of antibodies was not binding to other proteins as well. This control was not included in **Section 3.3.2**.

The fluorescence of anti-M13-PE antibody was measured for 30 phage anti-TIM-4 scFv antibody-displaying monoclones and the controls. The positive controls were expected to show the highest fluorescence whilst the negative controls were expected to show the lowest fluorescence.

Figure 3.8 showed that the anti-TIM-4 scFv antibody-displaying monoclones had very high fluorescence whilst the negative controls had very low fluorescence. Statistical tests were used to determine if there was a statistically significant difference between the fluorescence of TIM-4 monoclones and the negative controls. Each clone was compared to the no library control to determine binding to target protein TIM-4. Clones 2, 7-9, 12, 19, 21 and 27 were binding to TIM-4. These clones were found to exhibit high specificity to TIM-4, as evidenced by a significant difference in fluorescence

when comparing binding to the target protein TIM-4 versus the non-target protein SARS-CoV-2 RBD. Clone 20 showed a significantly lower binding to target protein than to non-target protein, however, the other results were as expected.

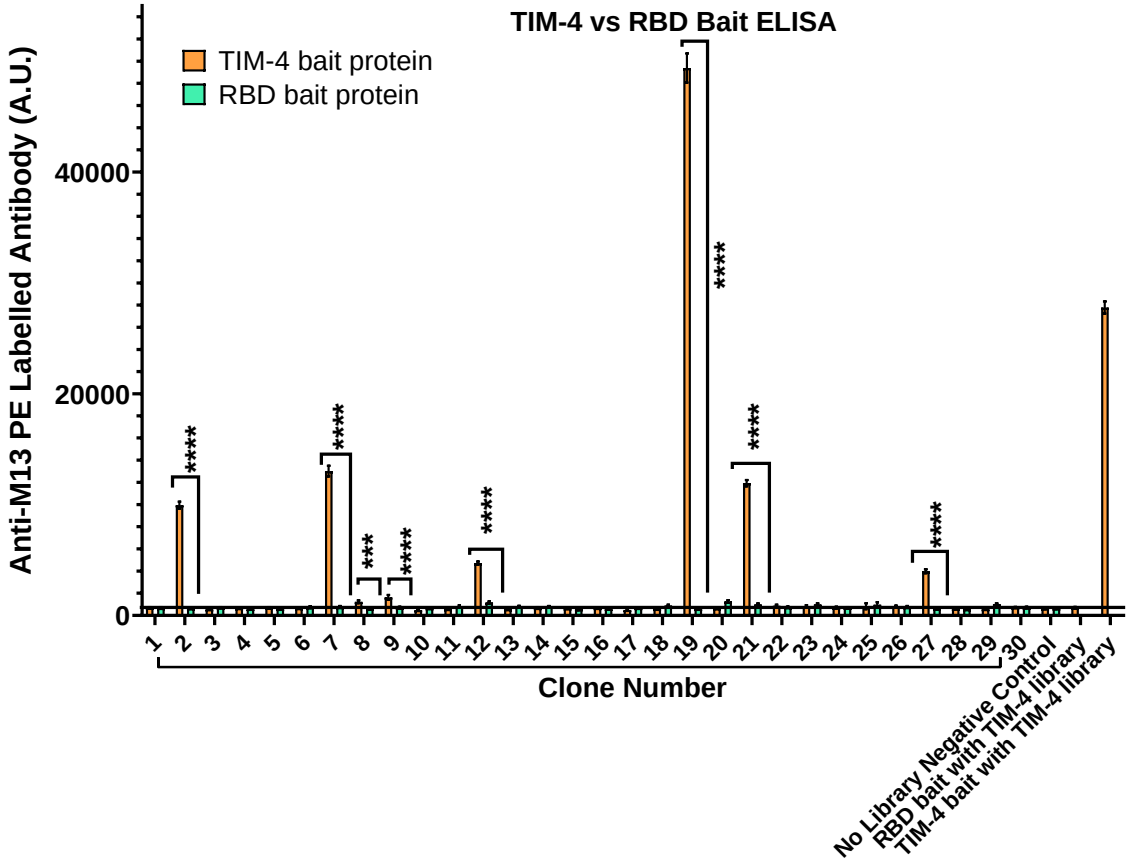

Figure 3.8: Graph of anti-TIM-4 scFv antibody-displaying monoclones vs anti-M13-PE antibody. *Graph of TIM-4 monoclones bound to TIM-4 bait protein vs SARS-CoV-2 RBD bait protein vs anti-M13-PE antibody. Each clone was analyzed with 12 technical replicates. The binding to target protein TIM-4 was determined by comparing the fluorescence of the negative control as demonstrated by the black line with the fluorescence of the clones. Clones 2, 7-9, 12, 19, 21 and 27 had significantly different fluorescence to the negative control indicating that these clones were binding to the target protein. The specificity of the monoclones was confirmed by comparing the fluorescence of the clones to the target protein TIM-4 vs non-target protein SARS-CoV-2 RBD. Once again, clones 2, 7-9, 12, 19, 21 and 27 had affinity to the target protein but not to the non-target protein. The no library control and the anti-TIM-4 scFv antibody-displaying polyclonal pool with SARS-CoV-2 RBD bait showed no binding whereas both anti-TIM-3-Fc and anti-TIM-4 scFv antibody-displaying polyclonal pools showed strong binding to their respective targets.*

3.4 Sanger sequencing

3.4.1 TIM-3

After performing the method in **Section 2.3** and confirming sample adequacy using the Nanodrop (refer to Appendix Section C), the samples were sent to LGC Genomics GmbH in Berlin for sanger sequencing. The sequencing data obtained was used to determine the amino acid sequence of the scFv displayed by each clone against target protein TIM-3-Fc. This was done using SnapGene [SnapGene By Dotmatics, GSL Biotech LLC, Boston, Massachusetts, US]. In total 30 clones were sent for sequencing, of which 12 were fully sequenced. Sequencing data was poor for some clones because a reverse primer was used, and sequencing tended to be less efficient at the beginning of an amino acid sequence read. The results obtained showed that several clones appeared to be identical. As can be seen in **Figure 3.9**, anti-TIM-3-Fc clones 1, 3, 4, 5, 9, 15, 16, 17, 20, 23, 24, 27 and 30 were identical. Clones 7, 8, 10, 13, 14, 21, 22, 25 and 29 were also identical. Additionally, clone 18 was identical to clone 26. Meanwhile, clones 2, 6, 11, 12, 19 and 28 were unique. Clone 2 showed a stop codon in the CDR1 of the VL chain and clones 18, 26 and 28 showed stop codons in CDR3-VL. This revealed that out of the 30 clones there were 9 differing amino acid sequences.

Figure 3.9: Alignments of anti-TIM-3-Fc scFv antibody-displaying monoclones grouped by sequence similarity. *The alignments of anti-TIM-3-Fc scFv antibody-displaying monoclones were categorized based on sequence similarity. A consensus approach utilizing a threshold exceeding 50% was employed to compare the sequence alignment. The designations 'CDR' and 'FR' in relation to clone 1 indicate the specific segments of the sequence corresponding to the Complementarity Determining Regions (CDR) and Framework Regions (FR). Stop codons in clones 2, 18, 26, and 28 were denoted by '*', while '-' signifies placeholders in cases where sequences for a region were shorter or not fully sequenced via Sanger sequencing. A total of nine distinct amino acid sequences were identified.*

SWISS-MODEL was used to produce a 3D structure of the scFv displayed by anti-TIM-3-Fc phage clone 11 as can be seen in **Figure 3.10** using the amino acid sequence from sanger sequencing. This was done to visualise the structure (refer to Appendix Section D.2 for the Ramachandran plot).

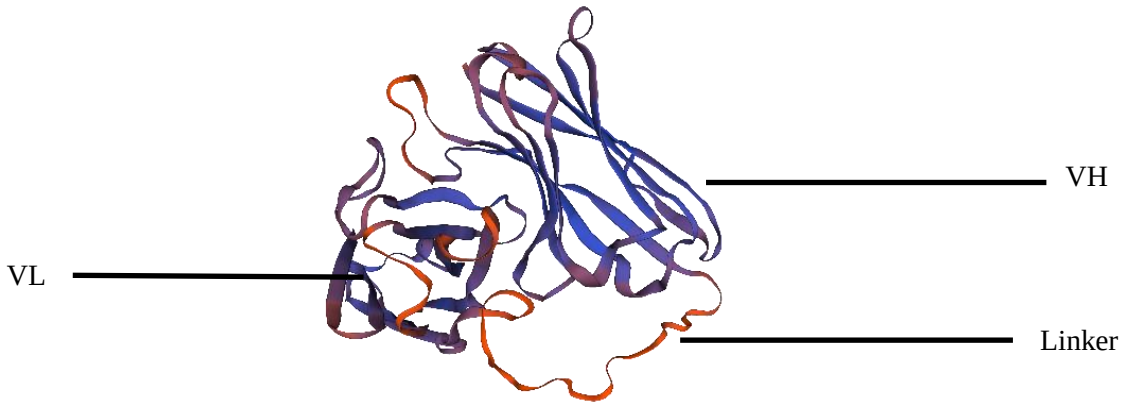

Figure 3.10: Structure of scFv displayed by anti-TIM-3-Fc scFv antibody-displaying phage clone 11. *The VH and VL domains are connected by a short flexible linker.*

3.4.2 IgG

The IgG monoclones were sequenced to determine if the scFv antibodies identified for IgG-Fc were similar in sequence to those identified for TIM-3-Fc. This was because both IgG and TIM-3 proteins used during biopanning had an Fc region (Recombinant Human TIM-3 Fc Chimera and Recombinant Human IgG_1 Fc R&D Systems package inserts). A total of 30 clones were sent for sequencing and 3 clones were fully sequenced. Anti-IgG-Fc clone 28 was also sequenced but had numerous stop codons throughout the amino acid sequence (as in Appendix Section D.1). From the sequencing data obtained, several clones appeared to be identical. As can be seen in **Figure 3.11**, clones 3, 4, 5, 8, 9, 12, 16, 18, 20, 21, 22, 24, 25 and 27 were identical. Apart from this, clones 6, 11, 15, 17 and 30 were also identical. Clones 1, 2, 7, 10, 14, 23, 26 and 29 were all unique. Ten different amino acid sequences were identified.

Figure 3.11: Alignments of anti-IgG-Fc scFv antibody-displaying monoclones grouped by sequence similarity. *The alignments of anti-IgG-Fc scFv antibody-displaying monoclones were categorized based on sequence similarity. A consensus approach utilizing a threshold exceeding 50% was employed to compare the sequence alignment. The designations 'CDR' and 'FR' in relation to clone 3 indicate the specific segments of the sequence corresponding to the CDRs and FRs. The '-' signifies placeholders in cases where sequences for a region were shorter or not fully sequenced via Sanger sequencing. Ten different amino acid sequences were identified.*

SWISS-MODEL was used to produce a 3D structure of the scFv displayed by anti-IgG-Fc phage clone 6 as can be seen in **Figure 3.12** using the amino acid sequence from sanger sequencing to visualise the structure (refer to Appendix Section D.2 for the Ramachandran plot).

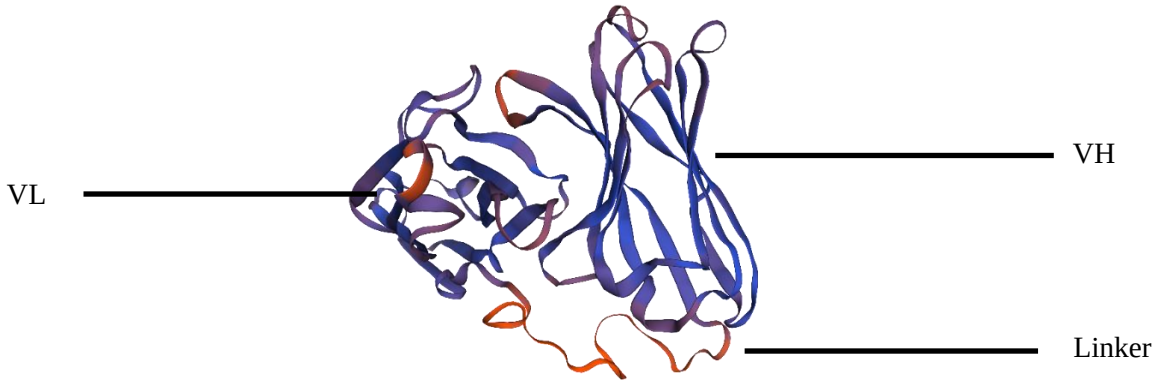

Figure 3.12: Structure of scFv displayed by anti-IgG-Fc scFv antibody-displaying phage clone 6. *The VH and VL domains are connected by a short flexible linker.*

3.4.3 TIM-4

Sixteen clones from biopanning against TIM-4 were sent to LGC Genomics GmbH in Berlin for sanger sequencing after plasmid extraction (refer to Appendix Section C for Nanodrop measurements). This was done to determine the amino acid sequence of the scFv displayed by each clone against target protein TIM-4 using SnapGene. Of the 16 clones sent, 1 was fully sequenced. The clones 2, 7, 8, 9, 12, 19, 21, and 27 were sequenced due to their binding to the target protein TIM-4, while clones 1, 4, 5, 6, 10, 11, and 13 were sequenced because they did not bind to the target protein TIM-4. This sequencing was conducted to elucidate any differences in the amino acid sequence alignment that might account for the observed binding or non-binding to the target protein TIM-4. From the sanger sequencing data obtained, it was elucidated that clones 1, 4, 6, 10, 11 and 13 contained a multitude of stop codons in their sequences (attached in Appendix Section D.1). Additionally, as can be seen in **Figure 3.13**, clones 2, 9 and 12 appeared to be identical. Clones 7, 21 and 27 were also seemingly identical. Meanwhile, clones 5, 8 and 19 had a completely unique sequence without stop codons. The number of different amino acid sequences identified without a multitude of stop codons was 5.

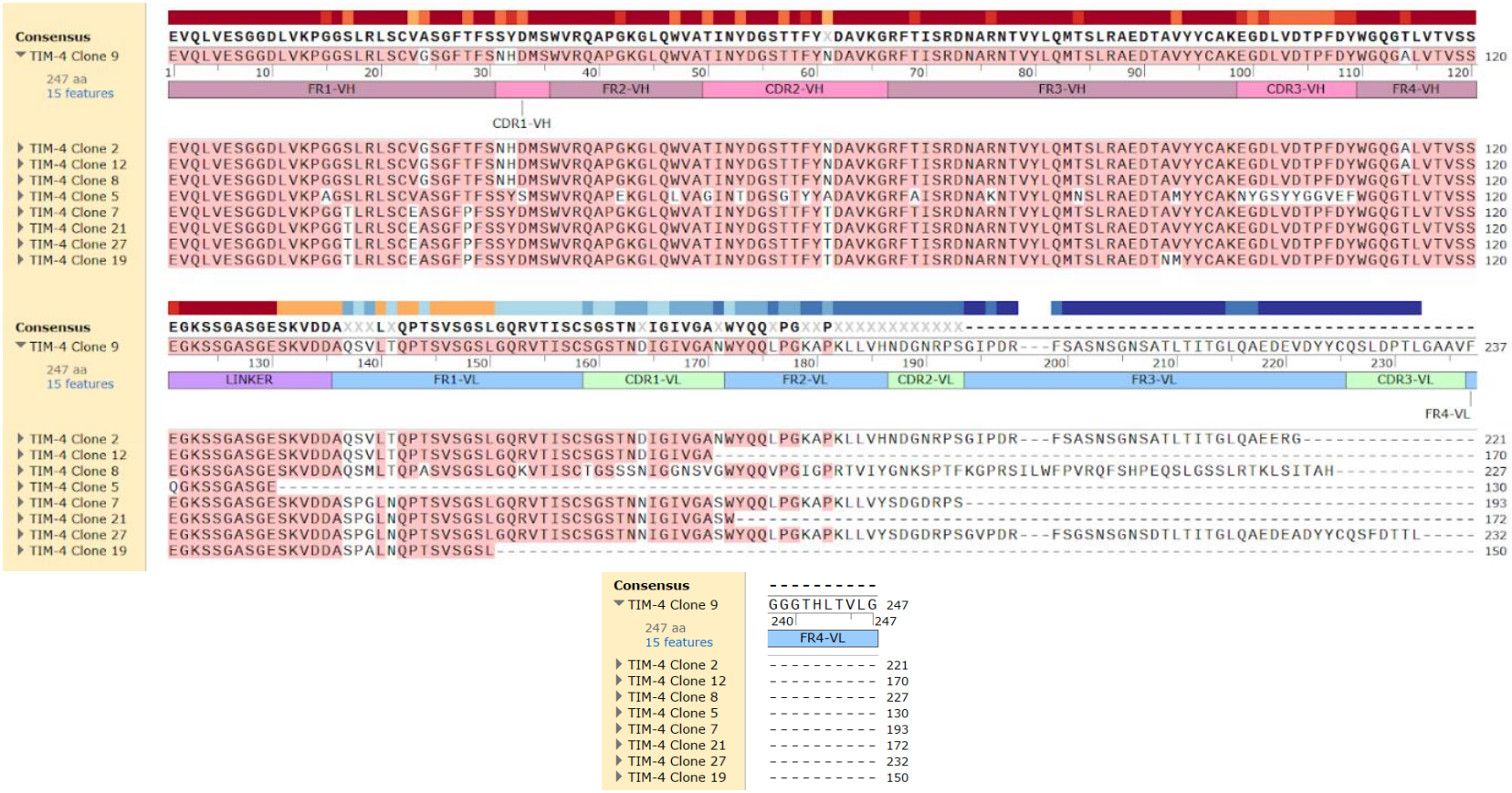

Figure 3.13: Alignments of TIM-4 monoclones grouped by sequence similarity. *The alignments of anti-TIM-4 scFv antibody-displaying monoclones were categorized based on sequence similarity. A consensus approach utilizing a threshold exceeding 50% was employed to compare the sequence alignment. The designations 'CDR' and 'FR' in relation to clone 9 indicate the specific segments of the sequence corresponding to the CDRs and FRs. The '-' signifies placeholders in cases where sequences were not fully sequenced via Sanger sequencing. Five different amino acid sequences were identified.*

SWISS-MODEL was used to produce a 3D structure of the scFv displayed by anti-TIM-4 phage clone 9 as in **Figure 3.14** using the amino acid sequence from sanger sequencing (refer to Appendix Section D.2 for the Ramachandran plot).

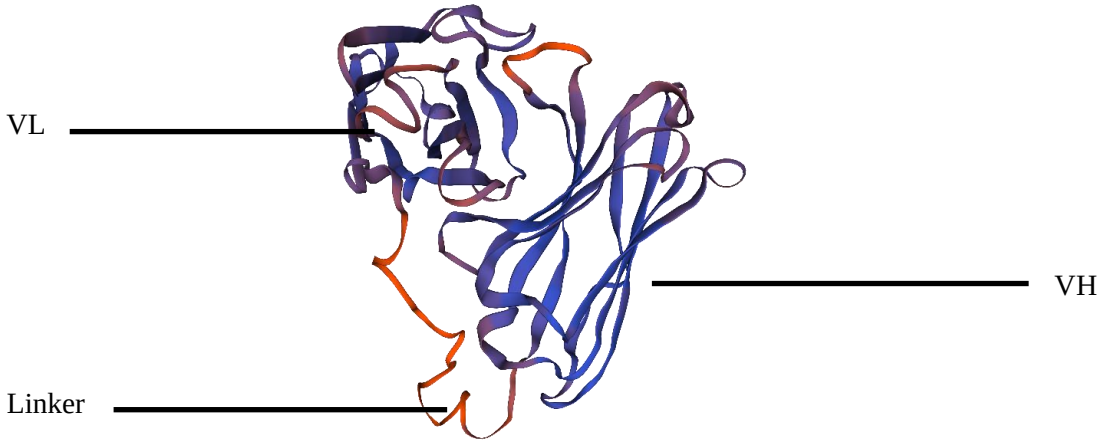

Figure 3.14: Structure of scFv displayed by anti-TIM-4 scFv antibody-displaying phage clone 9. *The VH and VL domains are connected by a short flexible linker.*

3.4.4 No protein control

The NPC which consisted of phage clones binding to the His-Tag beads and not specifically to any protein were sequenced to determine whether these were comparable to sequences of phage clones binding to the target protein TIM-4. In total 10 clones were sent for sequencing, of which 4 were fully sequenced. Two clones had nonsense sequences full of stop codons as in Appendix Section D.1. The results of the 2 fully sequenced clones in **Figure 3.15** showed that both fully sequenced clones were unique.

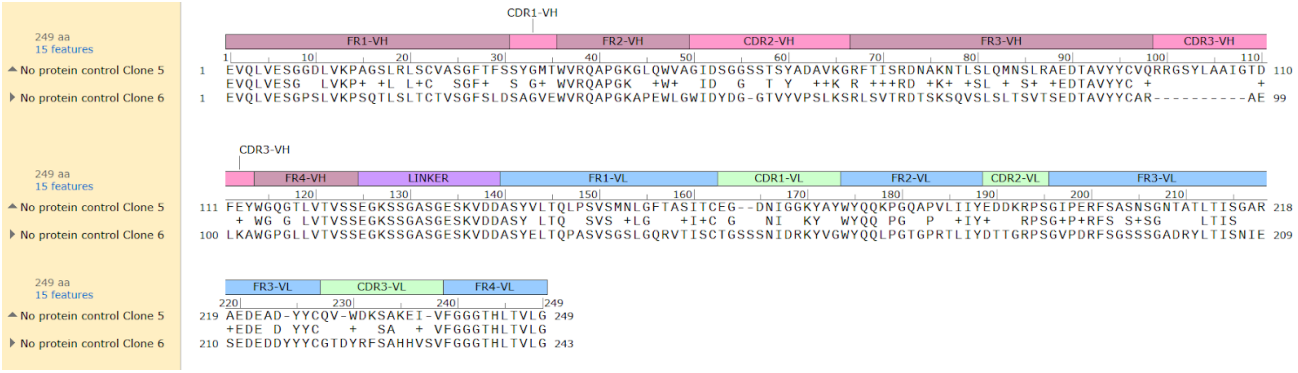

Figure 3.15: Alignments of NPC monoclones. *The alignments of no protein controls were categorized based on sequence similarity. A consensus approach utilizing a threshold exceeding 50% was employed to compare the sequence alignment. The designations 'CDR' and 'FR' indicate the specific segments of the sequence corresponding to the CDRs and FRs. The '-' signifies placeholders in cases where sequences for a region were shorter. The symbol '+' denotes regions where, despite variations in amino acid composition between sequences, there exists similarity in amino acid characteristics. Two different amino acid sequences were identified.*

SWISS-MODEL was used to produce a 3D structure of the scFv displayed by NPC phage clone 5 as in **Figure 3.16** using the amino acid sequence from sanger sequencing (refer to Appendix Section D.2 for the Ramachandran plot).

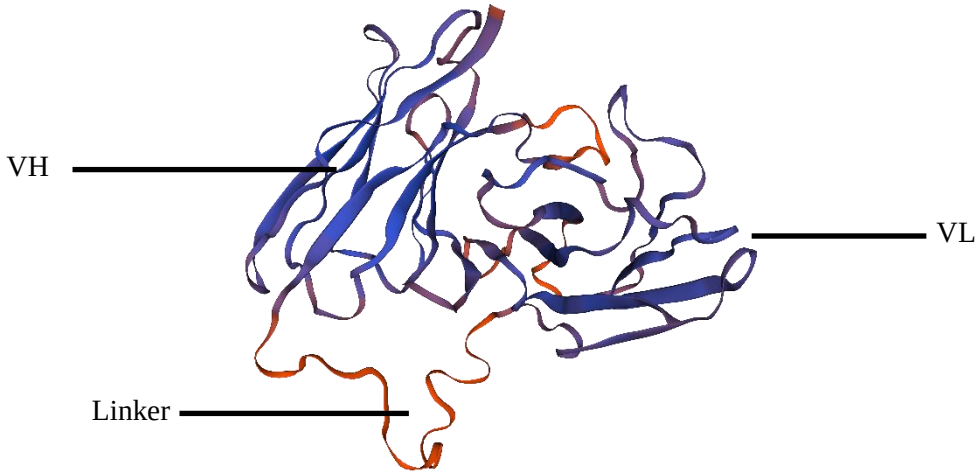

Figure 3.16: Structure of scFv displayed by NPC phage clone 5. *The VH and VL domains are connected by a short flexible linker.*

3.4.5 Comparison of all Fully Sequenced Monoclones

The fully sequenced clones were aligned using SnapGene to compare the amino acid sequences, aiming to establish whether clones binding to distinct target proteins exhibited identical or similar sequences. As per **Figure 3.17**, none of the anti-TIM-3-Fc scFv antibody-displaying clones were identical to the fully

sequenced anti-TIM-4 scFv antibody-displaying phage clone. Clones 1, 9, 17, 27 and 30 displaying anti-TIM-3-Fc scFv antibody were identical. Anti-TIM-3-Fc clones 7, 8, 11, 15 and 29 were unique while anti-TIM-3-Fc clones 13 and 21 were identical. Anti-TIM-4 clone 9 was the only fully sequenced clone against target protein TIM-4 and was unique in comparison to other clones targeting different proteins. The no protein control clones were also unique. The anti-IgG-Fc scFv antibody-displaying clones 3 and 27 were identical whilst clone 6 was unique. Since both NPC clones were unique, this indicated that none of the other clones were nonspecific binders. Additionally, all anti-TIM-3-Fc, anti-IgG-Fc and anti-TIM-4 scFv antibody-displaying clones were different when compared to each other indicating that all clones binding to different target proteins were unique.

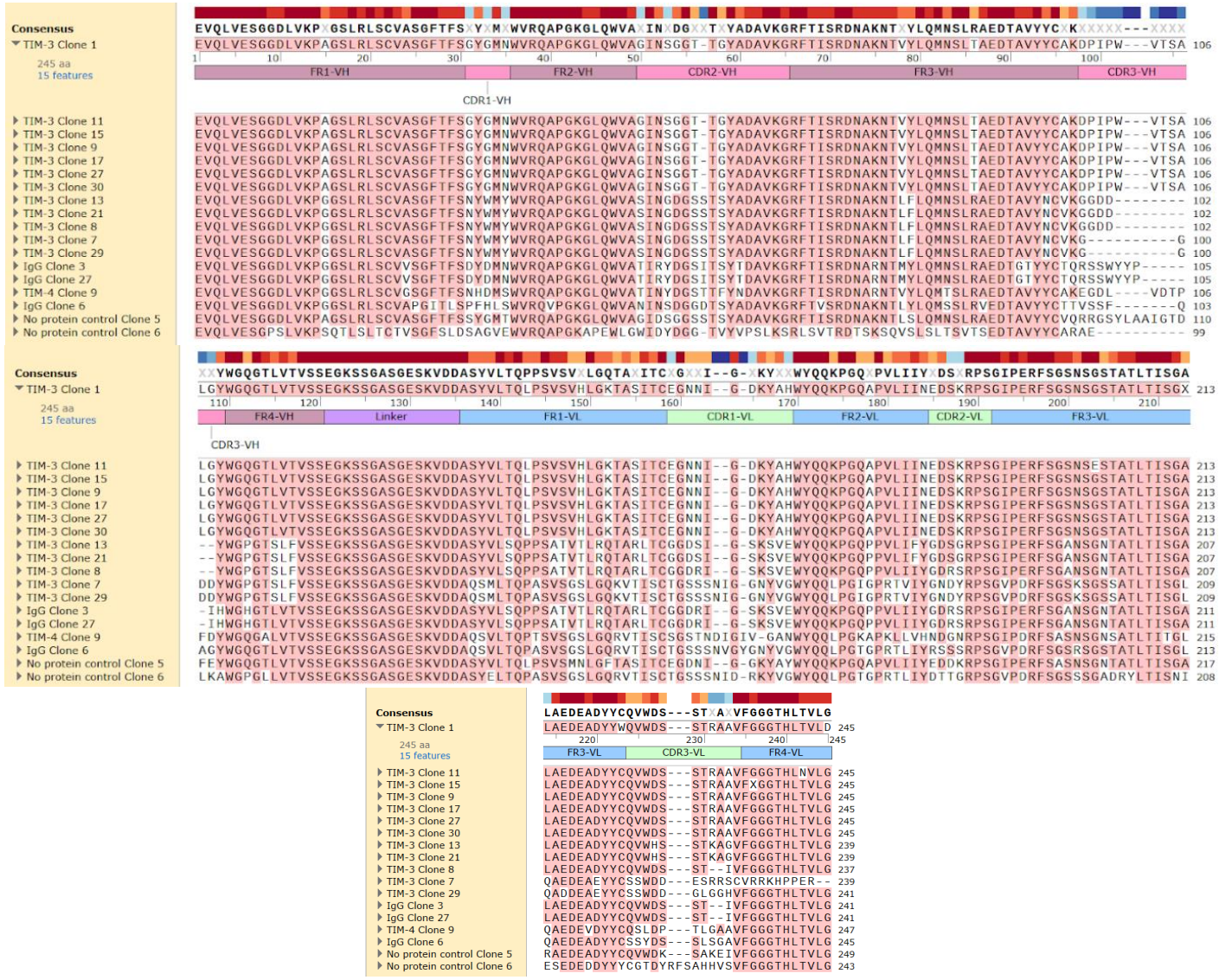

Figure 3.17: Alignments of fully sequenced monoclones grouped by sequence similarity. *A consensus with a threshold of >50% was used for comparison of the alignment. The complementarity-determining region demonstrated the largest variations in the amino acid sequences as was expected.*

BLAST analysis was carried out to compare the VH and VL chains of clones and the results can be found in Appendix Section D.3. Each CDR region was compared individually. Anti-TIM-3-Fc clones were compared to anti-IgG-Fc clones to confirm that the amino acid sequences were different. Anti-IgG-Fc clone 3 was not included in the analysis since its sequence was identical to anti-IgG-Fc clone 27. Anti-TIM-4 clones were compared to the no protein controls to check for similarities in the scFv amino acid sequences and anti-TIM-3-Fc and anti-TIM-4 clones were also compared to each other to check for similarities. If multiple similarities were found it would indicate that anti-TIM-3-Fc antibodies may bind to TIM-4 and *vice versa*. To check for similarities among the controls, anti-IgG-Fc clones 6 and 27 were compared to each other as were NPC clones 5 and 6.

Heatmaps were produced using GraphPad software using bit score values obtained in Blastp sequence similarity alignment to visualise the similarity of CDR regions as in **Figures 3.18** and **3.19**. In the context of smaller sequence alignments, the bit score was more important than the E-value because bit score measures sequence similarity independent of query sequence length and database size and was normalized based on the raw pairwise alignment score. On the other hand, the E-value was a statistical value that estimated the likelihood of finding a specific number of alignments with a bit score equal to or greater than the observed score when comparing query sequences to the target database meaning that the E-value depended on the bit score, query sequence length, and the size of the target database (Pearson 2013).

Taking note of the bit scores showed that most of the sequence similarities were insignificant which was the ideal result and expected. The lack of similarity in the sequences indicated that each comparison contained a unique clone and biopanning identified multiple different sequences which bind to the same and different targets. In comparing clones that bind to the target protein with those that bind to IgG-Fc or NPC, the lack of similarity between CDRs indicates that non-specific binders to target proteins were effectively removed during the washing process. In comparisons between TIM-3-Fc binders versus anti-TIM-4 clone 9, the lack of similarity indicated that scFv antibodies against TIM-3 were unlikely to bind to TIM-4 and *vice versa*. When comparing different clones binding to the same target protein, lack of sequence similarity indicated that a diverse set of clones was identified towards the same target protein. This

suggested that the diversity of clones from the original library was maintained throughout the rounds, and there was no over-amplification or biased identification of only one or a few clones.

Differences in the framework (FR) regions, especially from a polar amino acid to a non-polar amino acid or from an acidic to a basic amino acid may have impacted the structure of the scFv and potentially affected target binding. However, only CDR sequences were compared in blastp because these are responsible for the antigen-binding specificity of the scFv antibodies (Ahmad, Yeap et al. 2012). The CDRs were the most variable regions of the antibody, and they formed the antigen-binding site. The framework regions, on the other hand, provided the structural scaffold for the CDRs and were more conserved. While the framework regions contributed to the stability and folding of the antibody, they did not directly interact with the antigen. Therefore, differences in the framework regions were less likely to affect the antigen-binding specificity of the antibody than differences in the CDRs (Baran, Pszolla et al. 2017, Chan, Chan et al. 2011, Chiu, Goulet et al. 2019). Furthermore, each CDR made a distinct contribution to the binding of the antigen. For example, CDR3 and especially the heavy chain made a much bigger contribution to binding specificity than CDR2-VL (Asaadi, Jouneghani et al. 2021).

The anti-TIM-3-Fc scFv antibody-displaying clones chosen for sequence alignments were clone 30 as a representative for clones 1, 9, 17 and 27 since the sequences were identical. Clones 7, 8 and 29 since these were unique and clone 13 as a representative of clone 21 since these were identical. The CDR regions of clones 11 and 15 were the same as those of clone 30 and therefore were not included in the analysis.

Anti-TIM-3-Fc clone 8 which was not a binder in **Section 3.3.1** and was a weak binder in **Section 3.3.2** was compared to anti-TIM-3-Fc clone 13 which was a binder in both sections to check for similarities in the sequences. Anti-TIM-3-Fc clone 13 was chosen for comparison with clone 8 because the sequences were identical except regions CDR2-VL and CDR3-VL. This difference in the regions indicated that even small changes in these areas could significantly affect the binding of the clone to the target protein. For this comparison, there was also a single amino acid difference in FR2-VL of isoleucine instead of phenylalanine. However, both these amino acids were neutral and non-polar meaning that it was unlikely that this resulted in a significant change in protein structure. Comparison was also done between two clones

that were binding to the target protein TIM-3-Fc. Clones 7 and 30 were chosen because clone 30 had the most similar CDRs among all the clones and clone 7 was unique.

Most CDR comparisons between all clones showed no sequence similarity as was expected. Interestingly, anti-TIM-3 Fc clones 8 and 13 had more similar CDR sequences despite clone 8 being a very weak binder. However, only CDR2-VH was significantly similar for this comparison. More importantly, CDR3-VH was unique in all the clones. This CDR made the most vital contact with the antigens and tended to have the most variety in its conformation (Deiss, Vadnais et al. 2019, Asaadi, Jouneghani et al. 2021).

The CDR2-VH region was found to be similar in all comparisons except when NPC clones 5 and 6 were compared. This anomaly can be explained because NPC binding clones were non-specific meaning they were not binding to a target protein but rather randomly binding to the beads. Binding to His-tag beads may not have occurred through the scFv displayed by the phage but in some other orientation with a different part of the phage particle.

A)

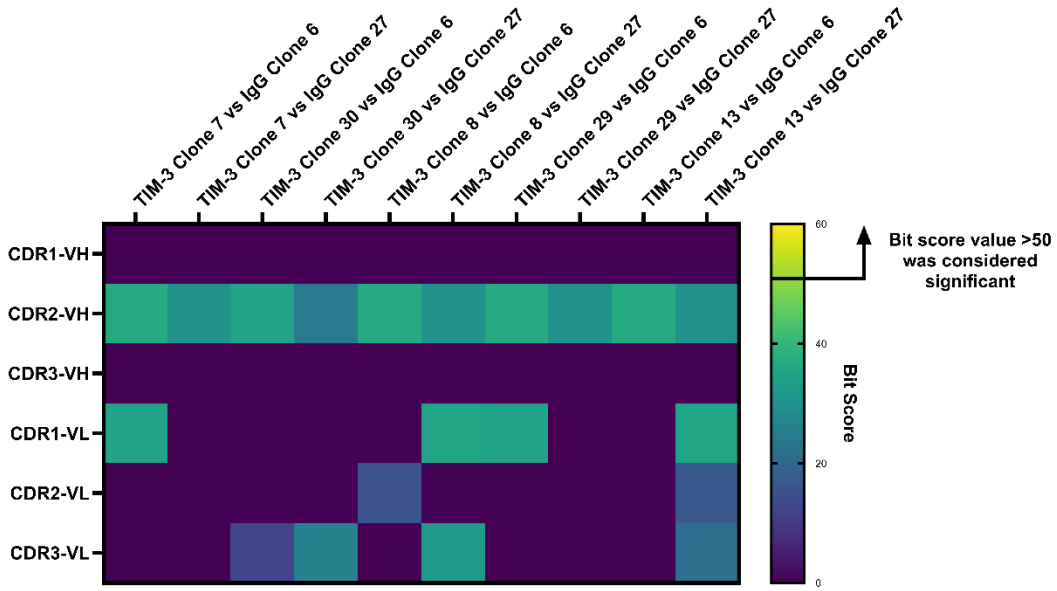

B)

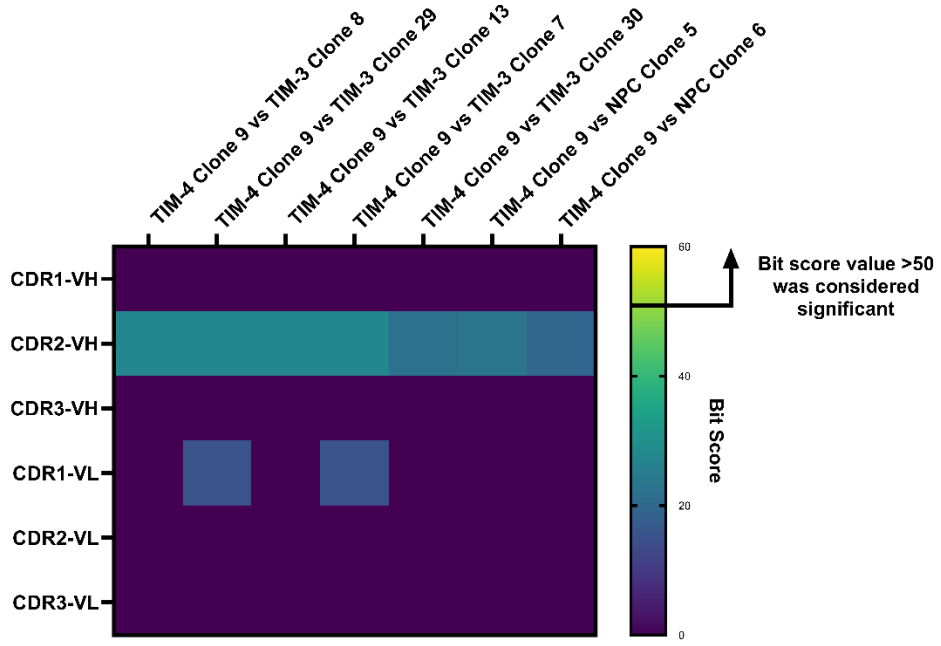

Figure 3.18: Heatmaps of CDR region comparisons between clones binding to different targets. *A) Comparisons of sequence similarities of anti-TIM-3-Fc clones to anti-IgG-Fc clones and NPC control clones and B) comparisons of sequence similarities of anti-TIM-4 clone 9 to anti-TIM-3-Fc clones. CDR2-VH was observed to have the most similarities throughout all comparisons. However, none of the sequence comparisons showed significant similarity.*

A) B)

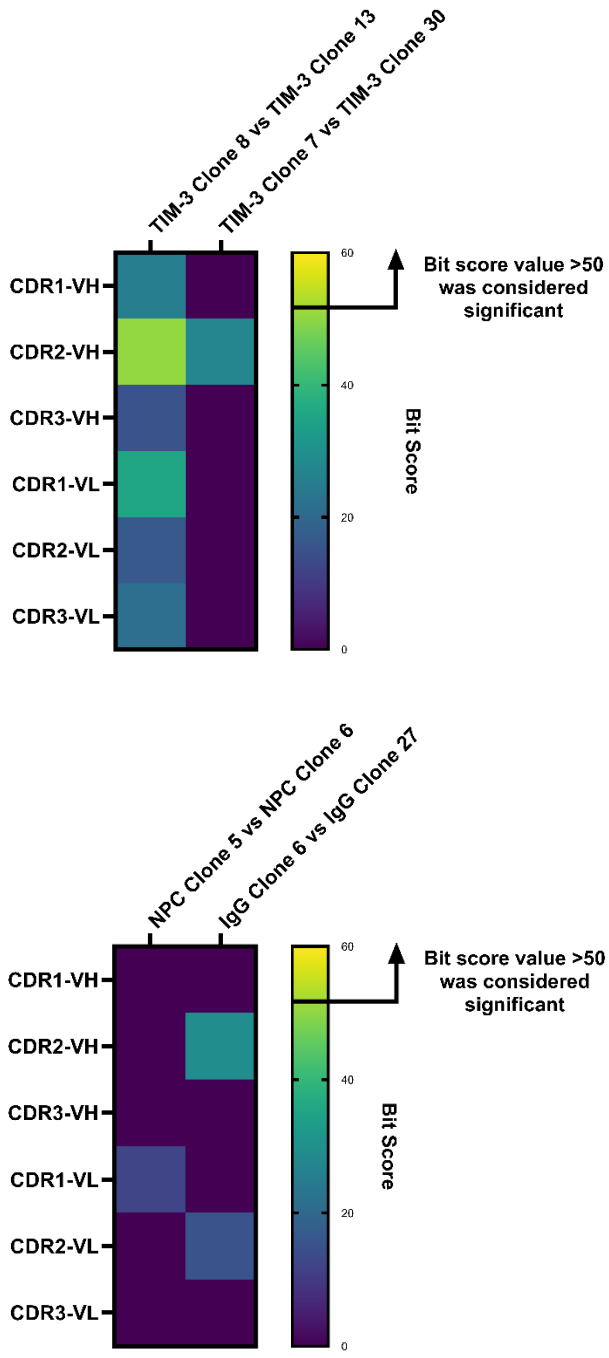

Figure 3.19: Heatmaps of CDR regions of clones binding to the same targets. *A) Comparison of CDR regions of TIM-3-binding clones and B) comparison of NPC and anti-IgG-Fc control clones. The highest sequence similarity observed in clones was between anti-TIM-3-Fc clones 8 and 13, especially CDR2-VH at a bit score of 50.3. This was only a slightly significant sequence similarity. The least sequence similarity was observed between NPC clones 5 and 6.*

Chapter 4: Discussion

This research studied the hypothesis that phage display biopanning identifies high affinity single chain variable fragment monoclonal antibodies specific to T cell co-inhibitory proteins TIM-3 and TIM-4. This objective was successfully achieved using phage display biopanning after 4 rounds. Considering the information at hand, it appears that this was the first reported anti-TIM-4 antibody successfully identified using phage display. The specificity of the phage pools and clones identified was determined using ELISA by comparing the binding of phages to target proteins TIM-3-Fc and TIM-4 versus to non-target proteins SARS-CoV-2 spike S1 and SARS-CoV-2 RBD proteins respectively as in **Figure 4.1**. A total of 21 anti-TIM-3-Fc scFv antibody phage monoclones with affinity and specificity to TIM-3-Fc and 8 anti-TIM-4 scFv antibody phage monoclones binding with affinity and specificity to TIM-4 were identified. BLAST was used to establish how structurally similar the target proteins TIM-3 and TIM-4 ECDs used during biopanning were. These were found to be highly homologous and the question arose whether antibodies identified against TIM-3-Fc might also bind to TIM-4 due to this homology. Analysis using Sanger sequencing data and SnapGene indicated that the monoclonal antibodies isolated were constructed of a variable heavy chain linked to a variable light chain and that the complementarity-determining regions differed for each monoclone. This indicated that the anti-TIM-3-Fc scFv antibodies likely did not bind to TIM-4 and *vice versa*.

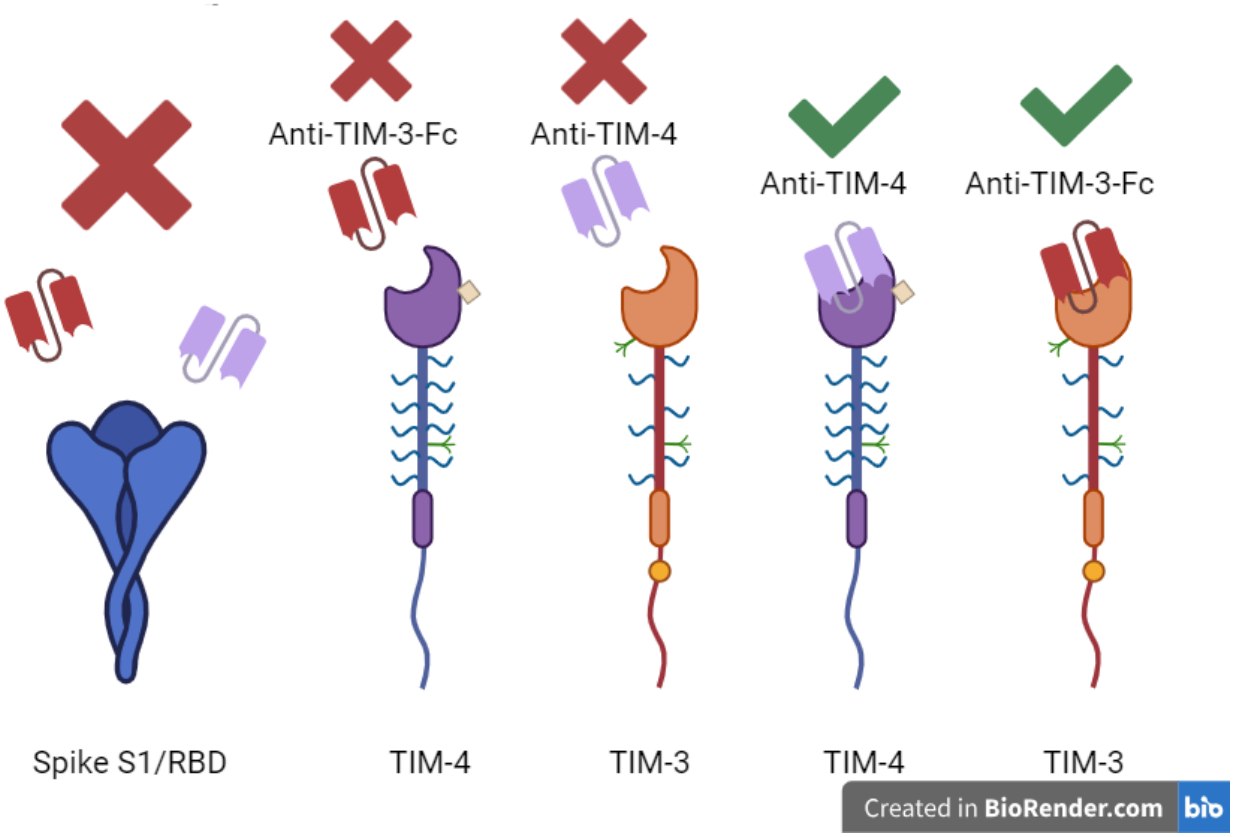

Figure 4.1: Binding specificity of scFv antibodies identified. *The antibody identified against TIM-3-Fc does not bind to SARS-CoV-2 spike S1 and should not bind to TIM-4. Additionally, the antibody identified against TIM-4 does not bind to SARS-CoV-2 RBD and should not bind to TIM-3 Fc.*

The use of checkpoint inhibitors in oncology has shown remarkable success with long lasting clinical benefit in a multitude of tumours (Brahmer, Tykodi et al. 2012, Patel, Bock et al. 2017, Peggs, Quezda et al. 2009). However, this efficacy has been restricted to 20-30% of the population and might not be as effective in more prevailing cancers such as breast and colorectal cancer (Buqué, Bloy et al. 2015, Lee, Cragg et al. 2013, Pardoll 2012). The phage display technology has aided the discovery of new antibodies, antigens and epitopes associated with tumours and has been vital in advancing anti-cancer strategies. Phage display also allowed for modified affinity, decreased immunogenicity and investigating biophysical properties that increase the drug-ability of therapeutic molecules (Lu, Hwang et al. 2020). Applications of this technique include research, clinical diagnosis and pharmaceuticals for therapeutic use (Christ, Lee et al. 2007).

Phage display relies on genetically engineered bacteriophages, multiple rounds of antigen-guided selection and amplification of phage (Barbas III, Burton et al. 2001) to select high affinity and specificity monoclonal antibodies towards target protein. The physical connection between the antibody fragment displayed on the coat protein and the genotype encoding this protein within the phage permits the study of genetic information and function of antigen-specific monoclonal antibodies (Hammers, Stanley 2014).

The immobilisation of target proteins during biopanning in this study was performed on beads rather than plates as it was found to be significantly more effective at isolating phage in previous studies (Grima 2022, Spiteri 2022, McConnell, Dinh et al. 1999). Furthermore, since using protein G beads for immobilisation of TIM-3-Fc resulted in clumping (Grima 2022, Spiteri 2022), His-tag beads were used instead for TIM-4 to test whether clumping still occurred. The clumping may have been partially caused by the binding of the detection antibody to the areas on the protein G beads that were not completely saturated with the target protein TIM-3-Fc. This was possible because protein G beads bound to the Fc portion of Fc tagged target proteins and/or to the Fc region of the detection antibody used (Dynabeads™ Protein G package insert, 2016). When His-tag beads were used, no clumping was observed.

The immobilisation of target protein TIM-3-Fc to the protein G beads achieved through binding of the Fc region to the protein G on the beads ensured that the target protein was binding in the correct orientation to the immobilisation surface (Liu, Yu 2015). Human TIMD4 extracellular domain was fused with a polyhistidine tag at the C-terminus (Human TIM4 / TIMD4 Protein (His Tag) Package Insert) and this bound to the cobalt beads through interaction between varying divalent metal ions. Co^{2+} was used in this case but Ni^{2+} could also have been used. Both interact with the basic imidazole ring of histidine in neutral or slightly basic pH of around 7.5-8 (The His-Tag: Fundamentals and Principles n.d., Liu, Yu 2015). During the washing steps of biopanning, loss of beads was noted (as in Grima 2022) especially for the no protein controls. This was compensated for by using a larger volume of beads as solid phase.

The first biopanning rounds carried out failed because any binding which took place was to the His-tag beads or other non-specific targets rather than to the TIM-4 target protein. This was confirmed by the no protein control. There were multiple possible causes for this. Most importantly, the original phage library

used for the first biopanning was stored incorrectly at -20°C and multiple freeze-thaw cycles over a year may have led to proteolytic cleavage of scFv from the surface of the phage particles (Andre, Moutinho et al. 2022, Baek, Suk 2002). Also, during the first biopanning attempt, a fixed centrifuge bucket was used which resulted in *E. coli* residue with the phage pellet observed as a yellowish plaque rather than a white pellet. Biopanning was successfully repeated using the swingout bucket to produce a more visible phage pellet for better recovery of phage and using a new original phage library properly stored at -80°C.

After each round of biopanning, the CFU/ml was calculated to ensure that phage titre remained the same throughout the rounds. The low multiplicity of infection meant that a host cell was infected by only one phage. Phage tire remained the same throughout the rounds for each target protein, confirming that any increase in phages binding to target throughout the rounds was not due to increased phage titres after round 4 but rather that with each round, phages specific to target were being identified and amplified while non-binding phages were being washed away. Satellite colonies were observed when performing titrations and counting the colonies. This could have been due to longer incubation times of around 16 hours. Other causes of satellite colony growth could have been old antibiotic stock, incorrect antibiotic concentration, addition of antibiotic to hot media and/or not enough mixing for antibiotic to be evenly distributed in the media before pouring into plates (Kroemer n.d.). For this reason, carbenicillin would be used instead of ampicillin in any future experiments due to its increased stability and its higher tolerance to heat and acidity (Patrick 2014).

ELISA was used to confirm the successful biopanning against TIM-3-Fc and TIM-4 and that monoclonal antibodies against said proteins were binding specifically to their target proteins. For TIM-3-Fc, the fluorescence of round 4 was lower than that of round 3. This could have occurred for multiple reasons such as oversaturation of the beads or ELISA wells. However, in this case since the library had been produced over a year previously and was being used frequently for multiple experiments, the titre of round 4 anti-TIM-3-Fc phages may have been reduced. That vial of round 4 polyclonal anti-TIM-3-Fc scFv antibody-displaying phage pool had also undergone more freeze thawing than the other rounds of TIM-3-Fc possibly contributing to proteolytic cleavage of some scFvs from the surface of M13 phages (Andre, Moutinho et

al. 2022, Baek, Suk 2002). Amplification of round 4 of TIM-3 was performed because of this and an increase in the number of phages binding to TIM-3 was observed as per Appendix Section B.

Importantly, during phage amplification it was very likely that the more abundant clone sequences out-amplified the rarer ones. Additionally, clones which amplified faster potentially out-competed other binding clones that amplified slower (Derda, Tang et al. 2011). Picking 30 clones from a library of more than 1 x 10^{11} PFU/ml meant that many clones were underrepresented, and the more prevalent ones were overrepresented. Furthermore, during the biopanning process, the diversity of the phage sample was reduced, while the proportion of phage displaying an scFv that bound to the target of interest increased. Therefore, some of the binders would have been lost or extremely diminished over the rounds and the chances of picking them up after titration would have become increasingly smaller (McGuire, Li et al. 2009). For this reason, less rounds were preferred. Since amplification of libraries decreases diversity and limits the number of binding clones that can be identified by screening, there can be greatly restricted identification of useful ligands for targets (Derda, Tang et al. 2011).

Several studies have been performed where the amplification step was completely avoided. However, this could have resulted in the ratio of binders to non-binders being lower. For example, Derda, Musah et al. (2010) performed an amplification-free experiment to isolate a population of approximately 10^5 clones that bound to the surface of pluripotent cells. This resulted in 6 binding clones from a total of 500 tested sequences after using ELISA for validation (Derda, Musah et al. 2010, Derda, Tang et al. 2011, Orner, Derda et al. 2004). This Masters research project on the other hand found through ELISAs that many of the antibodies identified were binding strongly and specifically to the target protein. For instance, 21 of the 30 anti-TIM-3-Fc clones tested were binding to TIM-3-Fc, 30 out of 30 anti-IgG-Fc clones picked were binding to IgG-Fc and 8 out of 30 anti-TIM-4 clones chosen were binding to TIM-4. Additionally, the scFv amino acid sequences against each target protein varied, with 9 different amino acid sequences identified for anti-TIM-3-Fc scFv antibodies, 10 different amino acid sequences identified for anti-IgG-Fc scFv antibodies, and 5 different scFv antibody sequences obtained for TIM-4. Therefore, comparing the outcomes of this study to that performed by Derda et al. (2010), it appears to be more efficient to perform

amplification as the benefit of finding more binders to the target protein of interest seems to outweigh the risk of picking identical clones.

The scFv sequence in the plasmid of the phage was situated between a pelB leader sequence and a myc tag sequence. pelB is a leader sequence of amino acids used to direct the protein of interest to the periplasm of the bacterial host where there is a favourable environment for proper protein folding and disulphide bond formation (Wlliams, Distel 2010). The myc tag is a polypeptide protein tag which is fused to the protein of interest to either the C- or N-terminus through recombinant DNA technology to allow detection and purification of the displayed protein (Duesberg, Vogt 1979, Evan, Lewis et al. 1985, Sheiness, Bishop 1979). The smallest unit of immunoglobulin with antigen-binding activity is the fragment variable region consisting of VH and VL connected with a disulphide bond. The scFvs used in this study were engineered so that instead of a disulphide bond there was a flexible linker connecting VH and VL. The length and amino acid composition of the linker has a key role in the folding of the protein, oligomeric state, expression level, affinity, specificity and stability (Ahmad, Yeap et al. 2012, Arslan, Karadag et al. 2022). It usually consists of 10-25 amino acids long with “EK” regions for better solubility and “GS” regions for flexibility in the final protein (Alfthan, Takkinen et al. 1995, Whitlow, Bell et al. 1993). Glycine-serine repeats are the most common linker sequence in scFv design, as glycines and serines are small and polar amino acids used in linkers due to their flexible nature and good solubility. Furthermore, the flexibility of glycine-serine linkers can be tuned to allow rational design of multidomain proteins such as scFvs (Van Rosmalen, Krom et al. 2017).

Linkers can also be improved to reduce aggregation (Arslan, Karadag et al. 2022). scFv fragments can dimerise or form higher-order oligomers and this is dependent on linker length, antibody sequence and external conditions which can affect the degrees of freedom of the scFv. For example, linkers longer than 12 amino acid residues are more likely to exist in a monomeric state, rather than forming dimers or higher-order oligomers (Arndt, Muller et al. 1998, Ludel, Bufe et al. 2019). To improve antigen-antibody binding and stability, scFv dimers can be constructed by shortening the linkers to 3-5 amino acid residues in the same orientation (Bie, Yang et al. 2010). Optimisation of the length and sequence content of linkers was

essential to improve it for the function it was intended to be used for. In this study the linker used was 15 amino acids long and the sequence was “EGKSSGASGESKVDD”.

In each of the VH and VL regions there are 3 hyper variable CDRs linked together by framework regions. CDRs are responsible for antigen binding and have a variable structure depending on the target epitope. The framework regions which are also variable acted as a scaffold and have much more limited variability compared to CDRs (Asaadi, Jouneghani et al. 2021).

Each CDR makes a distinct contribution to the binding of the antigen. For instance, the CDR3 in the heavy chain has a critical role by 29% contribution in binding specificity, while the involvement of CDR2-VL is just 4% (Asaadi, Jouneghani et al. 2021). These varying contributions of CDRs likely led to differences in binding affinity and specificity for the same target protein. Furthermore, the scFvs identified likely bound to different epitopes on the target protein, which could have led to the differences in CDRs for clones binding to the same target protein. For example, some scFvs may have bound to linear epitopes, while others may have bound to grooves and clefts (Asaadi, Jouneghani et al. 2021).

CDRs 1 and 2 are encoded by germline V genes whereas CDR3 are a product of gene recombination. The CDR3 region of the variable heavy chain in scFvs is considered the most important CDR region due to its significant role in antigen binding specificity and affinity. The CDR3, especially the heavy chain region is not only highly variable and diverse but also exhibited varied length and biochemical properties, contributing to its ability to recognize and bind diverse epitopes through enhanced sequence diversity (D'Angelo, Ferrara et al. 2018).

A study by Xu and Davis (2000) used mice which were constrained to use a single VH gene but full CDR3 diversity to generate their B cell repertoire against a variety of hapten and protein antigens. The development of primary and memory immune responses was monitored. They found that differences in CDR3-VH were enough to allow otherwise identical IgM molecules to differentiate between various hapten and protein antigens.

In this study, Sanger sequencing revealed that many clones for each target protein had similar framework sequences. As shown in this study, there were clones binding to the same target protein having identical

CDRs but varying frameworks. These differences in the frameworks were generally of only a few amino acids and the identification of clones with slightly different frameworks but the same CDRs suggested that these changes did not significantly impact the overall structure of the scFv since there was still binding to target protein.

In cases where the difference in amino acid framework sequence was of one polar amino acid instead of another polar amino acid, the protein structure likely would not have varied significantly. However, differences in framework resulting from a basic amino acid in one clone versus an acidic amino acid in another clone may have resulted in a change in protein structure. Perhaps the most important change in structure would be in clones that differed in amino acid sequence due to the presence of proline. Proline is highly anomalous and therefore has particular roles in protein structure. The nitrogen atom of proline is covalently locked in a ring as in **Figure 4.1** making it the only proteinogenic amino acid with a constrained phi angle. This can influence the conformation of the antibody's polypeptide chain especially if it occurs in the CDRs. Additionally, it can form *cis* or *trans* configurations depending on subtle influences such as changes in local charge distribution. This can also influence the conformation of the variable regions of antibodies and possibly influence the binding affinity and specificity of the antibody to its target antigen. Proline has a single hydrogen atom attached to its nitrogen and therefore it can't donate protons and serves rather as a proton acceptor. It can disrupt protein secondary structure by inhibiting the backbone from conforming to an alpha-helix or beta-sheet conformation. The impact of this on the secondary structure of the variable regions can affect the overall conformation of the antibody and therefore its antigen-binding properties. Nevertheless, it is commonly found as the first residue of an alpha helix and in the edge strands of beta sheets. In an alternate interpretation, proline imposes its own secondary structure with a confined phi angle that overrode other forms of secondary structures. This imposition may directly impact the conformation of the antibody, particularly in regions where proline is present, potentially influencing the overall structure and stability of the antibody (Cloutier, Sudrik et al. 2020, Guttman, Padte et al. 2020, Maseiro, Nelly et al. 2020, Morgan, Rubenstein 2013, Patriarca, Cermola et al. 2021, Vakilian 2022).

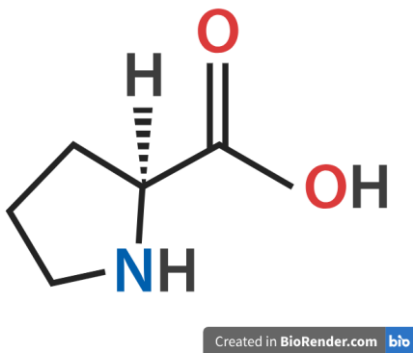

Figure 4.2: Structure of proline. *Proline is a unique amino acid that has a distinctive cyclic structure in its side chain, which gives it exceptional conformational rigidity compared to other amino acids.*

When comparing anti-IgG-Fc clones 6 and 27 it was noted that clone 6 had a proline (neutral-nonpolar) and clone 27 had a serine (neutral-polar) in FR1-VH. This also occurred in the CDR3-VH where some anti-TIM-3-Fc clones had proline instead of aspartic acid (acidic) and FR4-VH where some anti-TIM-3-Fc clones had proline instead of glutamine (neutral-polar). Modelling these clones in the future to observe any difference in structure due to the presence of proline would be interesting particularly in the context of different binding affinities. For instance, **Figure 3.6 B** indicated that anti-IgG-Fc clone 27 bound more strongly to the target protein IgG-Fc when compared to anti-IgG-Fc clone 6. Therefore, determining whether the increased affinity of anti-IgG-Fc clone 27 to target protein was partly due to the absence of proline would be interesting.

It was important to note that when comparing the CDR sequences of fully sequenced clones together, only CDR2-VH sequences of anti-TIM-3-Fc clones 8 and 13 were found to be statistically similar and only by a very small margin. The similarity in CDR2-VH among the clones was because it tends to have a more conserved nature. CDR2-VH was evolutionarily conserved in the germline so amino acid sequences in this region were highly conserved across different species and antibodies (Asaadi, Jouneghani et al. 2021). This conservation suggests that the CDR2 region plays a crucial role in maintaining the structural integrity and function of the antibody by forming a hydrogen bond network with the framework regions (Chiu, Goulet et al. 2019).

Very minor changes in the amino acid sequences of CDRs can result in different binding affinity because there can be structural changes, altered binding geometry which can influence the affinity of the interaction,

changes in hydrogen bonding, disulphide bond formation and electrostatic interactions between the scFv and the antigen and/or conformational changes (Ahmad, Yeap et al. 2012, Barderas, Desmet et al. 2008, Sarker, Rathore et al. 2022, Zahnd, Spinelli et al. 2004). This shows the importance of careful optimisation of CDRs during scFv antibody development for therapeutic applications (Sarker, Rathore et al. 2022 Teixeira, D'Angelo et al. 2022). This can be achieved through affinity maturation which involves the introduction of mutations into CDRs through *in vitro* evolution, genetic algorithms or machine learning techniques (Barderas, Desmet et al. 2008, Li, Gupta et al. 2023). For example, the introduction of charged residues into the framework region can improve the affinity of scFvs. scFvs can also be altered to introduce electrostatic interactions by introducing mutations that change the charge distribution of the scFv (Fukunaga, Tsumoto 2013). Small structural changes especially to CDR3-VH and CDR3-VL can result in significant improvements in affinity (Barderas, Desmet et al. 2008).

For multiple clones the reading of the sequences was incomplete, and this meant that not all the clones picked from the titrations could be properly analysed. Using forward primers would have solved the issues with incomplete sequencing since sanger sequencing tended to be less efficient at the beginning of an amino acid sequence read. Additionally, a primer for the middle of the sequence targeting the linker sequence can also be used. Several clones also had frameshifts, but these could still be analysed in SnapGene. Regardless of the issues encountered, the fully sequenced clones provided satisfactory information because it allowed for determination of how similar or different each clone was. The main aim was to determine whether clones binding to TIM-3-Fc had different sequences to clones binding to TIM-4 and the results confirmed that the sequences for these clones were different. The most commonly similar CDR throughout the comparisons was CDR2-VH. To determine whether the similarity can result in cross-binding to non-target molecules, ELISAs can be carried out between clones with highly similar CDRs to target versus to non-target protein.

Interestingly, there were 6 clones of anti-TIM-4, 2 clones of the NPC and 1 anti-IgG-Fc clone which had a plethora of stop codons in the sequence and may not have been displaying scFvs on their surface proteins (refer to Appendix D.1). The identification of such clones can be explained because even M13 bacteriophages displaying scFvs can bind non-specifically through other binding sites, specifically, through

the presence of multiple copies of the pIII, pVI, pVII, and pVIII proteins on their surface (Wang, Li et al. 2023). This multi-valency allows for multiple interactions with the target, which can lead to nonspecific binding. Additionally, even in cases where scFvs are displayed, because scFvs lack a constant region, there can be a less structured CDR, which may also result in nonspecific binding (Arimori, Kitago et al. 2017). This was important to know for the failed biopanning rounds and for no protein controls used during all biopanning. Any increase in phages binding to His-tag beads throughout the rounds could have been due to the above reasons.

The presence of stop codons in phage display libraries was also observed in commercial phage display libraries in a study by Sloth (2022). Next generation sequencing also identified many wild-type clones in the naïve library which could be attributed to the random nature of the library construction process and the natural diversity of the initial library. Some clones may have contained stop codons due to the diversity generating processes. Furthermore, the high abundance of wild-type clones in the naïve library could be due to the natural composition of the initial library which contained a large proportion of unaltered, wild-type sequences (Jaroszewicz, Morcinek-Oorlowska et al. 2022, Sloth, Bakhshinejad et al. 2022).

SWISS-Model was used to predict the structures of the protein targets used in biopanning and of the scFvs identified which were fully sequenced to visualise the structure. The Ramachandran plots indicated that the structures modelled were of good quality. However, these models predicted by SWISS-MODEL would need to be verified using methods such as X-ray crystallography, hydrogen deuterium exchange mass spectrometry, nuclear magnetic resonance spectroscopy or cryo-electron microscopy to ensure an accurate representation of the protein and scFv structures.

Information on a study by Lisowska, Worrall et al. was obtained through personal communication with Professor David Saliba and Ms Giuseppina Monda. A highly diverse naïve canine scFv antibody phage library (same library used for this study) was constructed by taking mRNA from canine B cells and amplifying these using 5’ Rapid amplification of cDNA ends-polymerase chain reaction to capture naïve expressed variable domain repertoire. A set of degenerate primers targeting the heavy and light chains from canine splenic tissue were designed and used to amplify and clone the heavy and light chain genes to hold

the plasmid libraries. These were fused to produce a bioactive scFv M13 phage library. Annotation of the heavy and light chain genes including CDR and FR length range and diversity was performed using long-read HiFi DNA sequencing which provided high accuracy. Additionally, validation of the functionality of the library was performed by performing six rounds of biopanning against recombinant enhanced green fluorescent protein (EGFP) and mCHERRY proteins which had very different amino acid sequences but similar structure using immunotubes for immobilisation. ELISA was used to determine specificity of each fluorescent protein. As with this study, binding to targets was observed after 4 rounds of biopanning. Individual clones were isolated and a representative anti-mCHERRY and anti-EGFP scFv antibody were assayed for binding using a dot blot. Binding was detected with HRP-conjugated protein-A followed by electrochemiluminescence. Comparing the amino acid sequences obtained against mCHERRY and EGFP with the sequences obtained in this study (anti-TIM-3-Fc and anti-TIM-4 scFv antibodies) also revealed some similarities. For example, the CDR1-VH region in their original phage library consisted of the sequence “FYGMS” and in this study, anti-TIM-3-Fc clones 1, 9, 11, 15, 17, 27 and 30 had a CDR1-VH sequence of “GYGMN”. These same anti-TIM-3-Fc clones had a CDR2-VH sequence of “GINSGGTTGYADAVKG” and the sequence in Lisowska’s study was “GISSDGSSTYYADAVK”. CDR3-VH seemed to be the most variable when comparing the original phage library to the clones identified in this study. CDR1-VL, CDR2-VL and CDR3-VL also shared some sequence similarities between the original phage library and the clones identified against TIM-3 and TIM-4.

In Monda’s research, sanger sequencing of clones biopanned against ZIKV envelope protein revealed clones with the presence of full VL regions but with a very short VH fragment. Only a single clone targeting the ZIKV envelope protein displayed the full scFv with both the VH and VL regions. These anti-ZIKV envelope protein clones showed 4 different amino acid sequences out of the 17 clones sequenced. From clones identified from bio panning against SARS-CoV-2 Spike trimer, all 30 clones sequenced were identical. Of the 28 clones identified from bio panning against SARS-CoV-2 S1 which were sequenced, all had the same sequence.

In a study by Mishima, Nakajima et al. (2021) there was successful development of a novel bispecific antibody against human TIM-3 to simultaneously block the galectin-9 binding site and the

phosphatidylserine binding site on the extracellular domain. Importantly, most anti-TIM-3 antibodies developed so far inhibited phosphatidylserine from binding to the TIM-3 IgV domain which did not prevent galectin-9 from binding to the carbohydrate motifs on the opposite side of the IgV domain. This binding of galectin-9 resulted in cell death of T cells expressing TIM-3 (Kuchroo, Zhu, 2005, Mishima, Nakajima et al. 2021). This antibody was developed through immunisation of mice with purified recombinant human TIM-3 protein and TIM-3 expressing mammalian cell line. Phage display libraries were constructed using complementary (c) DNAs of splenocytes and lymph node cells from the immunized mice. After this, biopanning was performed against recombinant TIM-3 proteins and the highly specific and high affinity scFvs identified were classified by epitope bin and inhibitory effects on TIM-3 binding to multiple ligands. A minimum of 5 classes of antibodies against TIM-3 were generated and each class was grouped into a different epitope bin and had unique inhibitory profiles for multiple TIM-3 ligands. The bispecific antibodies were generated by converting the scFvs to scFv-Fc. TIM-3 binding, inhibition of ligand binding and immune activation were tested, and the bispecific antibodies showed higher affinity and specificity when compared to monospecific antibodies. The galectin-9 and phosphatidylserine blocking antibody revealed significant potency on T cell activation, protection from exhaustion and apoptotic cell death of T cells and even resulted in increased anti-tumour efficacy. This antibody increased the number of IFNγ producing $CD8^+$ T cells by antigen stimulation and promoted TNFα and IFNγ cytokine production (Mishima, Nakajima et al. 2021).

The Sanger sequencing data obtained for the anti-TIM-3-Fc clones isolated in this study provides an opportunity to investigate the potential of the identified scFvs to inhibit the binding of phosphatidylserine to TIM-3, or alternatively, to inhibit the binding of galectin-9. This investigation could be conducted through computational methods, such as antibody-antigen docking software, or through experimental approaches such as competitive ELISAs between the anti-TIM-3-Fc scfv-displaying clones and galectin-9 and phosphatidylserine. It would also be interesting to determine the exact binding site of the anti-TIM-4 phage clone that was sequenced to understand which ligand it would inhibit from binding to the target protein TIM-4.

Furthermore, as previously mentioned, methods such as hydrogen deuterium exchange mass spectrometry could be used to map and compare the binding sites of the identified antibodies. Antibody stability analysis to assess the conformational, colloidal, and chemical stability of the antibodies identified could also be done. Techniques which could be used include nano differential scanning calorimetry, excitation-energy-dependent fluorescence edge-shift analysis, forced degradation studies and real-time stability testing (Knight, Woolley et al. 2020).

Additionally, antibody-antigen docking software would allow for studying of the paratopes of the antibodies identified. This could be used to empirically test the relationship between bit score and statistical significance by comparing the paratope structures of different scFv antibodies identified to the bit score values obtained (Davila, Xu et al. 2022, Desta, Kotelnikov et al. 2023a, Desta, Kotelnikov et al. 2023b, Reis, Barletta et al. 2022).

Another technique which can be used to study the antibody-antigen binding is amplified luminescent proximity homogenous (AlphaLISA) assay which is a bead-based, no-wash luminescent technology used to study biomolecular interactions in a microplate. This assay utilises Alpha Donor and Acceptor beads which are brought together through binding to target. Once the beads are near, there is a cascade of chemical reactions which results in a luminescent signal that can be detected and quantified. AlphaLISA have vast sample compatibility and require only a small sample size. These also offer wide detectable range and scalability (Hunt, Vogeli et al. 2023, Staerz, Lisabth et al. 2023, Waller, Chatterji et al. 2010).

Additional ELISAs which can be performed to build on this study include; polyclonal anti-TIM-4 phage library versus TIM-3-Fc bait and *vice versa* and monoclonal anti-TIM-4 phage clones versus TIM-3-Fc bait and *vice versa*. Furthermore, repetition of sanger sequencing using a forward primer or middle primer targeting the linker sequence can be performed to obtain more full sequences for the clones which were not fully sequenced. This would allow for more comparisons of clones and would allow more investigations into computational antibody-antigen docking.

Furthermore, the scFv antibody-displaying phages isolated through biopanning can be utilized for extraction of the scFvs, enabling their engineering into full length antibodies or other desired antibody

formats. For example, developing scFv-Fc as in the study by Mishima (2021) would retain desirable characteristics of IgG such as bivalency and a longer half-life while offering Fc-mediated effector functions. The scFv-Fc format allows for quick characterization of candidate scFvs before conversion to full-length IgG. The scFv-Fc format can be produced by fusing scFv molecules of the same or different specificity to the N- or C- terminus of the Fc region which enables the engineering of scFvs into full-length antibodies or other desired formats (Bujak, Matasci et al. 2014). IgG1 would be the most suitable choice of IgG isotype to develop the scFvs into since it is the most abundant in human serum and is also well-characterized. It is a common and versatile choice for therapeutic antibody development. Furthermore, IgG1 antibodies are known to produce strong effector functions including ADCC and complement-dependent cytotoxicity. This can be advantageous in therapeutic applications (Vidarsson, Dekkers et al. 2014).

In conclusion, this study successfully identified anti-TIM-3-Fc and anti-TIM-4 monoclonal antibodies which bound specifically towards the target proteins TIM-3 and TIM-4 respectively. Furthermore, the sequencing data indicated that the anti-TIM-3-Fc antibodies developed would not bind to TIM-4 and *vice versa*. Future research on the antibodies identified can lead to the development of new diagnostic tools or antibodies for therapeutic use in detection and treatment of TIM-3 and TIM-4 overexpressing cancers as monotherapy or combination therapy.

References

AGATA, Y., KAWASAKI, A., NISHIMURA, H., ISHIDA, Y., TSUBAT, T., YAGITA, H. and HONJO, T., 1996. Expression of the PD-1 antigen on the surface of stimulated mouse T and B lymphocytes. *International immunology,* **8**(5), pp. 765-772.

AHMAD, Z.A., YEAP, S.K., ALI, A.M., HO, W.Y., ALITHEEN, N.B.M. and HAMID, M., 2012. scFv Antibody: Principles and Clinical Application. *Clinical & developmental immunology,* **2012**, pp. 980250-15.

ALBACKER, L.A., KARISOLA, P., CHANG, Y., UMETSU, S.E., ZHOU, M., AKBARI, O., KOBAYASHI, N., BAUMGARTH, N., FREEMAN, G.J., UMETSU, D.T. and DEKRUYFF, R.H., 2010. TIM-4, a Receptor for Phosphatidylserine, Controls Adaptive Immunity by Regulating the Removal of Antigen-Specific T Cells. *The Journal of immunology (1950),* **185**(11), pp. 6839-6849.

ALCOCK, B.P., HUYNH, W., CHALIL, R., SMITH, K.W., RAPHENYA, A.R., WLODARSKI, M.A., EDALATMAND, A., PETKAU, A., SYED, S.A., TSANG, K.K., BAKER, S.J.C., DAVE, M., MCCARTHY, M.C., MUKIRI, K.M., NASIR, J.A., GOLBON, B., IMTIAZ, H., JIANG, X., KAUR, K., KWONG, M., LIANG, Z.C., NIU, K.C., SHAN, P., YANG, J.Y.J., GRAY, K.L., HOAD, G.R., JIA, B., BHANDO, T., CARFRAE, L.A., FARHA, M.A., FRENCH, S., GORDZEVICH, R., RACHWALSKI, K., TU, M.M., BORDELEAU, E., DOOLEY, D., GRIFFITHS, E., ZUBYK, H.L., BROWN, E.D., MAGUIRE, F., BEIKO, R.G., HSIAO, W.W.L., BRINKMAN, F.S.L., VAN DOMSELAAR, G. and MCARTHUR, A.G., 2023. CARD 2023: expanded curation, support for machine learning, and resistome prediction at the Comprehensive Antibiotic Resistance Database. *Nucleic acids research,* **51**(D1), pp. D690-D699.

ALFALEH, M., ARORA, N., YEH, M., DE BAKKER, C., HOWARD, C., MACPHERSON, P., ALLAVENA, R., CHEN, X., HARKNESS, L., MAHLER, S. and JONES, M., 2019. Canine CD117-Specific Antibodies with Diverse Binding Properties Isolated from a Phage Display Library Using Cell-Based Biopanning. *Antibodies,* **8**(1), pp. 15.

ALFALEH, M., JONES, M., HOWARD, C. and MAHLER, S., 2017. Strategies for Selecting Membrane Protein-Specific Antibodies using Phage Display with Cell-Based Panning. *Antibodies,* **6**(3), pp. 10.

ALFALEH, M.A., ALSAAB, H.O., MAHMOUD, A.B., ALKAYYAL, A.A., JONES, M.L., MAHLER, S.M. and HASHEM, A.M., 2020. Phage Display Derived Monoclonal Antibodies: From Bench to Bedside. Frontiers in immunology, 11, pp. 1986.

ALFTHAN, K., TAKKINEN, K., SIZMANN, D., SÖDERLUND, H. and TEERI, T.T., 1995. Properties of a single-chain antibody containing different linker peptides. Protein engineering, 8(7), pp. 725-731.

ALMO, S.C., SCHWARTZ, J.D., ZHANG, X. and NATHENSON, S.G., 2002. Structural mechanisms of costimulation. *Nature immunology,* **3**(5), pp. 427-434.

ALTSCHUL, S.F., MADDEN, T.L., SCHAFFER, A.A., ZHANG, J.H., ZHANG, Z., MILLER, W. and LIPMAN, D.J., 1997. Gapped BLAST and PSI-BLAST: a new generation of protein database search programs. *Nucleic acids research,* **25**(17), pp. 3389-3402.

ANDERSON, A.C., ANDERSON, D.E., BREGOLI, L., HASTINGS, W.D., KASSAM, N., LEI, C., CHANDWASKAR, R., KARMAN, J., SU, E.W., HIRASHIMA, M., BRUCE, J.N., KANE, L.P., KUCHROO, V.K. and HAFLER, D.A., 2007. Promotion of Tissue Inflammation by the Immune Receptor Tim-3 Expressed on Innate Immune Cells. *Science,* **318**(5853), pp. 1141-1143.

ANDERSON, N.M. and SIMON, M.C., 2020. The tumor microenvironment. *Current biology,* **30**(16), pp. R921-R925.

ANDRÉ, A.S., MOUTINHO, I., DIAS, J.N.R. and AIRES-DA-SILVA, F., 2022. In vivo Phage Display: A promising selection strategy for the improvement of antibody targeting and drug delivery properties. *Frontiers in microbiology,* **13**, pp. 962124.

ANSELL, S.M., LESOKHIN, A.M., BORRELLO, I., HALWANI, A., SCOTT, E.C., GUTIERREZ, M., SCHUSTER, S.J., MILLENSON, M.M., CATTRY, D., FREEMAN, G.J., RODIG, S.J., CHAPUY, B., LIGON, A.H., ZHU, L., GROSSO, J.F., KIM, S.Y., TIMMERMAN, J.M., SHIPP, M.A. and ARMAND, P., 2015. PD-1 Blockade with Nivolumab in Relapsed or Refractory Hodgkin's Lymphoma. *The New England journal of medicine,* **372**(4), pp. 311-319.

ARIMORI, T., KITAGO, Y., UMITSU, M., FUJII, Y., ASAKI, R., TAMURA-KAWAKAMI, K. and TAKAGI, J., 2017. Fv-clasp: An Artificially Designed Small Antibody Fragment with Improved Production Compatibility, Stability, and Crystallizability. Structure (London), 25(10), pp. 1611-1622.e4.

ARNDT, K.M., MÜLLER, K.M. and PLÜCKTHUN, A., 1998. Factors Influencing the Dimer to Monomer Transition of an Antibody Single-Chain Fv Fragment. *Biochemistry (Easton)*, **37**(37), pp. 12918-12926.

ARSLAN, M., KARADAG, M., ONAL, E., GELINCI, E., CAKAN-AKDOGAN, G. and KALYONCU, S., 2022. Effect of non-repetitive linker on in vitro and in vivo properties of an anti-VEGF scFv. *Scientific reports*, **12**(1), pp. 5449.

ASAADI, Y., JOUNEGHANI, F.F., JANANI, S. and RAHBARIZADEH, F., 2021. A comprehensive comparison between camelid nanobodies and single chain variable fragments. Biomarker research, 9(1), pp. 1-87.

BAEK, H., SUK, K., KIM, Y. and CHA, S., 2002. An improved helper phage system for efficient isolation of specific antibody molecules in phage display. *Nucleic acids research*, **30**(5), pp. e18.

BAGHDADI, M., NAGAO, H., YOSHIYAMA, H., AKIBA, H., YAGITA, H., DOSAKA-AKITA, H. and JINUSHI, M., 2013. Combined blockade of TIM-3 and TIM-4 augments cancer vaccine efficacy against established melanomas. *Cancer Immunology, Immunotherapy*, **62**(4), pp. 629-637.

BAGHDADI, M., YONEDA, A., YAMASHINA, T., NAGAO, H., KOMOHARA, Y., NAGAI, S., AKIBA, H., FORETZ, M., YOSHIYAMA, H., KINOSHITA, I., DOSAKA-AKITA, H., TAKEYA, M., VIOLLET, B., YAGITA, H. and JINUSHI, M., 2013a. TIM-4 Glycoprotein-Mediated Degradation of Dying Tumor Cells by Autophagy Leads to Reduced Antigen Presentation and Increased Immune Tolerance. *Immunity*, **39**(6), pp. 1070-1081.

BAI, J., LI, X., TONG, D., SHI, W., SONG, H. and LI, Q., 2013. T-cell immunoglobulin- and mucin-domain-containing molecule 3 gene polymorphisms and prognosis of non-small-cell lung cancer. *Tumor biology*, **34**(2), pp. 805-809.

BARAN, D., PSZOLLA, M.G., LAPIDOTH, G.D., NORN, C., DYM, O., UNGER, T., ALBECK, S., TYKA, M.D. and FLEISHMAN, S.J., 2017. Principles for computational design of binding antibodies. Proceedings of the National Academy of Sciences, 114(41), pp. 10900-10905.

BARBAS III, C.F., BURTON, D.R., SCOTT, J.K., SILVERMAN, G.J., 2001. *Phage display: a laboratory manual : pbk.* Cold Spring Harbor Laboratory Press.

BARBAS, C.F., KANG, A.S., LERNER, R.A. and BENKOVIC, S.J., 1991. Assembly of Combinatorial Antibody Libraries on Phage Surfaces: The Gene III Site. *Proceedings of the National Academy of Sciences - PNAS*, **88**(18), pp. 7978-7982.

BARDERAS, R., DESMET, J., TIMMERMAN, P., MELOEN, R. and CASAL, J.I., 2008. Affinity maturation of antibodies assisted by in silico modeling. *Proceedings of the National Academy of Sciences - PNAS*, **105**(26), pp. 9029-9034.

BARI, M.L. and YEASMIN, S., 2014. WATER QUALITY ASSESSMENT | Modern Microbiological Techniques. Encyclopedia of Food Microbiology. Second Edition edn. Elsevier Ltd, pp. 755-765.

BASS, S., GREENE, R. and WELLS, J.A., 1990. Hormone phage: An enrichment method for variant proteins with altered binding properties. *Proteins, structure, function, and bioinformatics*, **8**(4), pp. 309-314.

BATES, A. and POWER, C.A., 2019. David vs. Goliath: The Structure, Function, and Clinical Prospects of Antibody Fragments. *Antibodies*, **8**(2), pp. 28.

BEIER, K., HUTLOFF, A., DITTRICH, A., HEUCK, C., RAUCH, A., BÜCHNER, K., LUDEWIG, B., OCHS, H., MAGES, H. and KROCZEK, R., 2000. Induction, binding specificity and function of human ICOS. European journal of immunology, 30(12), pp. 3707-3717.

BENFAREMO, D., MANFREDI, L., LUCHETTI, M.M. and GABRIELLI, A., 2018. Musculoskeletal and Rheumatic Diseases Induced by Immune Checkpoint Inhibitors: A Review of the Literature. *Current Drug Safety*, **13**(3), pp. 150-164.

BENNETT, F., LUXENBERG, D., LING, V., WANG, I., MARQUETTE, K., LOWE, D., KHAN, N., VELDMAN, G., JACOBS, K.A., VALGE-ARCHER, V.E., COLLINS, M. and CARRENO, B.M., 2003. Program Death-1 Engagement Upon TCR Activation Has Distinct Effects on Costimulation and Cytokine-Driven Proliferation: Attenuation of ICOS, IL-4, and IL-21, But Not CD28, IL-7, and IL-15 Responses. *The Journal of immunology (1950)*, **170**(2), pp. 711-718.

BERGER, M., SHANKAR, V. and VAFAI, A., 2002. Therapeutic Applications of Monoclonal Antibodies. *The American Journal of the Medical Sciences*, **324**(1), pp. 14-30.

BIE, C., YANG, D., LIANG, X. and TANG, S., 2010. Construction of non-covalent single-chain Fv dimers for hepatocellular carcinoma and their biological functions. *World journal of hepatology*, **2**(5), pp. 185-191.

BLAZEK, D. and CELER, V., 2003. The production and application of single-chain antibody fragments. *Folia microbiologica*, **48**(5), pp. 687-698.

BLAZEK, D., CELER, V., NAVRÁTILOVÁ, I. and SKLÁDAL, P., 2004. Generation and characterization of single-chain antibody fragments specific against transmembrane envelope glycoprotein gp46 of maedi-visna virus. *Journal of virological methods*, **115**(1), pp. 83-92.

BOONTA, S. and BOONTHIEM, S., 2019. Symmetrical Trapezoidal Normal Distribution and its Parameter Estimation. *Annals of Pure and Applied Mathematics*, **20**(1), pp. 35-47.

BRAHMER, J.R., TYKODI, S.S., CHOW, L.Q.M., HWU, W., TOPALIAN, S.L., HWU, P., DRAKE, C.G., CAMACHO, L.H., KAUH, J., ODUNSI, K., PITOT, H.C., HAMID, O., BHATIA, S., MARTINS, R., EATON, K., CHEN, S., SALAY, T.M., ALAPARTHY, S., GROSSO, J.F., KORMAN, A.J., PARKER, S.M., AGRAWAL, S., GOLDBERG, S.M., PARDOLL, D.M., GUPTA, A. and WIGGINTON, J.M., 2012. Safety and Activity of Anti–PD-L1 Antibody in Patients with Advanced Cancer. *The New England journal of medicine*, **366**(26), pp. 2455-2465.

BREITLING, F., DÜBEL, S., SEEHAUS, T., KLEWINGHAUS, I. and LITTLE, M., 1991. A surface expression vector for antibody screening. *Gene*, **104**(2), pp. 147-153.

BRINKMAN, C.C., IWAMI, D., HRITZO, M.K., XIONG, Y., AHMAD, S., SIMON, T., HIPPEN, K.L., BLAZAR, B.R. and BROMBERG, J.S., 2016. Treg engage lymphotoxin beta receptor for afferent lymphatic transendothelial migration. *Nature communications*, **7**(1), pp. 12021.

BRUMMELMAN, J., MAZZA, E.M.C., ALVISI, G., COLOMBO, F.S., GRILLI, A., MIKULAK, J., MAVILIO, D., ALLOISIO, M., FERRARI, F., LOPCI, E., NOVELLIS, P., VERONESI, G. and LUGLI, E., 2018. High-dimensional single cell analysis identifies stem-like cytotoxic CD8+ T cells infiltrating human tumors. *The Journal of Experimental Medicine*, **215**(10), pp. 2520-2535.

BRUNET, J., DENIZOT, F., LUCIANI, M., ROUX-DOSSETO, M., SUZAN, M., MATTEI, M. and GOLSTEIN, P., 1987. A new member of the immunoglobulin superfamily-CTLA-4. *Nature (London)*, **328**(6127), pp. 267-270.

BUJAK, E., MATASCI, M., NERI, D. and WULHFARD, S., 2014. Reformatting of scFv Antibodies into the scFv-Fc Format and Their Downstream Purification. *Methods in molecular biology (Clifton, N.J.).* Totowa, NJ: Humana Press, pp. 315-334.

BUQUÉ, A., BLOY, N., ARANDA, F., CASTOLDI, F., EGGERMONT, A., CREMER, I., FRIDMAN, W.H., FUCIKOVA, J., GALON, J., MARABELLE, A., SPISEK, R., TARTOUR, E., ZITVOGEL, L., KROEMER, G. and GALLUZZI, L., 2015. Trial Watch: Immunomodulatory monoclonal antibodies for oncological indications. *Oncoimmunology,* **4**(4), pp. e1008814.

BUTLER, J.E., NAVARRO, P. and SUN, J., 1997. Adsorption-Induced Antigenic Changes and Their Significance in Elisa and Immunological Disorders. *Immunological investigations,* **26**(1-2), pp. 39-54.

BUTLER, J.E., NI, L., NESSLER, R., JOSHI, K.S., SUTER, M., ROSENBERG, B., CHANG, J., BROWN, W.R. and CANTARERO, L.A., 1992. The physical and functional behavior of capture antibodies adsorbed on polystyrene. *Journal of immunological methods,* **150**(1), pp. 77-90.

BYE, J.W., PLATTS, L. and FALCONER, R.J., 2014. Biopharmaceutical liquid formulation: a review of the science of protein stability and solubility in aqueous environments. *Biotechnology letters,* **36**(5), pp. 869-875.

CAI, C., WANG, L., WU, Z., LI, M., CHEN, W. and SUN, Y., 2012. T-Cell Immunoglobulin- and Mucin-Domain-Containing Molecule 3 Gene Polymorphisms and Renal Cell Carcinoma. *DNA and cell biology,* **31**(7), pp. 1285-1289.

CAO, W., RYAN, M., BUCKLEY, D., O'CONNOR, R. and CLARKSON, M.R., 2011. Tim-4 inhibition of T-cell activation and T helper type 17 differentiation requires both the immunoglobulin V and mucin domains and occurs via the mitogen-activated protein kinase pathway. *Immunology,* **133**(2), pp. 179-189.

CAO, W., RYAN, M., BUCKLEY, D., O'CONNOR, R. and CLARKSON, M.R., 2011. Tim-4 inhibition of T-cell activation and T helper type 17 differentiation requires both the immunoglobulin V and mucin domains and occurs via the mitogen-activated protein kinase pathway. Immunology, 133(2), pp. 179-189.

CAO, X., CAI, S.F., FEHNIGER, T.A., SONG, J., COLLINS, L.I., PIWNICA-WORMS, D.R. and LEY, T.J., 2007. Granzyme B and Perforin Are Important for Regulatory T Cell-Mediated Suppression of Tumor Clearance. *Immunity,* **27**(4), pp. 635-646.

CARONNI, N., PIPERNO, G.M., SIMONCELLO, F., ROMANO, O., VODRET, S., YANAGIHASHI, Y., DRESS, R., DUTERTRE, C., BUGATTI, M., BOURDELEY, P., DEL PRETE, A., SCHIOPPA, T., MAZZA, E.M.C., COLLAVIN, L., ZACCHIGNA, S., OSTUNI, R., GUERMONPREZ, P., VERMI, W., GINHOUX, F., BICCIATO, S., NAGATA, S. and BENVENUTI, F., 2021. TIM4 expression by dendritic cells mediates uptake of tumor-associated antigens and anti-tumor responses. *Nature communications,* **12**(1), pp. 2237.

CARTER, P.J. and LAZAR, G.A., 2018. Next generation antibody drugs: pursuit of the 'high-hanging fruit'. *Nature reviews. Drug discovery,* **17**(3), pp. 197-223.

CHAE, S., PARK, Y., LEE, Y., LEE, J. and CHUNG, H., 2004. The association of TIM-3 gene polymorphism with atopic disease in Korean population. *Human immunology,* **65**(12), pp. 1427-1431.

CHAN, C.E.Z., CHAN, A.H.Y., LIM, A.P.C. and HANSON, B.J., 2011. Comparison of the efficiency of antibody selection from semi-synthetic scFv and non-immune Fab phage display libraries against protein targets for rapid development of diagnostic immunoassays. Journal of Immunological Methods, 373(1-2), pp. 79-88.

CHAUDHARY, B. and ELKORD, E., 2016. Regulatory T Cells in the Tumor Microenvironment and Cancer Progression: Role and Therapeutic Targeting. *Vaccines,* **4**(3), pp. 28.

CHEN, D., HE, J., LU, C., ZHOU, J., FANG, K., LIU, X. and XU, L., 2015. Increased Expression of T Cell Immunoglobulin and Mucin Domain 4 Is Positively Associated with the Disease Severity of Patients with Ankylosing Spondylitis. *Inflammation,* **38**(3), pp. 935-940.

CHEN, L., DONG, H., ZHU, G. and TAMADA, K., 1999. B7-H1, a third member of the B7 family, co-stimulates T-cell proliferation and interleukin-10 secretion. *Nature medicine,* **5**(12), pp. 1365-1369.

CHEN, X., SONG, X., LI, K. and ZHANG, T., 2019. FcγR-Binding Is an Important Functional Attribute for Immune Checkpoint Antibodies in Cancer Immunotherapy. *Frontiers in Immunology,* **10**, pp. 292.

CHEN, X., ZARO, J.L. and SHEN, W., 2013. Fusion protein linkers: Property, design and functionality. *Advanced drug delivery reviews,* **65**(10), pp. 1357-1369.

CHENG, L. and RUAN, Z., 2015. Tim-3 and Tim-4 as the potential targets for antitumor therapy. *Human vaccines & immunotherapeutics,* **11**(10), pp. 2458-2462.

CHENNAMSETTY, N., VOYNOV, V., KAYSER, V., HELK, B. and TROUT, B.L., 2010. Prediction of Aggregation Prone Regions of Therapeutic Proteins. *The journal of physical chemistry. B,* **114**(19), pp. 6614-6624.

CHIBA, S., BAGHDADI, M., AKIBA, H., YOSHIYAMA, H., KINOSHITA, I., DOSAKA-AKITA, H., FUJIOKA, Y., OHBA, Y., GORMAN, J.V., COLGAN, J.D., HIRASHIMA, M., UEDE, T., TAKAOKA, A., YAGITA, H. and JINUSHI, M., 2012a. Tumor-infiltrating DCs suppress nucleic acid–mediated innate immune responses through interactions between the receptor TIM-3 and the alarmin HMGB1. *Nature Immunology,* **13**(9), pp. 832-842.

CHIBA, T., OHTANI, H., SATOMI, S., MIZOI, T., NAITO, Y., SATO, E., NAGURA, H., OHUCHI, A., OHUCHI, K., SHIIBA, K. and KUROKAWA, Y., 2004. Intraepithelial CD8 T-cell-count becomes a prognostic factor after a longer follow-up period in human colorectal carcinoma: possible association with suppression of micrometastasis. *British Journal of Cancer,* **91**(9), pp. 1711-1717.

CHINEN, T., KANNAN, A.K., LEVINE, A.G., FAN, X., KLEIN, U., ZHENG, Y., GASTEIGER, G., FENG, Y., FONTENOT, J.D. and RUDENSKY, A.Y., 2016. An essential role for the IL-2 receptor in Treg cell function. *Nature immunology,* **17**(11), pp. 1322-1333.

CHIU, M.L., GOULET, D.R., TEPLYAKOV, A. and GILLILAND, G.L., 2019. Antibody Structure and Function: The Basis for Engineering Therapeutics. Antibodies, 8(4), pp. 55.

CHRIST, D., LEE, C.M.Y., IORNO, N. and SIERRO, F., 2007. Selection of human antibody fragments by phage display. *Nature protocols,* **2**(11), pp. 3001-3008.

CLACKSON, T., HOOGENBOOM, H.R., GRIFFITHS, A.D. and WINTER, G., 1991. Making antibody fragments using phage display libraries. *Nature (London),* **352**(6336), pp. 624-628.

CLAYTON, K.L., HAALAND, M.S., DOUGLAS-VAIL, M.B., MUJIB, S., CHEW, G.M., NDHLOVU, L.C. and OSTROWSKI, M.A., 2014. T Cell Ig and Mucin Domain–Containing Protein 3 Is Recruited to the Immune Synapse, Disrupts Stable Synapse Formation, and Associates with Receptor Phosphatases. *The Journal of immunology (1950),* **192**(2), pp. 782-791.

CLOUTIER, T.K., SUDRIK, C., MODY, N., HASIGE, S.A. and TROUT, B.L., 2020. Molecular computations of preferential interactions of proline, arginine.HCl, and NaCl with IgG1 antibodies and their impact on aggregation and viscosity. *mAbs*, **12**(1), pp. 1816312.

COLLISON, L.W., WORKMAN, C.J., KUO, T.T., BOYD, K., YAO WANG, VIGNALI, K.M., CROSS, R., SEHY, D., BLUMBERG, R.S. and VIGNALI, D.A.A., 2007. The inhibitory cytokine IL-35 contributes to regulatory T-cell function. *Nature*, **450**(7169), pp. 566-569.

COUTELIER, J., GODFRAIND, C., DVEKSLER, G.S., WYSOCKA, M., CARDELLICHIO, C.B., NOËL, H. and HOLMES, K.V., 1994. B lymphocyte and macrophage expression of carcinoembryonic antigen-related adhesion molecules that serve as receptors for murine coronavirus. *European Journal of Immunology*, **24**(6), pp. 1383-1390.

CURIGLIANO, G., GELDERBLOM, H., MACH, N., DOI, T., TAI, D., FORDE, P.M., SARANTOPOULOS, J., BEDARD, P.L., LIN, C., HODI, F.S., WILGENHOF, S., SANTORO, A., SABATOS-PEYTON, C.A., LONGMIRE, T.A., XYRAFAS, A., SUN, H., GUTZWILLER, S., MANENTI, L. and NAING, A., 2021. Phase I/Ib Clinical Trial of Sabatolimab, an Anti–TIM-3 Antibody, Alone and in Combination with Spartalizumab, an Anti–PD-1 Antibody, in Advanced Solid Tumors. *Clinical cancer research*, **27**(13), pp. 3620-3629.

CURTIN, J.F., LIU, N., CANDOLFI, M., XIONG, W., ASSI, H., YAGIZ, K., EDWARDS, M.R., MICHELSEN, K.S., KROEGER, K.M., LIU, C., MUHAMMAD, A.K.M.G., CLARK, M.C., ARDITI, M., COMIN-ANDUIX, B., RIBAS, A., LOWENSTEIN, P.R. and CASTRO, M.G., 2009. HMGB1 Mediates Endogenous TLR2 Activation and Brain Tumor Regression. *PLoS Medicine*, **6**(1), pp. e10.

CURTSINGER, J.M., LINS, D.C. and MESCHER, M.F., 2003. Signal 3 determines tolerance versus full activation of naive CD8 T cells: dissociating proliferation and development of effector function. The Journal of experimental medicine, 197(9), pp. 1141-1151.

CURTSINGER, J.M., SCHMIDT, C.S., MONDINO, A., LINS, D.C., KEDL, R.M., JENKINS, M.K. and MESCHER, M.F., 1999. Inflammatory Cytokines Provide a Third Signal for Activation of Naive CD4+ and CD8+ T Cells. *The Journal of immunology (1950)*, **162**(6), pp. 3256-3262.

D'ANGELO, S., FERRARA, F., NARANJO, L., ERASMUS, M.F., HRABER, P. and BRADBURY, A.R.M., 2018. Many Routes to an Antibody Heavy-Chain CDR3: Necessary, Yet Insufficient, for Specific Binding. Frontiers in Immunology, 9, pp. 395.

DANTAS-BARBOSA, C., DE MACEDO BRIGIDO, M. and MARANHAO, A.Q., 2012. Antibody Phage Display Libraries: Contributions to Oncology. *International Journal of Molecular Sciences,* **13(**5), pp. 5420-5440.

DAS, S. and JOHNSON, D.B., 2019. Immune-related adverse events and anti-tumor efficacy of immune checkpoint inhibitors. *Journal for ImmunoTherapy of Cancer,* **7**(1), pp. 306.

DAVIDSON, D., SCHRAVEN, B. and VEILLETTE, A., 2007. PAG-Associated FynT Regulates Calcium Signaling and Promotes Anergy in T Lymphocytes. *Molecular and Cellular Biology,* **27**(5), pp. 1960-1973.

DAVILA, A., XU, Z., LI, S., ROZEWICKI, J., WILAMOWSKI, J., KOTELNIKOV, S., KOZAKOV, D., TERAGUCHI, S. and STANDLEY, D.M., 2022. AbAdapt: an adaptive approach to predicting antibody–antigen complex structures from sequence. *Bioinformatics advances,* **2**(1), pp. vbac015.

DE SOUSA LINHARES, A., KELLNER, F., JUTZ, S., ZLABINGER, G.J., GABIUS, H., HUPPA, J.B., LEITNER, J. and STEINBERGER, P., 2020. TIM-3 and CEACAM1 do not interact in cis and in trans. European journal of immunology, 50(8), pp. 1126-1141.

DE SOUSA LINHARES, A., LEITNER, J., GRABMEIER-PFISTERSHAMMER, K. and STEINBERGER, P., 2018. Not All Immune Checkpoints Are Created Equal. *Frontiers in Immunology*, **9**, pp. 1909.

DESTA, I.T., KOTELNIKOV, S., JONES, G., GHANI, U., ABYZOV, M., KHOLODOV, Y., STANDLEY, D.M., BEGLOV, D., VAJDA, S. and KOZAKOV, D., 2023b. The ClusPro AbEMap web server for the prediction of antibody epitopes. *Nature protocols,* **18**(6), pp. 1814-1840.

DESTA, I.T., KOTELNIKOV, S., JONES, G., GHANI, U., ABYZOV, M., KHOLODOV, Y., STANDLEY, D.M., SABITOVA, M., BEGLOV, D., VAJDA, S. and KOZAKOV, D., 2023a. Mapping of antibody epitopes based on docking and homology modeling. *Proteins, structure, function, and bioinformatics,* **91**(2), pp. 171-182.

DEISS, T.C., VADNAIS, M., WANG, F., CHEN, P.L., TORKAMANI, A., MWANGI, W., LEFRANC, M., CRISCITIELLO, M.F. and SMIDER, V.V., 2019. Immunogenetic factors driving formation of ultralong VH CDR3 in Bos taurus antibodies. Cellular & molecular immunology, 16(1), pp. 53-64.

DEKOSKY, B.J., IPPOLITO, G.C., DESCHNER, R.P., LAVINDER, J.J., WINE, Y., RAWLINGS, B.M., VARADARAJAN, N., GIESECKE, C., DÖRNER, T., ANDREWS, S.F., WILSON, P.C., HUNICKE-SMITH, S.P., WILLSON, C.G., ELLINGTON, A.D. and GEORGIOU, G., 2013. High-throughput sequencing of the paired human immunoglobulin heavy and light chain repertoire. *Nature biotechnology*, **31**(2), pp. 166-169.

DEKRUYFF, R.H., BU, X., BALLESTEROS, A., SANTIAGO, C., CHIM, Y.E., LEE, H., KARISOLA, P., PICHAVANT, M., KAPLAN, G.G., UMETSU, D.T., FREEMAN, G.J. and CASASNOVAS, J.M., 2010. T Cell/Transmembrane, Ig, and Mucin-3 Allelic Variants Differentially Recognize Phosphatidylserine and Mediate Phagocytosis of Apoptotic Cells. *The Journal of immunology (1950)*, **184**(4), pp. 1918-1930.

DELEEUW, R.J., KOST, S.E., KAKAL, J.A. and NELSON, B.H., 2012. The Prognostic Value of FoxP3+ Tumor-Infiltrating Lymphocytes in Cancer: A Critical Review of the Literature. *Clinical cancer research*, **18**(11), pp. 3022-3029.

DERDA, R., MUSAH, S., ORNER, B.P., KLIM, J.R., LI, L. and KIESSLING, L.L., 2010. High-Throughput Discovery of Synthetic Surfaces That Support Proliferation of Pluripotent Cells. *Journal of the American Chemical Society*, **132**(4), pp. 1289-1295.

DERDA, R., TANG, S.K.Y., LI, S.C., NG, S., MATOCHKO, W. and JAFARI, M.R., 2011. Diversity of Phage-Displayed Libraries of Peptides during Panning and Amplification. *Molecules*, **16**(2), pp. 1776-1803.

DERDA, R., WHERRITT, D.J. and KIESSLING, L.L., 2007. Solid-Phase Synthesis of Alkanethiols for the Preparation of Self-Assembled Monolayers. *Langmuir*, **23**(22), pp. 11164-11167.

DHATCHINAMOORTHY, K., COLBERT, J.D. and ROCK, K.L., 2021. Cancer Immune Evasion Through Loss of MHC Class I Antigen Presentation. *Frontiers in immunology*, **12**, pp. 636568.

DIXON, K.O., DAS, M. and KUCHROO, V.K., 2018. Human disease mutations highlight the inhibitory function of TIM-3. *Nature genetics*, **50**(12), pp. 1640-1641.

DOBSON, C.L., DEVINE, P.W.A., PHILLIPS, J.J., HIGAZI, D.R., LLOYD, C., POPOVIC, B., ARNOLD, J., BUCHANAN, A., LEWIS, A., GOODMAN, J., VAN DER WALLE, C.F., THORNTON, P., VINALL, L., LOWNE, D., AAGAARD, A., OLSSON, L., RIDDERSTAD WOLLBERG, A., WELSH, F., KARAMANOS, T.K., PASHLEY, C.L., IADANZA, M.G., RANSON, N.A., ASHCROFT, A.E., KIPPEN,

A.D., VAUGHAN, T.J., RADFORD, S.E. and LOWE, D.C., 2016. Engineering the surface properties of a human monoclonal antibody prevents self-association and rapid clearance in vivo. *Scientific Reports,* **6**(1), pp. 38644.

DONG, C., DAVIS, R.J. and FLAVELL, R.A., 2002. MAP KINASES IN THE IMMUNE RESPONSE. *Annual review of immunology,* **20**(1), pp. 55-72.

DORFMAN, DAVID M., MD, PHD, HORNICK, JASON L., MD, PHD, SHAHSAFAEI, A., MS and FREEMAN, G.J., PhD, 2010. The phosphatidylserine receptors, T cell immunoglobulin mucin proteins 3 and 4, are markers of histiocytic sarcoma and other histiocytic and dendritic cell neoplasms. *Human pathology,* **41**(10), pp. 1486-1494.

DUESBERG, P.H. and VOGT, P.K., 1979. Avian acute leukemia viruses MC29 and MH2 share specific RNA sequences: Evidence for a second class of transforming genes. *Proceedings of the National Academy of Sciences - PNAS,* **76**(4), pp. 1633-1637.

DUPAGE, M., CHEUNG, A.F., MAZUMDAR, C., WINSLOW, M.M., BRONSON, R., SCHMIDT, L.M., CROWLEY, D., CHEN, J. and JACKS, T., 2011. Endogenous T Cell Responses to Antigens Expressed in Lung Adenocarcinomas Delay Malignant Tumor Progression. *Cancer Cell,* **19**(1), pp. 72-85.

DUPAGE, M., MAZUMDAR, C., SCHMIDT, L.M., CHEUNG, A.F. and JACKS, T., 2012. Expression of tumour-specific antigens underlies cancer immunoediting. *Nature,* **482**(7385), pp. 405-409.

Dynabeads™ His-Tag Isolation & Pulldown package insert, Publication No. MAN0017121. Invitrogen, California, United States, 5/17. Accessed: 26/9/2023. [Online]. Available: https://tools.thermofisher.com/content/sfs/manuals/DynabeadsHisTagIsolationPulldown_man.pdf

Dynabeads™ Protein G package insert, Publication No. MAN0015809. Invitrogen, California, United States, 3/16. Accessed 28/9/2023. [Online]. Available: https://www.veritastk.co.jp/products/pdf/100.03D04D_Dynabeads_Protein_G_%28rev005%29.pdf

EISENHARDT, S.U., SCHWARZ, M., BASSLER, N. and PETER, K., 2007. Subtractive single-chain antibody (scFv) phage-display: tailoring phage-display for high specificity against function-specific conformations of cell membrane molecules. *Nature protocols,* **2**(12), pp. 3063-3073.

EISENHARDT, S.U., SCHWARZ, M., SCHALLNER, N., SOOSAIRAJAH, J., BASSLER, N., HUANG, D., BODE, C. and PETER, K., 2007. Generation of activation-specific human anti-alphaMbeta2 single-chain antibodies as potential diagnostic tools and therapeutic agents. *Blood,* **109**(8), pp. 3521-3528.

EVAN, G.I., LEWIS, G.K., RAMSAY, G. and BISHOP, J.M., 1985. Isolation of monoclonal antibodies specific for human c-myc proto-oncogene product. *Molecular and Cellular Biology,* **5**(12), pp. 3610-3616.

FACCIABENE, A., MOTZ, G.T. and COUKOS, G., 2012. T-Regulatory Cells: Key Players in Tumor Immune Escape and Angiogenesis. *Cancer research (Chicago, Ill.),* **72**(9), pp. 2162-2171.

FELLOUSE, F.A., ESAKI, K., BIRTALAN, S., RAPTIS, D., CANCASCI, V.J., KOIDE, A., JHURANI, P., VASSER, M., WIESMANN, C., KOSSIAKOFF, A.A., KOIDE, S. and SIDHU, S.S., 2007. High-throughput Generation of Synthetic Antibodies from Highly Functional Minimalist Phage-displayed Libraries. *Journal of molecular biology,* **373**(4), pp. 924-940.

FENG, BAI-SUI, MD, PHD, CHEN, X., MD, HE, SHAO-HENG, MD, PHD, ZHENG, PENG-YUAN, MD, PHD, FOSTER, J., PhD, XING, ZHOU, MD, PHD, BIENENSTOCK, J., MD and YANG, PING-CHANG, MD, PHD, 2008. Disruption of T-cell immunoglobulin and mucin domain molecule (TIM)–1/TIM4 interaction as a therapeutic strategy in a dendritic cell–induced peanut allergy model. *Journal of allergy and clinical immunology,* **122**(1), pp. 55-61.e7.

FISHER, D.T., APPENHEIMER, M.M. and EVANS, S.S., 2014. The two faces of IL-6 in the tumor microenvironment. *Seminars in immunology,* **26**(1), pp. 38-47.

FONTENOT, J.D., RASMUSSEN, J.P., WILLIAMS, L.M., DOOLEY, J.L., FARR, A.G. and RUDENSKY, A.Y., 2005. Regulatory T Cell Lineage Specification by the Forkhead Transcription Factor Foxp3. *Immunity,* **22**(3), pp. 329-341.

FOURCADE, J., SUN, Z., BENALLAOUA, M., GUILLAUME, P., LUESCHER, I.F., SANDER, C., KIRKWOOD, J.M., KUCHROO, V. and ZAROUR, H.M., 2010. Upregulation of Tim-3 and PD-1 expression is associated with tumor antigen–specific CD8+ T cell dysfunction in melanoma patients. *The Journal of experimental medicine,* **207**(10), pp. 2175-2186.

FOURCADE, J., ZHAOJUN SUN, HONG WANG, GUILLAUME, P., LUESCHER, I.F., KRIEG, A., ANDERSON, A.C., KUCHROO, V.K., ZAROUR, H.M., PAGLIANO, O., CHAUVIN, J., SANDER, C., JANJIC, B.,

TARHINI, A.A., TAWBI, H.A., KIRKWOOD, J.M. and MOSCHOS, S., 2014. PD-1 and Tim-3 Regulate the Expansion of Tumor Antigen–Specific CD8+ T Cells Induced by Melanoma Vaccines. *Cancer research (Chicago, Ill.)*, **74**(4), pp. 1045-1055.

FRANZIN, R., NETTI, G.S., SPADACCINO, F., PORTA, C., GESUALDO, L., STALLONE, G., CASTELLANO, G. and RANIERI, E., 2020. The Use of Immune Checkpoint Inhibitors in Oncology and the Occurrence of AKI: Where Do We Stand? *Frontiers in immunology*, **11**, pp. 574271.

FREEMAN, G.J., CASASNOVAS, J.M., UMETSU, D.T. and DEKRUYFF, R.H., 2010. TIM genes: a family of cell surface phosphatidylserine receptors that regulate innate and adaptive immunity. *Immunological reviews*, **235**(1), pp. 172-189.

FREEMAN, G.J., LATCHMAN, Y., WOOD, C.R., CHERNOVA, T., CHAUDHARY, D., BORDE, M., CHERNOVA, I., IWAI, Y., LONG, A.J., BROWN, J.A., NUNES, R., GREENFIELD, E.A., BOURQUE, K., BOUSSIOTIS, V.A., CARTER, L.L., CARRENO, B.M., MALENKOVICH, N., NISHIMURA, H., OKAZAKI, T., HONJO, T. and SHARPE, A.H., 2001. PD-L2 is a second ligand for PD-1 and inhibits T cell activation. *Nature immunology*, **2**(3), pp. 261-268.

FRENZEL, A., SCHIRRMANN, T. and HUST, M., 2016. Phage display-derived human antibodies in clinical development and therapy. mAbs, 8(7), pp. 1177-1194.

FRIEDLAENDER, A., ADDEO, A. and BANNA, G., 2019. New emerging targets in cancer immunotherapy: the role of TIM3. ESMO Open, 4(Suppl 3), pp. e000497.

FU, H., KISHORE, M., GITTENS, B., WANG, G., COE, D., KOMAROWSKA, I., INFANTE, E., RIDLEY, A.J., COOPER, D., PERRETTI, M. and MARELLI-BERG, F.M., 2014. Self-recognition of the endothelium enables regulatory T-cell trafficking and defines the kinetics of immune regulation. *Nature Communications*, **5**(1), pp. 3436.

FUKUNAGA, A. and TSUMOTO, K., 2013. Improving the affinity of an antibody for its antigen via long-range electrostatic interactions. *Protein engineering, design and selection*, **26**(12), pp. 773-780.

FUNFROCK, P. 2020, Why phage display for monoclonal antibody production remains an unrivaled technology [ProteoBlog], [Online]. Available: https://www.proteogenix.science/scientific-corner/antibody-production/phage-display-for-monoclonal-antibody-production/ [Feb 17, 2023].

GALON, J., COSTES, A., SANCHEZ-CABO, F., KIRILOVSKY, A., MLECNIK, B., LAGORCE-PAGÈS, C., TOSOLINI, M., CAMUS, M., BERGER, A., WIND, P., ZINZINDOHOUÉ, F., BRUNEVAL, P., CUGNENC, P., TRAJANOSKI, Z., FRIDMAN, W. and PAGÈS, F., 2006. Type, Density, and Location of Immune Cells Within Human Colorectal Tumors Predict Clinical Outcome. *Science,* **313**(5795), pp. 1960-1964.

GANDHI, A.K., KIM, W.M., SUN, Z.J., HUANG, Y., BONSOR, D.A., SUNDBERG, E.J., KONDO, Y., WAGNER, G., KUCHROO, V.K., PETSKO, G. and BLUMBERG, R.S., 2018. High resolution X-ray and NMR structural study of human T-cell immunoglobulin and mucin domain containing protein-3. *Scientific Reports,* **8**(1), pp. 17512-13.

GAO, X., YANG, J., HE, Y. and ZHANG, J., 2016. Quantitative assessment of TIM-3 polymorphisms and cancer risk in Chinese Han population. *Oncotarget,* **7**(24), pp. 35768-35775.

GAO, X., ZHU, Y., LI, G., HUANG, H., ZHANG, G., WANG, F., SUN, J., YANG, Q., ZHANG, X. and LU, B., 2012. TIM-3 Expression Characterizes Regulatory T Cells in Tumor Tissues and Is Associated with Lung Cancer Progression. *PLoS ONE,* **7**(2), pp. e30676.

GARIDEL, P., KUHN, A.B., SCHÄFER, L.V., KAROW-ZWICK, A.R. and BLECH, M., 2017. High-concentration protein formulations: How high is high? *European journal of pharmaceutics and biopharmaceutics,* **119**, pp. 353-360.

GAYDEN, T., SEPULVEDA, F.E., KHUONG-QUANG, D., PRATT, J., VALERA, E.T., GARRIGUE, A., KELSO, S., SICHERI, F., MIKAEL, L.G., HAMEL, N., BAJIC, A., DALI, R., DESHMUKH, S., DERVOVIC, D., SCHRAMEK, D., GUERIN, F., TAIPALE, M., NIKBAKHT, H., MAJEWSKI, J., MOSHOUS, D., CHARLEBOIS, J., ABISH, S., BOLE-FEYSOT, C., NITSCHKE, P., BADER-MEUNIER, B., MITCHELL, D., THIEBLEMONT, C., BATTISTELLA, M., GRAVEL, S., NGUYEN, V., CONYERS, R., DIANA, J., MCCORMACK, C., PRINCE, H.M., BESNARD, M., BLANCHE, S., EKERT, P.G., FRAITAG, S., FOULKES, W.D., FISCHER, A., NEVEN, B., MICHONNEAU, D., DE SAINT BASILE, G. and JABADO, N., 2018. Germline HAVCR2 mutations altering TIM-3 characterize subcutaneous panniculitis-like T cell lymphomas with hemophagocytic lymphohistiocytic syndrome. *Nature genetics,* **50**(12), pp. 1650-1657.

GE, R., ZENG, L., MO, L., XU, L., ZHANG, H., YU, H., ZHANG, M., LIU, Z., LIU, Z. and YANG, P., 2016. Interaction of TIM4 and TIM3 induces T helper 1 cell apoptosis. *Immunologic research,* **64**(2), pp. 470-475.

GEORGIOS KARAGKOUNIS, July 7, 2022-last update, What does the rectal cancer trial's 100% remission rate mean for young patients?. Available: https://utswmed.org/medblog/rectal-cancer-cure/#:~:text=Colorectal%20cancer%20diagnoses%20are%20increasing,specific%20form%20of%20rectal%20cancer [19/01/, 2023].

GIBSON, T.J., MCCARTY, K., MCFADYEN, I.J., CASH, E., DALMONTE, P., HINDS, K.D., DINERMAN, A.A., ALVAREZ, J.C. and VOLKIN, D.B., 2011. Application of a High-Throughput Screening Procedure with PEG-Induced Precipitation to Compare Relative Protein Solubility During Formulation Development with IgG1 Monoclonal Antibodies. *Journal of pharmaceutical sciences,* **100**(3), pp. 1009-1021.

GOLDEN-MASON, L. and ROSEN, H.R., 2017. Galectin-9: Diverse roles in hepatic immune homeostasis and inflammation. *Hepatology (Baltimore, Md.),* **66**(1), pp. 271-279.

GONÇALVES SILVA, I., YASINSKA, I.M., SAKHNEVYCH, S.S., FIEDLER, W., WELLBROCK, J., BARDELLI, M., VARANI, L., HUSSAIN, R., SILIGARDI, G., CECCONE, G., BERGER, S.M., USHKARYOV, Y.A., GIBBS, B.F., FASLER-KAN, E. and SUMBAYEV, V.V., 2017. The Tim-3-galectin-9 Secretory Pathway is Involved in the Immune Escape of Human Acute Myeloid Leukemia Cells. *EBioMedicine,* **22**(C), pp. 44-57.

GRIMA, M. 2022. Development of Recombinant Antibodies Targeting T Cell Co-Inhibitory Protein TIM-3. BSc Thesis, Malta: University of Malta.

GRIVENNIKOV, S.I., GRETEN, F.R. and KARIN, M., 2010. Immunity, Inflammation, and Cancer. Cell (Cambridge), 140(6), pp. 883-899.

GÜL, N., BABES, L., SIEGMUND, K., KORTHOUWER, R., BÖGELS, M., BRASTER, R., VIDARSSON, G., TEN HAGEN, T.L.M., KUBES, P. and VAN EGMOND, M., 2014. Macrophages eliminate circulating tumor cells after monoclonal antibody therapy. *The Journal of clinical investigation,* **124**(2), pp. 812-823.

GUTTMAN, M., PADTE, N.N., HUANG, Y., YU, J., ROCKLIN, G.J., WEITZNER, B.D., SCIAN, M., HO, D.D. and LEE, K.K., 2020. The influence of proline isomerization on potency and stability of anti-HIV antibody 10E8. *Scientific reports,* **10**(1), pp. 14313.

HAMMERS, C.M. and STANLEY, J.R., 2014. Antibody Phage Display: Technique and Applications. *Journal of Investigative Dermatology*, **134**(2), pp. 1-5.

HANAHAN, D. and WEINBERG, R., 2011. Hallmarks of Cancer: The Next Generation. Cell (Cambridge), 144(5), pp. 646-674.

HANSEN, J.A., HANASH, S.M., TABELLINI, L., BAIK, C., LAWLER, R.L., GROGAN, B.M., STORER, B., CHIN, A., JOHNSON, M., WONG, C., ZHANG, Q., MARTIN, P.J. and MCDONALD, G.B., 2013. A Novel Soluble Form of Tim-3 Associated with Severe Graft-versus-Host Disease. *Biology of Blood and Marrow Transplantation*, **19**(9), pp. 1323-1330.

HAQUE, A. and TONKS, N.K., 2012. The use of phage display to generate conformation-sensor recombinant antibodies. *Nature protocols*, **7**(12), pp. 2127-2143.

HARDING, F.A., MCARTHUR, J.G., GROSS, J.A., RAULET, D.H. and ALLISON, J.P., 1992. CD28-mediated signalling co-stimulates murine T cells and prevents induction of anergy in T-cell clones. Nature (London), 356(6370), pp. 607-609.

HARDING, J.J., MORENO, V., BANG, Y., HONG, M.H., PATNAIK, A., TRIGO, J., SZPURKA, A.M., YAMAMOTO, N., DOI, T., FU, S., CALDERON, B., VELEZ DE MENDIZABAL, N., CALVO, E., YU, D., GANDHI, L., LIU, Z.T., GALVAO, V.R., LEOW, C.C. and DE MIGUEL, M.J., 2021. Blocking TIM-3 in Treatment-refractory Advanced Solid Tumors: A Phase Ia/b Study of LY3321367 with or without an Anti-PD-L1 Antibody. *Clinical cancer research*, **27**(8), pp. 2168-2178.

HASHIMOTO, M., KAMPHORST, A.O., IM, S.J., KISSICK, H.T., PILLAI, R.N., RAMALINGAM, S.S., ARAKI, K. and AHMED, R., 2018. CD8 T Cell Exhaustion in Chronic Infection and Cancer: Opportunities for Interventions. *Annual review of medicine*, **69**(1), pp. 301-318.

HATHCOCK, K.S., LASZLO, G., PUCILLO, C., LINSLEY, P. and HODES, R.J., 1994. Comparative analysis of B7-1 and B7-2 costimulatory ligands: expression and function. The Journal of Experimental Medicine, 180(2), pp. 631-640.

HATIC, H., SAMPAT, D. and GOYAL, G., 2021. Immune checkpoint inhibitors in lymphoma: challenges and opportunities. *Annals of translational medicine*, **9**(12), pp. 1037.

HAUBNER, S., PERNA, F., KÖHNKE, T., SCHMIDT, C., BERMAN, S., AUGSBERGER, C., SCHNORFEIL, F.M., KRUPKA, C., LICHTENEGGER, F.S., LIU, X., KERBS, P., SCHNEIDER, S., METZELER, K.H., SPIEKERMANN, K., HIDDEMANN, W., GREIF, P.A., HEROLD, T., SADELAIN, M. and SUBKLEWE, M., 2019. Coexpression profile of leukemic stem cell markers for combinatorial targeted therapy in AML. *Leukemia,* **33**(1), pp. 64-74.

HAVEL, J.J., CHOWELL, D. and CHAN, T.A., 2019. The evolving landscape of biomarkers for checkpoint inhibitor immunotherapy. *Nature reviews. Cancer,* **19**(3), pp. 133-150.

HEATH, W.R. and CARBONE, F.R., 2001a. Cross-presentation in viral immunity and self-tolerance. *Nature reviews. Immunology,* **1**(2), pp. 126-134.

HEATH, W.R. and CARBONE, F.R., 2001b. CROSS-PRESENTATION, DENDRITIC CELLS, TOLERANCE AND IMMUNITY. *Annual review of immunology,* **19**(1), pp. 47-64.

HELLMANN, M.D., BIVI, N., CALDERON, B., SHIMIZU, T., DELAFONTAINE, B., LIU, Z.T., SZPURKA, A.M., COPELAND, V., HODI, F.S., ROTTEY, S., AFTIMOS, P., PIAO, Y., GANDHI, L., GALVAO, V.R., LEOW, C.C. and DOI, T., 2021. Safety and Immunogenicity of LY3415244, a Bispecific Antibody Against TIM-3 and PD-L1, in Patients With Advanced Solid Tumors. *Clinical cancer research,* **27**(10), pp. 2773-2781.

HERNÁNDEZ, J., AUNG, S., MARQUARDT, K. and SHERMAN, L.A., 2002. Uncoupling of Proliferative Potential and Gain of Effector Function by CD8+ T Cells Responding to Self-Antigens. *The Journal of Experimental Medicine,* **196**(3), pp. 323-333.

HO, J., TUMKAYA, T., ARYAL, S., CHOI, H. and CLARIDGE-CHANG, A., 2019. Moving beyond P values: data analysis with estimation graphics. Nature methods, 16(7), pp. 565-566.

HOLLINGSWORTH, S.A. and KARPLUS, P.A., 2010. A fresh look at the Ramachandran plot and the occurrence of standard structures in proteins. *Biomolecular concepts,* **1**(3-4), pp. 271-283.

HORI, S., NOMURA, T. and SAKAGUCHI, S., 2017. Pillars Article: Control of Regulatory T Cell Development by the Transcription Factor Foxp3. Science 2003. 299: 1057-1061. *The Journal of immunology (1950),* **198**(3), pp. 981-985.

HORST, A.K., BICKERT, T., BREWIG, N., LUDEWIG, P., VAN ROOIJEN, N., SCHUMACHER, U., BEAUCHEMIN, N., ITO, W.D., FLEISCHER, B., WAGENER, C. and RITTER, U., 2009. CEACAM1+ myeloid cells control angiogenesis in inflammation. *Blood,* **113**(26), pp. 6726-6736.

HÖTZEL, I., THEIL, F., BERNSTEIN, L.J., PRABHU, S., DENG, R., QUINTANA, L., LUTMAN, J., SIBIA, R., CHAN, P., BUMBACA, D., FIELDER, P., CARTER, P.J. and KELLEY, R.F., 2012. A strategy for risk mitigation of antibodies with fast clearance. *mAbs,* **4**(6), pp. 753-760.

HUANG, J.X., BISHOP-HURLEY, S.L. and COOPER, M.A., 2012. Development of Anti-Infectives Using Phage Display: Biological Agents against Bacteria, Viruses, and Parasites. *Antimicrobial Agents and Chemotherapy,* **56**(9), pp. 4569-4582.

HUANG, Y., ZHU, C., KONDO, Y., ANDERSON, A.C., GANDHI, A., RUSSELL, A., DOUGAN, S.K., PETERSEN, B., MELUM, E., PERTEL, T., CLAYTON, K.L., RAAB, M., CHEN, Q., BEAUCHEMIN, N., YAZAKI, P.J., PYZIK, M., OSTROWSKI, M.A., GLICKMAN, J.N., RUDD, C.E., PLOEGH, H.L., FRANKE, A., PETSKO, G.A., KUCHROO, V.K. and BLUMBERG, R.S., 2015. CEACAM1 regulates TIM-3-mediated tolerance and exhaustion. *Nature (London),* **517**(7534), pp. 386-390.

Human TIM4 / TIMD4 Protein (His Tag) Package Insert. Sino Biological Inc., Beijing, China. Accessed 13/10/2023. [Online]. Available: https://cdn1.sinobiological.com/reagent/12161-H08H.pdf

IM, S.J., HASHIMOTO, M., GERNER, M.Y., LEE, J., KISSICK, H.T., BURGER, M.C., SHAN, Q., HALE, J.S., LEE, J., NASTI, T.H., SHARPE, A.H., FREEMAN, G.J., GERMAIN, R.N., NAKAYA, H.I., XUE, H. and AHMED, R., 2016. Defining CD8+ T cells that provide the proliferative burst after PD-1 therapy. *Nature (London),* **537**(7620), pp. 417-421.

JAIN, T., SUN, T., DURAND, S., HALL, A., HOUSTON, N.R., NETT, J.H., SHARKEY, B., BOBROWICZ, B., CAFFRY, I., YU, Y., CAO, Y., LYNAUGH, H., BROWN, M., BARUAH, H., GRAY, L.T., KRAULAND, E.M., XU, Y., VÁSQUEZ, M. and WITTRUP, K.D., 2017. Biophysical properties of the clinical-stage antibody landscape. *Proceedings of the National Academy of Sciences - PNAS,* **114**(5), pp. 944-949.

JAN, M., CHAO, M.P., CHA, A.C., ALIZADEH, A.A., GENTLES, A.J., WEISSMAN, I.L. and MAJETI, R., 2011. Prospective separation of normal and leukemic stem cells based on differential expression of TIM3, a human acute myeloid leukemia stem cell marker. *Proceedings of the National Academy of Sciences - PNAS,* **108**(12), pp. 5009-5014.

JAROSZEWICZ, W., MORCINEK-ORŁOWSKA, J., PIERZYNOWSKA, K., GAFFKE, L. and WĘGRZYN, G., 2022. Phage display and other peptide display technologies. *FEMS microbiology reviews,* **46**(2),.

JENKINS, M.K., TAYLOR, P.S., NORTON, S.D. and URDAHL, K.B., 1991. CD28 delivers a costimulatory signal involved in antigen-specific IL-2 production by human T cells. The Journal of immunology (1950), 147(8), pp. 2461-2466.

JENKINS, R.W., BARBIE, D.A. and FLAHERTY, K.T., 2018. Mechanisms of resistance to immune checkpoint inhibitors. *British journal of cancer,* **118**(1), pp. 9-16.

JIANG, R., JIANG, Y., XIA, P., LUO, G., HUANG, W., HU, Z., CHENG, G., XIONG, Y., WANG, Y. and CUI, T., 2019. Cigarette Smoke Extract Promotes TIM4 Expression in Murine Dendritic Cells Leading to Th2 Polarization through ERK-Dependent Pathways. *International archives of allergy and immunology,* **178**(3), pp. 219-228.

JIN, H., ANDERSON, A.C., TAN, W.G., WEST, E.E., HA, S., ARAKI, K., FREEMAN, G.J., KUCHROO, V.K. and AHMED, R., 2010. Cooperation of Tim-3 and PD-1 in CD8 T-cell exhaustion during chronic viral infection. *Proceedings of the National Academy of Sciences - PNAS,* **107**(33), pp. 14733-14738.

JONES, M.L., ALFALEH, M.A., KUMBLE, S., ZHANG, S., OSBORNE, G.W., YEH, M., ARORA, N., HOU, J.J.C., HOWARD, C.B., CHIN, D.Y. and MAHLER, S.M., 2016. Targeting membrane proteins for antibody discovery using phage display. *Scientific Reports,* **6**(1), pp. 26240.

JONES, P.T., DEAR, P.H., FOOTE, J., NEUBERGER, M.S. and WINTER, G., 1986. Replacing the complementarity-determining regions in a human antibody with those from a mouse. *Nature (London),* **321**(6069), pp. 522-525.

JOSEFOWICZ, S.Z., LU, L. and RUDENSKY, A.Y., 2012. Regulatory T Cells: Mechanisms of Differentiation and Function. *Annual review of immunology,* **30**(1), pp. 531-564.

JOYCE, J.A. and POLLARD, J.W., 2009. Microenvironmental regulation of metastasis. Nature reviews. Cancer, 9(4), pp. 239-252.

JU, Y., SHANG, X., LIU, Z., ZHANG, J., LI, Y., SHEN, Y., LIU, Y., LIU, C., LIU, B., XU, L., WANG, Y., ZHANG, B. and ZOU, J., 2014. The Tim-3/galectin-9 pathway involves in the homeostasis of hepatic Tregs in a mouse model of concanavalin A-induced hepatitis. *Molecular immunology,* **58**(1), pp. 85-91.

KAMMERER, R., STOBER, D., SINGER, B.B., OBRINK, B. and REIMANN, J., 2001. Carcinoembryonic Antigen-Related Cell Adhesion Molecule 1 on Murine Dendritic Cells Is a Potent Regulator of T Cell Stimulation. *The Journal of immunology (1950),* **166**(11), pp. 6537-6544.

KANG, A.S., BARBAS, C.F., JANDA, K.D., BENKOVIC, S.J. and LERNER, R.A., 1991. Linkage of Recognition and Replication Functions by Assembling Combinatorial Antibody Fab Libraries Along Phage Surfaces. *Proceedings of the National Academy of Sciences - PNAS,* **88**(10), pp. 4363-4366.

KATAOKA, S., KONISHI, Y., NISHIO, Y., FUJIKAWA-ADACHI, K. and TOMINAGA, A., 2004. Antitumor Activity of Eosinophils Activated by IL-5 and Eotaxin against Hepatocellular Carcinoma. *DNA and cell biology,* **23**(9), pp. 549-560.

KAWAI, O., ISHII, G., KUBOTA, K., MURATA, Y., NAITO, Y., MIZUNO, T., AOKAGE, K., SAIJO, N., NISHIWAKI, Y., GEMMA, A., KUDOH, S. and OCHIAI, A., 2008. Predominant infiltration of macrophages and CD8+ T Cells in cancer nests is a significant predictor of survival in stage IV nonsmall cell lung cancer. *Cancer,* **113**(6), pp. 1387-1395.

KEHOE, J.W. and KAY, B.K., 2005. Filamentous Phage Display in the New Millennium. *Chemical reviews,* **105**(11), pp. 4056-4072.

KELLEY, B., 2020. Developing therapeutic monoclonal antibodies at pandemic pace. *Nature biotechnology,* **38**(5), pp. 540-545.

KHAIRNAR, V., DUHAN, V., PATIL, A.M., ZHOU, F., BHAT, H., THOENS, C., SHARMA, P., ADOMATI, T., FRIENDRICH, S., BEZGOVSEK, J., DREESEN, J.D., WENNEMUTH, G., WESTENDORF, A.M., ZELINSKYY, G., DITTMER, U., HARDT, C., TIMM, J., GÖTHERT, J.R., LANG, P.A., SINGER, B.B. and LANG, K.S., 2018. CEACAM1 promotes CD8 + T cell responses and improves control of a chronic viral infection. *Nature Communications,* **9**(1), pp. 2561-14.

KIKUSHIGE, Y. and MIYAMOTO, T., 2013. TIM-3 as a novel therapeutic target for eradicating acute myelogenous leukemia stem cells. *International journal of hematology,* **98**(6), pp. 627-633.

KIKUSHIGE, Y., MIYAMOTO, T., YUDA, J., JABBARZADEH-TABRIZI, S., SHIMA, T., TAKAYANAGI, S., NIIRO, H., YURINO, A., MIYAWAKI, K., TAKENAKA, K., IWASAKI, H. and AKASHI, K., 2015. A

TIM-3/Gal-9 Autocrine Stimulatory Loop Drives Self-Renewal of Human Myeloid Leukemia Stem Cells and Leukemic Progression. *Cell Stem Cell,* **17**(3), pp. 341-352.

KIKUSHIGE, Y., SHIMA, T., TAKAYANAGI, S., URATA, S., MIYAMOTO, T., IWASAKI, H., TAKENAKA, K., TESHIMA, T., TANAKA, T., INAGAKI, Y. and AKASHI, K., 2010. TIM-3 Is a Promising Target to Selectively Kill Acute Myeloid Leukemia Stem Cells. *Cell Stem Cell,* **7**(6), pp. 708-717.

KIM, H.S., KIM, H.S., LEE, C.W. and CHUNG, D.H., 2010. T Cell Ig Domain and Mucin Domain 1 Engagement on Invariant NKT Cells in the Presence of TCR Stimulation Enhances IL-4 Production but Inhibits IFN-γ Production. *The Journal of immunology (1950),* **184**(8), pp. 4095-4106.

KLEIN, C., SCHAEFER, W., REGULA, J.T., DUMONTET, C., BRINKMANN, U., BACAC, M. and UMAÑA, P., 2019. Engineering therapeutic bispecific antibodies using CrossMab technology. *Methods (San Diego, Calif.),* **154**, pp. 21-31.

KNIGHT, M.J., WOOLLEY, R.E., KWOK, A., PARSONS, S., JONES, H.B.L., GULÁCSY, C.E., PHAAL, P., KASSAAR, O., DAWKINS, K., RODRIGUEZ, E., MARQUES, A., BOWSHER, L., WELLS, S.A., WATTS, A., VAN DEN ELSEN, J.M.H., TURNER, A., O'HARA, J. and PUDNEY, C.R., 2020. Monoclonal antibody stability can be usefully monitored using the excitation-energy-dependent fluorescence edge-shift. *Biochemical journal,* **477**(18), pp. 3599-3612.

KOBAYASHI, N., KARISOLA, P., PEÑA-CRUZ, V., DORFMAN, D.M., JINUSHI, M., UMETSU, S.E., BUTTE, M.J., NAGUMO, H., CHERNOVA, I., ZHU, B., SHARPE, A.H., ITO, S., DRANOFF, G., KAPLAN, G.G., CASASNOVAS, J.M., UMETSU, D.T., DEKRUYFF, R.H. and FREEMAN, G.J., 2007a. TIM-1 and TIM-4 Glycoproteins Bind Phosphatidylserine and Mediate Uptake of Apoptotic Cells. *Immunity,* **27**(6), pp. 927-940.

KOYAMA, S., AKBAY, E.A., LI, Y.Y., HERTER-SPRIE, G.S., BUCZKOWSKI, K.A., RICHARDS, W.G., GANDHI, L., REDIG, A.J., RODIG, S.J., ASAHINA, H., JONES, R.E., KULKARNI, M.M., KURAGUCHI, M., PALAKURTHI, S., FECCI, P.E., JOHNSON, B.E., JANNE, P.A., ENGELMAN, J.A., GANGADHARAN, S.P., COSTA, D.B., FREEMAN, G.J., BUENO, R., HODI, F.S., DRANOFF, G., WONG, K. and HAMMERMAN, P.S., 2016. Adaptive resistance to therapeutic PD-1 blockade is associated with upregulation of alternative immune checkpoints. *Nature communications,* **7**(1), pp. 10501.

KRAG, D.N., SHUKLA, G.S., SHEN, G., PERO, S., ASHIKAGA, T., FULLER, S., WEAVER, D.L., BURDETTE-RADOUX, S. and THOMAS, C., 2006. Selection of Tumor-binding Ligands in Cancer Patients with Phage Display Libraries. *Cancer Research,* **66**(15), pp. 7724-7733.

KRISTENSEN, P. and SØRENSEN, M.D., 2011. Selection of antibodies against a single rare cell present in a heterogeneous population using phage display. *Nature protocols,* **6**(4), pp. 509-522.

KRISTENSEN, P. and WINTER, G., 1998. Proteolytic selection for protein folding using filamentous bacteriophages. *Folding & design,* **3**(5), pp. 321-328.

KROEMER, T. n.d., Troubleshooting: Satellite Colonies [GoldBio], [Online]. Available: https://goldbio.com/articles/article/satellite-colonies [Oct 13, 2023].

KUCHROO, V.K., MEYERS, J.H., CHAKRAVARTI, S., SCHLESINGER, D., ILLES, Z., WALDNER, H., UMETSU, S.E., KENNY, J., ZHENG, X.X., UMETSU, D.T., DEKRUYFF, R.H. and STROM, T.B., 2005. TIM-4 is the ligand for TIM-1, and the TIM-1-TIM-4 interaction regulates T cell proliferation. *Nature immunology,* **6**(5), pp. 455-464.

KUCHROO, V.K., MONNEY, L., SABATOS, C.A., GAGLIA, J.L., RYU, A., WALDNER, H., CHERNOVA, T., MANNING, S., GREENFIELD, E.A., COYLE, A.J., SOBEL, R.A. and FREEMAN, G.J., 2002. Th1-specific cell surface protein Tim-3 regulates macrophage activation and severity of an autoimmune disease. *Nature (London),* **415**(6871), pp. 536-541.

KUCHROO, V.K., ZHU, C., ANDERSON, A.C., SCHUBART, A., XIONG, H., IMITOLA, J., KHOURY, S.J., ZHENG, X.X. and STROM, T.B., 2005. The Tim-3 ligand galectin-9 negatively regulates T helper type 1 immunity. *Nature Immunology,* **6**(12), pp. 1245-1252.

KÜGLER, J., TOMSZAK, F., FRENZEL, A. and HUST, M., 2017. Construction of Human Immune and Naive scFv Libraries. *Methods in molecular biology (Clifton, N.J.).* New York, NY: Springer New York, pp. 3-24.

KURTULUS, S., MADI, A., ESCOBAR, G., KLAPHOLZ, M., NYMAN, J., CHRISTIAN, E., PAWLAK, M., DIONNE, D., XIA, J., ROZENBLATT-ROSEN, O., KUCHROO, V.K., REGEV, A. and ANDERSON, A.C., 2019. Checkpoint Blockade Immunotherapy Induces Dynamic Changes in PD-1−CD8+ Tumor-Infiltrating T Cells. *Immunity (Cambridge, Mass.),* **50**(1), pp. 181-194.e6.

KWON, N., KIM, Y. and LEE, J., 2019. Structural diversity and flexibility of diabodies. *Methods (San Diego, Calif.)*, **154**, pp. 136-142.

LABANI-MOTLAGH, A., ASHJA-MAHDAVI, M. and LOSKOG, A., 2020. The Tumor Microenvironment: A Milieu Hindering and Obstructing Antitumor Immune Responses. *Frontiers in immunology*, **11**, pp. 940.

LAVOISIER, A. and SCHLAEPPI, J., 2015. Early developability screen of therapeutic antibody candidates using Taylor dispersion analysis and UV area imaging detection. *mAbs*, **7**(1), pp. 77-83.

LEACH, D.R., KRUMMEL, M.F. and ALLISON, J.P., 1996. Enhancement of Antitumor Immunity by CTLA-4 Blockade. *Science*, **271**(5256), pp. 1734-1736.

LECERF, M., KANYAVUZ, A., LACROIX-DESMAZES, S. and DIMITROV, J.D., 2019. Sequence features of variable region determining physicochemical properties and polyreactivity of therapeutic antibodies. *Molecular immunology*, **112**, pp. 338-346.

LEDFORD, H., ELSE, H. and WARREN, M., 2018. Cancer immunologists scoop medicine Nobel prize. *Nature (London)*, **562**(7725), pp. 20-21.

LEE, C.S., CRAGG, M., GLENNIE, M. and JOHNSON, P., 2013. Novel antibodies targeting immune regulatory checkpoints for cancer therapy. *British journal of clinical pharmacology*, **76**(2), pp. 233-247.

LEE, J., PHONG, B., EGLOFF, A.M. and KANE, L.P., 2011. TIM polymorphisms—genetics and function. *Genes and immunity*, **12**(8), pp. 595-604.

LEFFERS, N., GOODEN, M.J.M., DE JONG, R.A., HOOGEBOOM, B., TEN HOOR, K.A., HOLLEMA, H., BOEZEN, H.M., VAN DER ZEE, ATE G. J, DAEMEN, T. and NIJMAN, H.W., 2009. Prognostic significance of tumor-infiltrating T-lymphocytes in primary and metastatic lesions of advanced stage ovarian cancer. *Cancer Immunology Immunotherapy*, **58**(3), pp. 449-459.

LEGOUFFE, E., LIAUTARD, J., GAILLARD, J.P., ROSSI, J., WIJDENES, J., BATAILLE, R., KLEIN, B. and BROCHIER, J., 1994. Human anti-mouse antibody response to the injection of murine monoclonal antibodies against IL-6. *Clinical and experimental immunology*, **98**(2), pp. 323-329.

LEGRAND, F., DRISS, V., DELBEKE, M., LOISEAU, S., HERMANN, E., DOMBROWICZ, D. and CAPRON, M., 2010. Human Eosinophils Exert TNF-α and Granzyme A-Mediated Tumoricidal Activity toward Colon Carcinoma Cells. *The Journal of immunology (1950)*, **185**(12), pp. 7443-7451.

LI, H., WU, K., TAO, K., CHEN, L., ZHENG, Q., LU, X., LIU, J., SHI, L., LIU, C., WANG, G. and ZOU, W., 2012. Tim-3/galectin-9 signaling pathway mediates T-cell dysfunction and predicts poor prognosis in patients with hepatitis B virus-associated hepatocellular carcinoma. *Hepatology (Baltimore, Md.)*, **56**(4), pp. 1342-1351.

LI, L., GUPTA, E., SPAETH, J., SHING, L., JAIMES, R., ENGELHART, E., LOPEZ, R., CACERES, R.S., BEPLER, T. and WALSH, M.E., 2023. Machine learning optimization of candidate antibody yields highly diverse sub-nanomolar affinity antibody libraries. *Nature communications*, **14**(1), pp. 3454.

LI, W., LI, X., XU, S., MA, X. and ZHANG, Q., 2016. Expression of Tim4 in Glioma and its Regulatory Role in LN-18 Glioma Cells. *Medical Science Monitor : International Medical Journal of Experimental and Clinical Research*, **22**, pp. 77-82.

LINDAU, D.S.U., GIELEN, P.R., KROESEN, M., WESSELING, P. and ADEMA, G.J., 2013. The immunosuppressive tumour network: myeloid-derived suppressor cells, regulatory T cells and natural killer T cells. *Immunology*, **138**(2), pp. 105-15.

LIPES, B.D., CHEN, Y., MA, H., STAATS, H.F., KENAN, D.J. and GUNN, M.D., 2008. An Entirely Cell-Based System to Generate Single-Chain Antibodies against Cell Surface Receptors. *Journal of molecular biology*, **379**(2), pp. 261-272.

LIU, W., XU, L., LIANG, X., LIU, X., ZHAO, Y., MA, C. and GAO, L., 2020. Tim-4 in Health and Disease: Friend or Foe? *Frontiers in Immunology*, **11**, pp. 537.

LIU, Y. and YU, J., 2015. Oriented immobilization of proteins on solid supports for use in biosensors and biochips: a review. Microchimica Acta, 183(1), pp. 1-19.

LIU, Z.-, LI, M.-, GENG, X.-, LIU, J., YANG, G., QIU, S.-, LIU, Z.- and YANG, P.-, 2017. Vitamin D regulates immunoglobulin mucin domain molecule-4 expression in dendritic cells. *Clinical and experimental allergy*, **47**(5), pp. 656-664.

LONBERG, N., 2005. Human antibodies from transgenic animals. *Nature biotechnology*, **23**(9), pp. 1117-1125.

LONBERG, N., TAYLOR, L.D., HARDING, F.A., TROUNSTINE, M., HIGGINS, K.M., SCHRAMM, S.R., KUO, C., MASHAYEKH, R., WYMORE, K., MCCABE, J.G., MUNOZ-O'REGAN, D., O'DONNELL, S.L., LAPACHET, E.S.G., BENGOECHEA, T., FISHWILD, D.M., CARMACK, C.E., KAY, R.M. and

HUSZAR, D., 1994. Antigen-specific human antibodies from mice comprising four distinct genetic modifications. *Nature (London)*, **368**(6474), pp. 856-859.

LOWE D., 2022, Pesky Sticky Proteins [Science], [Online]. Available: https://www.science.org/content/blog-post/pesky-sticky-proteins#:~:text=Small%20molecules%20and%20proteins%20alike,to%20worry%20about%20this%20effect. [Sept 27, 2023].

LOWMAN, H.B., BASS, S.H., SIMPSON, N. and WELLS, J.A., 1991. Selecting high-affinity binding proteins by monovalent phage display. *Biochemistry (Easton)*, **30**(45), pp. 10832-10838.

LÜDEL, F., BUFE, S., BLEYMÜLLER, W.M., DE JONGE, H., IAMELE, L., NIEMANN, H.H. and HELLWEG, T., 2019. Distinguishing Between Monomeric scFv and Diabody in Solution Using Light and Small Angle X-ray Scattering. *Antibodies*, **8**(4), pp. 48.

LU, R., HWANG, Y., LIU, I., LEE, C., TSAI, H., LI, H. and WU, H., 2020. Development of therapeutic antibodies for the treatment of diseases. *Journal of Biomedical Science*, **27**(1), pp. 1.

MAJ, T., WANG, W., CRESPO, J., ZHANG, H., WANG, W., WEI, S., ZHAO, L., VATAN, L., SHAO, I., SZELIGA, W., LYSSIOTIS, C., LIU, J.R., KRYCZEK, I. and ZOU, W., 2017. Oxidative stress controls regulatory T cell apoptosis and suppressor activity and PD-L1-blockade resistance in tumor. *Nature immunology*, **18**(12), pp. 1332-1341.

MANIS, J.P. 2023, – last updated. Overview of therapeutic monoclonal antibodies [Wolter Kluwer], [Online]. Available: https://www.uptodate.com/contents/overview-of-therapeutic-monoclonal-antibodies/print [Feb 21, 2023].

MARKS, J.D., HOOGENBOOM, H.R., BONNERT, T.P., MCCAFFERTY, J., GRIFFITHS, A.D. and WINTER, G., 1991. By-passing immunization: Human antibodies from V-gene libraries displayed on phage. *Journal of molecular biology*, **222**(3), pp. 581-597.

MARTIN, J.H. and EDWARDS, S.W., 1993. Changes in mechanisms of monocyte/macrophage-mediated cytotoxicity during culture. Reactive oxygen intermediates are involved in monocyte- mediated cytotoxicity, whereas reactive nitrogen intermediates are employed by macrophages in tumor cell killing. *The Journal of immunology (1950)*, **150**(8), pp. 3478-3486.

MARTINEZ, F.O., SICA, A., MANTOVANI, A. and LOCATI, M., 2008. Macrophage activation and polarization. Frontiers in Bioscience: A Journal and Virtual Library, 13, pp. 453-461.

MASIERO, A., NELLY, L., MARIANNE, G., CHRISTOPHE, S., FLORIAN, L., RONAN, C., CLAIRE, B., CORNELIA, Z., GRÉGOIRE, B., ERIC, L., LUDOVIC, L., DOMINIQUE, B., SYLVIE, A., MARIE, G., FRANCIS, D., FABIENNE, S., CÉCILE, C., ISABELLE, A., JACQUES, D., JÉRÔME, D., BRUNO, G., KATARINA, R., JEAN-MICHEL, M. and CATHERINE, P., 2020. The impact of proline isomerization on antigen binding and the analytical profile of a trispecific anti-HIV antibody. *mAbs,* **12**(1), pp. 1698128.

MCCAFFERTY, J., GRIFFITHS, A.D., WINTER, G. and CHISWELL, D.J., 1990. Phage antibodies: filamentous phage displaying antibody variable domains. *Nature (London),* **348**(6301), pp. 552-554.

MCCONNELL, S.J., DINH, T., LE, M. and SPINELLA, D.G., 1999. Biopanning Phage Display Libraries Using Magnetic Beads Vs. Polystyrene Plates. *BioTechniques,* **26**(2), pp. 208-214.

MCGUIRE, M.J., LI, S. and BROWN, K.C., 2009. Biopanning of Phage Displayed Peptide Libraries for the Isolation of Cell-Specific Ligands. *Biosensors and Biodetection.* Totowa, NJ: Humana Press, pp. 291-321.

MCINTIRE, J.J., 2002. *Identification of Tapr, a T cell and airway phenotype regulatory locus, and positional cloning of the Tim gene family*, Stanford University.

MENDEZ, M.J., GREEN, L.L., CORVALAN, J.R.F., JIA, X., MAYNARD-CURRIE, C.E., YANG, X., GALLO, M.L., LOUIE, D.M., LEE, D.V., ERICKSON, K.L., LUNA, J., ROY, C.M.-., ABDERRAHIM, H., KIRSCHENBAUM, F., NOGUCHI, M., SMITH, D.H., FUKUSHIMA, A., HALES, J.F., FINER, M.H., DAVIS, C.G., ZSEBO, K.M. and JAKOBOVITS, A., 1997. Functional transplant of megabase human immunoglobulin loci recapitulates human antibody response in mice. *Nature genetics,* **15**(2), pp. 146-156.

MENENDEZ, A. and SCOTT, J.K., 2005. The nature of target-unrelated peptides recovered in the screening of phage-displayed random peptide libraries with antibodies. *Analytical biochemistry,* **336**(2), pp. 145-157.

MEYERS, J.H., SABATOS, C.A., CHAKRAVARTI, S. and KUCHROO, V.K., 2005. The TIM gene family regulates autoimmune and allergic diseases. *Trends in molecular medicine,* **11**(8), pp. 362-369.

MICHEL, M.C., MURPHY, T.J. and MOTULSKY, H.J., 2020. New Author Guidelines for Displaying Data and Reporting Data Analysis and Statistical Methods in Experimental Biology. Molecular pharmacology, 97(1), pp. 49-60.

MILLER, B.C., SEN, D.R., AL ABOSY, R., BI, K., VIRKUD, Y.V., LAFLEUR, M.W., YATES, K.B., LAKO, A., FELT, K., NAIK, G.S., MANOS, M., GJINI, E., KUCHROO, J.R., ISHIZUKA, J.J., COLLIER, J.L., GRIFFIN, G.K., MALERI, S., COMSTOCK, D.E., WEISS, S.A., BROWN, F.D., PANDA, A., ZIMMER, M.D., MANGUSO, R.T., HODI, F.S., RODIG, S.J., SHARPE, A.H. and HAINING, W.N., 2019. Subsets of exhausted CD8+ T cells differentially mediate tumor control and respond to checkpoint blockade. *Nature immunology,* **20**(3), pp. 326-336.

MISHIMA, Y., NAKAJIMA, K., SHIRAISHI, M., MATSUMURA, H., ARAMAKI, T., MATSUMOTO, N. and NAKAMURA, N., 2021. 235 Novel biparatopic TIM-3 antibody effectively blocks multiple inherent ligands and activates anti-tumor immunity. *Journal for immunotherapy of cancer,* **9**(Suppl 2), pp. A251.

MISHRA, P., PANDEY, C., SINGH, U., GUPTA, A., SAHU, C. and KESHRI, A., 2019. Descriptive statistics and normality tests for statistical data. *Annals of Cardiac Anaesthesia,* **22**(1), pp. 67-72.

MIZUI, M., SHIKINA, T., ARASE, H., SUZUKI, K., YASUI, T., RENNERT, P.D., KUMANOGOH, A. and KIKUTANI, H., 2008. Bimodal regulation of T cell-mediated immune responses by TIM-4. *International immunology,* **20**(5), pp. 695-708.

MÖLLER-HACKBARTH, K., DEWITZ, C., SCHWEIGERT, O., TRAD, A., GARBERS, C., ROSE-JOHN, S. and SCHELLER, J., 2013. A Disintegrin and Metalloprotease (ADAM) 10 and ADAM17 Are Major Sheddases of T Cell Immunoglobulin and Mucin Domain 3 (Tim-3). *The Journal of biological chemistry,* **288**(48), pp. 34529-34544.

Monarch® Plasmid Miniprep Kit Instruction Manual, version 3.1. New England BioLabs Inc., Massachusetts, United States, 9/2021. Accessed: 26/9/2023. [Online]. Available: https://www.neb.com/en/-/media/nebus/files/manuals/manualt1010.pdf?rev=e79c527b32dd4c7f823db7a05ce6ad62&hash=51FAD6BD033A756986A666A8FC99CCE7

MORGAN, A.A. and RUBENSTEIN, E., 2013. Proline: The Distribution, Frequency, Positioning, and Common Functional Roles of Proline and Polyproline Sequences in the Human Proteome. PloS one, 8(1), pp. e53785.

MORRISON, S.L. and OI, V.T., 1989. Genetically Engineered Antibody Molecules. *Advances in Immunology.* United States: Elsevier Science & Technology, pp. 65-92.

MUELLER, D.L., JENKINS, M.K. and SCHWARTZ, R.H., 1989. Clonal Expansion Versus Functional Clonal Inactivation: A Costimulatory Signalling Pathway Determines the Outcome of T Cell Antigen Receptor Occupancy. *Annual review of immunology,* **7**(1), pp. 445-480.

MUKHERJEE, S., URA, M., HOEY, R.J. and KOSSIAKOFF, A.A., 2015. A New Versatile Immobilization Tag Based on the Ultra High Affinity and Reversibility of the Calmodulin–Calmodulin Binding Peptide Interaction. *Journal of molecular biology,* **427**(16), pp. 2707-2725.

MURTAZA, A., LAKEN, H., DA SILVA CORREIA, J., MCNEELEY, P., ALTOBELL, L., ZHANG, J., VANCUTSEM, P., WILCOXEN, K. and JENKINS, D., 2016. Discovery of TSR-022, a novel, potent anti-human TIM-3 therapeutic antibody. *European journal of cancer (1990),* **69**, pp. S102.

NAGY, P., FRIEDLANDER, E., TANNER, M., KAPANEN, A.I., CARRAWAY, K.L., ISOLA, J. and JOVIN, T.M., 2005. Decreased Accessibility and Lack of Activation of ErbB2 in JIMT-1, a Herceptin-Resistant, MUC4-Expressing Breast Cancer Cell Line. *Cancer Research,* **65**(2), pp. 473-482.

NAKAHARA, T., MOROI, Y., UCHI, H. and FURUE, M., 2006. Differential role of MAPK signaling in human dendritic cell maturation and Th1/Th2 engagement. *Journal of dermatological science,* **42**(1), pp. 1-11.

NAKAYAMA, M., AKIBA, H., TAKEDA, K., KOJIMA, Y., HASHIGUCHI, M., AZUMA, M., YAGITA, H. and OKUMURA, K., 2009. Tim-3 mediates phagocytosis of apoptotic cells and cross-presentation. *Blood,* **113**(16), pp. 3821-3830.

NanoDrop 2000/2000c Spectrophotometer User Manual, version 1.0. ThermoScientific, Massachusetts, United States, 3/09. Accessed: 26/9/2023. [Online]. Available: https://assets.thermofisher.com/TFS-Assets/CAD/manuals/NanoDrop-2000-User-Manual-EN.pdf

NDHLOVU, L.C., LOPEZ-VERGÈS, S., BARBOUR, J.D., JONES, R.B., JHA, A.R., LONG, B.R., SCHOEFFLER, E.C., FUJITA, T., NIXON, D.F. and LANIER, L.L., 2012. Tim-3 marks human natural killer cell maturation and suppresses cell-mediated cytotoxicity. *Blood,* **119**(16), pp. 3734-3743.

NOH, J., KIM, O., JUNG, Y., HAN, H., KIM, J., KIM, S., LEE, S., PARK, J., JUNG, R.H., KIM, S.I., PARK, J., HAN, J., LEE, H., YOO, D.K., LEE, A.C., KWON, E., RYU, T., CHUNG, J. and KWON, S., 2019. High-throughput retrieval of physical DNA for NGS-identifiable clones in phage display library. *mAbs,* **11**(3), pp. 532-545.

O'CALLAGHAN, R., BRADLEY, R. and PARANCHYCH, W., 1973. The effect of M13 phage infection upon the F pili of E. coli. *Virology (New York, N.Y.),* **54**(1), pp. 220-229.

OOMIZU, S., ARIKAWA, T., NIKI, T., KADOWAKI, T., UENO, M., NISHI, N., YAMAUCHI, A. and HIRASHIMA, M., 2012. Galectin-9 suppresses Th17 cell development in an IL-2-dependent but Tim-3-independent manner. *Clinical immunology (Orlando, Fla.),* **143**(1), pp. 51-58.

ORNER, B.P., DERDA, R., LEWIS, R.L., THOMSON, J.A. and KIESSLING, L.L., 2004. Arrays for the Combinatorial Exploration of Cell Adhesion. *Journal of the American Chemical Society*, **126**(35), pp. 10808-10809.

PADUCH, M., KOIDE, A., UYSAL, S., RIZK, S.S., KOIDE, S. and KOSSIAKOFF, A.A., 2013. Generating conformation-specific synthetic antibodies to trap proteins in selected functional states. *Methods (San Diego, Calif.),* **60**(1), pp. 3-14.

PANDE, J., SZEWCZYK, M.M. and GROVER, A.K., 2010. Phage display: Concept, innovations, applications and future. *Biotechnology advances,* **28**(6), pp. 849-858.

PARDOLL, D.M., 2012. The blockade of immune checkpoints in cancer immunotherapy. *Nature reviews. Cancer,* **12**(4), pp. 252-264.

PATEL, R., BOCK, M., POLOTTI, C.F. and ELSAMRA, S., 2017. Pharmacokinetic drug evaluation of atezolizumab for the treatment of locally advanced or metastatic urothelial carcinoma. *Expert opinion on drug metabolism & toxicology,* **13**(2), pp. 225-232.

PATRIARCA, E.J., CERMOLA, F., D'ANIELLO, C., FICO, A., GUARDIOLA, O., DE CESARE, D. and MINCHIOTTI, G., 2021. The Multifaceted Roles of Proline in Cell Behavior. *Frontiers in cell and developmental biology,* **9**, pp. 728576.

PATRICK, M. 2014, Plasmids 101: Antibiotic Resistance Genes [addgene Blog], [Online]. Available: https://blog.addgene.org/plasmids-101-everything-you-need-to-know-about-antibiotic-resistance-genes [Oct 13, 2023].

PEARSON, W.R., 2013. An Introduction to Sequence Similarity ("Homology") Searching. *Current Protocols in Bioinformatics,* **42**(1), pp. 3.1.1-3.1.8.

PEGGS, K.S., QUEZADA, S.A. and ALLISON, J.P., 2009. Cancer immunotherapy: co-stimulatory agonists and co-inhibitory antagonists. *Clinical and experimental immunology,* **157**(1), pp. 9-19.

PENG, L., ZHUANG, Y., SHI, Y., ZHAO, Y., WANG, T., CHEN, N., CHENG, P., LIU, T., LIU, X., ZHANG, J., ZUO, Q., MAO, X., GUO, G., LU, D., YU, P. and ZOU, Q., 2012. Increased tumor-infiltrating CD8+Foxp3+ T lymphocytes are associated with tumor progression in human gastric cancer. *Cancer Immunology, Immunotherapy,* **61**(11), pp. 2183-2192.

PERAZELLA, M.A. and SHIRALI, A.C., 2020. Immune checkpoint inhibitor nephrotoxicity: what do we know and what should we do? *Kidney international,* **97**(1), pp. 62-74.

PETERSEN, R.P., CAMPA, M.J., SPERLAZZA, J., CONLON, D., JOSHI, M., HARPOLE, D.H. and PATZ, E.F., 2006. Tumor infiltrating Foxp3+ regulatory T-cells are associated with recurrence in pathologic stage I NSCLC patients. *Cancer,* **107**(12), pp. 2866-2872.

PHONG, B.L., AVERY, L., SUMPTER, T.L., GORMAN, J.V., WATKINS, S.C., COLGAN, J.D. and KANE, L.P., 2015. Tim-3 enhances FcεRI-proximal signaling to modulate mast cell activation. *The Journal of Experimental Medicine,* **212**(13), pp. 2289-2304.

PINEDA, C., CASTAÑEDA HERNÁNDEZ, G., JACOBS, I.A., ALVAREZ, D.F. and CARINI, C., 2016. Assessing the Immunogenicity of Biopharmaceuticals. *BioDrugs : clinical immunotherapeutics, biopharmaceuticals, and gene therapy,* **30**(3), pp. 195-206.

POLPRASERT, C., TAKEUCHI, Y., KAKIUCHI, N., YOSHIDA, K., ASSANASEN, T., SITTHI, W., BUNWORASATE, U., PIRUNSARN, A., WUDHIKARN, K., LAWASUT, P., UAPRASERT, N., KONGKIATKAMON, S., MOONLA, C., SANADA, M., AKITA, N., TAKEDA, J., FUJII, Y., SUZUKI, H., NANNYA, Y., SHIRAISHI, Y., CHIBA, K., TANAKA, H., MIYANO, S., ROJNUCKARIN, P., OGAWA, S. and MAKISHIMA, H., 2019. Frequent germline mutations of HAVCR2 in sporadic subcutaneous panniculitis-like T-cell lymphoma. *Blood advances,* **3**(4), pp. 588-595.

POSNETT, D.N., EDINGER, J.W., MANAVALAN, J.S., IRWIN, C. and MARODON, G., 1999. Differentiation of human CD8 T cells: implications for in vivo persistence of CD8+CD28– cytotoxic effector clones. *International immunology,* **11**(2), pp. 229-241.

RADER, C. and BARBAS, C.F., 1997. Phage display of combinatorial antibody libraries. *Current opinion in biotechnology*, **8**(4), pp. 503-508.

RAKONJAC, J., BENNETT, N.J., SPAGNUOLO, J., GAGIC, D. and RUSSEL, M., 2011. Filamentous Bacteriophage: Biology, Phage Display and Nanotechnology Applications. *Current Issues in Molecular Biology*, **13**(2), pp. 51-76.

RAMSDELL, F., KHATTRI, R., COX, T. and YASAYKO, S., 2003. An essential role for Scurfin in CD4 + CD25 + T regulatory cells. *Nature immunology*, **4**(4), pp. 337-342.

RANGACHARI, M., ZHU, C., SAKUISHI, K., XIAO, S., KARMAN, J., CHEN, A., ANGIN, M., WAKEHAM, A., GREENFIELD, E.A., SOBEL, R.A., OKADA, H., MCKINNON, P.J., MAK, T.W., ADDO, M.M., ANDERSON, A.C. and KUCHROO, V.K., 2012. Bat3 promotes T cell responses and autoimmunity by repressing Tim-3–mediated cell death and exhaustion. *Nature medicine*, **18**(9), pp. 1394-1400.

RAYBOULD, M.I.J., MARKS, C., KRAWCZYK, K., TADDESE, B., NOWAK, J., LEWIS, A.P., BUJOTZEK, A., SHI, J. and DEANE, C.M., 2019. Five computational developability guidelines for therapeutic antibody profiling. *Proceedings of the National Academy of Sciences - PNAS*, **116**(10), pp. 4025-4030.

Recombinant Human IgG_1 Fc Package Insert. R&D Systems, Minnesota, United States. Accessed 20/11/2023. [Online]. Available: https://resources.rndsystems.com/pdfs/datasheets/110-hg.pdf?v=20231120&_ga=2.235356679.7060452.1700467527-1214292294.1700467526

Recombinant Human TIM-3 Fc Chimera Package Insert. R&D Systems, Minnesota, United States. Accessed 13/10/2023. [Online]. Available: https://resources.rndsystems.com/pdfs/datasheets/2365-tm.pdf?v=20231012&_ga=2.83305874.548896509.1697115122-904647627.1696520704

REIS, P.B.P.S., BARLETTA, G.P., GAGLIARDI, L., FORTUNA, S., SOLER, M.A. and ROCCHIA, W., 2022. Antibody-Antigen Binding Interface Analysis in the Big Data Era. *Frontiers in molecular biosciences*, **9**, pp. 945808.

RODI, D.J. and MAKOWSKI, L., 1999. Phage-display technology – finding a needle in a vast molecular haystack. Current Opinion in Biotechnology, 10(1), pp. 87-93.

RODRIGUEZ-MANZANET, R., MEYERS, J.H., BALASUBRAMANIAN, S., SLAVIK, J., KASSAM, N., DARDALHON, V., GREENFIELD, E.A., ANDERSON, A.C., SOBEL, R.A., HAFLER, D.A., STROM,

T.B. and KUCHROO, V.K., 2008. TIM-4 Expressed on APCs Induces T Cell Expansion and Survival. *The Journal of immunology (1950)*, **180**(7), pp. 4706-4713.

RUBENSTEIN, E., 2000. Biologic Effects of and Clinical Disorders Caused by Nonprotein Amino Acids. Medicine (Baltimore), 79(2), pp. 80-89.

RULIFSON, I.C., SPERLING, A.I., FIELDS, P.E., FITCH, F.W. and BLUESTONE, J.A., 1997. CD28 costimulation promotes the production of Th2 cytokines. The Journal of immunology (1950), 158(2), pp. 658-665.

RUSSEL, M., LINDEROTH, N.A. and ŠALI, A., 1997. Filamentous phage assembly: variation on a protein export theme1Presented at the Workshop on `Type-4 Pili – Biogenesis, Adhesins, Protein Export, and DNA Import', Schloss Ringberg, Germany, 26–29 November 1995.1. Gene, 192(1), pp. 23-32.

SABATOS-PEYTON, C.A., NEVIN, J., BROCK, A., VENABLE, J.D., TAN, D.J., KASSAM, N., XU, F., TARASZKA, J., WESEMANN, L., PERTEL, T., ACHARYA, N., KLAPHOLZ, M., ETMINAN, Y., JIANG, X., HUANG, Y., BLUMBERG, R.S., KUCHROO, V.K. and ANDERSON, A.C., 2018. Blockade of Tim-3 binding to phosphatidylserine and CEACAM1 is a shared feature of anti-Tim-3 antibodies that have functional efficacy. *Oncoimmunology*, **7**(2), pp. e1385690.

SAKAGUCHI, S., MIYARA, M., COSTANTINO, C.M. and HAFLER, D.A., 2010. [FOXP3.sup.+] regulatory T cells in the human immune system. *Nature reviews. Immunology*, **10**(7), pp. 490.

SAKAGUCHI, S., YAMAGUCHI, T., NOMURA, T. and ONO, M., 2008. Regulatory T Cells and Immune Tolerance. *Cell*, **133**(5), pp. 775-787.

SAKUISHI, K., APETOH, L., SULLIVAN, J.M., BLAZAR, B.R., KUCHROO, V.K. and ANDERSON, A.C., 2010. Targeting Tim-3 and PD-1 pathways to reverse T cell exhaustion and restore anti-tumor immunity. *The Journal of Experimental Medicine*, **207**(10), pp. 2187-2194.

SALEH, R. and ELKORD, E., 2020. Acquired resistance to cancer immunotherapy: Role of tumor-mediated immunosuppression. *Seminars in cancer biology*, **65**, pp. 13-27.

SANTIAGO, C., BALLESTEROS, A., MARTÍNEZ-MUÑOZ, L., MELLADO, M., KAPLAN, G.G., FREEMAN, G.J. and CASASNOVAS, J.M., 2007. Structures of T Cell Immunoglobulin Mucin Protein 4 Show a Metal-Ion-Dependent Ligand Binding Site where Phosphatidylserine Binds. *Immunity*, **27**(6), pp. 941-951.

SANTOS, R., URSU, O., GAULTON, A., BENTO, A.P., DONADI, R.S., BOLOGA, C.G., KARLSSON, A., AL-LAZIKANI, B., HERSEY, A., OPREA, T.I. and OVERINGTON, J.P., 2017. A comprehensive map of molecular drug targets. *Nature reviews. Drug discovery,* **16**(1), pp. 19-34.

SARKAR, C.A., DODEVSKI, I., KENIG, M., DUDLI, S., MOHR, A., HERMANS, E. and PLÜCKTHUN, A., 2008. Directed evolution of a G protein-coupled receptor for expression, stability, and binding selectivity. *Proceedings of the National Academy of Sciences - PNAS,* **105**(39), pp. 14808-14813.

SARKER, A., RATHORE, A.S., KHALID, M.F. and GUPTA, R.D., 2022. Structure-guided affinity maturation of a single-chain variable fragment antibody against the Fu-bc epitope of the dengue virus envelope protein. *The Journal of biological chemistry,* **298**(4), pp. 101772.

SASIDHARAN NAIR, V. and ELKORD, E., 2018. Immune checkpoint inhibitors in cancer therapy: a focus on T-regulatory cells. *Immunology and cell biology,* **96**(1), pp. 21-33.

SATO, E., OLSON, S.H., AHN, J., BUNDY, B., NISHIKAWA, H., QIAN, F., JUNGBLUTH, A.A., FROSINA, D., GNJATIC, S., AMBROSONE, C., KEPNER, J., ODUNSI, T., RITTER, G., LELE, S., CHEN, Y., OHTANI, H., OLD, L.J. and ODUNSI, K., 2005. Intraepithelial CD8+ Tumor-Infiltrating Lymphocytes and a High $CD8^+/regulatory$ T Cell Ratio Are Associated with Favorable Prognosis in Ovarian Cancer. *Proceedings of the National Academy of Sciences - PNAS,* **102**(51), pp. 18538-18543.

SAW, P.E. and SONG, E., 2019. Phage display screening of therapeutic peptide for cancer targeting and therapy. Protein & cell, 10(11), pp. 787-807.

SCHIRRMANN, T., MEYER, T., SCHÜTTE, M., FRENZEL, A. and HUST, M., 2011. Phage Display for the Generation of Antibodies for Proteome Research, Diagnostics and Therapy. *MOLECULES,* **16**(1), pp. 412-426.

SCHMIDT, C.S. and MESCHER, M.F., 1999. Adjuvant Effect of IL-12: Conversion of Peptide Antigen Administration from Tolerizing to Immunizing for CD8+ T Cells In Vivo. *The Journal of immunology (1950),* **163**(5), pp. 2561-2567.

SCHMIDT, C.S. and MESCHER, M.F., 2002. Peptide Antigen Priming of Naive, But Not Memory, CD8 T Cells Requires a Third Signal That Can Be Provided by IL-12. *The Journal of immunology (1950),* **168**(11), pp. 5521-5529.

SCHWARZ, M., MEADE, G., STOLL, P., YLANNE, J., BASSLER, N., CHEN, Y.C., HAGEMEYER, C.E., AHRENS, I., MORAN, N., KENNY, D., FITZGERALD, D., BODE, C. and PETER, K., 2006. Conformation-Specific Blockade of the Integrin GPIIb/IIIa: A Novel Antiplatelet Strategy That Selectively Targets Activated Platelets. *Circulation Research,* **99**(1), pp. 25-33.

SCHWARZ, M., RÖTTGEN, P., TAKADA, Y., LE GALL, F., KNACKMUSS, S., BASSLER, N., BÜTTNER, C., LITTLE, M., BODE, C. and PETER, K., 2004. Single-chain antibodies for the conformation-specific blockade of activated platelet integrin alphaIIbbeta3 designed by subtractive selection from naive human phage libraries. *The FASEB journal,* **18**(14), pp. 1704-1706.

SCHWEIGERT, O., DEWITZ, C., MÖLLER-HACKBARTH, K., TRAD, A., GARBERS, C., ROSE-JOHN, S. and SCHELLER, J., 2014. Soluble T cell immunoglobulin and mucin domain (TIM)-1 and -4 generated by A Disintegrin And Metalloprotease (ADAM)-10 and -17 bind to phosphatidylserine. *Biochimica et Biophysica Acta (BBA) - Molecular Cell Research,* **1843**(2), pp. 275-287.

SEKTIOGLU, I.M., CARRETERO, R., BULBUC, N., BALD, T., TÜTING, T., RUDENSKY, A.Y. and HÄMMERLING, G.J., 2017. Basophils Promote Tumor Rejection via Chemotaxis and Infiltration of CD8+ T Cells. *Cancer research (Chicago, Ill.),* **77**(2), pp. 291-302.

SEOANE, J. and GOMIS, R.R., 2017. TGF-β Family Signaling in Tumor Suppression and Cancer Progression. *Cold Spring Harbor perspectives in biology,* **9**(12), pp. a022277.

SHANG, B., LIU, Y., JIANG, S. and LIU, Y., 2015. Prognostic value of tumor-infiltrating FoxP3+ regulatory T cells in cancers: a systematic review and meta-analysis. *Scientific Reports,* **5**(1), pp. 15179.

SHARMA, P., HU-LIESKOVAN, S., WARGO, J.A. and RIBAS, A., 2017. Primary, Adaptive, and Acquired Resistance to Cancer Immunotherapy. *Cell,* **168**(4), pp. 707-723.

SHARPE, A.H., 2009. Mechanisms of Costimulation. Immunological reviews, 229(1), pp. 5-11.

SHEEHAN, J. and MARASCO, W.A., 2015. Phage and Yeast Display. *Microbiology spectrum,* **3**(1), pp. AID-2014.

SHEINESS, D. and BISHOP, J.M., 1979. DNA and RNA from uninfected vertebrate cells contain nucleotide sequences related to the putative transforming gene of avian myelocytomatosis virus. *Journal of Virology,* **31**(2), pp. 514-521.

SHEN, W., LI, S., PARK, M., ZHANG, Z., CHENG, Z., PETRENKO, V.A. and CHIN, B.A., 2012. Blocking Agent Optimization for Nonspecific Binding on Phage Based Magnetoelastic Biosensors. *Journal of the Electrochemical Society,* **159**(10), pp. B818-B823.

SHENTAL-BECHOR, D. and LEVY, Y., 2008. Effect of glycosylation on protein folding: A close look at thermodynamic stabilization. *Proceedings of the National Academy of Sciences - PNAS,* **105**(24), pp. 8256-8261.

SHIER, R., 2004, Statistics: 2.3 The Mann-Whitney U Test [Mathematics Learning Support Centre], [Online]. Available: https://www.statstutor.ac.uk/resources/uploaded/mannwhitney.pdf [21/4/22].

SHIMIZU, J., YAMAZAKI, S. and SAKAGUCHI, S., 1999. Induction of Tumor Immunity by Removing CD25+CD4+ T Cells: A Common Basis Between Tumor Immunity and Autoimmunity. *The Journal of immunology (1950),* **163**(10), pp. 5211-5218.

SHITARA, K. and NISHIKAWA, H., 2018. Regulatory T cells: a potential target in cancer immunotherapy. *Annals of the New York Academy of Sciences,* **1417**(1), pp. 104-115.

SIDDIQUI, I., SCHAEUBLE, K., CHENNUPATI, V., FUERTES MARRACO, S.A., CALDERON-COPETE, S., PAIS FERREIRA, D., CARMONA, S.J., SCARPELLINO, L., GFELLER, D., PRADERVAND, S., LUTHER, S.A., SPEISER, D.E. and HELD, W., 2019. Intratumoral Tcf1+PD-1+CD8+ T Cells with Stem-like Properties Promote Tumor Control in Response to Vaccination and Checkpoint Blockade Immunotherapy. *Immunity (Cambridge, Mass.),* **50**(1), pp. 195-211.e10.

SIDHU, S.S., 2001. Engineering M13 for phage display. *Biomolecular engineering,* **18**(2), pp. 57-63.

SIDHU, S.S., WEISS, G.A. and WELLS, J.A., 2000. High Copy Display of Large Proteins on Phage for Functional Selections. *Journal of molecular biology,* **296**(2), pp. 487-495.

SIMPSON, T.R., LI, F., MONTALVO-ORTIZ, W., SEPULVEDA, M.A., BERGERHOFF, K., ARCE, F., RODDIE, C., HENRY, J.Y., YAGITA, H., WOLCHOK, J.D., PEGGS, K.S., RAVETCH, J.V., ALLISON, J.P. and QUEZADA, S.A., 2013. Fc-dependent depletion of tumor-infiltrating regulatory T cells co-defines the efficacy of anti–CTLA-4 therapy against melanoma. *The Journal of Experimental Medicine,* **210**(9), pp. 1695-1710.

SIVA, A.C., KIRKLAND, R.E., LIN, B., MARUYAMA, T., MCWHIRTER, J., YANTIRI-WERNIMONT, F., BOWDISH, K.S. and XIN, H., 2008. Selection of anti-cancer antibodies from combinatorial libraries by whole-cell panning and stringent subtraction with human blood cells. *Journal of immunological methods,* **330**(1), pp. 109-119.

SLOTH, A.B., BAKHSHINEJAD, B., JENSEN, M., STAVNSBJERG, C., LIISBERG, M.B., ROSSING, M. and KJAER, A., 2022. Analysis of Compositional Bias in a Commercial Phage Display Peptide Library by Next-Generation Sequencing. *Viruses,* **14**(11), pp. 2402.

SMITH G.P. and PETRENKO V.A. 1997. Phage Display. Chem Rev, 97(2), pp. 391-410.

SMITH, G.P. and SCOTT, J.K., 1993. [15] Libraries of peptides and proteins displayed on filamentous phage. *Methods in Enzymology.* United States: Elsevier Science & Technology, pp. 228-257.

SMITH, G.P., 1985. Filamentous fusion phage: novel expression vectors that display cloned antigens on the virion surface. *Science,* **228**(4705), pp. 1315-1317.

SOKULLU, E., SOLEYMANI ABYANEH, H. and GAUTHIER, M.A., 2019. Plant/Bacterial Virus-Based Drug Discovery, Drug Delivery, and Therapeutics. *Pharmaceutics,* **11**(5), pp. 211.

SOLÁ, R.J. and GRIEBENOW, K., 2009. Effects of glycosylation on the stability of protein pharmaceuticals. *Journal of pharmaceutical sciences,* **98**(4), pp. 1223-1245.

SØRENSEN, M.D., AGERHOLM, I.E., CHRISTENSEN, B., KØLVRAA, S. and KRISTENSEN, P., 2010. Microselection – affinity selecting antibodies against a single rare cell in a heterogeneous population. *Journal of cellular and molecular medicine,* **14**(7), pp. 1953-1961.

SORMANNI, P., AMERY, L., EKIZOGLOU, S., VENDRUSCOLO, M. and POPOVIC, B., 2017. Rapid and accurate in silico solubility screening of a monoclonal antibody library. *Scientific Reports,* **7**(1), pp. 8200-9.

SORMANNI, P., APRILE, F.A. and VENDRUSCOLO, M., 2018. Third generation antibody discovery methods: in silico rational design. *Chemical Society reviews,* **47**(24), pp. 9137-9157.

SPAGNUOLO, A. and GRIDELLI, C., 2018. "Comparison of the toxicity profile of PD-1 versus PD-L1 inhibitors in non-small cell lung cancer": is there a substantial difference or not? *Journal of thoracic disease,* **10**(Suppl 33), pp. S4065-S4068.

SPECTHRIE, L., BULLITT, E., HORIUCHI, K., MODEL, P., RUSSEL, M. and MAKOWSKI, L., 1992. Construction of a microphage variant of filamentous bacteriophage. *Journal of molecular biology,* **228**(3), pp. 720-724.

SPITERI, J. 2022, Development of Recombinant Antibodies Targeting T Cell Co-Inhibitory Molecule VISTA. BSc Thesis, Malta: University of Malta.

SS, S., 2000. Phage display in pharmaceutical biotechnology. Current Opinion in Biotechnology, 11(6), pp. 610-616.

STUDNICKA, G.M., SOARES, S., BETTER, M., WILLIAMS, R.E., NADELL, R. and HORWITZ, A.H., 1994. Human-engineered monoclonal antibodies retain full specific binding activity by preserving non-CDR complementarity-modulating residues. *Protein engineering,* **7**(6), pp. 805-814.

SU, E.W., BI, S. and KANE, L.P., 2011. Galectin-9 regulates T helper cell function independently of Tim-3. *Glycobiology (Oxford),* **21**(10), pp. 1258-1265.

SWANN, J.B. and SMYTH, M.J., 2007. Immune surveillance of tumors. *The Journal of clinical investigation,* **117**(5), pp. 1137-1146.

TAFLIN, C., FAVIER, B., BAUDHUIN, J., SAVENAY, A., HEMON, P., BENSUSSAN, A., CHARRON, D., GLOTZ, D. and MOONEY, N., 2011. Human endothelial cells generate Th17 and regulatory T cells under inflammatory conditions. *Proceedings of the National Academy of Sciences - PNAS,* **108**(7), pp. 2891-2896.

TAKEUCHI, Y. and NISHIKAWA, H., 2016. Roles of Regulatory T Cells in Cancer Immunity. *International Immunology,* **28**(8), pp. 401-409.

TAN, X., ZHANG, Z., YAO, H. and SHEN, L., 2018. Tim-4 promotes the growth of colorectal cancer by activating angiogenesis and recruiting tumor-associated macrophages via the PI3K/AKT/mTOR signaling pathway. *Cancer letters,* **436**, pp. 119-128.

TANG, D. and LOTZE, M.T., 2012. Tumor immunity times out: TIM-3 and HMGB1. Nature immunology, 13(9), pp. 808-810.

TAYLOR, A., VERHAGEN, J., BLASER, K., AKDIS, M. and AKDIS, C.A., 2006. Mechanisms of immune suppression by interleukin-10 and transforming growth factor-β: the role of T regulatory cells. *Immunology,* **117**(4), pp. 433-442.

TAYLOR, P.A., LEES, C.J., FOURNIER, S., ALLISON, J.P., SHARPE, A.H. and BLAZAR, B.R., 2004. B7 Expression on T Cells Down-Regulates Immune Responses through CTLA-4 Ligation via R-T Interactions. The Journal of immunology (1950), 172(1), pp. 34-39.

TEIXEIRA, A.A.R., D'ANGELO, S., ERASMUS, M.F., LEAL-LOPES, C., FERRARA, F., SPECTOR, L.P., NARANJO, L., MOLINA, E., MAX, T., DEAGUERO, A., PEREA, K., STEWART, S., BUONPANE, R.A., NASTRI, H.G. and BRADBURY, A.R.M., 2022. Simultaneous affinity maturation and developability enhancement using natural liability-free CDRs. *mAbs*, **14**(1), pp. 2115200.

TESNIERE, A., SCHLEMMER, F., MENDIBOURE, J., PIGNON, J.-., JOOSTE, V., VAN ENDERT, P., DUCREUX, M., ZITVOGEL, L., PIARD, F., KROEMER, G., BOIGE, V., KEPP, O., MARTINS, I., GHIRINGHELLI, F., AYMERIC, L., MICHAUD, M., APETOH, L. and BARAULT, L., 2010. Immunogenic death of colon cancer cells treated with oxaliplatin. *Oncogene*, **29**(4), pp. 482-491.

The BLAST Sequence Analysis Tool, The NCBI Handbook. The National Library of Medicine, Maryland, United States, Chapter 16. Accessed: 26/9/2023. [Online]. Available: https://www.unmc.edu/bsbc/docs/NCBI_blast.pdf

The His-Tag: Fundamentals And Principles [Cube Biotech], [Online]. Available: https://cube-biotech.com/knowledge/protein-purification/his-tag/#:~:text=The%20purification%20of%20a%20protein,7.5%20–%208%20is%20typical). [Oct 17, 2023]

THORNTON, A.M., LU, J., KORTY, P.E., KIM, Y.C., MARTENS, C., SUN, P.D. and SHEVACH, E.M., 2019. Helios+ and Helios− Treg subpopulations are phenotypically and functionally distinct and express dissimilar TCR repertoires. *European journal of immunology*, **49**(3), pp. 398-412.

TIAN, T. and LI, Z., 2021. Targeting Tim-3 in Cancer With Resistance to PD-1/PD-L1 Blockade. *Frontiers in oncology*, **11**, pp. 731175.

TONG, D., ZHOU, Y., CHEN, W., DENG, Y., LI, L., JIA, Z. and QI, D., 2012. T cell immunoglobulin- and mucin-domain-containing molecule 3 gene polymorphisms and susceptibility to pancreatic cancer. *Molecular biology reports*, **39**(11), pp. 9941-9946.

TREVINO, S.R., SCHOLTZ, J.M. and PACE, C.N., 2008. Measuring and Increasing Protein Solubility. *Journal of pharmaceutical sciences*, **97**(10), pp. 4155-4166.

TSENG, S.Y., OTSUJI, M., GORSKI, K., HUANG, X., SLANSKY, J.E., PAI, S.I., SHALABI, A., SHIN, T., PARDOLL, D.M. and TSUCHIYA, H., 2001. B7-Dc, a New Dendritic Cell Molecule with Potent Costimulatory Properties for T Cells. *The Journal of Experimental Medicine,* **193**(7), pp. 839-846.

UCHIYAMA, Y., KOIKE, M., KITAMURA, T., NAGATA, S., MIYANISHI, M. and TADA, K., 2007. Identification of Tim4 as a phosphatidylserine receptor. *Nature,* **450**(7168), pp. 435-439.

URBAN, J.H., MOOSMEIER, M.A., AUMÜLLER, T., THEIN, M., BOSMA, T., RINK, R., GROTH, K., ZULLEY, M., SIEGERS, K., TISSOT, K., MOLL, G.N. and PRASSLER, J., 2017. Phage display and selection of lanthipeptides on the carboxy-terminus of the gene-3 minor coat protein. Nature Communications, 8(1), pp. 1-10.

URBAN, J.L., SHEPARD, H.M., ROTHSTEIN, J.L., SUGARMAN, B.J. and SCHREIBER, H., 1986. Tumor Necrosis Factor: A Potent Effector Molecule for Tumor Cell Killing by Activated Macrophages. *Proceedings of the National Academy of Sciences - PNAS,* **83**(14), pp. 5233-5237.

URQUHART, L., 2020. Top companies and drugs by sales in 2019. *Nature reviews. Drug discovery,* **19**(4), pp. 228.

VADDEPALLY, R.K., KHAREL, P., PANDEY, R., GARJE, R. and CHANDRA, A.B., 2020. Review of Indications of FDA-Approved Immune Checkpoint Inhibitors per NCCN Guidelines with the Level of Evidence. *Cancers,* **12**(3), pp. 738.

VAKILIAN, M., 2022. A review on the effect of prolyl isomerization on immune response aberration and hypersensitivity reactions: A unifying hypothesis. *Clinical immunology (Orlando, Fla.),* **234**, pp. 108896.

VAN DE WEYER, P.S., MUEHLFEIT, M., KLOSE, C., BONVENTRE, J.V., WALZ, G. and KUEHN, E.W., 2006. A highly conserved tyrosine of Tim-3 is phosphorylated upon stimulation by its ligand galectin-9. *Biochemical and biophysical research communications,* **351**(2), pp. 571-576.

VAN ROSMALEN, M., KROM, M. and MERKX, M., 2017. Tuning the Flexibility of Glycine-Serine Linkers To Allow Rational Design of Multidomain Proteins. *Biochemistry (Easton),* **56**(50), pp. 6565-6574.

VAN WEZENBEEK, P.M.G.F., HULSEBOS, T.J.M. and SCHOENMAKERS, J.G.G., 1980. Nucleotide sequence of the filamentous bacteriophage M13 DNA genome: comparison with phage fd. *Gene,* **11**(1), pp. 129-148.

VIDARSSON, G., DEKKERS, G. and RISPENS, T., 2014. IgG Subclasses and Allotypes: From Structure to Effector Functions. *Frontiers in immunology,* **5**, pp. 520.

VINAY, D.S., RYAN, E.P., PAWELEC, G., TALIB, W.H., STAGG, J., ELKORD, E., LICHTOR, T., DECKER, W.K., WHELAN, R.L., KUMARA, H.M.C.S., SIGNORI, E., HONOKI, K., GEORGAKILAS, A.G., AMIN, A., HELFERICH, W.G., BOOSANI, C.S., GUHA, G., CIRIOLO, M.R., CHEN, S., MOHAMMED, S.I., AZMI, A.S., KEITH, W.N., BILSLAND, A., BHAKTA, D., HALICKA, D., FUJII, H., AQUILANO, K., ASHRAF, S.S., NOWSHEEN, S., YANG, X., CHOI, B.K. and KWON, B.S., 2015. Immune evasion in cancer: Mechanistic basis and therapeutic strategies. *Seminars in Cancer Biology,* **35**, pp. S185-S198.

VINCKE, C. and MUYLDERMANS, S., 2012. Introduction to Heavy Chain Antibodies and Derived Nanobodies. *Methods in molecular biology (Clifton, N.J.).* Totowa, NJ: Humana Press, pp. 15-26.

WALUNAS, T.L., LENSCHOW, D.J., BAKKER, C.Y., LINSLEY, P.S., FREEMAN, G.J., GREEN, J.M., THOMPSON, C.B. and BLUESTONE, J.A., 1994. CTLA-4 can function as a negative regulator of T cell activation. *Immunity (Cambridge, Mass.),* **1**(5), pp. 405-413.

WANG, R., LI, H., CAO, Y., WANG, Z., YANG, T. and WANG, J., 2023. M13 phage: a versatile building block for a highly specific analysis platform. Analytical and bioanalytical chemistry, 415(18), pp. 3927-3944.

WANG, S., CAMPOS, J., GALLOTTA, M., GONG, M., CRAIN, C., NAIK, E., COFFMAN, R.L. and GUIDUCCI, C., 2016. Intratumoral injection of a CpG oligonucleotide reverts resistance to PD-1 blockade by expanding multifunctional $CD8^+$ T cells. *Proceedings of the National Academy of Sciences - PNAS,* **113**(46), pp. E7240-E7249.

WANG, Z., CHEN, C., SU, Y. and KE, N., 2023. Function and characteristics of TIM-4 in immune regulation and disease (Review). International journal of molecular medicine, 51(2), pp. 1.

WARD, R.L., CLARK, M.A., LEES, J. and HAWKINS, N.J., 1996. Retrieval of human antibodies from phage-display libraries using enzymatic cleavage. *Journal of immunological methods,* **189**(1), pp. 73-82.

WHITE, S.H. and WIMLEY, W.C., 1999. MEMBRANE PROTEIN FOLDING AND STABILITY: Physical Principles. *Annual review of biophysics and biomolecular structure,* **28**(1), pp. 319-365.

WHITESIDE, T.L., 2008. The tumor microenvironment and its role in promoting tumor growth. Oncogene, 27(45), pp. 5904-5912.

WHITLOW, M., BELL, B.A., FENG, S., FILPULA, D., HARDMAN, K.D., HUBERT, S.L., ROLLENCE, M.L., WOOD, J.F., SCHOTT, M.E., MILENIC, D.E., YOKOTA, T. and SCHLOM, J., 1993. An improved linker

for single-chain Fv with reduced aggregation and enhanced proteolytic stability. Protein engineering, 6(8), pp. 989-995.

WIENER, Z., KOHALMI, B., POCZA, P., JEAGER, J., TOLGYESI, G., TOTH, S., GORBE, E., PAPP, Z. and FALUS, A., 2007. TIM-3 Is Expressed in Melanoma Cells and Is Upregulated in TGF-Beta Stimulated Mast Cells. *Journal of Investigative Dermatology*, **127**(4), pp. 906-914.

WILLIAMS, C. and DISTEL, B., 2010. Chapter 296 - Protein Quality Control in Peroxisomes: Ubiquitination of the Peroxisomal Targeting Signal Receptors. *Handbook of Cell Signaling, 2/e.* Second Edition edn. Elsevier Inc, pp. 2489-2497.

WINTER, G. and MILSTEIN, C., 1991. Man-made antibodies. *Nature (London)*, **349**(6307), pp. 293-299.

WITKOWSKA, M. and SMOLEWSKI, P., 2018. Immune Checkpoint Inhibitors to Treat Malignant Lymphomas. *Journal of Immunology Research*, **2018**, pp. 1982423-10.

WOLF PÉREZ, A., SORMANNI, P., ANDERSEN, J.S., SAKHNINI, L.I., RODRIGUEZ-LEON, I., BJELKE, J.R., GAJHEDE, A.J., DE MARIA, L., OTZEN, D.E., VENDRUSCOLO, M. and LORENZEN, N., 2019. In vitro and in silico assessment of the developability of a designed monoclonal antibody library. *mAbs*, **11**(2), pp. 388-400.

WOLF, Y., ANDERSON, A.C. and KUCHROO, V.K., 2020. TIM3 comes of age as an inhibitory receptor. *Nature reviews. Immunology*, **20**(3), pp. 173-185.

WONG, K., VALDEZ, P.A., TAN, C., YEH, S., HONGO, J. and OUYANG, W., 2010. Phosphatidylserine receptor Tim-4 is essential for the maintenance of the homeostatic state of resident peritoneal macrophages. *Proceedings of the National Academy of Sciences - PNAS*, **107**(19), pp. 8712-8717.

WU, C., THALHAMER, T., FRANCA, R., XIAO, S., WANG, C., HOTTA, C., ZHU, C., HIRASHIMA, M., ANDERSON, A. and KUCHROO, V., 2014. Galectin-9-CD44 Interaction Enhances Stability and Function of Adaptive Regulatory T Cells. *Immunity*, **41**(2), pp. 270-282.

WU, T., JI, Y., MOSEMAN, E.A., XU, H.C., MANGLANI, M., KIRBY, M., ANDERSON, S.M., HANDON, R., KENYON, E., ELKAHLOUN, A., WU, W., LANG, P.A., GATTINONI, L., MCGAVERN, D.B. and SCHWARTZBERG, P.L., 2016. The TCF1-Bcl6 axis counteracts type I interferon to repress exhaustion and maintain T cell stemness. *Science immunology*, **1**(6),.

XU, B., YUAN, L., GAO, Q., YUAN, P., ZHAO, P., YUAN, H., FAN, H., LI, T., QIN, P., HAN, L., FANG, W. and SUO, Z., 2015. Circulating and tumor-infiltrating Tim-3 in patients with colorectal cancer. *Oncotarget,* **6**(24), pp. 20592-20603.

XU, J.L. and DAVIS, M.M., 2000. Diversity in the CDR3 Region of VH Is Sufficient for Most Antibody Specificities. Immunity, 13(1), pp. 37-45.

XU, L., QI, J., LIU, X., MA, H., YUAN, W., ZHAO, P., LIANG, X., XU, Y., WANG, H., XU, X., WANG, W., MA, C. and GAO, L., 2015. Tim-4 Inhibits NO Generation by Murine Macrophages. *PLoS ONE,* **10**(4), pp. e0124771.

XU, L., QI, J., ZHAO, P., LIANG, X., JU, Y., LIU, P., LIU, B., GUO, C., ZHANG, L., MA, C. and GAO, L., 2010a. T cell immunoglobulin- and mucin-domain-containing molecule-4 attenuates concanavalin A-induced hepatitis by regulating macrophage. *Journal of leukocyte biology,* **88**(2), pp. 329-336.

XU, L., XIAO, H., XU, M., ZHOU, C., YI, L. and LIANG, H., 2011. Glioma-derived T Cell Immunoglobulin- and Mucin Domain-containing Molecule-4 (TIM4) Contributes to Tumor Tolerance. *The Journal of biological chemistry,* **286**(42), pp. 36694-36699.

YAMANISHI, Y., KITAURA, J., IZAWA, K., KAITANI, A., KOMENO, Y., NAKAMURA, M., YAMAZAKI, S., ENOMOTO, Y., OKI, T., AKIBA, H., ABE, T., KOMORI, T., MORIKAWA, Y., KIYONARI, H., TAKAI, T., OKUMURA, K. and KITAMURA, T., 2010. TIM1 is an endogenous ligand for LMIR5/CD300b: LMIR5 deficiency ameliorates mouse kidney ischemia/reperfusion injury. *The Journal of Experimental Medicine,* **207**(7), pp. 1501-1511.

YAMASHITA, M., SHINNAKASU, R., ASOU, H., KIMURA, M., HASEGAWA, A., HASHIMOTO, K., HATANO, N., OGATA, M. and NAKAYAMA, T., 2005. Ras-ERK MAPK Cascade Regulates GATA3 Stability and Th2 Differentiation through Ubiquitin-Proteasome Pathway. *The Journal of biological chemistry,* **280**(33), pp. 29409-29419.

YAMAZAKI, T., AKIBA, H., IWAI, H., MATSUDA, H., AOKI, M., TANNO, Y., SHIN, T., TSUCHIYA, H., PARDOLL, D.M., OKUMURA, K., AZUMA, M. and YAGITA, H., 2002. Expression of Programmed Death 1 Ligands by Murine T Cells and APC. *The Journal of immunology (1950),* **169**(10), pp. 5538-5545.

YAN, J., ZHANG, Y., ZHANG, J., LIANG, J., LI, L. and ZHENG, L., 2013. Tim-3 Expression Defines Regulatory T Cells in Human Tumors. *PLoS ONE,* **8**(3), pp. e58006.

YANG, B., LUO, Y., LIU, Z., YANG, P. and GUI, Y., 2018. Probiotics SOD inhibited food allergy via downregulation of STAT6-TIM4 signaling on DCs. *Molecular immunology,* **103**, pp. 71-77.

YANG, Y., 2015. Cancer immunotherapy: harnessing the immune system to battle cancer. *The Journal of clinical investigation,* **125**(9), pp. 3335-3337.

YEUNG, M.Y., MCGRATH, M.M., NAKAYAMA, M., SHIMIZU, T., BOENISCH, O., MAGEE, C.N., ABDOLI, R., AKIBA, H., UENO, T., TURKA, L.A. and NAJAFIAN, N., 2013. Interruption of Dendritic Cell–Mediated TIM-4 Signaling Induces Regulatory T Cells and Promotes Skin Allograft Survival. *The Journal of immunology (1950),* **191**(8), pp. 4447-4455.

YOO, D.K., LEE, S.R., JUNG, Y., HAN, H., LEE, H.K., HAN, J., KIM, S., CHAE, J., RYU, T. and CHUNG, J., 2020. Machine Learning-Guided Prediction of Antigen-Reactive In Silico Clonotypes Based on Changes in Clonal Abundance through Bio-Panning. *Biomolecules,* **10**(3), pp. 421.

YOON, H.H., ORROCK, J.M., FOSTER, N.R., SARGENT, D.J., SMYRK, T.C. and SINICROPE, F.A., 2012. Prognostic Impact of FoxP3+ Regulatory T Cells in Relation to CD8+ T Lymphocyte Density in Human Colon Carcinomas. *PLoS ONE,* **7**(8), pp. e42274.

YU, P., LEE, Y., LIU, W., KRAUSZ, T., CHONG, A., SCHREIBER, H. and FU, Y., 2005. Intratumor depletion of CD4+ cells unmasks tumor immunogenicity leading to the rejection of late-stage tumors. *The Journal of Experimental Medicine,* **201**(5), pp. 779-791.

ZAHND, C., SPINELLI, S., LUGINBUEHL, B., AMSTUTZ, P., CAMBILLAU, C. and PLUECKTHUN, A., 2004. Directed in Vitro Evolution and Crystallographic Analysis of a Peptide-binding Single Chain Antibody Fragment (scFv) with Low Picomolar Affinity. *The Journal of biological chemistry,* **279**(18), pp. 18870-18877.

ZHANG, Q., WANG, H., WU, X., LIU, B., LIU, W., WANG, R., LIANG, X., MA, C. and GAO, L., 2015a. TIM-4 promotes the growth of non-small-cell lung cancer in a RGD motif-dependent manner. *British Journal of Cancer,* **113**(10), pp. 1484-1492.

ZHANG, X., GU, J., ZHOU, L. and MI, Q., 2016. TIM-4 is expressed on invariant NKT cells but dispensable for their development and function. *Oncotarget*, **7**(44), pp. 71099-71111.

ZHANG, Y., CAI, P., LIANG, T., WANG, L. and HU, L., 2017. TIM-3 is a potential prognostic marker for patients with solid tumors: A systematic review and meta-analysis. *Oncotarget*, **8**(19), pp. 31705-31713.

ZITVOGEL, L., GALLUZZI, L., SMYTH, M. and KROEMER, G., 2013. Mechanism of Action of Conventional and Targeted Anticancer Therapies: Reinstating Immunosurveillance. *Immunity*, **39**(1), pp. 74-88.

Appendix

Appendix A: CFU measurements

A.1 CFU of previously biopanned proteins after fresh titering

Table A.1: CFU of previously biopanned proteins after fresh titering. *Phage count was sufficient at 10^{12}.*

Protein & Round	Dilution Factor	Number of Colonies	Colony Forming Unit (CFU/ml)
Round 4 TIM-3	10^{10}	46	9.2×10^{12}
Round 4 IgG	10^{9}	124	2.5×10^{12}

A.2 CFU counts for TIM-4 in failed TIM-4 biopanning

Table A.2: CFU counts for TIM-4 in failed TIM-4 biopanning. *Phage count for TIM-4 after 5 rounds of biopanning was maintained at 10^{12}.*

Protein & Round	Dilution Factor	Number of Colonies	Colony Forming Unit (CFU/ml)
Round 1 TIM-4	10^{10}	68	1.4×10^{13}
Round 2 TIM-4	10^{9}	118	2.4×10^{12}
Round 3 TIM-4	10^{9}	57	1.1×10^{12}
Round 4 TIM-4	10^{9}	102	2.0×10^{12}
Round 5 TIM-4	10^{9}	>300	$> 6.0 \times 10^{12}$

A.3 CFU counts for NPC in failed TIM-4 biopanning

Table A.3: CFU counts for NPC in failed TIM-4 biopanning. *Phage count for the NPC was maintained at $10^{11\text{-}12}$ throughout the 5 rounds of biopanning.*

Protein & Round	Dilution Factor	Number of Colonies	Colony Forming Unit (CFU/ml)
Round 1 NPC	10^{10}	20	4.0×10^{12}
Round 2 NPC	10^{9}	85	1.7×10^{12}
Round 3 NPC	10^{8}	205	4.1×10^{11}
Round 4 NPC	10^{9}	82	1.6×10^{12}
Round 5 NPC	10^{9}	>300	$> 6.0 \times 10^{12}$

A.4 CFU counts for TIM-4 in successful TIM-4 biopanning

Table A.4: CFU counts for TIM-4 in successful TIM-4 biopanning. *Phage count for TIM-4 was maintained at $10^{12\text{-}13}$ throughout the 4 rounds of biopanning.*

Protein & Round	Dilution Factor	Number of Colonies	Colony Forming Unit (CFU/ml)
Round 1 TIM-4	10^{10}	177	3.5×10^{13}
Round 2 TIM-4	10^{10}	63	1.3×10^{13}
Round 3 TIM-4	10^{10}	61	1.2×10^{13}
Round 4 TIM-4	10^{10}	31	6.2×10^{12}

A.5 CFU counts for NPM in successful TIM-4 biopanning

Table A.5: CFU counts for NPM in successful TIM-4 biopanning. *Phage count for NPC was maintained at $10^{12\text{-}13}$ throughout the 4 rounds of biopanning.*

Protein & Round	Dilution Factor	Number of Colonies	Colony Forming Unit (CFU/ml)
Round 1 NPC	10^{10}	114	2.3×10^{13}
Round 2 NPC	10^{10}	40	8.0×10^{12}
Round 3 NPC	10^{10}	47	9.4×10^{12}
Round 4 NPC	10^{9}	93	1.9×10^{12}

A.6 CFU counts for trimer in successful TIM-4 biopanning

Table A.6: CFU counts for trimer in successful TIM-4 biopanning. *Phage titre for trimer was maintained at 10^{12} throughout the rounds.*

Protein & Round	Dilution Factor	Number of Colonies	Colony Forming Unit (CFU/ml)
Round 1 Trimer	10^{10}	>300	$> 6.0 \times 10^{12}$
Round 2 Trimer	10^{10}	>300	$> 6.0 \times 10^{12}$
Round 3 Trimer	10^{9}	240	4.8×10^{12}
Round 4 Trimer	10^{10}	>300	$> 6.0 \times 10^{12}$

Appendix B: Amplification of Round 4 of TIM-3

From the experiments performed on the TIM-3 rounds as per **Section 3.2.2** it was determined that the round 4 of TIM-3 needed to be amplified. The amplification steps from **Section 2.2.1** were performed on round 4 of TIM-3 and ELISA was used to confirm that the amplification was successful. The ELISA wells were

coated with TIM-3 and 1/10, 1/100 and 1/100 serial dilutions were made of the old round 4 of TIM-3 and the new amplified round 4 of TIM-3 and added to the wells. The negative control used was a no library control. For this control no phage library was added to the TIM-3-bound ELISA wells. The fluorescence of anti-M13-PE detection antibody was used to create a graph of phage dilutions against anti-M13-PE antibody.

As expected, **Figure B.1** showed that amplification was successful since the fluorescence of the new amplified round 4 of TIM-3 was higher than that of the old round 4 of TIM-3. The negative no library control had the lowest fluorescence as was expected.

The AUC of the old and new TIM-3 round 4 was calculated and Welch's t test was used to compare the AUCs and determine if there was a statistically significant difference between the old and new TIM-3 round 4 libraries. Statistical analysis showed no statistically significant difference between the AUCs of the old and amplified libraries.

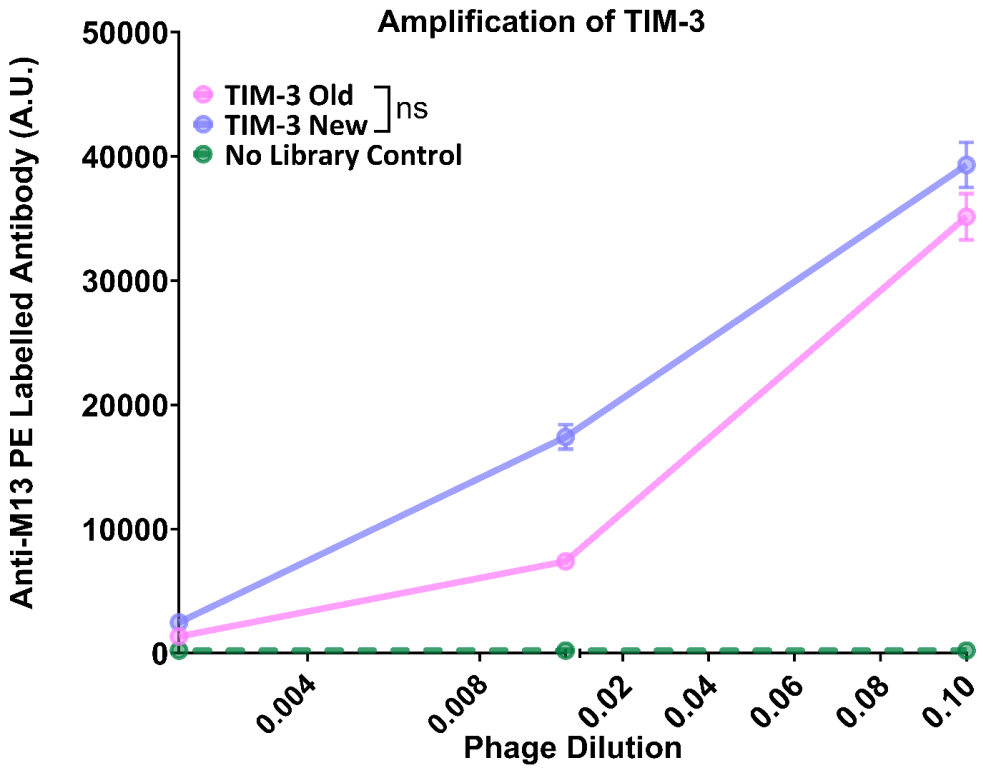

Figure B.1: Graph of phage dilutions against anti-M13-PE antibody. *The amplification of TIM-3 round 4 resulted in a higher fluorescence. However, statistical analysis showed that this increase in fluorescence was not significant.*

Appendix C: Nanodrop measurements

C.1 Nanodrop measurements for TIM-3

Table C.1: Nanodrop measurements for TIM-3. *Measurements taken on the nanodrop were considered sufficient for the samples to be sent for sanger sequencing.*

Anti-TIM-3-Fc phage clones	Concentration (Ng/ul)	260/280	260/230
Clone 1	81.5	1.87	2.18
Clone 2	116.4	1.86	2.04
Clone 3	113.6	1.92	2.37
Clone 4	77.6	1.84	1.55
Clone 5	69.3	1.86	1.77
Clone 6	63.2	1.88	1.87
Clone 7	92.4	1.91	2.2
Clone 8	87.5	1.91	2.19
Clone 9	93.5	1.91	2.18
Clone 10	94	1.92	2.26
Clone 11	65	1.91	1.87
Clone 12	116.9	1.85	2.31
Clone 13	93.1	1.87	1.81
Clone 14	107.3	1.76	1.48
Clone 15	86.4	1.91	2.2
Clone 16	117.6	1.87	2.15
Clone 17	105	1.90	2.03
Clone 18	128.4	1.92	2.27
Clone 19	116.9	1.90	2.03
Clone 20	116.2	1.88	2.26
Clone 21	107.2	1.93	2.12
Clone 22	122.1	1.92	2.11
Clone 23	106.1	1.89	2.34
Clone 24	111	1.88	2.23
Clone 25	103.4	1.91	2.09
Clone 26	74.9	1.92	2.14
Clone 27	106.4	1.88	2.02
Clone 28	80.2	1.87	1.91
Clone 29	58.6	1.83	1.69
Clone 30	65.4	1.88	2.19

C.2 Nanodrop measurements for IgG

Table C.2: Nanodrop measurements for IgG. *Measurements taken on the nanodrop were considered sufficient for the samples to be sent for sanger sequencing.*

Anti-IgG-Fc phage clones	Concentration (Ng/ul)	260/280	260/230
Clone 1	49.7	1.92	2.11
Clone 2	117.3	1.89	2.17
Clone 3	106.4	1.95	2.46
Clone 4	125.8	1.92	2.19
Clone 5	112.5	1.89	2.19
Clone 6	110.9	1.91	2.25
Clone 7	122.3	1.89	2.11
Clone 8	113.1	1.89	1.94
Clone 9	130.8	1.91	2.16
Clone 10	122.3	1.88	1.86
Clone 11	127	1.92	2.22
Clone 12	133.2	1.90	2.19
Clone 13	111	1.90	2.23
Clone 14	113.9	1.89	2.18
Clone 15	125	1.90	2.3
Clone 16	102.8	1.88	2.14
Clone 17	108.7	1.91	2.13
Clone 18	94.2	1.90	2.17
Clone 19	51.4	1.97	2.1
Clone 20	136.9	1.91	2.18
Clone 21	131.8	1.92	2.09
Clone 22	130.8	1.91	2.15
Clone 23	146.2	1.92	2.08
Clone 24	127.7	1.92	2.12
Clone 25	124	1.92	2.09
Clone 26	145.3	1.89	1.91
Clone 27	100.7	1.94	2.16
Clone 28	131.1	1.93	2.11
Clone 29	135.6	1.90	2.06
Clone 30	155.9	1.91	2.13

C.3 Nanodrop measurements for TIM-4

Table C.3: Nanodrop measurements for TIM-4. *Measurements taken on the nanodrop were considered sufficient for the samples to be sent for sanger sequencing.*

Anti-TIM-4 phage clones	Concentration (Ng/ul)	260/280	260/230
Clone 1	63.7	1.96	2.07
Clone 2	114.3	1.90	2.11
Clone 3	33.4	1.99	1.62
Clone 4	58	1.89	1.6
Clone 5	99.6	1.92	2.07
Clone 6	55.5	1.96	1.98
Clone 7	109.4	1.89	2.06
Clone 8	99.8	1.91	2.02
Clone 9	105.1	1.90	2.16
Clone 10	44.7	1.93	1.75
Clone 11	44	1.93	1.67
Clone 12	111.8	1.92	2.1
Clone 13	59.9	1.98	1.94
Clone 19	103	1.94	2.15
Clone 21	108.5	1.90	2.03
Clone 27	110.9	1.93	2.11

C.4 Nanodrop measurements for original library

Table C.4: Nanodrop measurements for original library. *Measurements taken on the nanodrop were considered sufficient for the samples to be sent for sanger sequencing.*

Original Library	Concentration (Ng/ul)	260/280	260/230
Clone 1	61.5	1.80	1.85
Clone 2	69.7	1.75	1.62
Clone 3	59.3	1.77	1.68
Clone 4	57.4	1.85	2.08
Clone 5	75.9	1.83	2.12
Clone 6	51.0	1.81	1.96
Clone 7	42.5	1.81	2.02
Clone 8	88.8	1.86	2.22
Clone 9	73.8	1.81	1.95
Clone 10	53.6	1.85	2.14
Clone 11	48.3	1.82	2.00
Clone 12	54.4	1.83	1.82
Clone 13	65.0	1.83	2.02
Clone 14	44.4	1.82	2.13
Clone 15	48.8	1.78	1.85

C.5 Nanodrop measurements for no protein control

Table C.5: Nanodrop measurements for no protein control. *Measurements taken on the nanodrop were considered sufficient for the samples to be sent for sanger sequencing.*

Original Library	Concentration (Ng/ul)	260/280	260/230
Clone 1	88.8	1.82	2.03
Clone 2	61.3	1.80	2.04
Clone 3	136	1.80	2.10
Clone 4	81.7	1.99	2.03
Clone 5	121	1.89	2.06
Clone 6	116	1.90	1.89
Clone 7	111.4	1.92	2.01
Clone 8	105.5	1.86	2.17
Clone 9	96	1.77	1.97
Clone 10	121	1.95	2.21

Appendix D: Sanger Sequencing Data

Appendix D.1 of Original Phage Library and Nonsense Clones

The original phage library was sequenced to try and determine the most common scFv sequences in the phages prior to biopanning. A consensus with a threshold of >50% was used for comparison of the alignment. All the original phage library clones that were successfully sequenced had a nonsense amino acid sequence full of stop codons. This was also observed for some anti-TIM-4 clones, an anti-IgG-Fc clone and some of the no protein control (refer to **Figure D.1**). The binding of these clones to the target proteins, His-tag beads and containers could be explained by the fact that smaller proteins or peptides are known to be stickier (Lowe 2022). It would be interesting to determine why the only sequenced clones of the original phage library were those with a nonsense amino acid sequence full of stop codons. As per **Figure D.1**, anti-TIM-4 clones 1, 4, 6, 10 and 13 show the same nonsense amino acid sequences as the no protein control clones 8 and 9. Anti-TIM-4 clone 11 is unique and so are all the clones of the original phage library. Anti-IgG-Fc clone 28 is also unique.

Figure D.1: Alignments of high quality sequenced monoclones grouped by sequence similarity. *The sequences were very similar and contained a multitude of stop codons.*

Appendix D.2 Swiss-Model Ramachandran Plots and Superposition of Structures

The proteins and clones visualized using SWISS-MODEL were analyzed using Ramachandran plots as in **Figures D.2 to D.6** which are graphical representations of dihedral angles of amino acid residues in protein structures. The ψ values were plotted in the x-axis and the φ values were plotted in the y-axis to predict the potential conformation of the proteins and clones. The plot also assessed the sterically allowed and disallowed conformations in the proteins' backbone and aided in the assessment of the quality of protein structures produced. It was also used to understand the energetically favorable regions of protein folding (Hollingsworth, Karplus 2010).

A) Ramachandran plot for TIM-3

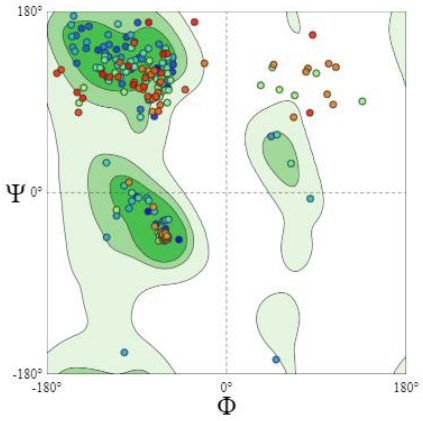

B) Ramachandran plot for TIM-3 ECD

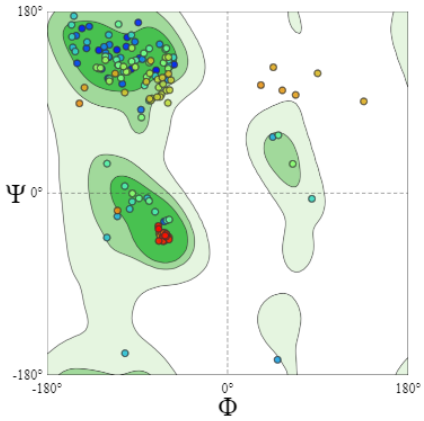

C) Ramachandran plot for TIM-4

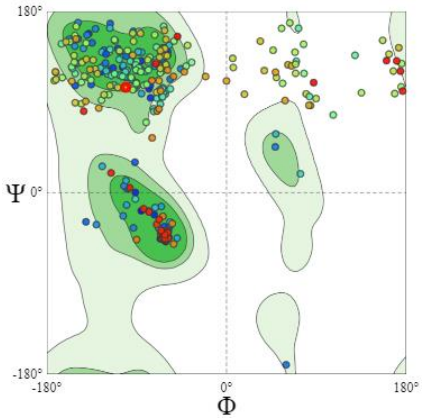

D) Ramachandran plot for TIM-4 ECD

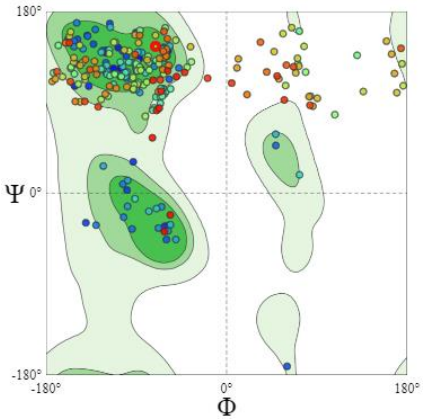

Figure D.2: Ramachandran plots for TIM-3 and TIM-4. *Ramachandran plot for A) TIM-3 protein, B) TIM-3 ECD, C) TIM-4 protein and D) TIM-4 ECD.*

A) TIM-3 clone 11 closed structure

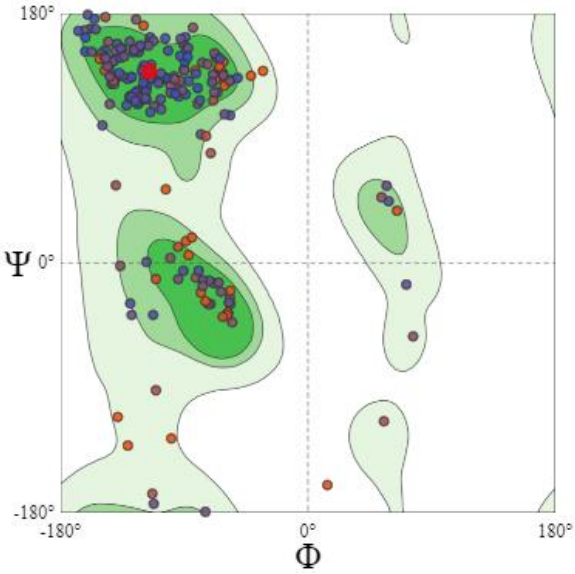

B) TIM-3 clone 11 open structure

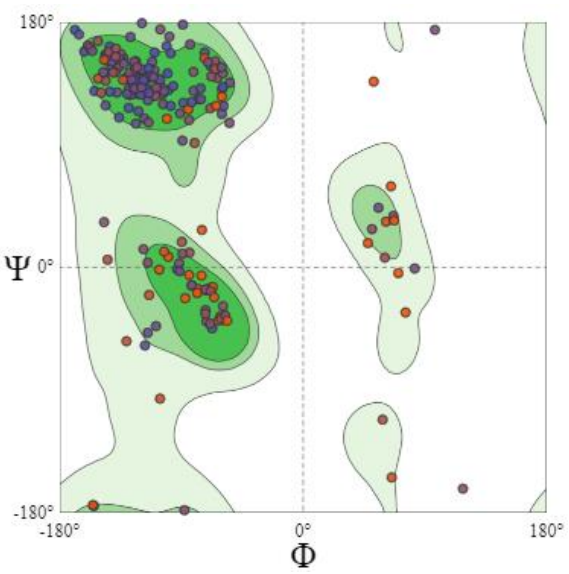

C) TIM-3 structures superposed

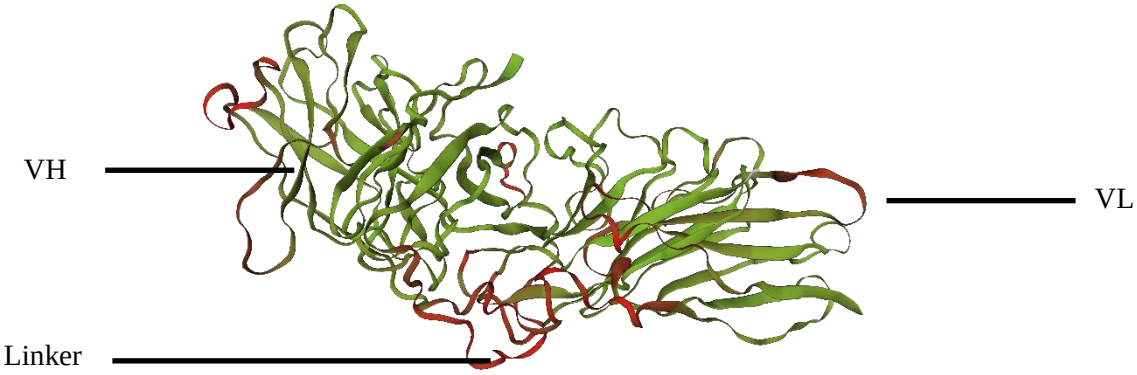

Figure D.3: Ramachandran plots for TIM-3 clone 11. *SWISS-MODEL predicted two different structures for TIM-3 clone 11. A) Ramachandran plot for the closed structure of the scFv and C) Ramachandran plot for the more open scFv structure predicted. C) Superposition of the two predicted models.*

Ramachandran plot for IgG Clone 6

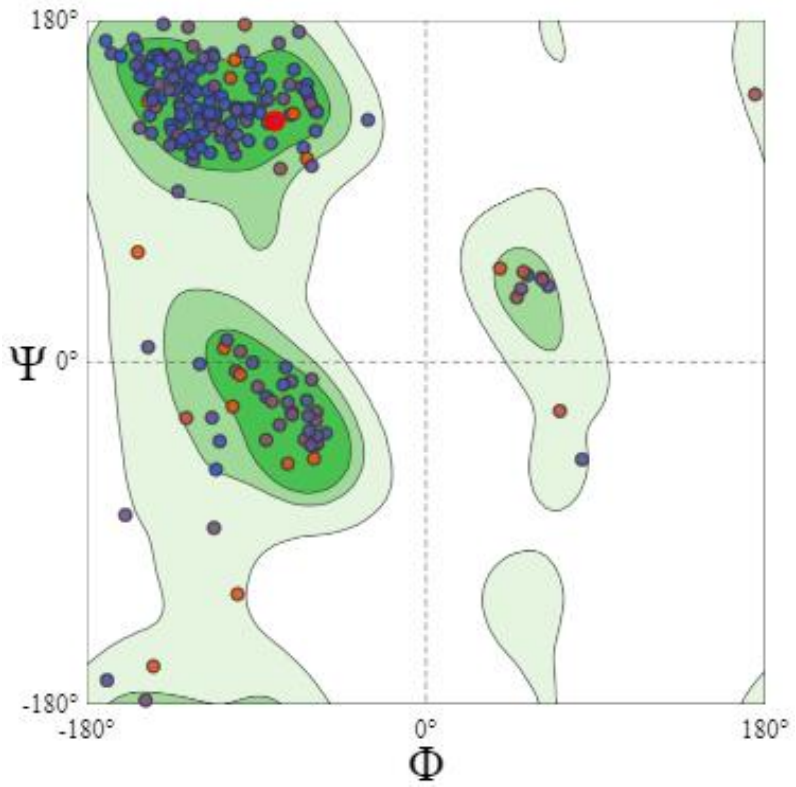

Figure D.4: Ramachandran plots for IgG Clone 6. *The model predicted one potential 3D structure for IgG clone 6. Despite SWISS-MODEL only predicting the closed scFv structure, there may still be a possibility of an open structure which would be determined through methods such as X-ray crystallography or hydrogen deuterium exchange mass spectrometry.*

A) TIM-4 clone 9 closed structure

B) TIM-4 clone 9 open structure

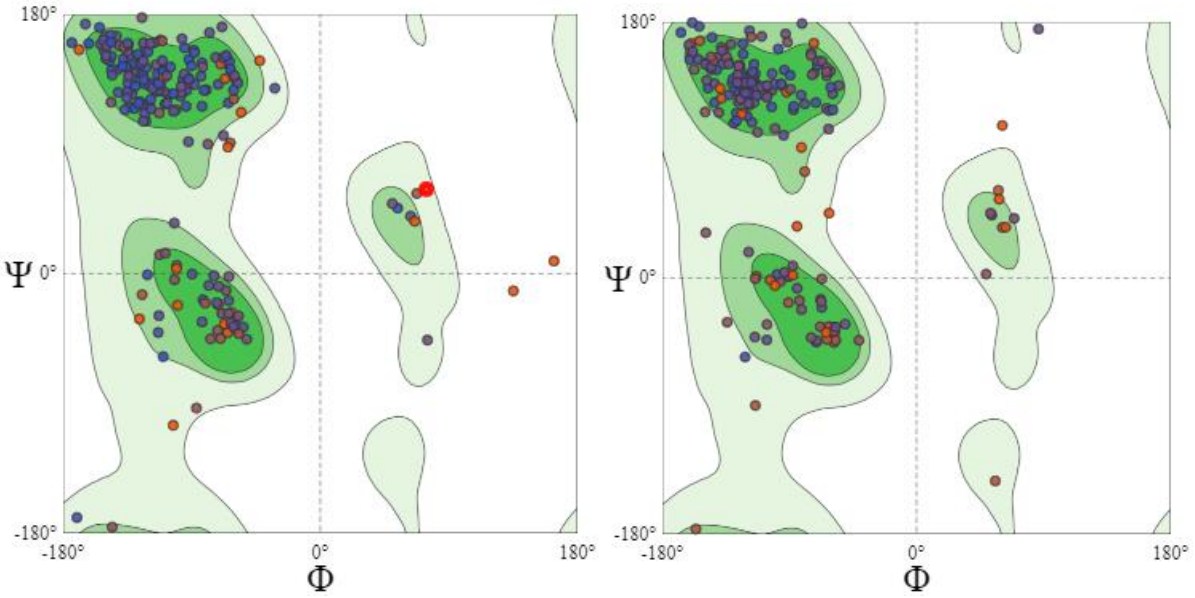

C) Superposition of open and closed structures of TIM-4 clone 9

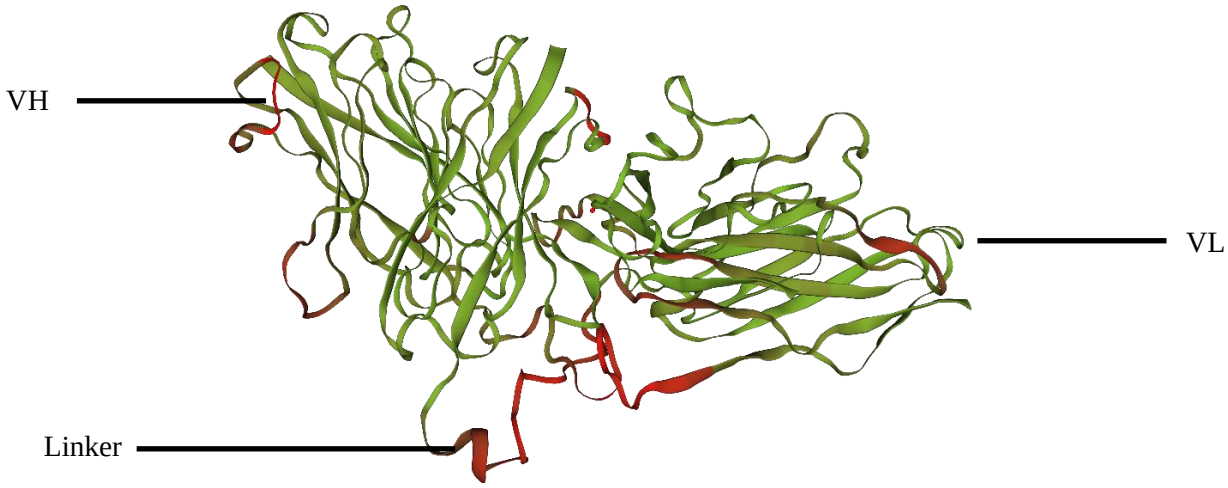

Figure D.5: Ramachandran plots for TIM-4 clone 9. *SWISS-MODEL predicted two different structures for TIM-4 clone 9. A) Ramachandran plot for the closed structure of the scFv and C) Ramachandran plot for the more open scFv structure predicted. C) Superposition of the two predicted models.*

A) NPC clone 5 closed structure

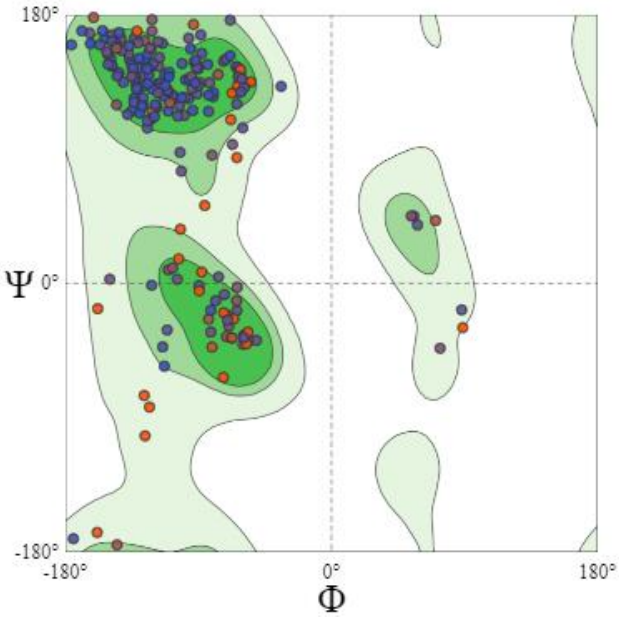

B) NPC clone 5 open structure

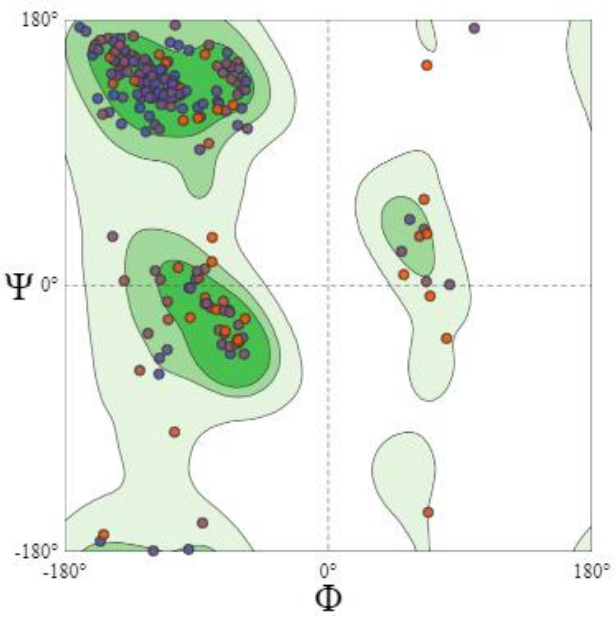

C) NPC clone 5 structures superposed

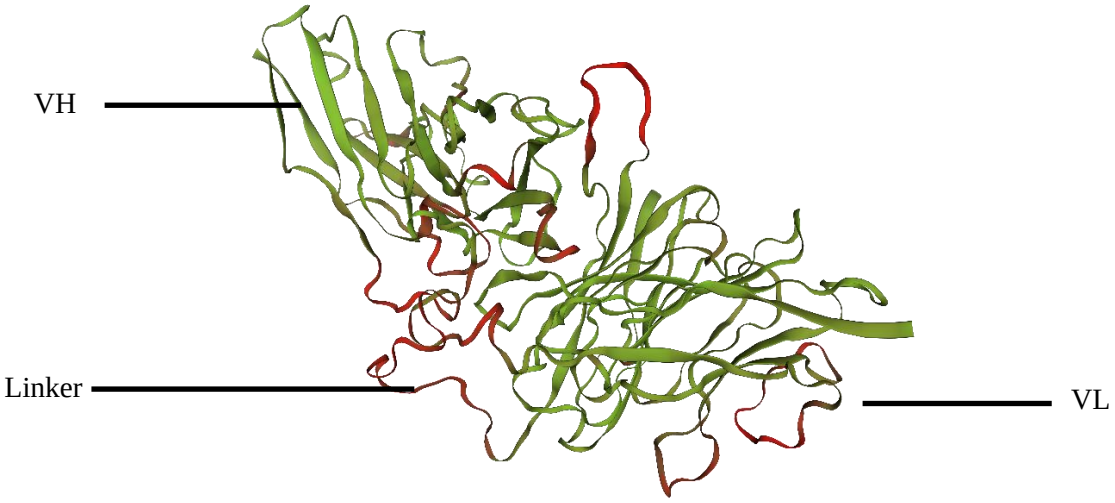

Figure D.6: Ramachandran plots for NPC clone 5. *SWISS-MODEL predicted two different structures for NPC clone 5. A) Ramachandran plot for the closed structure of the scFv and C) Ramachandran plot for the more open scFv structure predicted. C) Superposition of the two predicted models.*

Appendix D.3 BLAST Results for Comparisons Between Clones

Table D.1: Schematic showing similarities in CDR regions of fully sequenced clones. *The green represented sequence comparisons that showed no similarity and red represented sequence comparisons that showed some level of similarity. The labels "A), B), C) etc." refer to the BLAST alignments in* ***Figure D.7****.*

Sequence Comparison	CDR1-VH Bit Score	CDR2-VH Bit Score	CDR3-VH Bit Score	CDR1-VL Bit Score	CDR2-VL Bit Score	CDR3-VL Bit Score
Anti-TIM-3 Fc clone 7 vs Anti-IgG-Fc clone 6	0	A) 36.7	0	B) 34.6	0	0
Anti-TIM-3 Fc clone 7 vs Anti-IgG-Fc clone 27	0	C) 29.9	0	0	0	0
Anti-TIM-3 Fc clone 30 vs Anti-IgG-Fc clone 6	0	D) 34.6	0	0	0	E) 12.1
Anti-TIM-3 Fc clone 30 vs Anti-IgG-Fc clone 27	0	F) 24.4	0	0	0	G) 26.5
Anti-TIM-3 Fc clone 8 vs Anti-IgG-Fc clone 6	0	H) 36.7	0	0	I) 15.1	0
Anti-TIM-3 Fc clone 8 vs Anti-IgG-Fc clone 27	0	J) 29.9	0	K) 35.4	0	L) 32.9
Anti-TIM-3 Fc clone 29 vs Anti-IgG-Fc clone 6	0	M) 36.7	0	N) 34.6	0	0
Anti-TIM-3 Fc clone 29 vs Anti-IgG-Fc clone 27	0	O) 29.9	0	0	0	0
Anti-TIM-3 Fc clone 13 vs Anti-IgG-Fc clone 6	0	P) 36.7	0	0	0	0
Anti-TIM-3 Fc clone 13 vs Anti-IgG-Fc clone 27	0	Q) 29.9	0	R) 35.4	S) 16.3	T) 21.4
Anti-TIM-3 Fc clone 8 vs Anti-TIM-4 clone 9	0	U) 27.4	0	0	0	0
Anti-TIM-3 Fc clone 29 vs Anti-TIM-4 clone 9	0	V) 27.4	0	W) 15.1	0	0
Anti-TIM-3 Fc clone 13 vs Anti-TIM-4 clone 9	0	X) 27.4	0	0	0	0
Anti-TIM-4 clone 9 vs Anti-TIM-3 Fc clone 7	0	Y) 27.4	0	Z) 15.1	0	0
Anti-TIM-4 clone 9 vs Anti-TIM-3 Fc clone 30	0	AA) 22.3	0	0	0	0
Anti-TIM-4 clone 9 vs NPC Clone 5	0	AB) 23.1	0	0	0	0
Anti-TIM-4 clone 9 vs NPC Clone 6	0	AC) 19.7	0	0	0	0

Table D.2: Schematic showing similarities in CDR regions of fully sequenced clones. *The green represented sequence comparisons that showed no similarity and red represented sequence comparisons that showed some level of similarity. The labels "A), B), C) etc." refer to the BLAST alignments in* ***Figure D.8.***

Comparison	CDR1-VH Bit Score	CDR2-VH Bit Score	CDR3-VH Bit Score	CDR1-VL Bit Score	CDR2-VL Bit Score	CDR3-VL Bit Score
NPC Clone 5 vs NPC Clone 6	0	0	0	A) 12.1	0	0
Anti-IgG-Fc clone 6 vs Anti-IgG-Fc clone 27	0	B) 29.1	0	0	C) 15.1	0
Anti-TIM-3 Fc clone 8 vs Anti-TIM-3 Fc clone 13	D) 25.2	E) 50.3	F) 15.1	G) 35.4	H) 16.3	I) 21.4
Anti-TIM-3 Fc clone 7 vs Anti-TIM-3 Fc clone 30	0	J) 27.4	0	0	0	0

A) Anti-TIM-3 Fc clone 7 vs Anti-IgG-Fc clone 6 CDR2-VH

IgG Clone 6 CDR2-VH

Sequence ID: Query_227777 Length: 17 Number of Matches: 1

Range 1: 2 to 16 Graphics ▼ Next Match ▲ Previous Match

Score	Expect	Identities	Positives	Gaps
36.7 bits(79)	2e-11	12/15(80%)	12/15(80%)	0/15(0%)

```
Query  2   INGDGSSTSYADAVK  16
           IN DG  TSYADAVK
Sbjct  2   INSDGGDTSYADAVK  16
```

B) Anti-TIM-3 Fc clone 7 vs Anti-IgG-Fc clone 6 CDR1-VL

IgG Clone 6 CDR1-VL

Sequence ID: Query_261361 Length: 14 Number of Matches: 1

Range 1: 1 to 14 Graphics ▼ Next Match ▲ Previous Match

Score	Expect	Identities	Positives	Gaps
34.6 bits(74)	5e-11	12/14(86%)	13/14(92%)	1/14(7%)

```
Query  1   TGSSSNIG-GNYVG  13
           TGSSSN+G GNYVG
Sbjct  1   TGSSSNVGYGNYVG  14
```

C) Anti-TIM-3 Fc clone 7 vs Anti-IgG-Fc clone 27 CDR2-VH

IgG Clone 27 CDR2-VH

Sequence ID: Query_57071 Length: 17 Number of Matches: 1

Range 1: 5 to 16 Graphics ▼ Next Match ▲ Previous Match

Score	Expect	Identities	Positives	Gaps
29.9 bits(63)	9e-09	10/12(83%)	10/12(83%)	0/12(0%)

```
Query  5   DGSSTSYADAVK  16
           DGS TSY DAVK
Sbjct  5   DGSITSYTDAVK  16
```

D) Anti-TIM-3 Fc clone 30 vs Anti-IgG-Fc clone 6 CDR2-VH

IgG Clone 6 CDR2-VH

Sequence ID: Query_63699 Length: 17 Number of Matches: 1

Range 1: 2 to 17 Graphics ▼ Next Match ▲ Previous Match

Score	Expect	Identities	Positives	Gaps
34.6 bits(74)	1e-10	13/16(81%)	13/16(81%)	1/16(6%)

```
Query  2   INS-GGTTGYADAVKG  16
           INS GG T YADAVKG
Sbjct  2   INSDGGDTSYADAVKG  17
```

E) Anti-TIM-3 Fc clone 30 vs Anti-IgG-Fc clone 6 CDR3-VL

IgG Clone 6 CDR3-VL

Sequence ID: Query_469827 Length: 11 Number of Matches: 1

Range 1: 4 to 11 Graphics ▼ Next Match ▲ Previous Match

Score	Expect	Identities	Positives	Gaps
12.1 bits(21)	0.015	5/8(63%)	5/8(62%)	0/8(0%)

```
Query  4   DSSTRAAV  11
           DSS  AV
Sbjct  4   DSSLSGAV  11
```

F) Anti-TIM-3-Fc clone 30 vs Anti-IgG-Fc clone 6 CDR2-VH

IgG Clone 27 CDR2-VH

Sequence ID: Query_506513 Length: 17 Number of Matches: 1

Range 1: 6 to 17 Graphics ▼ Next Match ▲ Previous Match

Score	Expect	Identities	Positives	Gaps
24.4 bits(50)	1e-06	8/12(67%)	8/12(66%)	0/12(0%)

```
Query  5   GGTTGYADAVKG  16
           G  T Y DAVKG
Sbjct  6   GSITSYTDAVKG  17
```

G) Anti-TIM-3-Fc clone 30 vs Anti-IgG-Fc clone 27 CDR3-VL

IgG Clone 27 CDR3-VL

Sequence ID: Query_502921 Length: 9 Number of Matches: 1

Range 1: 1 to 7 Graphics ▼ Next Match ▲ Previous Match

Score	Expect	Identities	Positives	Gaps
26.5 bits(55)	2e-08	7/7(100%)	7/7(100%)	0/7(0%)

```
Query  1  QVWDSST  7
          QVWDSST
Sbjct  1  QVWDSST  7
```

H) Anti-TIM-3-Fc clone 8 vs Anti-IgG-Fc clone 6 CDR2-VH

IgG Clone 6 CDR2-VH

Sequence ID: Query_47547 Length: 17 Number of Matches: 1

Range 1: 2 to 16 Graphics ▼ Next Match ▲ Previous Match

Score	Expect	Identities	Positives	Gaps
36.7 bits(79)	2e-11	12/15(80%)	12/15(80%)	0/15(0%)

```
Query  2   INGDGSSTSYADAVK  16
           IN DG  TSYADAVK
Sbjct  2   INSDGGDTSYADAVK  16
```

I) Anti-TIM-3-Fc clone 8 vs Anti-IgG-Fc clone 6 CDR2-VL

IgG Clone 6 CDR2-VL

Sequence ID: Query_89665 Length: 7 Number of Matches: 1

Range 1: 4 to 7 Graphics ▼ Next Match ▲ Previous Match

Score	Expect	Identities	Positives	Gaps
15.1 bits(28)	2e-04	4/4(100%)	4/4(100%)	0/4(0%)

```
Query  4  SRPS  7
          SRPS
Sbjct  4  SRPS  7
```

J) Anti-TIM-3-Fc clone 8 vs Anti-IgG-Fc clone 27 CDR2-VH

IgG Clone 27 CDR2-VH

Sequence ID: Query_71079 Length: 17 Number of Matches: 1

Range 1: 5 to 16 Graphics ▼ Next Match ▲ Previous Match

Score	Expect	Identities	Positives	Gaps
29.9 bits(63)	9e-09	10/12(83%)	10/12(83%)	0/12(0%)

```
Query  5   DGSSTSYADAVK  16
           DGS TSY DAVK
Sbjct  5   DGSITSYTDAVK  16
```

K) Anti-TIM-3-Fc clone 8 vs Anti-IgG-Fc clone 27 CDR1-VL

IgG Clone 27 CDR1-VL

Sequence ID: Query_41455 Length: 11 Number of Matches: 1

Range 1: 1 to 11 Graphics ▼ Next Match ▲ Previous Match

Score	Expect	Identities	Positives	Gaps
35.4 bits(76)	1e-11	11/11(100%)	11/11(100%)	0/11(0%)

```
Query  1   GGDRIGSKSVE  11
           GGDRIGSKSVE
Sbjct  1   GGDRIGSKSVE  11
```

L) Anti-TIM-3-Fc clone 8 vs Anti-IgG-Fc clone 27 CDR3-VL

IgG Clone 27 CDR3-VL

Sequence ID: Query_117545 Length: 9 Number of Matches: 1

Range 1: 1 to 9 Graphics ▼ Next Match ▲ Previous Match

Score	Expect	Identities	Positives	Gaps
32.9 bits(70)	5e-11	9/9(100%)	9/9(100%)	0/9(0%)

```
Query  1  QVWDSSTIV  9
          QVWDSSTIV
Sbjct  1  QVWDSSTIV  9
```

M) Anti-TIM-3-Fc clone 29 vs Anti-IgG-Fc clone 6 CDR2-VH

IgG Clone 6 CDR2-VH

Sequence ID: Query_66125 Length: 17 Number of Matches: 1

Range 1: 2 to 16 Graphics ▼ Next Match ▲ Previous Match

Score	Expect	Identities	Positives	Gaps
36.7 bits(79)	2e-11	12/15(80%)	12/15(80%)	0/15(0%)

```
Query  2   INGDGSSTSYADAVK  16
           IN DG  TSYADAVK
Sbjct  2   INSDGGDTSYADAVK  16
```

N) Anti-TIM-3-Fc clone 29 vs Anti-IgG-Fc clone 6 CDR1-VL

IgG Clone 6 CDR1-VL

Sequence ID: Query_11155 Length: 14 Number of Matches: 1

Range 1: 1 to 14 Graphics ▼ Next Match ▲ Previous Match

Score	Expect	Identities	Positives	Gaps
34.6 bits(74)	5e-11	12/14(86%)	13/14(92%)	1/14(7%)

```
Query  1   TGSSSNIG-GNYVG  13
           TGSSSN+G GNYVG
Sbjct  1   TGSSSNVGYGNYVG  14
```

O) Anti-TIM-3-Fc clone 29 vs Anti-IgG-Fc clone 27 CDR2-VH

IgG Clone 27 CDR2-VH

Sequence ID: Query_50505 Length: 17 Number of Matches: 1

Range 1: 5 to 16 Graphics ▼ Next Match ▲ Previous Match

Score	Expect	Identities	Positives	Gaps
29.9 bits(63)	9e-09	10/12(83%)	10/12(83%)	0/12(0%)

```
Query  5   DGSSTSYADAVK  16
           DGS TSY DAVK
Sbjct  5   DGSITSYTDAVK  16
```

P) Anti-TIM-3-Fc clone 13 vs Anti-IgG-Fc clone 6 CDR2-VH

IgG Clone 6 CDR2-VH

Sequence ID: Query_60521 Length: 17 Number of Matches: 1

Range 1: 2 to 16 Graphics ▼ Next Match ▲ Previous Match

Score	Expect	Identities	Positives	Gaps
36.7 bits(79)	2e-11	12/15(80%)	12/15(80%)	0/15(0%)

```
Query  2   INGDGSSTSYADAVK  16
           IN DG  TSYADAVK
Sbjct  2   INSDGGDTSYADAVK  16
```

Q) Anti-TIM-3-Fc clone 13 vs Anti-IgG-Fc clone 27 CDR2-VH

IgG Clone 27 CDR2-VH

Sequence ID: **Query_39197** **Length:** **17** **Number of Matches:** **1**

Range 1: 5 to 16 Graphics ▼ Next Match ▲ Previous Match

Score	Expect	Identities	Positives	Gaps
29.9 bits(63)	9e-09	10/12(83%)	10/12(83%)	0/12(0%)

```
Query  5   DGSSTSYADAVK  16
           DGS TSY DAVK
Sbjct  5   DGSITSYTDAVK  16
```

R) Anti-TIM-3-Fc clone 13 vs Anti-IgG-Fc clone 27 CDR1-VL

IgG Clone 27 CDR1-VL

Sequence ID: **Query_83707** **Length:** **11** **Number of Matches:** **1**

Range 1: 1 to 11 Graphics ▼ Next Match ▲ Previous Match

Score	Expect	Identities	Positives	Gaps
35.4 bits(76)	1e-11	11/11(100%)	11/11(100%)	0/11(0%)

```
Query  1   GGDRIGSKSVE  11
           GGDRIGSKSVE
Sbjct  1   GGDRIGSKSVE  11
```

S) Anti-TIM-3-Fc clone 13 vs Anti-IgG-Fc clone 27 CDR2-VL

IgG Clone 27 CDR2-VL

Sequence ID: **Query_28109** **Length:** **7** **Number of Matches:** **1**

Range 1: 1 to 7 Graphics ▼ Next Match ▲ Previous Match

Score	Expect	Identities	Positives	Gaps
16.3 bits(31)	8e-05	5/7(71%)	5/7(71%)	0/7(0%)

```
Query  1  GDSGRPS  7
          GD  RPS
Sbjct  1  GDRSRPS  7
```

T) Anti-TIM-3-Fc clone 13 vs Anti-IgG-Fc clone 27 CDR3-VL

IgG Clone 27 CDR3-VL

Sequence ID: **Query_460281** **Length:** **9** **Number of Matches:** **1**

Range 1: 1 to 7 Graphics ▼ Next Match ▲ Previous Match

Score	Expect	Identities	Positives	Gaps
21.4 bits(43)	2e-06	6/7(86%)	6/7(85%)	0/7(0%)

```
Query  1  QVWHSST  7
          QVW SST
Sbjct  1  QVWDSST  7
```

U) Anti-TIM-3-Fc clone 8 vs Anti-TIM-4 clone 9 CDR2-VH

TIM-4 Clone 9 CDR2-VH

Sequence ID: **Query_115121** **Length:** **16** **Number of Matches:** **1**

Range 1: 2 to 16 Graphics ▼ Next Match ▲ Previous Match

Score	Expect	Identities	Positives	Gaps
27.4 bits(57)	7e-08	11/15(73%)	11/15(73%)	0/15(0%)

```
Query  2   INGDGSSTSYADAVK  16
           IN DGS T Y DAVK
Sbjct  2   INYDGSTTFYNDAVK  16
```

V) Anti-TIM-3-Fc clone 29 vs Anti-TIM-4 clone 9 CDR2-VH

TIM-4 Clone 9 CDR2-VH

Sequence ID: **Query_94479** **Length:** **16** **Number of Matches:** **1**

Range 1: 2 to 16 Graphics ▼ Next Match ▲ Previous Match

Score	Expect	Identities	Positives	Gaps
27.4 bits(57)	7e-08	11/15(73%)	11/15(73%)	0/15(0%)

```
Query  2   INGDGSSTSYADAVK  16
           IN DGS T Y DAVK
Sbjct  2   INYDGSTTFYNDAVK  16
```

W) Anti-TIM-3-Fc clone 29 vs Anti-TIM-4 clone 9 CDR1-VL

TIM-4 Clone 9 CDR1-VL

Sequence ID: **Query_117405** **Length:** **15** **Number of Matches:** **1**

Range 1: 4 to 10 Graphics ▼ Next Match ▲ Previous Match

Score	Expect	Identities	Positives	Gaps
15.1 bits(28)	0.002	4/7(57%)	5/7(71%)	0/7(0%)

```
Query  2  GSSSNIG  8
          GS  +IG
Sbjct  4  GSTNDIG  10
```

X) Anti-TIM-3-Fc clone 13 vs Anti-TIM-4 clone 9 CDR2-VH

TIM-4 Clone 9 CDR2-VH

Sequence ID: **Query_20189** **Length:** **16** **Number of Matches:** **1**

Range 1: 2 to 16 Graphics ▼ Next Match ▲ Previous Match

Score	Expect	Identities	Positives	Gaps
27.4 bits(57)	7e-08	11/15(73%)	11/15(73%)	0/15(0%)

```
Query  2   INGDGSSTSYADAVK  16
           IN DGS T Y DAVK
Sbjct  2   INYDGSTTFYNDAVK  16
```

Y) Anti-TIM-4 clone 9 vs Anti-TIM-3-Fc clone 7 CDR2-VH

TIM-3 Clone 7 CDR2-VH

Sequence ID: **Query_35893** **Length:** **16** **Number of Matches:** **1**

Range 1: 2 to 16 Graphics ▼ Next Match ▲ Previous Match

Score	Expect	Identities	Positives	Gaps
27.4 bits(57)	7e-08	11/15(73%)	11/15(73%)	0/15(0%)

```
Query  2   INYDGSTTFYNDAVK  16
           IN DGS T Y DAVK
Sbjct  2   INGDGSSTSYADAVK  16
```

Z) Anti-TIM-4 clone 9 vs Anti-TIM-3-Fc clone 7 CDR1-VL

TIM-3 Clone 7 CDR1-VL

Sequence ID: **Query_124397** **Length:** **13** **Number of Matches:** **1**

Range 1: 2 to 8 Graphics ▼ Next Match ▲ Previous Match

Score	Expect	Identities	Positives	Gaps
15.1 bits(28)	0.002	4/7(57%)	5/7(71%)	0/7(0%)

```
Query  4  GSTNDIG  10
          GS  +IG
Sbjct  2  GSSSNIG  8
```

AA) Anti-TIM-4 clone 9 vs Anti-TIM-3-Fc clone 30 CDR2-VH

TIM-3 Clone 30 CDR2-VH

Sequence ID: **Query_75235** **Length:** **16** **Number of Matches:** **1**

Range 1: 2 to 15 Graphics ▼ Next Match ▲ Previous Match

Score	Expect	Identities	Positives	Gaps
22.3 bits(45)	6e-06	10/15(67%)	10/15(66%)	1/15(6%)

```
Query  2   INYDGSTTFYNDAVK  16
           IN  G TT Y DAVK
Sbjct  2   IN-SGGTTGYADAVK  15
```

AB) Anti-TIM-4 clone 9 vs NPC Clone 5 CDR2-VH

NPC Clone 5 CDR2-VH

Sequence ID: **Query_83625** **Length:** **16** **Number of Matches:** **1**

Range 1: 6 to 16 Graphics ▼ Next Match ▲ Previous Match

Score	Expect	Identities	Positives	Gaps
23.1 bits(47)	3e-06	8/11(73%)	8/11(72%)	0/11(0%)

```
Query  6   GSTTFYNDAVK  16
           GS T Y DAVK
Sbjct  6   GSSTSYADAVK  16
```

AC) Anti-TIM-4 clone 9 vs NPC Clone 6 CDR2-VH

NPC Clone 6 CDR2-VH

Sequence ID: **Query_22853** **Length:** **16** **Number of Matches:** **1**

Range 1: 2 to 8 Graphics ▼ Next Match ▲ Previous Match

Score	Expect	Identities	Positives	Gaps
19.7 bits(39)	6e-05	5/7(71%)	6/7(85%)	0/7(0%)

```
Query  2  INYDGST  8
          I+YDG T
Sbjct  2  IDYDGGT  8
```

Figure D.7: Comparison of CDR regions of controls vs clones binding to target proteins in high quality and fully sequenced clones. *Each CDR region was compared individually. Anti-TIM-3-Fc clones were compared to Anti-IgG-Fc clones and Anti-TIM-4 clones were compared to NPC clones and Anti-TIM-3-Fc clones.*

A) NPC Clone 5 vs NPC Clone 6 CDR1-VL

NPC Clone 6 CDR1-VL

Sequence ID: Query_54821 **Length:** 13 **Number of Matches:** 1

Range 1: 6 to 11 Graphics ▼ Next Match ▲ Previous Match

Score	Expect	Identities	Positives	Gaps
12.1 bits(21)	0.018	4/6(67%)	4/6(66%)	0/6(0%)

```
Query  4   NIGGKY  9
           NI  KY
Sbjct  6   NIDRKY  11
```

B) Anti-IgG-Fc clone 6 vs Anti-IgG-Fc clone 27 CDR2-VH

IgG Clone 27 CDR2-VH

Sequence ID: Query_302397 **Length:** 17 **Number of Matches:** 1

Range 1: 5 to 17 Graphics ▼ Next Match ▲ Previous Match

Score	Expect	Identities	Positives	Gaps
29.1 bits(61)	2e-08	10/13(77%)	10/13(76%)	0/13(0%)

```
Query  5   DGGDTSYADAVKG  17
           DG  TSY DAVKG
Sbjct  5   DGSITSYTDAVKG  17
```

C) Anti-IgG-Fc clone 6 vs Anti-IgG-Fc clone 27 CDR2-VL

IgG Clone 27 CDR2-VL

Sequence ID: Query_83729 **Length:** 7 **Number of Matches:** 1

Range 1: 4 to 7 Graphics ▼ Next Match ▲ Previous Match

Score	Expect	Identities	Positives	Gaps
15.1 bits(28)	2e-04	4/4(100%)	4/4(100%)	0/4(0%)

```
Query  4  SRPS  7
          SRPS
Sbjct  4  SRPS  7
```

D) Anti-TIM-3-Fc clone 8 vs Anti-TIM-3-Fc clone 13 CDR1-VH

TIM-3 Clone 13 CDR1-VH

Sequence ID: Query_19893 **Length:** 5 **Number of Matches:** 1

Range 1: 1 to 5 Graphics ▼ Next Match ▲ Previous Match

Score	Expect	Identities	Positives	Gaps
25.2 bits(52)	1e-08	5/5(100%)	5/5(100%)	0/5(0%)

```
Query  1  NYWMY  5
          NYWMY
Sbjct  1  NYWMY  5
```

E) Anti-TIM-3-Fc clone 8 vs Anti-TIM-3-Fc clone 13 CDR2-VH

TIM-3 Clone 13 CDR2-VH

Sequence ID: Query_86733 **Length:** 16 **Number of Matches:** 1

Range 1: 1 to 16 Graphics ▼ Next Match ▲ Previous Match

Score	Expect	Identities	Positives	Gaps
50.3 bits(111)	8e-17	16/16(100%)	16/16(100%)	0/16(0%)

```
Query  1   SINGDGSSTSYADAVK  16
           SINGDGSSTSYADAVK
Sbjct  1   SINGDGSSTSYADAVK  16
```

F) Anti-TIM-3-Fc clone 8 vs Anti-TIM-3-Fc clone 13 CDR3-VH

TIM-3 Clone 13 CDR3-VH

Sequence ID: Query_54709 **Length:** 4 **Number of Matches:** 1

Range 1: 1 to 4 Graphics ▼ Next Match ▲ Previous Match

Score	Expect	Identities	Positives	Gaps
15.1 bits(28)	5e-05	4/4(100%)	4/4(100%)	0/4(0%)

```
Query  1  GGDD  4
          GGDD
Sbjct  1  GGDD  4
```

G) Anti-TIM-3-Fc clone 8 vs Anti-TIM-3-Fc clone 13 CDR1-VL

TIM-3 Clone 13 CDR1-VL

Sequence ID: Query_34219 **Length:** 11 **Number of Matches:** 1

Range 1: 1 to 11 Graphics ▼ Next Match ▲ Previous Match

Score	Expect	Identities	Positives	Gaps
35.4 bits(76)	1e-11	11/11(100%)	11/11(100%)	0/11(0%)

```
Query  1   GGDRIGSKSVE  11
           GGDRIGSKSVE
Sbjct  1   GGDRIGSKSVE  11
```

H) Anti-TIM-3-Fc clone 8 vs Anti-TIM-3-Fc clone 13 CDR2-VL

TIM-3 Clone 13 CDR2-VL

Sequence ID: Query_118067 **Length:** 7 **Number of Matches:** 1

Range 1: 1 to 7 Graphics ▼ Next Match ▲ Previous Match

Score	Expect	Identities	Positives	Gaps
16.3 bits(31)	8e-05	5/7(71%)	5/7(71%)	0/7(0%)

```
Query  1  GDRSRPS  7
          GD  RPS
Sbjct  1  GDSGRPS  7
```

I) Anti-TIM-3-Fc clone 8 vs Anti-TIM-3-Fc clone 13 CDR3-VL

TIM-3 Clone 13 CDR3-VL

Sequence ID: **Query_84011** **Length:** **11** **Number of Matches:** **1**

Range 1: 1 to 7 Graphics ▼ Next Match ▲ Previous Match

Score	Expect	Identities	Positives	Gaps
21.4 bits(43)	2e-06	6/7(86%)	6/7(85%)	0/7(0%)

```
Query  1  QVWDSST  7
          QVW SST
Sbjct  1  QVWHSST  7
```

J) Anti-TIM-3-Fc clone 7 vs Anti-TIM-3-Fc clone 30 CDR2-VH

TIM-3 Clone 30 CDR2-VH

Sequence ID: **Query_35851** **Length:** **16** **Number of Matches:** **1**

Range 1: 2 to 15 Graphics ▼ Next Match ▲ Previous Match

Score	Expect	Identities	Positives	Gaps
27.4 bits(57)	7e-08	10/15(67%)	10/15(66%)	1/15(6%)

```
Query  2   INGDGSSTSYADAVK  16
           IN  G  T YADAVK
Sbjct  2   INS-GGTTGYADAVK  15
```

Figure D.8: Comparison of CDR regions for controls and binders to target proteins against themselves in high quality and fully sequenced clones. *Comparison of NPC and IgG controls together and comparison of the non-binding clone anti-TIM-3-Fc clone 8 with binding clone anti-TIM-3-Fc clone 13 and comparison of two binding clones anti-TIM-3-Fc clone 7 and anti-TIM-3-Fc clone 30.*